Durham E-Theses

Unveiling the molecular determinants of mammalian skin ageing: A proteomic and transcriptomic approach

O'MAHONY, KATHERINE,MARGARET

Department of Biosciences

Unveiling the molecular determinants of mammalian skin ageing: a proteomic and transcriptomic approach

Katherine Margaret O'Mahony

January 2017

A thesis submitted for the degree of Doctor of Philosophy

Declaration

The work described herein was carried out in the School of Biosciences, University of Durham between October 2013 and January 2017. All of the work is my own, except where specifically stated otherwise. No part has previously been submitted for a degree at this or any other university.

Statement of Copyright

Abstract

As the limits of human lifespan continue to expand, ageing biologists must address the decline in the integrity of bodily tissues with time. Our skin is drastically impacted by both intrinsic and extrinsic ageing processes, driven by gradual accumulation of cellular damage and environmental insults like ultra-violet irradiation.

Together intrinsic and extrinsic skin ageing give rise to clinical issues such as xerosis, pruritus and neoplasms. Cosmetic issues, such as unsightly wrinkling, thinning and sagging of the skin also impact human psychological and social wellbeing. Given these issues, studying the molecular mechanisms of intrinsic and extrinsic skin ageing processes is an important element of biological research, as a better understanding of how these processes contribute to reduced tissue integrity will allow us to develop therapies to attenuate the ageing process.

Using tissues taken from C57BL/6 male mice and female humans as our models, we analysed skin at early, middle and late stages within both the murine and human lifespans to assess the impact of ageing on changes in the epidermis, dermis and at the basement membrane. By considering tissue taken from photo-protected and photo-exposed sites of humans, we additionally studied the differential changes occurring during intrinsic and extrinsic skin ageing (photo-ageing).

Our studies showed that several morphometric changes occur to the epidermis with age in mouse skin, where we observed thinning and cellular loss. Cell proliferation and lamin B1 levels declined, which was coupled with decreased expression of dermal and basement membrane collagens. Many of these observations were ubiquitous in intrinsically aged human skin, where we additionally show unique transcriptional changes at the basement membrane. One little studied pathway in skin ageing is the Hippo pathway, which has crucial roles in epidermal development through its control of epidermal cell proliferation. We identify a novel modulation of the Hippo pathway effector YAP1 in aged mouse and human skin, where we show that nuclear localisation of YAP1 increases during epidermal ageing.

Together this body of work demonstrates that C57BL/6 mouse skin ageing shares common mechanisms of intrinsic human skin ageing. Additionally, we show that YAP1 localisation is altered during epidermal ageing, which suggests that the Hippo pathway is sensitive to both changes in the extra-cellular matrix content, and cell-proliferation properties of skin over time.

Acknowledgements

First and foremost, I want to thank Akis for his ideas, his patience and his encouragement. The circumstances of him becoming my supervisor were exceptional, and his un-questioning will to take me on was crucial to my progression as a scientist.

Secondly, this PhD would have been much harder without the unconditional love and support of my family- you are all amazing and always there to help.

Thirdly I am so grateful for my friends- Claire, Ines, Mariama, Steph, Jen, Kasia, everyone at Durham University Triathlon club, Durham University Cycling club and Durham City Harriers. Thank you for helping me to maintain the belief that I could do this and for helping me to keep a balance in my life away from the bench and computer.

Within the department I would like to thank Pamela Ritchie, Mathilde Roger, Nicola Fullard, Colin Jahoda, Carrier Ambler and Frederique Tholozan for always being there to help. The technical support from Christine Richardson, Helen Grindley, Tim Hawkins and Joanne Robson with all things microscopy. Within the LINK grant: Thomas von Zglinicki, Arto Maatta and Stefan Przyborski for your excellent input. Also to Keith Lindsey for overseeing the BBSRC DTP programme that has given me so many opportunities along with financial support.

Over at Newcastle- Glyn Nelson- I am so grateful for all your technical and informative help! Also to Diana Jurk for your help with all things IHC. Thank you to Gavin Richardson for providing further mouse tissue. I also want to thank Bob Binder, Bob Isfort, Charlie Bascom and everyone at Procter and Gamble for kindly providing some of the materials contributing to the work in section 4 of this thesis and for supporting me financially.

I dedicate this thesis to everyone above and feel very special that you gave me your time and energy.

Table of Contents

List of Figures

List of Tables

Abbreviations

- %= percentage
- °C= degrees Celsius
- μl=microliters
- 2D= Two-dimensional
- AD-EDMD= Autosomal-dominant Emery-Dreifuss muscular dystrophy
- AFM= Atomic force microscopy
- ANOVA= analysis of variance
- Appendix 1: Abbreviations
- AT-probe-set= above-threshold probe sets
- BE= basal epidermal
- BM= basement membrane
- BPAG-1= Bullous pemphigoin antigen 1
- BRB/T= Blot rinse buffer with tween 20
- BSA= bovine serum albumin
- CE= cornified envelope
- CLSM= confocal laser scanning microscopy
- DAPI= 4',6-diamidino-2-phenylindole
- DDF= Dna damage foci
- de= dermis
- DEJ= dermal-epidermal junction
- dH_20= distilled water
- DMEM= Dulbecco's modified eagle's medium
- DNA DF= DNA damage foci
- DNA= deoxyribonucleic acid
- DP= Desmoplakin
- e= epidermis
- ECL= enhanced chemiluminescence substrate
- ECM= extra-cellular matrix
- EDTA= Ethylenediaminetetraacetic acid
- EM- electron microscopy
- Enz AR= enzyme induced antigen retrieval
- Epi SC= Epidermal stem cell
- EtOH= ethanol
- FBS= foetal bovine serum
- FDR= false discovery rate
- F-IHC= fluorescent immunohistochemistry
- FRAP= fluorescence recovery after photo-bleaching
- FTS= Full thickness skin
- GAPDH= Glyceraldehyde 3-phosphate dehydrogenase
- GWAS= genome-wide association studies
- H+E= Haematoxylin and Eosin
- hd= hypodermis
- HDF's= human dermal fibroblasts
- hf= hair follicle (legend)
- HF= hair follicle (text)
- HFC= hair follicle cycle
- HGF= human growth factor
- HGPS= Hutchison Gilford Progeria Syndrome

- HIAR= heat induced antigen retrieval
- hr= hours
- HSP's= highly significant mRNA probe sets
- IF IHC= immunofluorescent immunohistochemistry
- IFE= inter-follicular epidermis
- IGF's= Insulin-like growth factors
- IHC= immunohistochemical
- IL-6= Interleukin 6
- IL-8= Interleukin 8
- INM= inner nuclear membrane
- K10=Keratin 10
- K14= Keratin 14
- K5= Keratin 5
- kDa= kilodaltons
- LCM= Laser Capture Microdissection
- LHS =left hand side
- LINC= linker of nucleoskeleton and cytoskeleton
- lncRNA= long non-coding RNA
- mo= months
- mAmp= milliampere
- mESC's= mouse embryonic stem cells
- mg=milligrams
- min= minutes
- miRNA= micro RNA
- ml= millilitres
- mm= milli-metres
- mM= milli-molar
- MMP-1= Matrix metalloproteinase-1
- MMP-9= Matrix metalloproteinase-9
- mRNA= messenger RNA
- ms= muscle
- MW= molecular weight
- N:C= Nuclear to cytoplasmic ratio
- NCS= newborn calf serum
- ng= nanograms
- OCT= optimal cutting temperature medium
- p53= tumour protein p53
- P53BP1= (also TP53BP1) Tumor suppressor p53-binding protein 1
- PBS= phospho-buffered saline
- PD= papillary dermis
- PE= photo-exposed
- PE= photo-exposed
- PE=Old photo-exposed
- PFA= paraformaldehyde
- PG= Plakoglobin
- PKC= Protein Kinase C
- PKP1= Plakophillin 1
- POD= peroxidase
- PP= Old photo-protected

- PP= photo-protected
- PP= photo-protected
- pRb= retinoblastoma protein
- RD= reticular dermis
- RHS= right hand side
- ROS= reactive oxygen species
- RPM= revolutions per minute
- rRNA= ribosomal RNA
- RT-PCR= Reverse transcription polymerase chain reaction
- SASP= senescence-associated secretory phenotype
- SC= Stratum Corneum
- SDS-PAGE= sodium dodecyl sulfate polyacrylamide gel electrophoresis
- sec= seconds
- sen-β-gal= Senescence-associated β-galactosidase staining
- sg= sebaceous gland
- siRNA= small-interfering RNA
- SPR's= Small Proline rich proteins
- SUN1= SUN domain-containing protein 1
- TAZ= transcriptional co-activator with a PDZ-binding motif
- TBS/T= Tris-buffered saline with tween 20
- TBS/T= tris-buffered saline with tween 20
- TEM=transmission electron microscopy
- TJ= tight junctions
- UV= ultraviolet
- V= volts
- wk= week
- WT= wild type
- YAP1= yes-associated protein 1
- Y-PE= Young photo-exposed
- Y-PP= Young photo-protected

Chapter 1: Introduction and Objectives

1.1   Skin structure and function

Our skin is the largest organ in the human body, accounting for around 15% of the total body weight in adult humans. As a highly evolved, multifunctional organ, skin prevents excess water loss, excludes toxins, resists mechanical stress, maintains our body temperature and participates in immune responses (Kanitakis, J. 2002). In order to fulfill its many functions, skin has an elaborate layered structure, with the outermost layer being the epidermis, followed by the dermis and then the hypodermis. Within the dermal region adnexal structures such as hair follicles, sweat glands, sebaceous glands, lymphatic vessels and blood vessels are present, which all play a role in skin biology. A representative example of human skin is shown in figure 1.1.
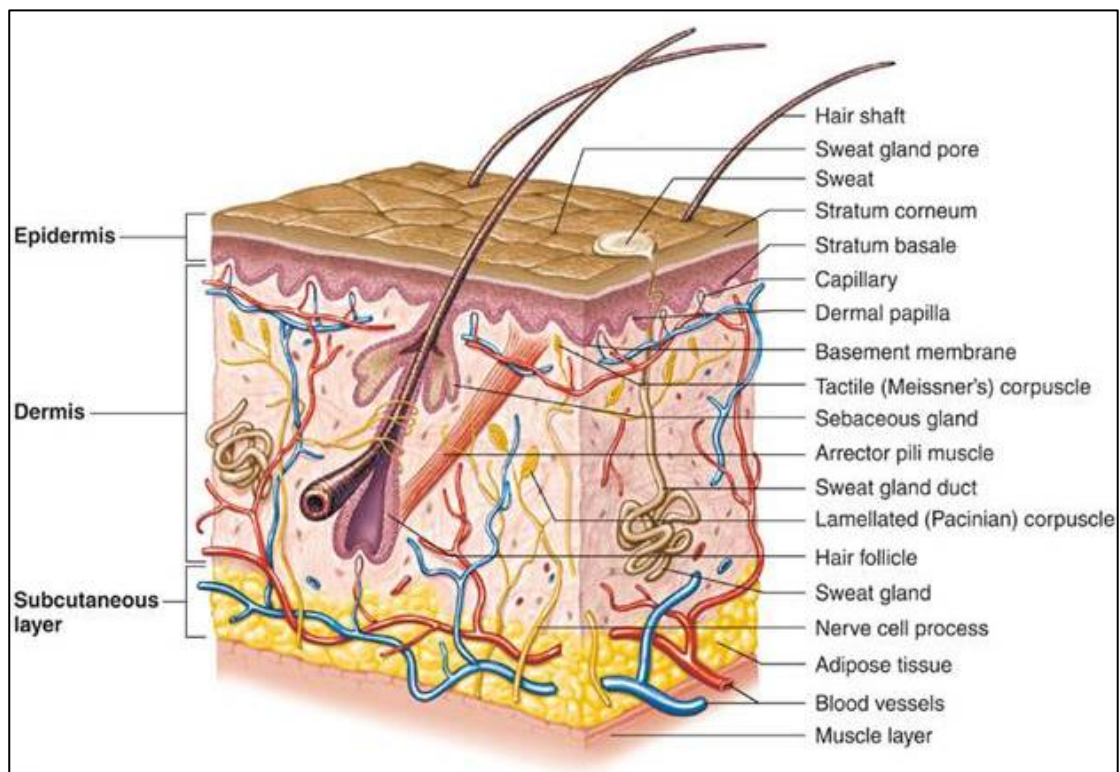
Figure 1.1: An example of a cross section of human skin showing the 3 main layers: epidermis, dermis and subcutaneous layer (also known as hypodermis). The epidermis does not have a vascular network of its own, and depends on the vasculature present in the dermis for nutrient supply. The skin is a highly sensory organ, and therefore present in the dermis are many nerve endings (Lamellated corpuscle's). The subcutaneous (fatty) layer provides insulation to the body, preventing excess heat loss and thus allowing us to maintain our core temperature. (Image taken from Hole's Human Anatomy and Physiology, Chapter 6).

1.2   The epidermis of our skin is a multilayered, specialized epithelium

Our epidermis is our first line of defence against water loss, pathogens and mechanical stress (Sandilands et al, 2009). This multi-layered epithelium has evolved over time to consist of several different cellular layers, which are made primarily from keratinocytes. The epidermal layers are histologically distinct (figure 1.2) and in ascending order, are called the basal layer (*stratum basale*), spinous layer (*stratum spinosum*), granular layer (*stratum granulosum*) and cornified envelope (*stratum corneum*).
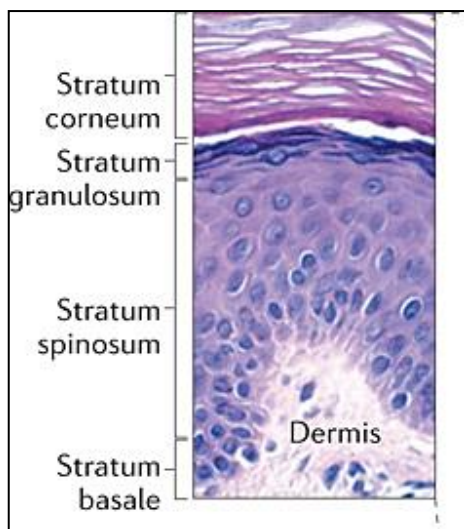
Figure 1.2: The epidermal layers are histologically distinct from one another. Epidermal layers stained with haematoxylin and eosin showing the different *strata* (layers) (image from Simpson et al, 2011).

Although keratinocytes make up the vast majority of the cellular population in this compartment, other specialized cells are also present in small quantities such as antigen-presenting Langerhans cells, which play a role in the skin immune response and make up 2-5% of the epidermal cell population in humans (Chomiczewska et al, 2009). Merkel cells are also present, and these mechanosensory cells are usually associated with several nerve endings, allowing touch sensations to be signaled from the skin to the brain. This sensory cell population accounts for 6-10% of the whole epidermis in humans. Finally, melanocytes are resident in the basal layer, and these cells produce the pigment melanin, which gives skin its colour and protects DNA from UV-induced damage. Melanocytes make up around 5% of the total epidermal cell population in human skin (Cichorek et al, 2013).

The resident keratinocytes within each epidermal layer have their own unique cellular morphology, keratin expression profile and cell junction expression profile. This phenotypic change in the different layers is a result of the terminal differentiation process that occurs starting in the basal layer and ending in the cornified envelope (CE) (Simpson et al, 2011). Figure 1.3 depicts the basal layer (*stratum basale*), which is connected to the basement

membrane (BM) by several cell-matrix adhesion complexes (focal contacts), such as integrin proteins, which tether the basal keratinocytes to this region. Several cellular junctions are present between the basal epidermal cells, which confer mechanical stability and also allow cell-cell communication (Lai-Cheong et al, 2007). In the spinous layer cells begin to synthesize the machinery needed to form the CE, whilst also increasing their expression of adhesion proteins such as E-cadherin, desmoplakin (DP), plakophilin 1 (PKP1) and plakoglobin (PG). These molecules contribute to the formation of cadherin-based cell junctions and desmosomes, aiding in both the mechanical resistance and barrier properties of the epidermis (Bazzoni and Dejana, 2002). In the granular layer (figure 1.3), cells begin to assemble the components of the CE before eventually becoming anuclear components of the stratum corneum (SC). Finally, dead corneocytes are shed from the outer epidermis, ensuring that basal keratinocyte proliferation is balanced with cellular loss.
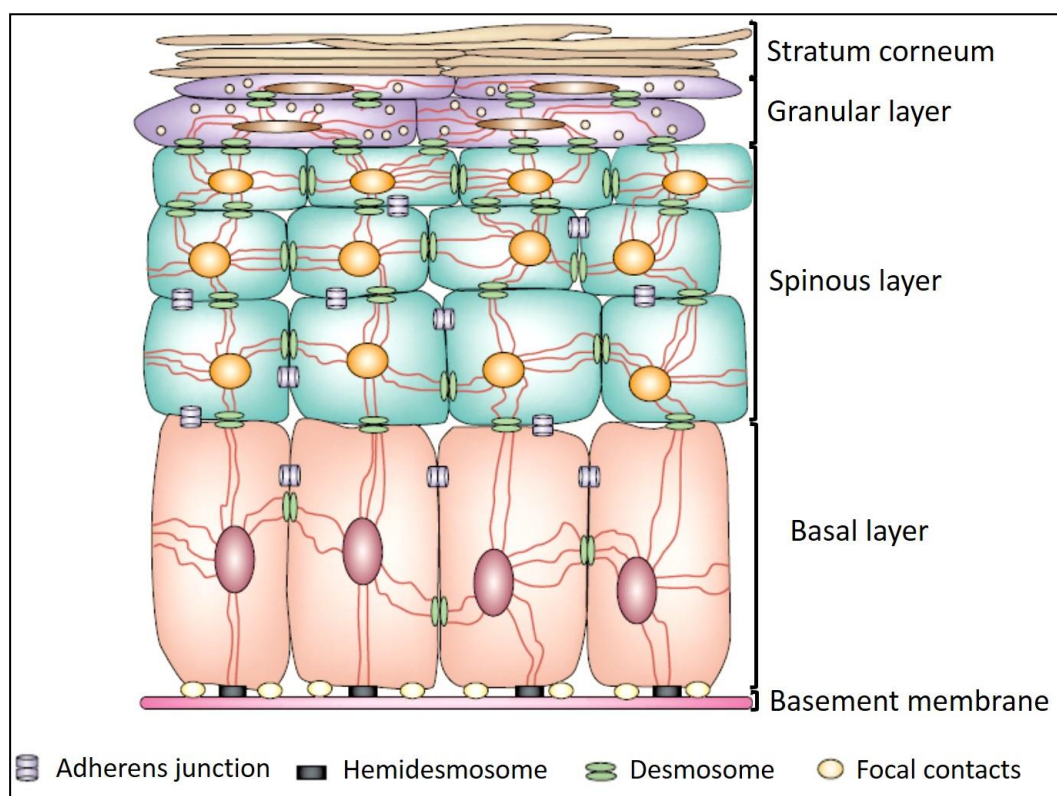
Figure 1.3: Structure of the keratinocytes within each epidermal layer. Basal layer cells are connected to the basement membrane via hemidesmosomes and integrin-containing focal adhesions. Cells of the spinous layer are reduced in size compared to basal cells and express many cell adhesion molecules so that cells can be connected via desmosomes and adherens junctions, which allow inter-cell communication. In the granular layer cell flattening and synthesis of lipid vesicles and other protein components occurs so that terminally differentiated keratinocytes can form the components of the stratum corneum. Image from Fuchs and Raghavan, 2002.

1.3   Epidermal stem cells in the basal layer drive epidermal homeostasis

The epidermal basal layer (*stratum basale*) is the central hub of epidermal mitosis, as it houses keratinocyte stem cells which are contained within a protective niche. Cells of this layer express the keratins K5 and K14, which help to maintain them in an un-differentiated state (Fuchs and Raghavan, 2002). Epidermal stem cell (Epi SC) proliferation in this layer is believed to be driven in part by extracellular signals derived from cells within the dermis, which secrete mitogens such as insulin-like growth factors (IGF's), causing the initiation of cell division (Hsu et al, 2014). Epi SC's proliferate and subsequently migrate upwards and differentiate in to the cells forming the spinous layer (*stratum spinosum*). The precise mechanics of Epi SC proliferation and differentiation have been contested in several reports, with some authors providing support for a hierarchical model (Clayton et al, 2007; Lim et al, 2013), and others a stochastic mechanism of epidermal renewal (Mascré et al, 2012) (both mechanisms depicted in figure 1.4). Whatever the precise mechanics of Epi SC proliferation, it is hypothesized that loss of cellular contact with the basement membrane (BM), via down-regulated expression of integrins on the cell surface, allows subsequent keratinocyte differentiation processes to occur (Watt, F.M. 2002).
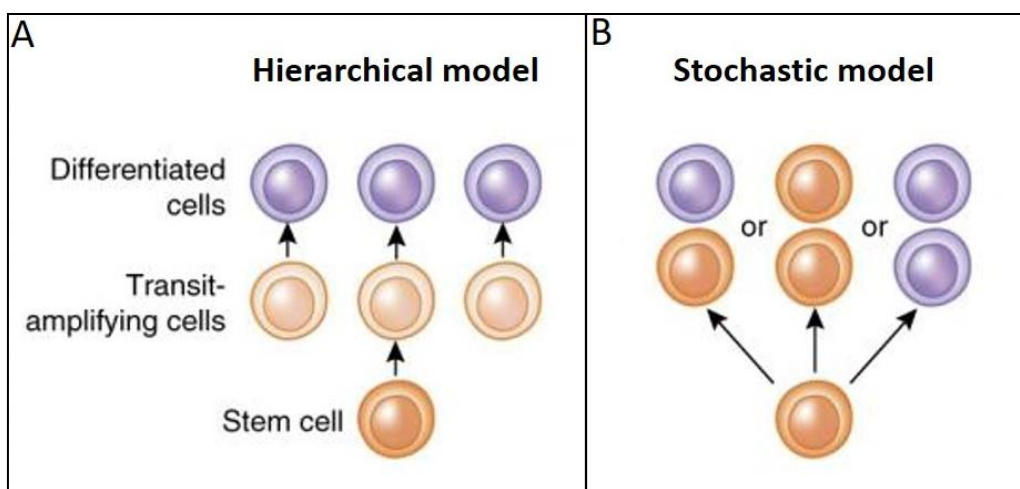
Figure 1.4: Two proposed models of Epi SC proliferation. In the **Hierarchical model** (A) rarely placed stem cells in the basal layer divide giving rise to rapidly diving transit amplifying cells also occupying the basal layer. These TA cells then go on to differentiate and form the upper epidermal layers. In the **Stochastic model** (B) all of the basal cells are identical and random assignment of cell fate can result in 3 outcomes. 1: one cell becomes a differentiated daughter cell (purple) and one remains a progenitor and continues to reside in the basal layer (orange). 2: both cells become progenitors, or 3: both cells become differentiated daughter cells. In this model equal probability of the 3 outcomes ensures that overall epidermal homeostasis is maintained (image from Hsu et al, 2014).

In the absence of cell-matrix contact, daughter cells of Epi SC's undergo alterations in their cell polarity and cytoskeletal architecture, eventually becoming post-mitotic cellular residents of the spinous layer. Both biochemical and mechanical cues are thought to drive this

process (Connelly et al, 2010), which results in down-regulation of the expression of basal epidermal keratins K5 and K14 and up-regulation of keratin 1 (K1) and keratin 10 (K10). Additionally, the intercellular adhesion profile in this layer is altered, with cells expressing greater amounts of E-cadherin and desmoglein 1, which contribute to the formation of adherens junctions and desmosomes respectively (Simpson et al, 2011). At this stage, cells begin to lay the foundations for later CE formation, by depositing glutamine and lysine-rich envelope proteins such as involucrin on the inner surface of the plasma membrane of each cell. Additionally, lipid synthesis and packing into vesicles begins to occur (Fuchs, E. 1990).

1.4   Spinous to granular transition

The phenotypic transition of keratinocytes in the spinous layer to the granular layer is controlled by several signaling mechanisms, some of which are dependent on the presence of a calcium gradient within the epidermal layer. The Protein Kinase C (PKC) pathway initiates expression of the CE components loricrin, filaggrin and transglutaminases whilst also causing a down-regulation in expression of K10 and K1 (Koster and Roop, 2007). Filaggrin acts to bundle keratin filaments into parallel rope-like structures that cause the cell to collapse and become flattened. The filaggrin bundled cytoskeleton then forms a platform for the assembly of the components of the CE, which is a proteinaceous barrier that resists mechanical stress and prevents water loss (Steven and Steinert, 1994). The structure of the CE is depicted in figure 1.5.
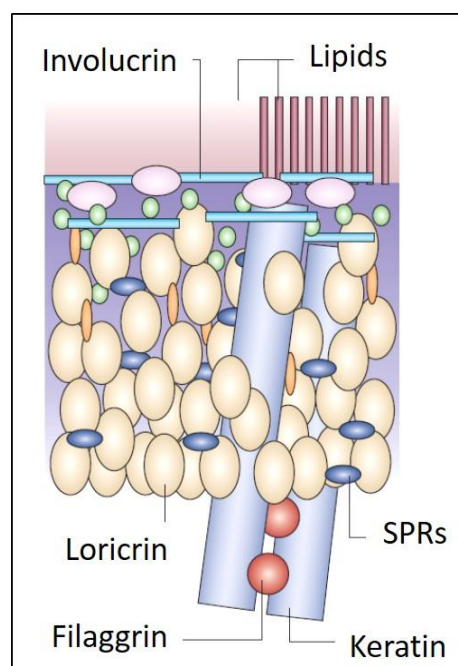
Figure 1.5: Proteins of the CE. In corneocytes the plasma membrane is replaced with a specialized protein cage that is formed from structural proteins like **involucrin** and **loricrin** which give the CE elasticity and **keratin** which promote mechanical resilience in this layer. Involucrin and loricrin are cross-linked through isopeptide bonds catalyzed by transglutaminase enzymes and small-proline rich proteins (**SPRs**). Keratins are bundled in large macrofilaments by filaggrin. Additionally, lipids such as ceramides, cholesterol, fatty acids and cholesterol esters are released between the corneocytes, allowing a hydrophobic barrier to be formed in the outer epidermal layers. (Picture from Candi et al, 2005).

1.5   Formation of the CE

The formation of the outermost epidermal layer involves a unique cell death programme called cornification. During cornification, proteases such as cathepsins degrade organelles and DNase enzymes degrade nuclear material, causing an associated reduction in cell body size. Apoptotic signaling mechanisms are suppressed during this process, so that the remaining cell body, now known as a squame, remains present on the outer epidermal surface, fulfilling its function as a barrier structure (Eckhart et al, 2013). By this stage the terminally differentiated keratinocytes are free from organelles and contain only cytoskeletal and other structural proteins of the CE. The squames are joined to one another by special inter-cellular adhesions in this area, known as corneodesmosomes (Lippens et al, 2009). Additionally, the formation of the CE involves inter-cellular lipid release from lamellar bodies within the cells, resulting in a lipid coating to be formed in the spaces between squames. The eventual structure of the CE has been likened to "bricks" within a lipid-based "mortar", which is adept in its role as a hydrophobic barrier that prevents microorganism entry (Nemes and Steinert, 1999). The final process of de-squamification involves shedding of corneocytes due to proteolytic activity that degrades the corneodesmosomes. Removal and changes to the surrounding lipids are also thought to aid in this process (Lin et al, 2012).

1.6   The Basement membrane of skin is situated at the dermal-epidermal junction

The basement membrane (BM) in skin is a specialized ECM layer that separates the epidermal and dermal compartments and provides a platform for adherence of basal epidermal keratinocytes. The structure of the BM promotes mechanical stability at the dermal-epidermal junction (DEJ) and also provides a protective niche for epidermal stem cells (Kalluri, R 2003). BM's are complex structures consisting of several layers and molecular components, including their own unique collagen protein profile. Ultra-structural imaging of the BM using an electron microscope depicts two layers, known as the electron-lucid, upper *lamina lucida* and the electron-dense, lower *lamina densa* (Natsuga, K. 2013) (see figure 1.6). Collagen IV is a crucial part of the *lamina densa*, and it confers mechanical stability to this region and can be found in the BM's of many epithelia and also blood vessel endothelia (Hasegawa et al, 2007). Unlike collagen IV, the expression of collagen VII is restricted to the BM zone beneath stratified squamous epithelia, like the skin epidermis, and this protein acts to form anchoring fibrils that connect the BM to the underlying dermis (Langton et al, 2016). *In vitro* studies from Ryynanen et al, (1992) have shown that epidermal keratinocytes are primary synthesizers of collagen VII,

although dermal fibroblasts also express collagen VII mRNA at low levels. Both fibroblasts (Olsen et al, 1989) and keratinocytes (Schafer et al, 1991) have also been shown to synthesize collagen IV demonstrating the potential for both epidermal and dermal cell populations to contribute to the production of the basement membrane collagens.
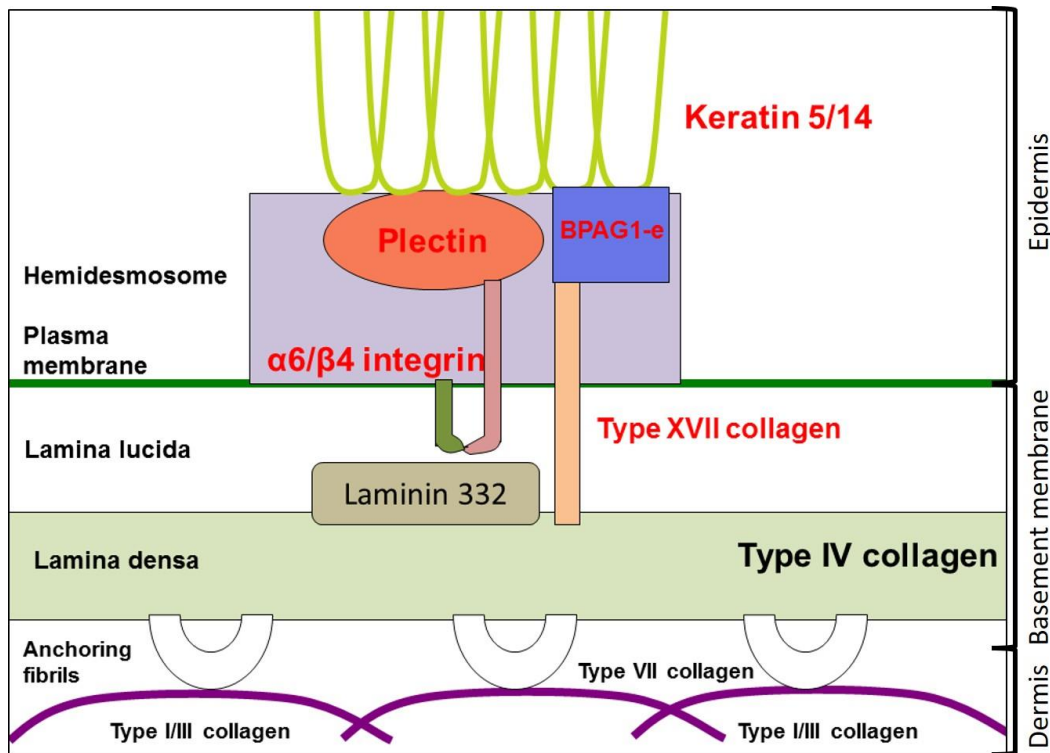
Figure 1.6: Structure of the basement membrane at the dermal-epidermal junction. The figure shows a keratinocyte (components in red font) in the basal epidermis tethered to the basement membrane by **α6β4 integrin** and **type XVII collagen**. Also present in the diagram are the cytoskeletal linker proteins **plectin** and **BPAG1** (Bullous pemphigoid antigen 1) that tether the intermediate filaments in the keratinocyte to the **hemidesmosomes** at the cellular plasma membrane. The diagram indicates the two morphologically distinct layers in the BM, the **lamina lucida**, which is rich in **laminin 332** protein, and **lamina densa,** rich in **type IV collagen**. **Collagen VII** anchoring fibrils join the BM to the type I and type III collagens present in the dermis. (Image from Natsuga, K. 2013)

1.7   Structure and functions of the dermal compartment

The dermis is a thick, extra-cellular matrix (ECM) rich skin layer that is relatively acellular compared to the epidermis, although fibroblasts and immune cells do populate this layer, which houses appendages such as hair follicles, sweat and sebaceous glands. The structural constituents of the dermal matrix, notably collagens, elastins and fibrillins form a basket-weave structure that confers tensile strength and mechanical resilience to the skin (Brincat et al, 2005). Several non-fibrillar molecules interact with dermal collagens and elastins such as glycosaminoglycans. These unbranched polysaccharide chains are able to bind large

quantities of water and give the dermis a soft, gel-like consistency that constitutes suppleness (Calleja-Agius et al, 2013).

Type I and Type III collagens make up the bulk of dermal protein (97.5%) and are arranged in a ratio of approximately 3:1 in young skin (Cheng et al, 2011). Their distribution is different in the two histologically distinctive dermal layers. In the upper papillary dermis, which is fibroblast-dense and consists of loosely arranged collagen, there is less type I collagen and more type III. In contrast, in the lower reticular dermis the collagen fibrils are densely packed and the region is rich in type I collagen (Oikarinen, A 1990)(see figure 1.7.). Each region has been shown to have its own distinct fibroblast populations, with a genetic and secretory profile unique to that region (Janson et al, 2012).
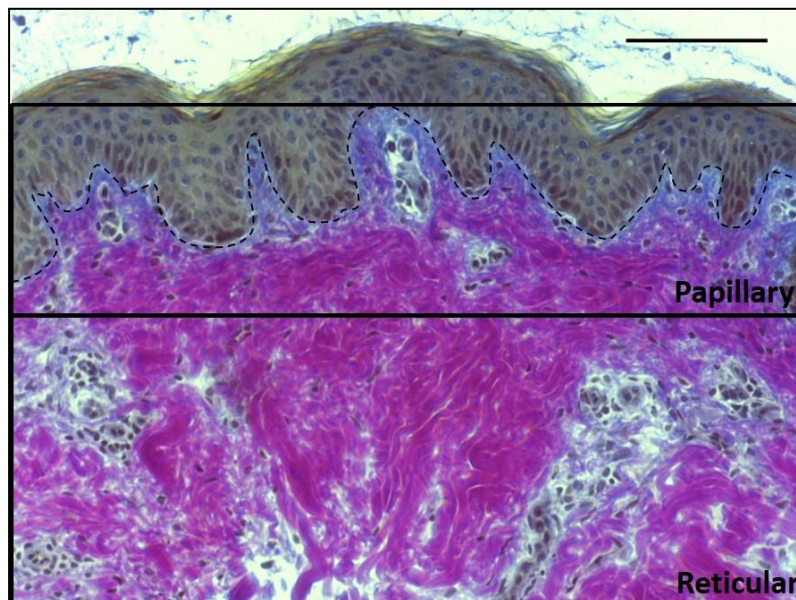
Figure 1.7: The two dermal layers are histologically distinct. Human skin stained with Herovici's stain for young (blue) and mature (magenta) collagen. Nuclei are stained blue/black. Black dotted line= DEJ. The papillary dermis resides in the upper dermal layer and contains high levels of young, type III collagens. In the reticular dermis mature, type I collagens are pre-dominant. Scale bar= 100µm. Image= authors own.

1.8   Dermal collagen fibrillogenesis

Collagens I and III of the dermis are proteins with a triple-helical structure and multiple *in vivo* binding partners (Di Lullo et al, 2002). Fibroblasts synthesize pro-collagen molecules that are assembled into triple helices in the rough endoplasmic reticulum then secreted into the surrounding ECM. Once they have been secreted, resident metalloproteinase enzymes cleave pro-peptides present at the N and C terminus of each protein molecule (Mouw et al, 2014-see figure 1.8). Cross-linking between collagen molecules by lysyl oxidases then occurs, which allows higher order assembly of collagen molecules into nano-fibrils and collagen fibre's (Fratzl,

P et al, 1998). Type III collagen is believed to be important in the regulation of type I collagen fibril assembly, and thus the two are commonly found localized together (Liu et al, 1997). AFM (atomic force microscopy) studies have shown that the papillary dermis, where collagen III predominates, is softer than the reticular dermis, where collagen I predominates and thus both of these dermal regions have differences in their biomechanical properties due to the different collagen fibril arrangements (Achterberg et al, 2014)
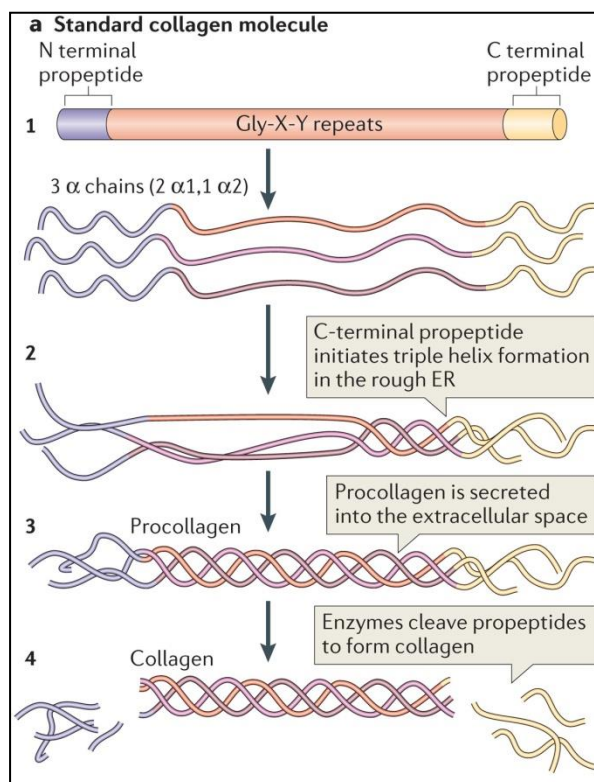
Figure 1.8: Overview of collagen molecule synthesis. Collagen molecules are synthesized in fibroblasts and each individual molecule has both an N and C –terminal pro-peptide (a1). The majority of collagen molecules are made of up glycine-rich repeats, which assist in the assembly of the triple helix formation. The individual collagen alpha chains (depicted here are the 3 alpha chains for collagen I) form triple helices in the rough ER (2) and are then secreted from the cell through vesicles formed in the Golgi (3). Finally, enzymes in the ECM cleave away the N and C-terminal pro-peptides before extra-cellular higher order collagen assembly occurs. (Image from Mouw et al, 2014)

1.9   The dermis houses a prominent vascular network

Unlike the epidermis, the dermis is home to a prominent vascular network, which originates from cutaneous branches of musculoskeletal arteries. Deep in the reticular dermis these artery branches spread to form a vascular plexus, which resides in the reticular dermis, running parallel to the skin's surface. In the superficial papillary dermis, extensions from reticular parent vessels are arranged into smaller arterioles, forming the superficial plexus. This vascular supply provides the cells of the epidermis and dermis with oxygen and nutrients, allowing them to carry out normal metabolism (figure 1.9). (Brehmer-Andersson, E. 2006)
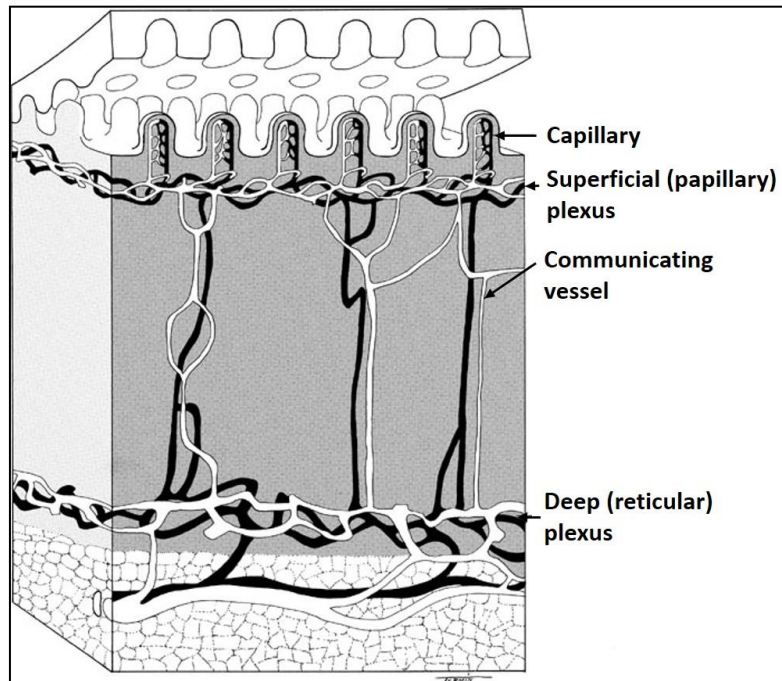
Figure 1.9: Schematic of the dermal vascular network showing how the deep vascular plexus in the reticular dermis is joined to the superficial plexus in the papillary dermis by communicating blood vessels. Further branching of the vessels allows a fine capillary network to reside in the papillary dermis. (Image from Ackerman et al, 2005)

1.10   The Hair Follicle is a key skin appendage

Along with a prominent vascular supply, the dermis also houses one of the key appendages found within all mammalian skin types- hair follicles. These keratin-rich structures provide a thermo-regulatory protective covering that shields the skin from the outer environment (Otberg et al, 2008) and a cross-sectional image of a hair follicle is shown in figure 1.10, which depicts the organ with its auxiliary structures. Together the hair follicle, the arrector pili muscle, sebaceous gland and sebaceous duct are known as a "pilo-sebaceous unit".

Key differences in the structure and organisation of hair follicles are demonstrated between mammalian species, and within organisms themselves, distinct follicle types are situated on different bodily regions. In mice, 8 distinct hair types are present, including those found at the eye lashes, tail, ears, vibrissae (whiskers) and most abundant of all, the pelage (coat hairs). In humans, two distinct follicle populations are present: the highly pigmented terminal hairs found in regions such as the scalp, and the finer, less-pigmented villus hairs found on the face and abdomen (Schneider et al, 2009). Mouse pelage hairs are highly abundant compared to human hairs, and within an anatomical-site matched region, the density of hair follicles within mouse skin can be more than 100 times that of human skin (Mangelsdorf et al, 2014).
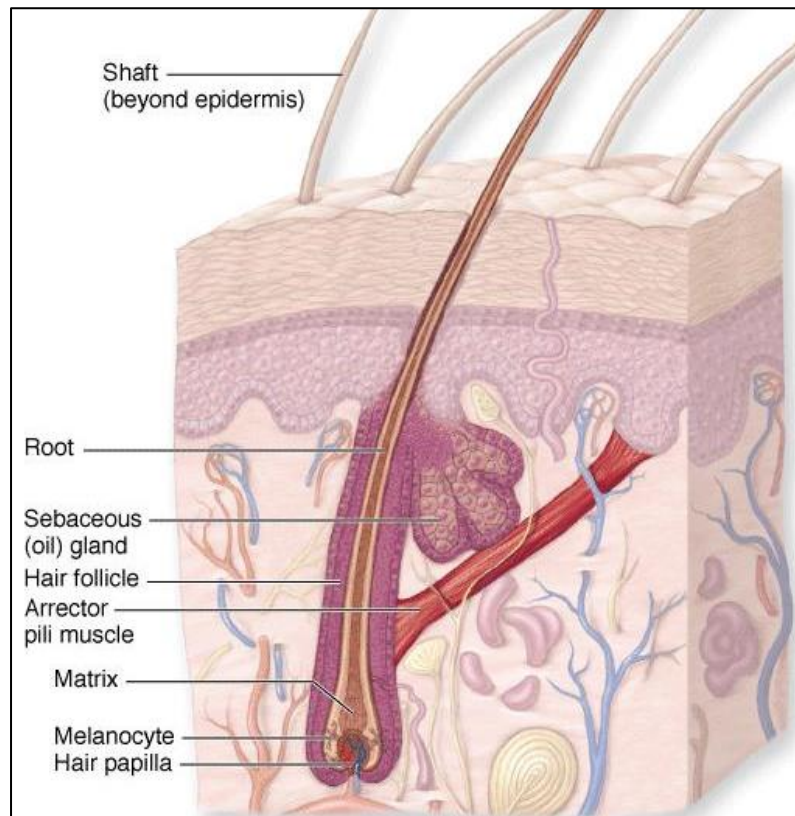
Figure 1.10: Structure of a pilosebaceous unit. The majority of the hair follicle and its auxiliary structures are situated in the dermis, with the most inferior structure being the dermal (hair) papilla. The hair root is surrounded by a protective root sheath (not labelled), which is connected to an adjacent sebaceous gland that secretes sebum (oil) onto the surface of the skin. The arrector pili muscle determines the angular position of the hair next to the skin, and when contracted, the hair shaft stands upwards, allowing air to be trapped between the hairs on the skin which provides insulation to the body. (Image from Mescher, A.L: Junqueira's Basic Histology: Text and Atlas, 12th edition)

1.11 Hair Follicles demonstrate cyclical regeneration that is impacted during physiological ageing

Across all species, the hair follicles are recognised as self-regenerating mini-organs, which undergo a cycle of active growth (anagen), regression (catagen) and rest (telogen) (Schneider et al, 2009). The molecular circuitry that regulates the transitions between the hair follicle cycle (HFC) stages is highly complex, and is dependent on the impact of growth factors and mitogenic pathways such as Wnt signalling, which control stem cell activity within the bulge region. In order for a new HFC to occur, cells within the bulge proliferate and migrate downwards into the hair bulb to initiate growth of a new hair (Fuchs, E. 2009). At each stage of the HFC the follicle takes on a unique structure, making anagen follicles visually distinct from both catagen and telogen follicles. This is depicted in figure 1.11 (Müller-Röver et al, 2001).
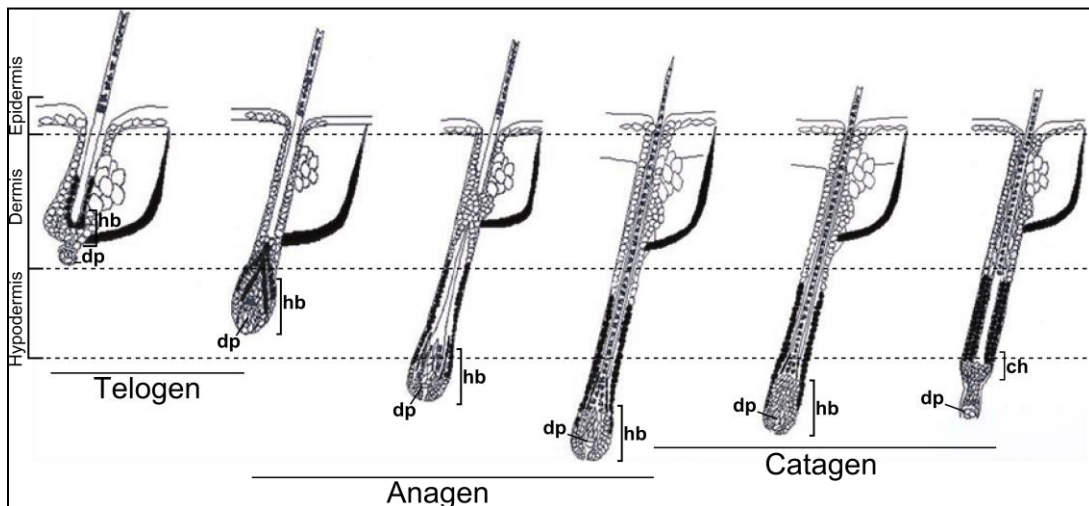
Figure 1.11: The stages in the hair follicle cycle are structurally distinct. A hair follicle in telogen is typically short, contained within the dermal region, and the dermal papilla (dp) is situated below the hair bulb (hb). Once entry into anagen has occurred, the follicle grows in length and extends downwards into the hypodermis, and the dermal papilla is engulfed within the hair bulb. During catagen the follicle regresses upwards back to the dermal region, and separation of the dermal papilla from the resulting club hair (ch) is initiated. (Image adapted from Foitzik et al, 2003)

In post-natal mice the first two HFC's are highly synchronised across the entire body, with the first anagen occurring 1 month after birth and the second anagen 3 months after birth (Paus and Cotsarelis, 1999). Following this, sections of the pelage begin to grow asynchronously in distinct domains across the body, and the initiation of active growth (anagen) in each bodily domain is dependent on BMP signalling factors originating from the dermal environment (Plikus and Chuong, 2008).

Growth of the mouse pelage is impacted by the ageing process, and after 18 months the number of actively cycling, anagen follicles is reduced. The hair follicles spend a greater amount of time resting (in telogen) and hair growth domains become fragmented into smaller regions (Chen et al, 2014). The potential causes of reduced HFC activity with age are numerous, and it has been shown that hair follicle stem cells accumulate chromatin modifications during the ageing process as a result of deterioration in DNA damage repair capacities (Schuler and Rübe, 2013). Additionally the extracellular environment can play a role, as transplanting aged donor mouse skin to a young host restored donor HFC capacity, demonstrating that changes in the extra-follicular environment in the ageing dermal matrix impacts the activity of hair follicles (Chen et al, 2014).

1.12   The hair follicle is a rich resource of distinct stem cell populations

Hair follicles have recently gained attention due to a vastly expanding field of knowledge concerning the presence and behavior of several stem cell pools within the follicle structure (figure 1.12). Stem cells can be found within the hair follicle bulge, above the bulge in

the isthmus, in sebaceous glands and also within the dermal papilla, indicating that the hair follicle can be a rich resource of stem cell activity. Cells of the dermal papilla have recently gained attention due evidence supporting their ability to be re-programmed into induced-pluripotent stem cells, which under varying culture conditions can be directed to form adipogenic, osteogenic and haematopoietic lineages (Driskell et al, 2011). The plasticity of stem cells within the follicle is also demonstrated during skin insults such as in wounding, where stem cells present in the sebaceous glands and hair follicles have been shown to contribute to inter-follicular epidermal repair by stimulating cellular proliferation in order to restore homeostasis (Solanas and Benitah, 2013).
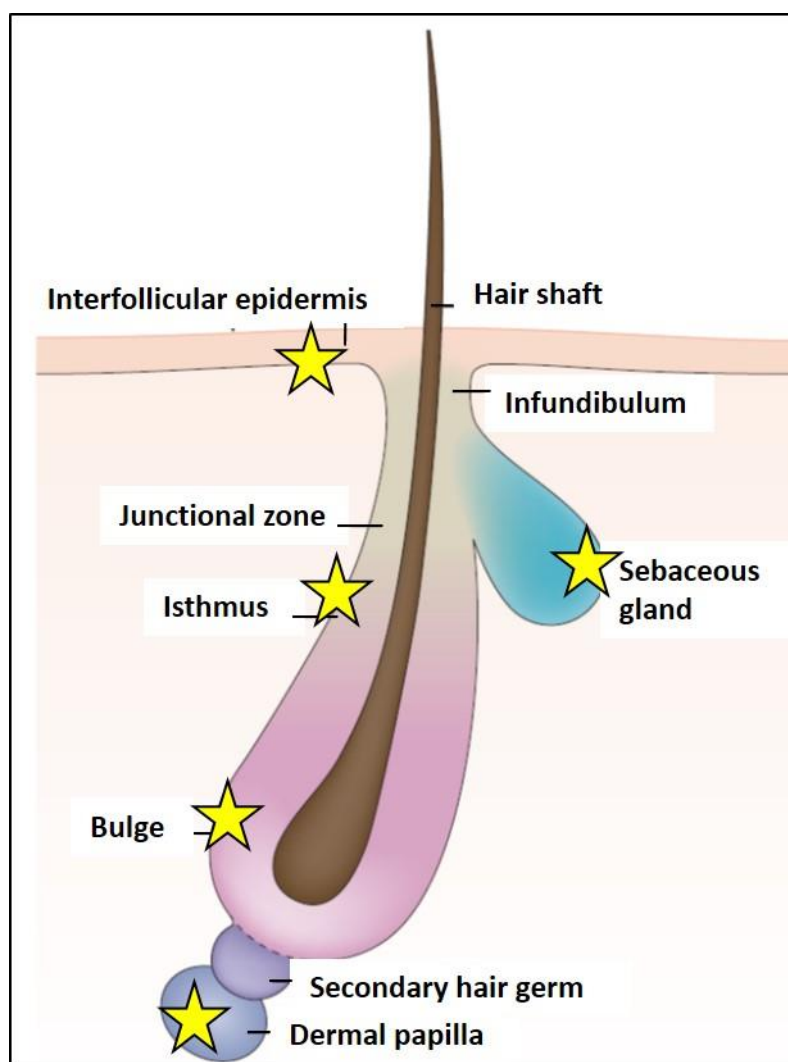
Figure 1.12: Diagram of the stem cell populations in the hair follicle. Unique stem cell pools (depicted by yellow stars) have been identified in the **bulge**, above the bulge in the **isthmus**, in **sebaceous glands**, in the **dermal papilla** as well as in the **inter-follicular epidermis**. The hair follicle is continuous with the inter-follicular epidermis and provides a further layer of protection to the skin barrier (Image from Solanas and Benitah, 2013).

1.13 Skin ageing impacts the epidermis and dermis

Profound morphological and physiological changes occur during ageing of the skin, which have both clinical and cosmetic consequences (Binic et al, 2013). Skin ageing within the dermis comes as a result of age-related changes in the proliferative and metabolic properties of collagen-producing fibroblasts. One of the many contributing factors to decreased fibroblast health in aged skin is due to age-related atrophying of the vascular network within the dermis, which results in a reduced delivery of oxygen and nutrients to cells within the dermis (Mine et al., 2008). A reduction in the number and biosynthetic capacity of fibroblasts leads to a decrease in their secretion of the extracellular matrix proteins type I and type III collagen and elastin, causing atrophying of the dermal matrix (Varani et al., 2008). Additionally, aged fibroblasts secrete Matrix Metalloproteinases (MMPs) that cause collagen degradation and disorganization of the remaining fibrils (Quan et al., 2013). Decreased production and increased degradation of collagen and elastin results in a thinned and wrinkled appearance to the skin and reduces its ability to withstand mechanical stress (Zouboulis and Makrantonaki, 2011). In the epidermis slowing of stem cell activity in the basal layer results in a reduced cellular output, which causes a decline in epidermal turnover. This results in epidermal thinning and a reduction in the efficiency of the epidermal barrier. The aged stratum corneum is less adept to exclude environmental pathogens, resulting in an increased frequency of infections in the skin of the elderly (Rawlings, A.V. 2010).

Changes in the protein component of the basement membrane also occur during skin ageing, making it less able to withstand mechanical stress which, coupled with dermal changes, results in flattening of the dermal-epidermal junction and a reduced surface area for oxygen transport from the vasculature in dermis to the cells within the epidermis (Langton et al, 2016).

1.14 Clinical and cosmetic consequences of skin ageing

The external nature of skin gives it special importance, as the appearance of our body, and especially the facial area, greatly influences individual personal and social identity (Oberg and Tornstam, 1999). However, profound morphological and physiological changes occur during ageing of the skin, which have both clinical and cosmetic consequences (Binic et al, 2013). Cosmetically, the aged skin phenotype is characterized by unsightly changes such as wrinkling, sagging, presence of irregular pigmentations (wrinkling and pigmentary changes depicted in figure 1.13) and telangiectases (visible broken capillaries on the skin surface). Clinically, the consequences of skin ageing can be severe, and skin disorders, like xerosis, pigmentation disorders and neoplastic formations, are one of the main reasons that elderly patients visit their

doctors (St. Sauver et al, 2013). Aside from the pathological issues occurring in ageing skin, the unsightly physical appearance of wrinkles, pigmentary spots and age-associated hair loss can cause serious psychological consequences. The source of many of these issues are due to increased negative connotations associated with old age, leading to societal and cultural pressures to maintain a youthful appearance (Gupta and Gilchrest, 2005). For these reasons many elderly patients suffer decreased self-esteem and poorer social relations as a result of ageing skin (Kligman and Koblenzer, 1997).

Figure 1.13: Visual changes to ageing skin. Pigmentary spots can accumulate around the eye (A, B) and lip regions (C). Wrinkles can also be observed around the eyes (D), lips (E) and in the forehead region (F) (Image from Flament et al, 2015).

1.15   Intrinsic and extrinsic ageing share common and distinct mechanisms

Skin ageing is driven by intrinsic cellular processes and also external environmental insults and therefore both "intrinsic" and "extrinsic" mechanisms contribute to the aged skin phenotype (figure 1.14). The main causative factors in "intrinsic" skin ageing concern the gradual accumulation of cellular damage as a result of normal oxidative metabolism (Naylor et al, 2011). DNA damage accumulates in both ageing fibroblasts and keratinocytes, which

instigates the process of cellular senescence as a result of this genomic instability. Cellular senescence results in cell cycle arrest, thus resulting in a depletion of dermal and epidermal cell populations in the absence of restorative cellular proliferation (Campisi, J, 1998). These processes also occur during, "extrinsic" ageing, but are compounded by additional cellular damage that occurs as a result of external factors within the environment. Air pollution and exposure to ultra-violet (UV) rays from sunlight have been shown to drive skin ageing, but it is commonly accepted that the most potent external driver of skin ageing mechanisms is UV-irradiation (Fisher et al, 2002). UV-rays have such a profound effect on the aged skin phenotype that the term "photoageing" is used to describe sun-exposed skin that can adopt a prematurely aged phenotype due to the damaging effect of these agents (Naylor et al, 2011).
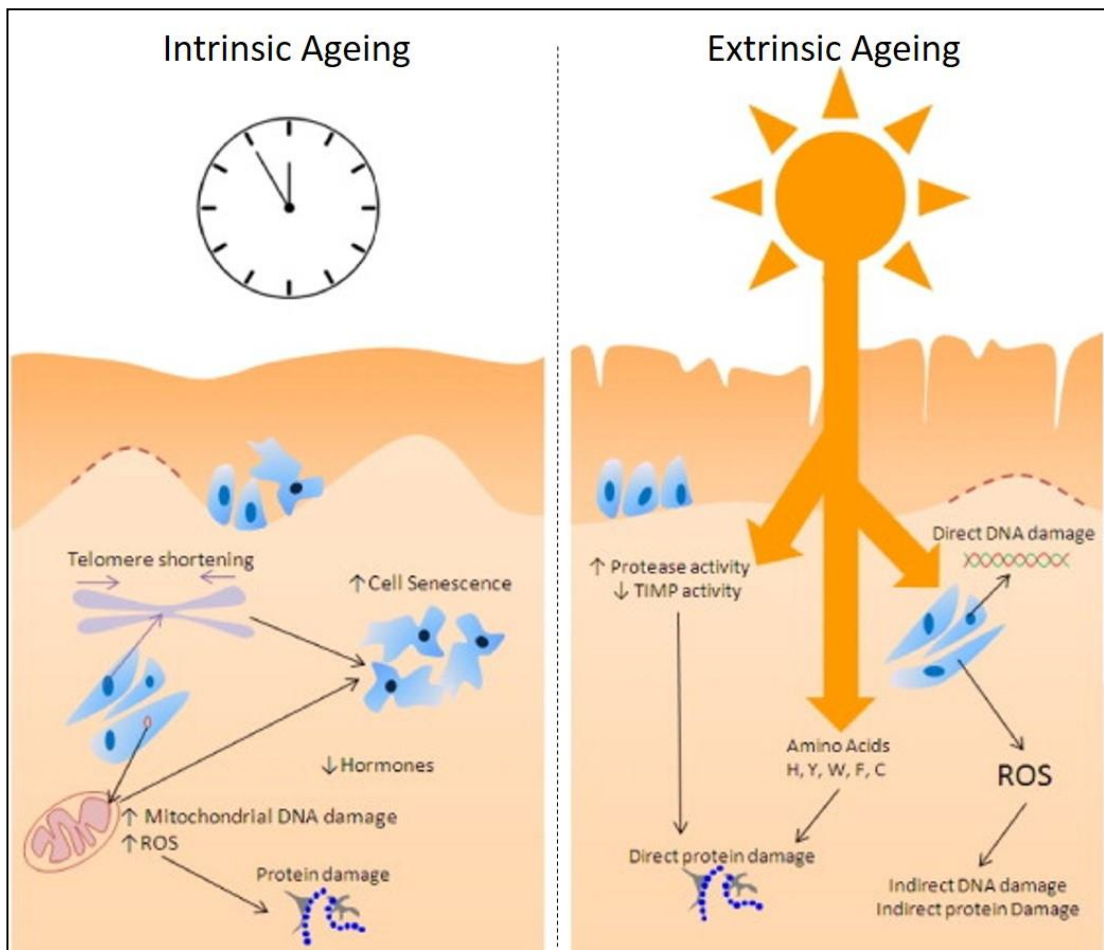
Figure 1.14: Pathomechanisms of intrinsic and extrinsic (photo-ageing). Intrinsic skin ageing (left hand side) is a result of the accumulation of critically short telomeres in fibroblasts and keratinocytes, along with other genomic instabilities, which induces cellular senescence. Extrinsic ageing (right hand side) is primarily caused by the deleterious effects of UV rays from sunlight, which directly damage DNA and protein. Additionally, UV-induced cellular damage stimulates the production of excess ROS, which causes further damage to cellular organelles and genetic material (image from Naylor et al, 2011).

1.16　Lamin proteins: intermediate filaments of a nuclear meshwork

Nuclear lamins are type V intermediate filaments of A-type and B-type that form a stress-resistant network underneath the inner nuclear membrane (Broers et al., 2006). Lamin monomers consist of an N-terminal head domain, a C-terminal globular tail and a central alpha-helical rod domain (structure depicted in figure 1.15) and they are assembled in the nucleus through dimerization, polymerization and higher order assembly (Goldman et al, 2002). B-type lamins (lamin B1 and lamin B2) are generally ubiquitously expressed in human tissues, whereas A-type lamins (lamin A and lamin C) are restricted to differentiated cells (Constantinescu et al, 2006). Lamin B1 and B2 are encoded for by the *LMNB1* and *LMNB2* genes whereas lamin A and lamin C are produced through alternative splicing of the single *LMNA* gene (Dittmer and Misteli, 2011). Lamin A protein is translated as a pre-cursor protein that undergoes several post-translational modifications in order to form mature lamin A, including the enzymatic cleavage of the full length pre-cursor protein (figure 1.16).
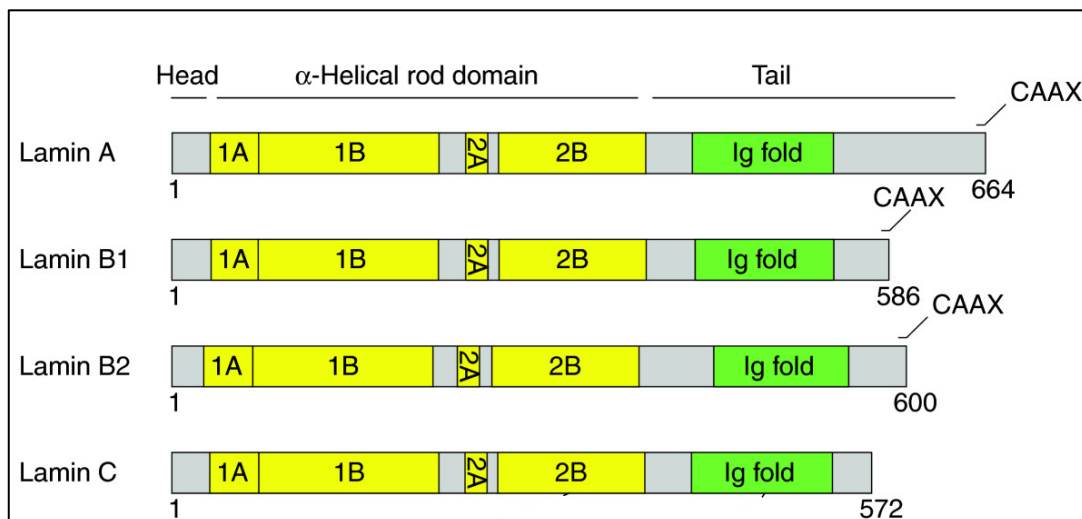
Figure 1.10: Structure of the nuclear lamins showing how the proteins all share a common α-helical rod domain. The tail domain contains a nuclear localization signal, an immunoglobulin domain (green), and a conserved CAAX box, which undergoes farnesylation. Numbers indicate their amino-acid lengths. Arrows point to the presence of the CAAX motif in the carboxy termina of lamin A, lamin B1 and lamin B2 (Taken from Ditmer and Misteli, 2011).
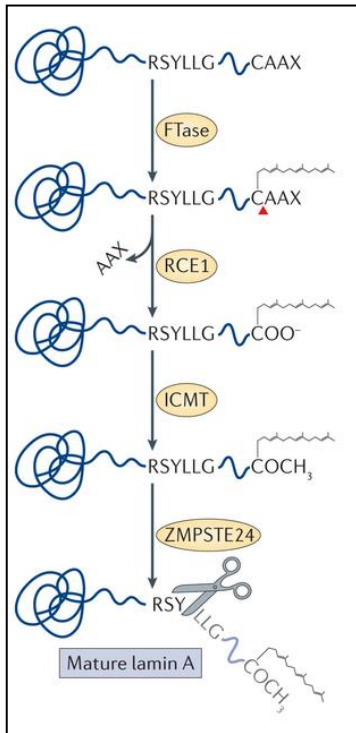
Figure 1.11: Pre lamin A processing requires several stages: Maturation of lamin A from the precursor pre-lamin A involves firstly farnesylation by farnesyl transferase (FTase), then RAS-converting CAAX endopeptidase 1 (RCE1)-mediated proteolysis. Next the cleaved protein is methylated by an isoprenylcysteine carboxymethyltransferase enzyme (ICMT). Finally the ZMPSTE24 protease cleaves the carboxy-terminal residues from prelamin A to produce mature lamin A (Image from Wang and Casey, 2016)

Aberrant lamin A processing, which allows the nuclear accumulation of pre-lamin A intermediates, is the cause of several age-related degenerative diseases known as laminopathies (Broers et al, 2006). The location of the nuclear lamina, and the spectrum of diseases that are a result of mutations in the *LMNA* gene suggests a multifunctional role for A-type lamin proteins in both genetic and structural aspects of cell physiology, including tumour progression, control of nuclear architecture, regulation of gene expression, senescence, apoptosis and chromatin organization and segregation (Foster et al, 2010; Ho and Lammerding 2012).

B-type lamins are thought to have crucial functions in DNA replication, chromatin organisation and gene expression at the nuclear periphery (Ho and Lammerding, 2012). Genetic ablation of either *LMNB1* or *LMNB2* in HeLa cells leads to growth arrest and apoptosis, leading to the theory that B-type lamins are essential for cellular growth and division (Harborth et al, 2001). In mouse embryonic stem cells (mESC's) however, this concept has been refuted, as mESCs without B-type lamins or both A and B-type lamins grow and differentiate normally (Kim et al, 2011). *Lmnb1*^{-/-} and *Lmnb2*^{-/-} knockout mice are unable to survive after birth however, indicating that both B-type lamins are essential for post-natal life. *Lmnb1*^{-/-} knockouts showed severe defects in brain, lung and bone tissues, whereas the defects in the *Lmnb2*^{-/-} knockouts were restricted to the brain (Vergnes et al, 2004). These findings highlight that although

dispensable in embryonic cells, B-type lamins clearly have important roles in the building of tissues and particularly in the brain (Yang et al, 2011a).

1.17   Role of lamins in skin development and homeostasis

As rapidly dividing cells contributing to a self-renewing epithelium, one would think that the keratinocytes of the basal epidermal layer would require normal levels of B-type lamins in order to fulfil their function, but this has been disproved in conditional knock-out mice where both lamin B1 and lamin B2 expression is absent from the epidermis (*Lmnb1*$^{-/-}$ *Lmnb2*$^{-/-}$). The epidermis and hair follicles of *Lmnb1*$^{-/-}$ *Lmnb2*$^{-/-}$ mice developed normally and showed normal levels of proliferation. This demonstrates that for the epidermis at least, B-type lamins are not essential, and raises questions about their dispensability in other tissues (Yang et al, 2011b).

Similar epidermal-specific genetic knock-out studies have been performed in order to deduce the importance of the A-type lamins in epidermal development. Epidermal *Lmna*$^{-/-}$ mice present with abnormalities in the form of a thickened epidermis, thinner dermis and reduced hair follicle density, suggesting that unlike B-type, proper A-type lamin levels are essential for normal epidermal development where they allow cells to differentiate into the lineages needed for hair follicle and inter-follicular epidermis formation (Wang et al, 2008). As a more severe phenotype is demonstrated by epidermal-specific *Lmna*$^{-/-}$ knockouts compared to *Lmnb1*$^{-/-}$ *Lmnb2*$^{-/-}$ knockouts, this suggests that A-type lamins play a more pivotal role in epidermal development.

Complete genetic ablation of both A and B-type lamins from the epidermis of developing mice presents with the most dramatic phenotype at all (see figure 1.17). The absence of lamins in the epidermis causes severe abnormalities, including ichthyosis (dry, thickened epidermis), complete loss of epidermal barrier function and abnormal accumulation of endoplasmic reticulum components in keratinocyte nuclei. The mice die a few days after birth from severe dehydration (Jung et al, 2014). The more dramatic phenotype seen in the combined epidermal-specific A and B-type lamin knock-out compared to the separate A-type or B-type lamin knockouts suggests that although not essential when removed in isolation, the absence of B-type lamins in the presence of abolished A-type lamin expression exacerbates poor skin development and maintenance, and the resultant phenotype implies both a lack of cellular proliferation and differentiation mechanisms needed for normal epidermal barrier formation.
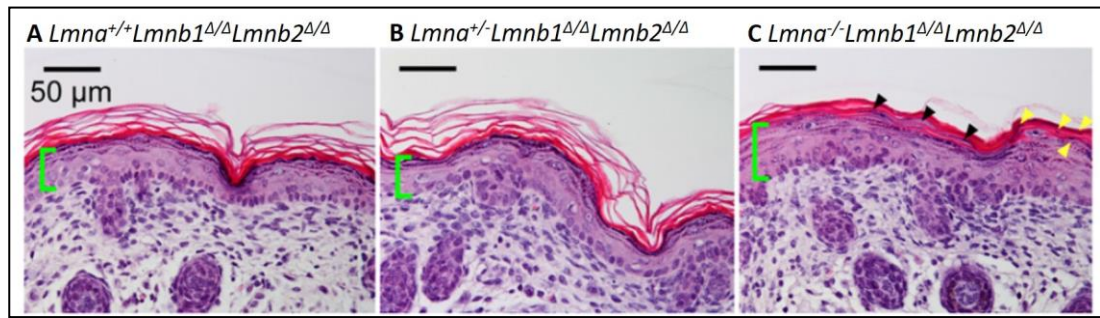
Figure 1.17: Complete ablation of lamin expression in the epidermis results in a dramatic phenotype. Histological presentation of skin as shown by haematoxylin and eosin staining in mice with homozygous expression of A-type lamins, and no epidermal B-type lamins (A-Lmna$^{+/+}$Lmnb1$^{\Delta/\Delta}$Lmnb2$^{\Delta/\Delta}$), mice with heterozygous expression of A-type lamins and no epidermal B-type lamins (B- Lmna$^{+/-}$Lmnb1$^{\Delta/\Delta}$Lmnb2$^{\Delta/\Delta}$) and mice with no A-type lamins and epidermal-specific knock-out of B-type lamins (C- Lmna$^{-/-}$Lmnb1$^{\Delta/\Delta}$Lmnb2$^{\Delta/\Delta}$). Epidermis and dermis in the absence of B-type lamins only (A and B) shows no obvious phenotype whereas in the absence of all lamins (C), epidermal hyperplasia is present (green bracket-C). Additionally, the stratum granulosum and stratum corneum were disorganised (black arrowheads) and nuclei were present in the stratum corneum (yellow arrowheads). Image from Jung et al, 2014.

1.18 Lamins modulate cellular senescence programmes

Cellular senescence is a state of permanent cell cycle arrest that occurs as a result of DNA lesions and critically short telomeres. This nuclear instability triggers a permanent DNA damage response, preventing subsequent cell cycle progression. Cellular senescence can be induced in cells by multiple rounds of replication, oncogene expression and DNA damage caused by ionising radiation (d'Adda di Fagagna et al, 2003).

Changes in the shape of the nuclear lamina are shown in senescent cells and cells that undergo premature ageing due to lamin protein mutations (Righolt et al, 2011). Additionally, several recent publications have shown that levels of the nuclear lamina component lamin B1 are decreased in cells induced to senescence by a variety of mechanisms (Freund et al, 2012). Dreesen et al (2013) have further shown that reduced lamin B1 is a hallmark of cellular senescence, but is not a cause. The relevance of having appropriate levels of both nuclear A-type and B-type lamins has also been demonstrated by the fact that lamin B1 overexpression in cells depleted of lamin A results in telomere dysfunction, DNA damage accumulation and premature entry into a senescent state. These studies implicate that lamin expression can be modulated by senescence effector programmes and this may be due to the fact that lamins have roles in both stress signaling and cell cycle control (Hutchison, C.J. 2012).

1.19   Laminopathies and lamins in normal skin ageing

Laminopathies impact several tissues within the body and can result from a variety of mutations in the *LMNA* gene. The premature ageing disease Hutchison-Gilford Progeria Syndrome (HGPS) is a result of a single point mutation in exon 11 of the *LMNA* gene. This mutation creates the appearance of a cryptic splice site, which leads to the elimination of a 50 amino acid residue sequence within the lamin A tail. This truncated form of lamin A is called progerin. Progerin lacks the cleavage site recognised by ZMPSTE24 and in the absence of normal processing, progerin is permanently farnesylated and thus anchored at the inner nuclear membrane (INM). Although lamins A and C are products of the same gene, lamin C formation remains unaffected as, unlike lamin A, it does not require complex processing for normal sub-nuclear localisation (Burke and Stewart, 2013).

Abnormal accumulation of progerin at the INM in cells is cytotoxic and drives the premature ageing phenotype in this disease that results in alopecia, short stature and early death from cardiovascular disease (De Sandre-Giovannali et al, 2003). Skin fibroblasts isolated from Progeria patients show chromosomal abnormalities, reduced proliferation in culture compared to WT fibroblasts and tend to senesce prematurely due to accumulation of irreparable levels of DNA damage (Burtner and Kennedy, 2010). Further reports show that the accumulation of cellular progerin increases sensitivity to oxidative stress leading to the formation of DNA lesions that slow the cell cycle (Richards et al, 2011). Progerin has also been found to increase in level in the skin of subjects during healthy ageing (Mc Clintock et al, 2007). Studies on fibroblasts isolated from elderly individuals show that the accumulation of progerin was associated with decreased heterochromatin, shortened telomeres and a slower cell cycle (Scaffidi and Misteli, 2006). These observations show that normal lamin A processing becomes altered in ageing fibroblasts and implicate lamin A in proliferative changes to skin cells in both normal physiological ageing and diseases associated with premature ageing syndromes.

Restrictive Dermopathy (RD) is a skin-specific laminopathy, which is caused by either a splicing mutation in exon 11 of *LMNA* (like in HGPS) or a base-pair insertion in ZMPSTE24. The mutation in ZMPSTE24 leads to the production of a truncated form of the enzyme that is highly unlikely to be an active protease, thus preventing its wild type activity (Navarro et al, 2004). Although the two predisposing mutations are in different genes, they both result in loss of normal cellular levels of mature lamin A due to an inhibition of proper lamin A processing. Instead, accumulation of truncated lamin A causes an embryonic lethal disease presenting with a severe skin phenotype showing dermal thinning, alopecia and epidermal hyperkeratosis. Of interest, many of these maladies are shared by the epidermal *Lmna*^{-/-} knockout mice (Wang et

al, 2008). The phenotype is severe, and new-borns that survive normally die just a few weeks after birth from other anomalies such as respiratory defects due to pulmonary hyperplasia (Lu et al, 2013). The phenotype of RD indicates that altered levels of mature lamin A and the accumulation of truncated lamin A during foetal development drastically impacts normal skin development along with other tissues found in the lungs.

Despite a plethora of *in vitro* work looking at the roles of lamins in cellular senescence and physiological ageing (Dreesen et al, 2013; Hutchison et al, 2012; Freund et al, 2013), studies on changes in the nuclear lamina in ageing skin *in vivo* are rare. In a small study, Dreesen et al (2013) have shown that lamin B1 protein decreases in intrinsically aged 60y human skin along with a decline in cell proliferation and the expression of LAP2α (a polypeptide associated with the nuclear lamina) compared to 1yr old skin (see figure 1.18) . In this study epidermal lamin A/C levels were constant along with the keratinocyte differentiation marker K10 in the aged skin, implicating an association of decreased epidermal lamin B1 levels with age but not lamin A/C. Lamin B1 has also been shown to decline in the fat body organ of aged *Drosophila melanogaster*, here lamin B1 loss was associated with an increased inflammatory response (Chen et al. 2014).
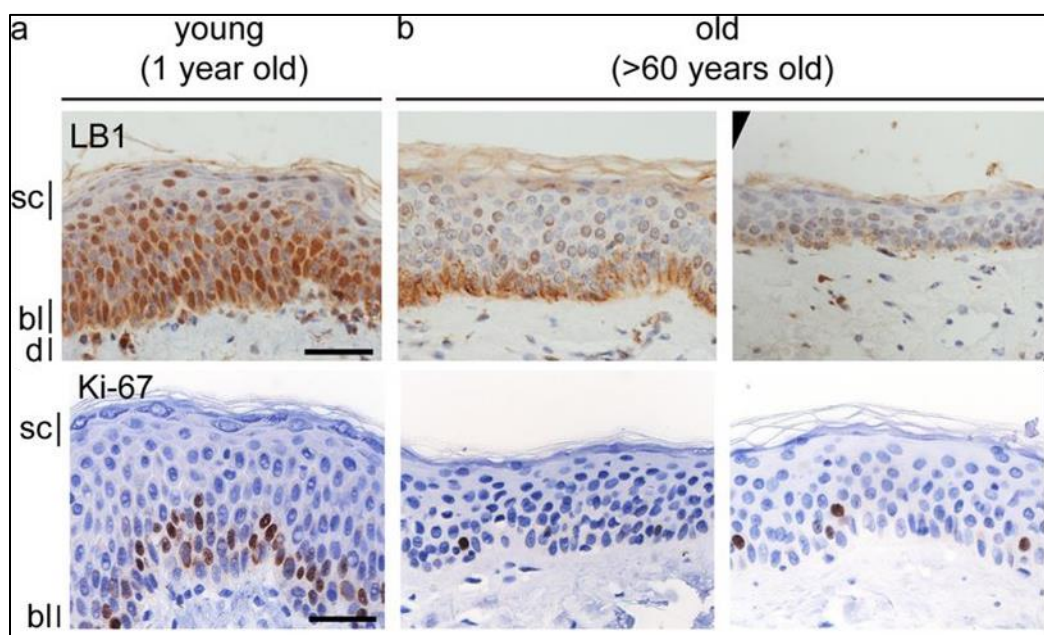
Figure 1.18: Decreased lamin B1 and cellular proliferation in the epidermis of aged human skin. Young human epidermis had strong lamin B1 (LB1) staining and many cells positive for Ki-67 (cellular proliferation). In contrast, aged skin (b) had dramatically reduced lamin B1 and cellular proliferation levels. bl= basal layer, d= dermis, sc= stratum corneum. Scale bar= 50 μm. Image taken from Dreesen et al, 2013.

1.20   Role of lamins in oxidative defence

Reactive Oxygen Species (ROS) are small, short-lived molecules that at normal levels, regulate cellular proliferation, differentiation, gene-expression and migration. However, abnormally high levels of ROS are associated with age-related protein and genome damage, cellular death and senescence (Callaghan and Wilhelm, 2008). Both intrinsic cellular ageing and extrinsic photo-ageing of the skin have been shown to be associated with increased (ROS), which in excess contribute to cellular ageing by causing protein oxidation, telomere shortening and DNA damage (Sieprath et al, 2012).

Maintenance of normal lamin A levels has been shown to be important in cellular ROS defence mechanisms. Silenced *LMNA* and *ZMPSTE24* human cells both have elevated basal levels of ROS compared to controls and both cell types show increased levels of ROS detoxifying enzymes such as SOD3 (superoxide dismutase 3)(Sieprath et al, 2015). Under identical levels of oxidative insult, both cell lines were less able to tolerate oxidative insult in comparison to control cells with normal A-type lamin expression. During exposure to oxidative stress, mutant *LMNA* fibroblasts underwent apoptosis whereas the fibroblasts that accumulated farnesylated pre-lamin A due to the *ZMPSTE24* silencing became prematurely senescent (Sieprath et al, 2015).

The bifurcation in cellular response shown in *LMNA*^{-/-} and *ZMPSTE24*^{-/-} cells could be due to another identified role for lamin A during oxidative insult. The C-terminus of mammalian lamin A contains 3 unique, highly conserved cysteine residues, and it was shown that di-sulphide bond formation at these residues can occur under oxidising conditions. Removal of these residues resulted in premature senescence under oxidative stress, leading to the theory that lamin A is able to chelate excess ROS in human dermal fibroblasts (HDF's) undergoing oxidative insult. This mechanism is thought to be unrelated to disease causing mutations to *LMNA* however, as HDF's expressing progerin showed control levels of ROS tolerance in comparison to cells where the cysteine residues were removed. The authors concluded that inter and intra-molecular di-sulphide bond formation at these specific cysteine residues could allow lamin A to behave as a ROS "sink", thus protecting the cell from excessive genetic and protein damage and prolonging its fitness (Pekovic et al, 2011). It thus follows that the presence of these cysteine residues in the *ZMPSTE*^{-/-} cells allowed them to tolerate more ROS in comparison to the *LMNA*^{-/-} cells where they were absent. This tolerance could explain why oxidative insult directed a senescent cell fate in *ZMPSTE*^{-/-} cells whereas the more ROS-sensitive *LMNA*^{-/-} cells underwent apoptosis (Sieprath et al, 2015).

In addition to the studies looking at A-type lamins and ROS, several authors have deduced a link between B-type lamins, ROS and cell cycle control. ROS levels are known to increase as cells progress through the cell cycle and anti-oxidant treatment can induce cell cycle arrest in late G1 (Verbon et al, 2012). Furthermore, modest increases in ROS from pro-oxidant treatment increase the proliferation rates of cells in culture and whole organisms (Shimi and Goldman, 2014). The presence of cellular ROS is therefore crucial for cell cycle progression. Shimi et al (2011) uncovered a role for lamin B1 in this process by showing that silencing of lamin B1 promoted cell cycle arrest via p53 signalling, which was accompanied by a decrease in mitochondrial ROS levels. By re-introducing small levels of ROS, cell cycle progression occurred, therefore showing a link between lamin B1 expression, cell division and ROS. A correlation between lamin B1 levels and ROS was also shown by Barascu et al (2012), where treatment of fibroblasts with excess ROS induced an increase in expression of lamin B1, which was directly linked to an induction of the p38-MAPK stress-induced signalling pathway. These two findings implicate lamin B1 as a mediator of normal redox balance through two independent pathways, cell cycle control and stress signalling and implicate lamin B1 in the maintenance of cellular fitness during oxidative insult (Hutchison, C, 2012). As oxidative insult is a key modulator of skin ageing, and photo-ageing in particular, uncovering whether lamin proteins play a role in oxidative defence in the skin is an important future step in this research.

1.21 Lamins form part of the LINC complex which tethers the nucleus to the cytoskeleton

In addition to their roles as modulators of the cell cycle, senescence programmes and redox balance, the nuclear lamins are important structural components of the LINC (linker of nucleoskeleton and cytoskeleton) complex, which connects the nucleus to the cytoskeleton via a protein structure that spans the nuclear envelope (figure 1.19). An intact nuclear lamina is important for cytoskeletal organization, and cells lacking A-type lamins show defective motility due to the presence of a disorganized cytoskeleton as a result of disruptions of the LINC network (Ho and Lammerding, 2012). Furthermore, the LINC complex is a sensor of mechanical force, and in response to cellular tension placed on nesprin proteins, lamin A/C is recruited at the nuclear envelope in order to induce nuclear stiffening in response to this force (Guilluy et al, 2014).

Studies have also shown that lamins are important for the anchoring of other LINC complex components such emerin (Vaughan et al, 2001) and SUN1 (Chen et al, 2012) at the nuclear membrane. In HeLa cells without lamin A, emerin accumulated abnormally in the endoplasmic reticulum and lamin C was also mislocalised within cells. In *Lmna* null mice, SUN1

accumulated in the golgi of cells and surprisingly, deletion of SUN1 in the *Lmna* null background resulted in partial rescue of the premature ageing phenotype displayed by these mice. This showed that the mis-localisation of SUN1 in the golgi could be involved in the cellular pathogenesis mechanism observed in diseases resulting from mutations in the *LMNA* gene- like the autosomal dominant form of Emery-Dreifuss Muscular Dystrophy (AD-EDMD). This report further showed that properly localized components of LINC is crucial for cellular fitness.
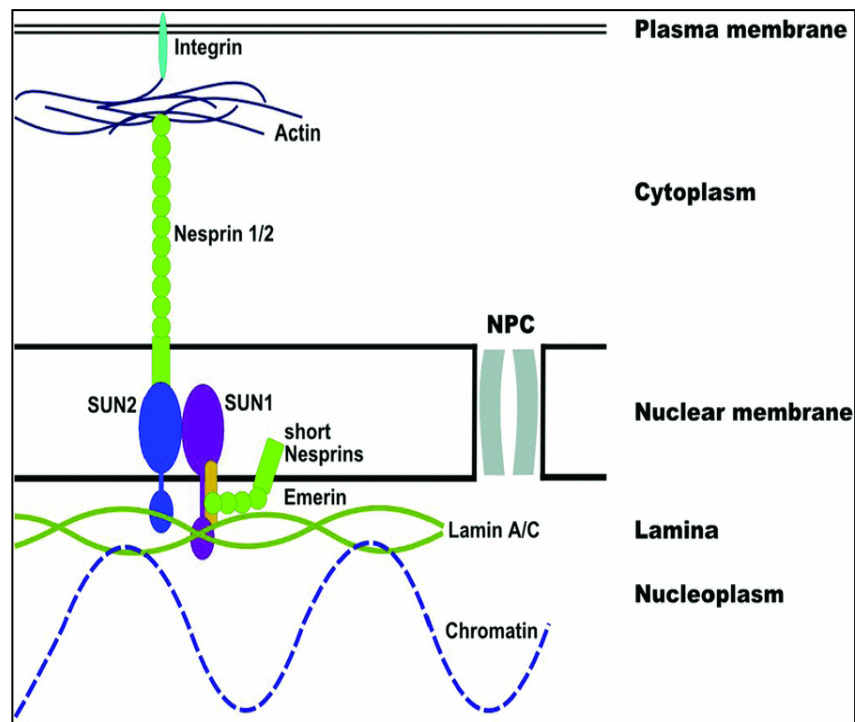
Figure 1.12: The lamina forms part of the LINC complex which tethers the nucleus to the cytoskeleton. Nuclear lamins (B-type lamins not shown in this diagram but also present) interact with chromatin (nuclear material) in the nucleoplasm and also the structural complex that spans the nuclear membrane consisting of **emerin**, **nesprins** and **SUN** proteins. Nesprins link this complex to cytoskeletal actin located in the cytoplasm, and in this way, the LINC complex forms a bridge from the nucleus to the cytoskeleton (image from Meinke et al, 2011).

1.22 The Hippo Pathway is a crucial modulator of tissue development and homeostasis

The Hippo kinase signaling pathway is a highly conserved signaling pathway that controls cell growth, homeostasis, apoptosis, differentiation and senescence (Lo Sardo et al, 2014). The pathway was originally identified in *Drosophila*, where mutations in its component kinases resulted in an overgrown phenotype (figure 1.20). The core signaling components are conserved in mammals and their final targets are the transcriptional co-activator Yes-associated protein (YAP1) and Transcriptional co-activator with a PDZ-binding motif (TAZ), which are protein homologs with 46% amino-acid sequence identity (Kodaka and Hata, 2015) (Core kinase cascade depicted in figure 1.21).

Along with normal roles in cellular physiology, the Hippo pathway effector YAP1 has been identified as an oncogene. Many human cancers show overexpression or hyper-activation of YAP1 (Wang et al, 2013; Hayashi et al, 2015; see Lo Sardo et al, 2014 for additional references). Furthermore, in mouse, overexpression of YAP1 in the liver resulted in an overgrown phenotype which eventually lead to development of hepatocellular carcinoma (Camargo et al, 2007).
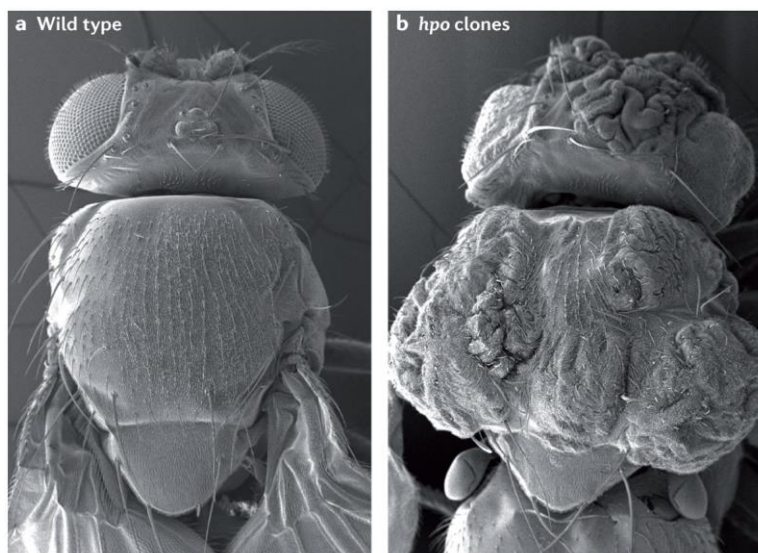
Figure 1.20: Mutations in the gene encoding the core kinase Hpo (hpo gene- MST1/2 in mammals) results in cellular overgrowth in Drosophila. Scanning electron micrographs of a wild-type fruitfly (a) and a fruitfly with patches of cells that are homozygous mutant for the Hippo (hpo) gene (b) are shown. The hpo-mutant fly exhibits an overgrown phenotype, shown by large clumps of cells forming on the body (Image from Johnson and Halder, 2014).
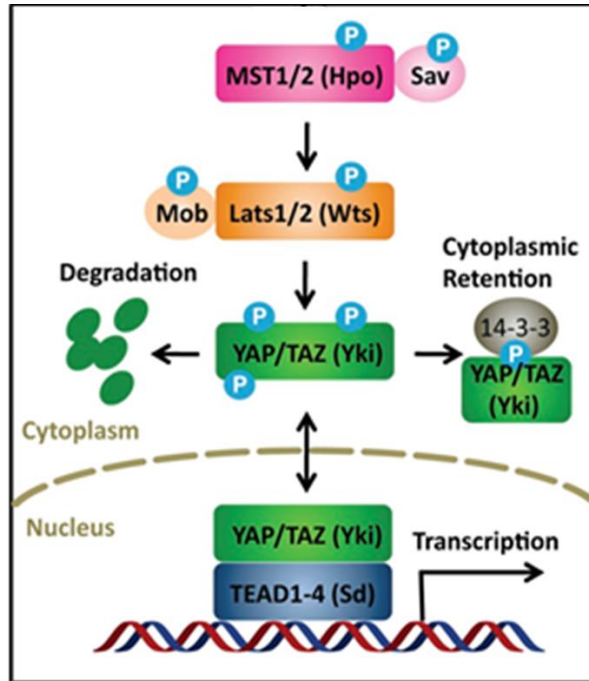
Figure 1.21: Core elements of the Hippo kinase cascade in vertebrates. Following upstream signals, MST1/2 phosphorylates Sav, Lats1/2, and Mob. Lats1/2 then phosphorylates the transcription factor YAP/TAZ. Phosphorylated YAP/TAZ interacts with 14-3-3, which results in cytoplasmic retention and subsequent degradation, thus preventing activation of downstream target genes. In the absence of phosphorylation, YAP/TAZ enter nuclei and induce gene transcription by interacting with the TEAD family of transcription factors. Drosophila orthologs for these core components are shown in brackets. (Image from Yu and Guan 2013).

1.23   Hippo pathway regulators

Many up-stream regulators modulate Hippo, including cell junction proteins, G-protein-coupled receptor signaling components and proteins that dictate cell polarity. Cell junction and cell polarity proteins work together to maintain the normal structure of epithelia, and organize the cytoskeleton and position of the nucleus. One notable complex that modulates Hippo activity is the Kibra complex, which is located at the apical surface of epithelial cells. This complex acts upstream of the core Hippo kinase cascade and negatively regulates YAP1 by cytoplasmic retention (Genevet et al, 2010) (see figure 1.22). Additionally, Hippo regulators can be found in tight junctions and adherens junctions (Lo Sardo et al, 2014).
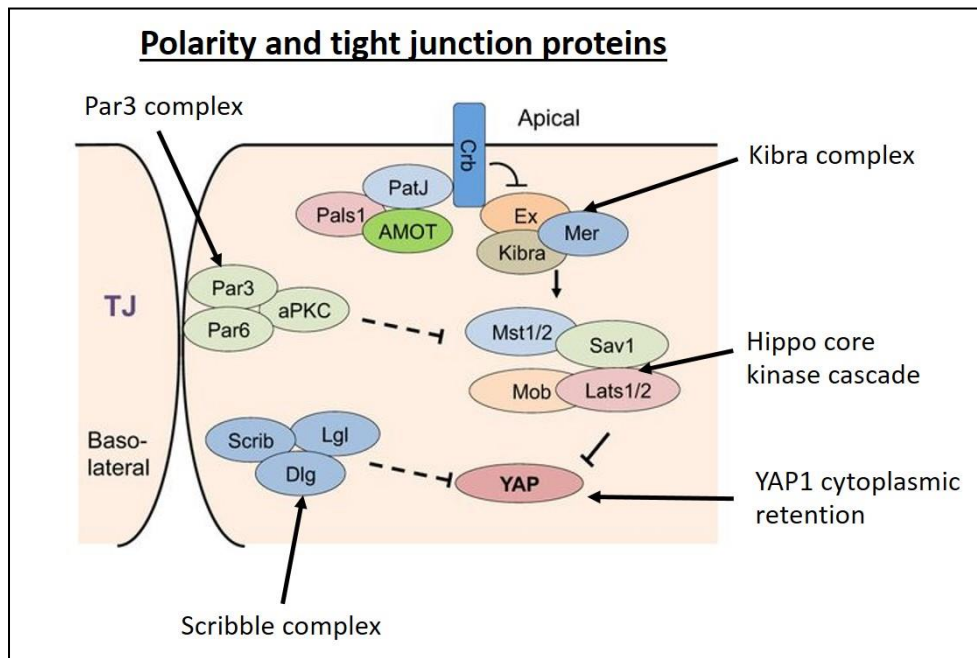
Figure 1.22: Polarity and tight-junction protein complexes negatively regulate YAP1 activity. The Kibra complex at the apical surface of the cell, the **Par3** complex at tight junction (TJ) cellular adhesions and the **Scribble** complex at the baso-lateral surface of the cell are all modulators of YAP1 activity. In this way the proteins that control tissue architecture contribute to the activity of YAP1, thus allowing tissue homeostasis to be maintained. This is particularly important in the maintenance of epithelia. (Image from Kim and Gumbiner, 2015).

1.24   The Hippo Pathway is a mechano-sensory effector

Mechanical cues are also crucial in the regulation of YAP1 activity, and changes to the properties of the cell culture substrate can modulate the activity of the Hippo pathway. Dupont et al, (2011) have shown that culture on stiff substrates drove nuclear localisation of YAP1 whereas culture on soft substrates allowed YAP1 to be retained in the cytoplasm. Furthermore, cell density is an important modulator of YAP1 localisation, and cells cultured at low cell density, where cells are flattened and spread out, show nuclear localization of YAP1. When cells are at high cell density, and a tightly packed together, YAP1 is predominantly localized to the cytoplasm (Yu and Guan, 2013). In this way, the hippo pathway behaves as an extra-cellular "sensor" and cues from the surrounding tissue microenvironment direct cell fate through the cellular localization of YAP1. (Aragona et al, 2013; Wada et al, 2011) (Piccolo et al, 2014- see figure 1.23).
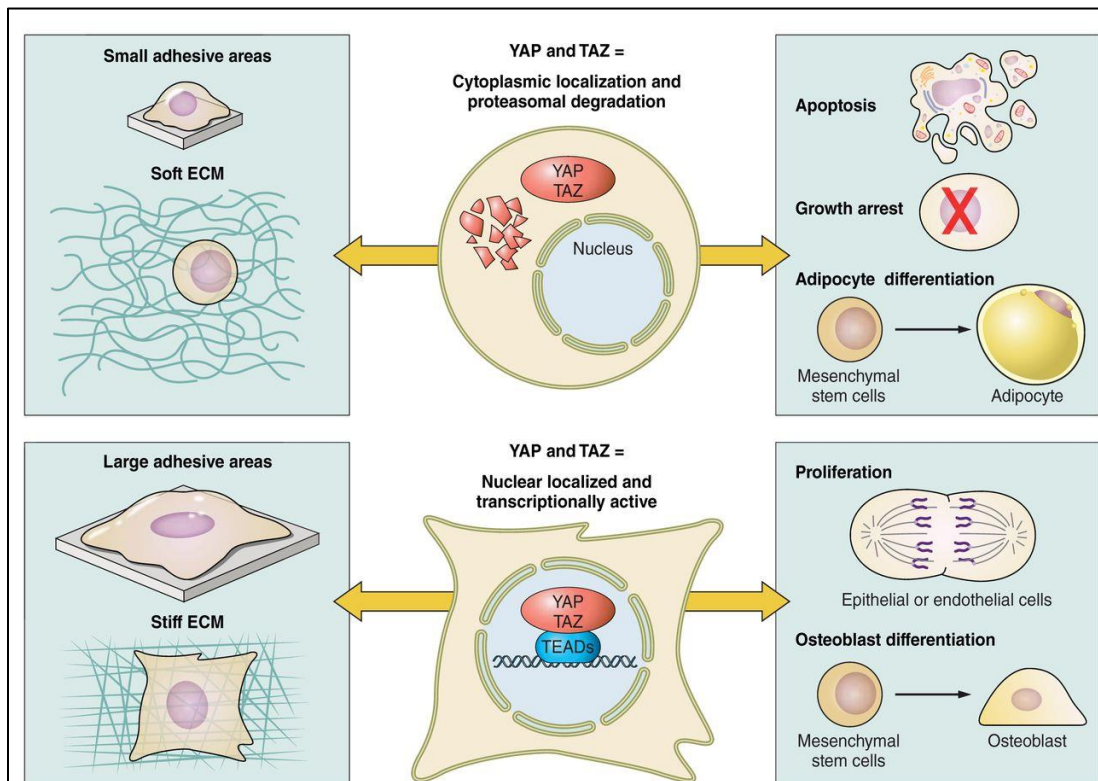
Figure 1.13: Extra-cellular mechanical cues drive YAP1 localization and impact cell fate: In the presence of a small adhesive area or a soft ECM, YAP1 is sequestered in the cytoplasm and is targeted for degradation. This allows apoptosis pathways to be effected and also the formation of soft tissue components like adipocytes. Conversely, if a cell is subjected to a large adhesive area of a stiff ECM environment, YAP1 translocates to the nucleus and induces transcription of target genes that control proliferation and formation of stiff tissues like bone. (Image from Piccolo et al, 2014.)

Both the mechano-sensory and cell-density sensing properties of YAP1 are thought to be modulated via the actin cytoskeleton, and studies have shown that actin cytoskeleton modulators, like Rho GTPase, can affect the localization of YAP1 independently of the core, phosphorylation dependent signaling cascade (Dupont et al, 2011). In line with this, cellular detachment from the ECM, which causes actin cytoskeletal re-arrangements, results in activation of the Hippo pathway and sequestration of YAP1 in the cytoplasm, ultimately resulting in its degradation. Detachment-induced YAP inactivation is required for anoikis, which is a form of apoptosis resulting from cell-ECM detachment. This mechanism forms part of the underlying biology of tumour metastasis, as transformed cells which are resistant to anoikis present with growth-maintaining nuclear YAP1, thus allowing them to disperse to various anatomic sites within the body where they can form secondary tumours (Zhao et al, 2012).

1.25   YAP1 plays crucial roles in epidermal homeostasis and wound healing

The epidermis is a self-renewing epithelial sheet that depends on a careful balance of proliferative and differentiative cues to maintain homeostasis and given that control of both stem cell proliferation and differentiation are crucial aspects of epidermal biology, it is unsurprising that the Hippo pathway has been shown to play a role in epidermal homeostasis in a body of work completed in mice.

Key publications from the Camargo and Fuchs labs have used genetic studies to determine how YAP1, the hippo pathway effector, contributes to epidermal biology. The Camargo lab used Cre-Lox technology to generate epidermal-specific YAP1 knock-out mice. An aberrant phenotype was the result, with thin, fragile, underdeveloped skin showing complete loss of barrier function. In addition, the mouse mutants showed cellular loss in the epidermis, particularly within the basal layer. Importantly, existing basal cells had lost their normal columnar morphology, and exhibited pronounced cellular flattening. Staining of the epidermis with proliferation markers indicated reduced basal keratinocyte division compared to WT mice. Finally, the mutant skin showed loss of Loricrin expression in the outer epidermal layers, which indicated that the barrier function was compromised (Schlegelmilch et al, 2011-see Figure 1.24).
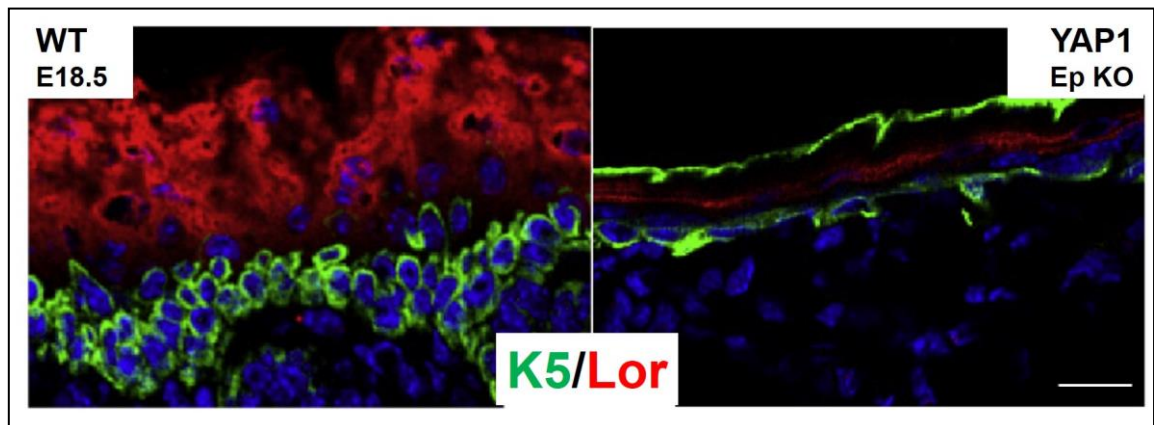
Figure 1.14:YAP1 is crucial for epidermal development in mouse. The figure depicts staining in wild type E18.5 mouse skin and epidermal-specific YAP1 knock-out mice (YAP1 deletion under control of K14 promoter-YAP1 Ep KO). In the WT skin, the basal epidermal keratinocyte marker K5 (green) is abundant, and the mice have a thick stratum corneum, depicted by loricrin expression (red). In the knock-out mice the epidermis is much thinner, and both K5 and loricrin expression are dramatically reduced. Image from Schlegelmilch et al, 2011.

Zhang et al, (2011- Fuchs lab) generated transgenic mice that expressed a mutated form of YAP1 protein (S127A YAP1) under the control of the K14 promoter. The resulting mutation ablated the YAP1 phosphorylation sites needed for cytoplasmic retention, causing abnormal nuclear YAP1 accumulation in basal keratinocytes. This caused a hyper-thickened

epidermis to form with abnormal hair follicles. Cells isolated from the epidermis and cultured *in vivo* divided rapidly and showed reduced levels of both differentiation and apoptosis cues compared to WT keratinocytes. Altogether the paper showed, like in Schlegelmilch et al, 2011, that YAP1 controlled epidermal cell proliferation. Furthermore, the results indicated that sequestration of YAP1 into the cytoplasm was crucial for proliferation to cease and for differentiation to occur so that a normal epidermis could be formed. Together, these two studies show that proper YAP1 levels and sub-cellular localisation are crucial in the balance between proliferation and differentiation in epidermal stem and progenitor cells in developing mice.

The requirement for normal Hippo Pathway action is also important in dermal physiology. This has been shown in wound healing studies using siRNA (small-interfering RNA) knockdown of YAP and its protein homolog TAZ. During normal wounding, YAP and TAZ levels were observed to be elevated in the cells at the wounded site where induction of wounding creates an area of low cell density. At this site nuclear YAP and TAZ caused TGFβ signaling, which induced fibroblast proliferation, migration and collagen synthesis in order to close the wound. Silencing of YAP and TAZ at the wound site delayed its closure, showing that in the absence of cell-density sensing cues orchestrated by the Hippo Pathway, skin repair upon wounding was defective (Lee et al, 2014).

1.26   Objectives of this thesis

Clinical and cosmetic issues associated with skin ageing outline a clear need for the development of therapeutics to address the incidence of pathology and the poor presentation of aged skin. However, a crucial pre-requisite to therapeutic development is a sound understanding of the underlying molecular causes that drive the age-related changes in skin architecture. The objectives of this thesis were therefore to:

1. The mouse strain C57BL/6 is a commonplace model for studies of biological ageing but a comprehensive overview of skin ageing changes in this rodent has not been produced. We therefore aimed to understand the morphological and protein changes that occur to the skin over the lifespan of the mouse in the epidermal, dermal and basement membrane compartments. In our studies we also wished to conclude if evidence of cellular senescence occurred in the highly cellular epidermal compartment during ageing (Relevant data sections: 3.2-3.5).

2. Numerous studies have identified a link between alterations in both the expression levels and organisation of nuclear lamina intermediate filaments during ageing at both the cell and tissue level. We aimed to build on what is already uncovered in two ways: Firstly we wished to understand whether lamin B1 expression was altered in ageing mouse epidermis and secondly, we wished to characterise the unique transcriptional and protein changes of lamina constituents during human intrinsic ageing and photo-ageing (Relevant data sections: 3.3.6, 4.4)

3. The tissue pools used in our human transcriptomic studies are unprecedented in terms of sample size numbers and age-range; and by separating the epidermis and dermis in some of our experiments we increased our ability to un-cover transcriptional changes that are highly specific to either the epidermal or dermal compartment. We therefore aimed to use this highly powerful data set to uncover novel findings with regards to well-studied areas of skin ageing biology such as dermal collagen gene transcription and also basement membrane collagen gene transcription. (Relevant data sections: 4.2-4.3)

4. Discrete roles for the Hippo pathway have been identified in organ development and skin homeostasis but little is known about the role of Hippo during skin ageing. One of our goals was therefore to assess whether the expression levels and localisation of the Hippo effector YAP1 changed during ageing in our mouse and human models. (Relevant data sections 3.5, 4.5)

5. Once we had established a greater understanding of skin ageing processes in our C57BL/6 mice and human cohorts, our final aim was to understand the similarities and differences in ageing skin between these two models at the protein level.

Chapter 2: Materials and Methods

2.1   C57BL/6 mouse skin histology

2.1.1   Mice

Statement of Ethics: Ethical approval was granted by the LERC Newcastle University, UK. The work was licensed by the UK Home Office (PPL 60/3864) and complied with the guiding principles for the care and use of laboratory animals published by the National Research Council.

Ad-libitum fed, male C57BL/6J mice of ages 3 mo, 12 mo, 15 mo, 24 mo and 30 mo were housed and prepared at the Newcastle University Institute for Ageing. Four individual mice from each age group were used in the generation of experimental data.

2.1.2   Preparation of paraffin-embedded samples.

Preparation of mice and paraffin embedding was completed by Clara Correia Melo at Newcastle University. The back skin of each mouse was removed and the excess hair was shaved away. A square of skin was taken from this region and placed with the epidermis facing upwards onto a square of cardboard and the edges were pulled to ensure no folding or crumpling of the skin occurred. The skin was then placed in histological cassettes and was fixed in 4% paraformaldehyde (w/v) prepared in PBS [8 mM Na_2HPO_4, 2 mM KH_2PO_4, 137 mM NaCl, and 2.7 mM KCl, (all reagents Sigma) pH 7.4] overnight at 4℃. Excess fixative was removed and the skin was washed in 3 changes of PBS for 10 min each. Skin was then subjected to dehydration in sequential changes of ethanol before embedding in paraffin. Skin samples were orientated so that longitudinal cross sections would be taken upon subsequent sectioning. Paraffin blocks were covered with aluminium foil and stored in an airtight container.

2.1.3   Sectioning of mouse skin

Prior to sectioning, skin was placed at -20℃ to cool the paraffin blocks and assist in the cutting process. A microtome blade (Thermo Fisher) was loaded into a manual microtome (Leica RM 2235) and the block was trimmed to remove the outer layer. 5µm sections were then cut and floated briefly on the surface of a water bath set to 37℃ to expand the sections before collection on charged microscope slides (Superfrost™ Plus- Thermo Fisher). Slides were left to dry overnight on a slide drying bench before being placed in microscope slide boxes and sealed with paraffin to exclude air.

2.1.4 Deparaffinisation and re-hydration of mouse skin sections

Slides were incubated sequentially in 2x 5 min changes of histological grade xylene (Sigma, cat #534056), 2x5 min changes of 100% EtOH and 2x 5 min changes dH$_2$0 and then stored in PBS for up to 24 hrs.

2.1.5 Haematoxylin and Eosin staining

Skin sections were prepared as described in 2.1.3 and 2.1.4. Nuclei were then stained using Mayer's haematoxylin (Sigma- H9267) solution [0.1% (w/v) haematoxylin, 0.02% (v/v) sodium iodate, 5% (v/v) aluminium potassium sulphate, 5% (v/v) chloral hydrate and 0.1% (v/v) citric acid (all reagents Sigma) in dH$_2$0] for 5 min then excess reagent was briefly washed away in distilled water for 30 sec. Slides were then incubated in alkaline alcohol [3% (v/v) ammonia in 70% EtOH] to blue nuclei. Slides were then passed through 30 sec changes of 2x 70% EtOH and 2x 95% EtOH before incubation in 0.5% (w/v) eosin (Sigma- E4009) prepared in 95% EtOH for 1 minute to stain protein components in the skin. Excess eosin solution was removed by passing the slides through 2x 30 sec changes in 95% EtOH followed by 2x 20 sec changes in 100% EtOH. Slides were then cleared in 2x 3 min sequential changes of xylene (Sigma, cat #534056) before mounting in DPX (Fisher, 10050080) and coverslipping. Slides were left to dry overnight at room temperature then imaged using a Leica DM500 light microscope with ICC50 Camera and 20x and 40x objective lenses. Images were exported and processed using LAS EZ (Leica) software.

2.1.6 Herovici staining for young and mature collagen

Skin sections were prepared as described in 2.1.3 and 2.1.4. The acid resistant nuclear stain Weigert's Iron Hamematoxylin was prepared by mixing equal parts of solution A [1% (w/v) haematoxylin in 95% EtOH] and solution B [0.8% (w/v) ferric chloride (Sigma), 1.5% (w/v) ferrous sulphate (Sigma) and 1% (v/v) hydrochloric acid prepared in dH$_2$0] just prior to use. To stain nuclei, slides were incubated in staining solution for 15 min and then placed under a running tap for 15 min to remove excess stain (care was taken to ensure tissue was not disturbed during the rinsing period). Next, to differentially stain young and mature collagen Herovici's polychrome solution was prepared according to Turner et al (2013). Solution A [0.1% Van Gieson stain prepared from 495ml picric acid and 5ml 1% (w/v) acid fuchsin (Sigma)] was used in a 2:1 ratio with solution B [0.05% (w/v) methyl blue (Sigma) prepared in 1% acetic acid in dH$_2$0]. Slides were incubated in polychrome staining solution for 4 min then differentiated in 1% acetic acid in dH$_2$0 for 2 min. Excess reagent was rinsed away by incubating slides in 2x 1 min changes of 100% EtOH under gentle agitation. Slides were then cleared in 2x 3 min changes of xylene before mounting in DPX and coverslipping. Slides were left to dry overnight at room

temperature then imaged using a Leica DM500 light microscope with ICC50 Camera and 20x, 40x and 100x objective lenses. Images were exported and processed using LAS EZ (Leica) software.

2.2   Mouse skin western blotting

2.2.1   Sample Collection

The back skin of three different C57BL/6 mice aged 3 mo and three different C57BL/6 mice aged 30 mo snap frozen in liquid nitrogen and stored at -150℃ were provided by Glyn Nelson from Newcastle University. Samples travelled to Durham University on dry ice and were stored for 24 hours before lysate preparation began.

2.2.2   Whole skin lysate preparation

Skin was handled using sterile forceps and placed into a Petri dish containing ice. Using a scalpel, excess hair was removed from each sample and they were briefly rinsed in ice-cold PBS to remove any loose hair. Samples were then cut into small 1mm pieces and placed in shatter-proof test tubes. Ice-cold RIPA buffer [150mM NaCl, 50mM Tris-HCl pH 8.0, 0.1% (v/v) Triton X-100, 0.5% (w/v) sodium deoxycholate, 0.1% (w/v) SDS- all reagents- Sigma] with the addition of 1% proteinase inhibitor cocktail (PIC Sigma) was added at a volume of 300µl buffer per 5 mg skin with the total volume being at least 1 ml in each tube. Tubes were kept on ice wherever possible during this procedure.

Test tubes containing skin were then subjected to homogenisation (using VWR NDI 25 homogeniser) in brief bursts, and upon sample rotation the homogeniser blade was cleaned thoroughly with dH_2O and 70% ethanol. Each sample was subjected to 6x 20 sec homogenisation steps or until no visible tissue clumps were present in the homogenate. All samples were prepared in the same time frame and were kept on ice when not in use. Test tubes containing homogenate were then placed in a 4℃ room and subjected to agitation on a laboratory shaker for 30 min.

The homogenate from each sample was then dispensed into a clean Eppendorf tube (one for each sample) and mechanical break-down of sample components was performed by passing each sample through a 24G hypodermic needle using a 2 ml syringe. Samples were syringed 5 times each to shear DNA and ensure breakdown of cellular components. Lysates were then subjected to centrifugation at 13,000 RPM for 20min. On ice, the supernatant was then carefully removed and pipetted into a new, pre-labelled Eppendorf. The supernatant was briefly mixed then 10 µl of each sample was taken for protein assay quantification. Samples were then aliquotted into two Eppendorf tubes each. In one tube 2x sample buffer [125mM

Tris-HCl pH 6.8, 2% (v/v) SDS, 2mM DTT, 20% (v/v) glycerol, 5% (v/v) β-mercaptoethanol and 0.25% (w/v) bromophenol blue (all reagents- Sigma)] was added in a 1:1 ratio of sample to buffer. The samples containing sample buffer were heated to 99℃ for 4 minutes then cooled and stored at -20℃. The Eppendorf containing the remaining sample was stored at -80℃. All of the 6 samples prepared were subjected to an identical procedure and stored on ice wherever possible.

2.2.3   Bradford Assay

Approximate protein concentrations for each lysate were determined by Bradford Assay. In order to produce a standard curve for use in determination of the unknown protein concentration of whole cell extracts, a protein assay kit was used (Bio Rad). Standards were prepared according to the manufacturer's instructions along with skin lysate samples (all in triplicate). Both low (2.5µl) and high (5µl) amounts of skin lysate samples were prepared to glean accurate readings. All samples were prepared in 96 well plates and readings were recorded on a plate reader (Nanodrop 8000- Thermo Scientific). A standard curve was then generated from the results using the average absorbance at the test BSA concentrations, omitting any anomalous values from the analysis. The results of the assay are shown in figure 2.1. For each sample of un-known protein concentration, the equation shown on the standard curve graph was subsequently used to solve for x (the unknown protein concentration of each sample) where the absorbance values were represented on the y-axis.
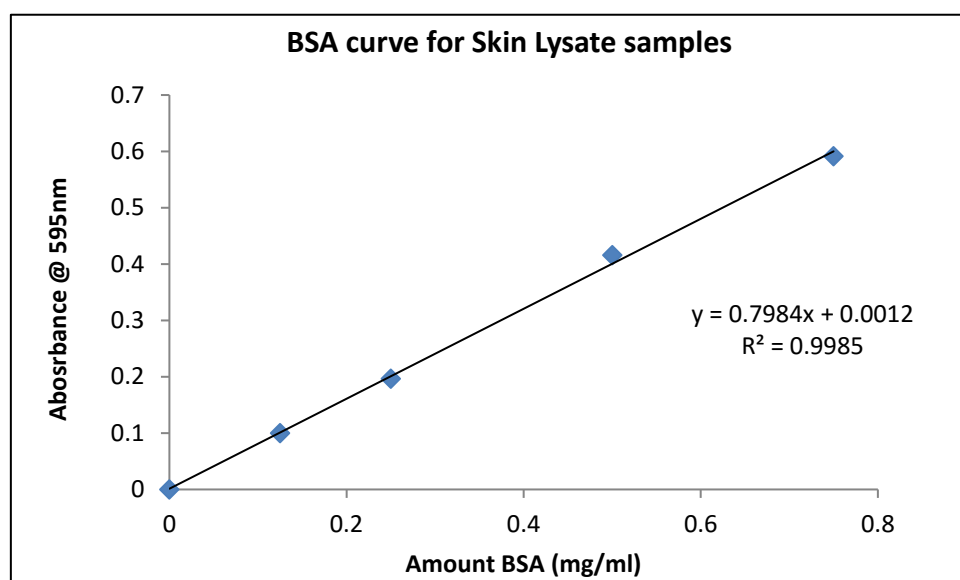
Figure 2.1: Protein standard curve produced for skin lysate protein assay. The equation of the graph represents the slope of the line of best fit (regression line). The R-squared value indicates how closely data points fit the line of regression.

2.2.4 Coomassie blue based in-gel validation of equal protein loading

Once protein concentration had been determined for each sample, equal protein loading was validated by Coomassie staining of samples subjected to gel electrophoresis. 10% polyacrylamide gels were cast in casting chambers (Bio-Rad) using the reagents detailed in table 2.1. Resolving gel was pipetted between gel plates and topped with isobutanol (Sigma) and left for 45min to set. Once resolving gel was set, isobutanol was removed by pouring and a 5% stacking gel solution (see table 2.1) was poured on the surface of the resolving gel. A comb was then inserted to form wells and the gel was left to set for 15 min.

Table 2.1: Quantities of reagents used for acrylamide gel casting

Reagent (measurement in ml/μl)	Amount used: Resolving Gel- 10%	Amount used: Stacking Gel- 5%
ProSieve® 50 acrylamide gel solution (Cambrex BioScience Wokingham, Ltd., UK), (ml)	2.00	0.50
Milli-Q™ H$_2$0 (ml)	5.30	3.96
1.5M Tris-HCl pH 8.8 (ml)	2.50	0.50
10% SDS solution (μl)	100	50
10% Ammonium persulphate solution (μl) (Fisher Biosciences)	100	50
TEMED (μl) ((N,N,N',N'-Tetramethylethylenediamine).(Sigma)	4	5

2.2.5 SDS Polyacrylamide gel electrophoresis (SDS PAGE)

Once gels had set, they were placed in a tank (BioRad) and submerged in tank buffer [25mM Tris pH 8.3, 192mM Glycine, 0.1% (v/v) SDS (all reagents-Sigma)] Combs were then removed from gels and equal protein concentrations (10 μg of protein per well) were loaded into the gel using a fine pipette tips. The volume of sample in each well was standardised with excess sample buffer as needed. A protein standard (PageRuler™ Plus- Thermo Fischer) was also loaded into one of the wells to behave as a reference. Gel electrophoresis was subsequently performed at 100V and 40mAmp until samples migrated to the bottom of the resolving gel. This took around 2 hours.

2.2.6 Coomassie blue staining of gels

Separated in-gel proteins were stained with Coomassie brilliant blue reagent (ThermoFischer) prepared in gel staining solution [0.1% (w/v) Coomassie R-250, 10% (v/v) glacial acetic acid, 50% (v/v) methanol, 40% dH$_2$0] by incubating the gel in solution in a plastic staining dish under agitation for at least 1 hour at room temperature. Gel was then subjected to de-staining (to allow band visualisation) overnight in de-staining solution [10% (v/v) glacial acetic acid, 50% (v/v) methanol, 40% dH$_2$0]. In the morning the de-staining solution was changed and replenished then gels were visualised over a white light box (ThermoFisher) to enhance contrast between protein bands. Equal loading of protein bands was determined by considering the intensity of staining and distribution of protein bands from each sample across the whole gel (see figure 2.2). Small adjustments in protein amounts for each sample were made accordingly until equal protein loading was achieved between samples.
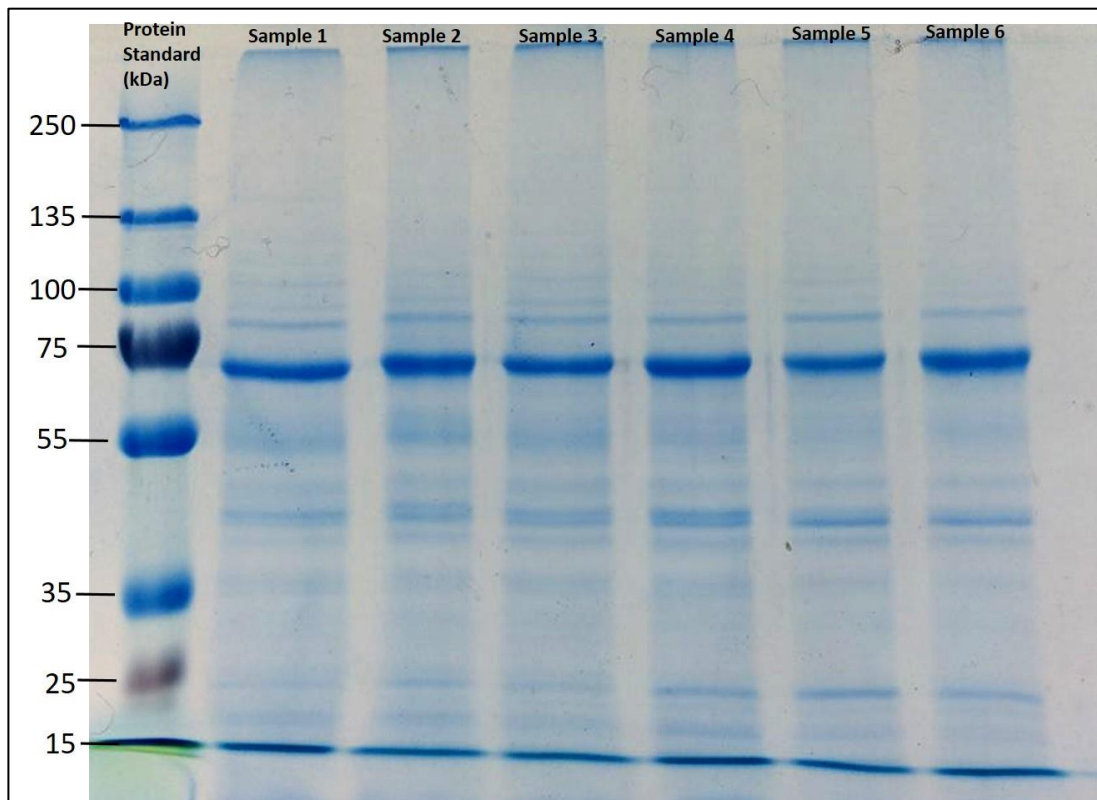
Figure 2.2: Coomassie blue in-gel staining of skin lysate samples to validate equal loading. Proteins within samples were separated by weight using gel electrophoresis. Equal sample loading was determined by the intensity and distribution of protein bands in each lane.

2.2.7 Resolving gels for C57BL/6 skin blots

The percentage acrylamide for each resolving gel was determined by the molecular weight of the protein(s) of interest and 8%, 10% and 12% acrylamide gels were used. The

stacking gel was the same for all gels cast. Reagents for 8% and 12% resolving gels are shown below in table 2.2 (10% gel reagent volumes are in table 2.1). and details of the resolving gel percentages for each protein, along with the antibody used, its host animal and the working dilution are shown in table 2.3.

Table 2.2: Reagents and their volumes used in preparation of 8% and 12% acrylamide resolving gels for SDS-PAGE

Reagent (measurement in ml/µl)	Amount used: Resolving Gel- 8%	Amount used: Resolving Gel- 12%
ProSieve® 50 acrylamide gel solution (Lonza), (ml)	1.60	2.40
Milli-Q™ H$_2$0 (ml)	5.70	4.90
1.5M Tris-HCl pH 8.8 (ml)	2.50	2.50
10% SDS solution (µl)	100	100
10% Ammonium persulphate solution (µl) (Fisher Biosciences)	100	100
TEMED (µl) ((N,N,N',N'-Tetramethylethylenediamine).(Sigma)	4	4

Table 2.3: Primary antibodies, host animals, percentage gel and working dilutions used for western blots of C57BL/6 mouse skin lysates.

Antibody	Supplier/ (cat#)	Host	Resolving gel percentage	Dilution of antibody
Collagen I	Abcam (ab34710)	Rabbit	8	1:1000
Collagen III	Abcam (ab7778)	Rabbit	8	1:1000
Lamin B1	Abcam (ab16048)	Rabbit	10	1:1000
Keratin 14	Abcam (ab181595)	Rabbit	10	1:2000
Keratin 10	Abcam (ab76318)	Rabbit	10	1:3000
Loricrin	Abcam (ab83679)	Rabbit	12	1:1000
GAPDH	Abcam (ab9485)	Mouse	10 or 12	1:2000
β-Actin	Sigma (A2228)	Mouse	10 or 12	1:1000
β-Tubulin	Sigma (T8328)	Mouse	10 or 12	1:2000
YAP1	Novus Biologicals (NB110-58358)	Rabbit	10	1:1000
E-Cadherin	Cell Signalling (#14472)	Mouse	8	1:1000

All protein gels were cast as described in 2.3.4 and underwent electrophoresis as described in 2.3.5. Glass gel plates were then separated and the gel was carefully removed from plates and equilibrated in transfer buffer [192mM Glycine, 25mM Tris HCl pH 9.2, 20% (v/v) methanol, 0.1% (v/v) SDS] for 1 minute.

2.2.8 Electrophoretic transfer of proteins in polyacrylamide gels onto PVDF membranes

PVDF transfer membrane was activated prior to use by soaking in methanol (1 min), dH20 (1 min) then transfer buffer (5 min). Transfer cassettes (Bio Rad) consisting of (from negative to positive electrode- a fibre pad (VWR), Whatman paper soaked in transfer buffer, SDS-PAGE gel and activated PVDF membrane, Whatman paper and fibre pad) were assembled into a transfer equipment rack and tank (Bio Rad) and fully covered in transfer buffer. For subsequent immunoblotting of proteins with a molecular weight under 80 kDa, transfer was performed at 100V, 250 mAmp for 1.5 hours at room temperature (25°C). For proteins over 80 kDa, transfer was performed overnight at 4°C using a current of 20V, 100 mAmps and constant stirring of transfer buffer within the tank.

2.2.9 Membrane blocking for non-specific binding and immunoblotting

Following transfer, cassettes were disassembled and membranes were transferred to plastic incubation dishes using clean, flat ended tweezers. The protein standard bands present on the membrane were checked to verify efficient protein transfer and were then marked in pencil for future reference (as bands faded during storage). Membranes were then blocked for non-specific antibody binding in 4% (w/v) non-fat dry milk (Sigma) in Blot Rinse Buffer/Tween-20® [BRB/T- 150mM NaCl, 10mM Tris pH 7.4, 1mM EDTA, 0.1% (v/v) (Sigma) Tween-20®] for 1 hour at room temperature. Membranes were then washed briefly in 2 changes of BRB/T before being carefully placed into a 50ml falcon tube (Greiner Bio One) with the transferred proteins on the membrane facing upwards. Primary antibodies prepared in antibody diluent [1% (v/v) NCS in BRB/T] were then added to the tubes using the working dilutions shown in table 2.4 and volumes were made up to 3 mol of solution. Tubes were then incubated on a roller overnight at 4°C so that the solution remained in contact with the membrane for the entire incubation period.

Membranes were then removed from falcon tubes using clean, flat ended tweezers and were placed, protein side up in plastic dishes. Membranes were then washed three times for 10 min in BRB/T and then placed in a fresh falcon tube for addition of the secondary antibody (Either goat anti-mouse POD –P4416 or goat anti-rabbit POD- A9037 both purchased from Sigma). Secondary antibodies were prepared at a working dilution of 1:2000 in antibody diluent with the final volume being made up to 3 mol. Membranes were then carefully placed in fresh falcon tubes, which were were placed on a roller and secondary antibody incubation was performed for 1 hr at room temperature. Following secondary antibody incubation, membranes were washed as for the primary antibody.

2.2.10 ECL-based protein band detection

Enhanced chemiluminescence (ECL) detection solution [250 mM luminol (Sigma) prepared in DMSO (Sigma), 90mM P-coumaric acid (Sigma) prepared in DMSO, 1M Tris-HCl pH 8.5 and 0.01% (v/v) 30% hydrogen peroxide solution (Sigma)] was prepared fresh just prior to film exposure. Excess wash buffer was blotted away from membranes at their edges using absorbent paper towel and membranes were placed flat on a surface prepared with cling film. ECL substrate was pipetted onto membrane surface (protein side up) and left for 1 min. Excess ECL was then removed and the membranes were covered in a single layer of cling film and mounted in a developing cassette. Membranes were then exposed to high-performance photographic film (GE Healthcare Life Sciences) in a Dark Room and films were developed using a Compact X4 Automatic X-ray Film Processor (Xograph Imaging Systems Ltd., Gloucestershire, UK).

2.3 C57BL/6 mouse skin Immunohistochemistry

2.3.1   Heat induced antigen retrieval (HIAR):

Prior to HIAR, mouse skin sections were prepared on slides and were processed as shown in sections 2.1.3-2.1.4. Citrate buffer [10 mM Sodium Citrate 0.05% Tween 20, pH 6.0] was prepared using a tri-sodium citrate di-hydrate salt (Sigma- S1804). Buffer solution was heated in a small, plastic, thermostable box (ThermoFisher, cat#195) in a microwave until boiling. As soon as boiling had subsided, the solution was stirred to evenly distribute heat and temperature was checked using a thermometer to ensure it was between 95-99℃. Slides were then placed in a compatible staining rack (ThermoFisher, cat# 196) and subsequently in a water-bath preheated to 98℃ (under boiling). The water-bath was topped up with freshly boiled water from a kettle to ensure that the water level was just below the lid of the box. Slides were incubated for 16 min in the water-bath before being removed and left to cool in the box (lid taken off) for 15 min. Slides were then placed under a running tap to complete the cooling process and wash away excess buffer then stored in PBS for up to 2 hrs.

2.3.2   Enzymatic antigen retrieval (Enz AR)

For enzymatic antigen retrieval, proteinase K enzyme (Sigma) (stock solution was 10 mg/ml enzyme in PBS stored at -20℃ and defrosted prior to use) was prepared in Tris-EDTA buffer [50 mM Tris Base, 1 mM EDTA, 0.5% (v/v) Triton X-100, pH 8.0] at a concentration of 20 μg/ml. Tris-EDTA buffer was subjected to gentle microwave heating to obtain a temperature of 37℃ before addition of the enzyme. Slides were placed in the buffer and incubated in a water-

bath preheated to 37℃ for 15 minutes. Slides were then removed and placed under a running tap and washed several times to quench the enzymatic activity. They were then stored in PBS for up to 2 hrs.

2.3.3 Blocking of non-specific antibody binding

To reduce subsequent reagent use, the region around skin sections was marked with a hydrophobic barrier pen (VectorLabs- H-4000). Excess fluid was blotted away from this region using paper towel with care taken to ensure that the skin sections were not disturbed. Blocking solution [10% normal goat serum (Sigma) prepared in 0.1% BSA (bovine serum albumin) in PBS] was applied to skin sections and incubated at room temperature for 1 hr.

2.3.4 Antibody preparation

Antibodies were prepared in antibody diluent [0.1% BSA in PBS] at the concentrations shown in table 2.4. To avoid issues associated with non-specific binding of secondary antibody, all primary antibodies used on mouse tissue were made in rabbits. The antigen retrieval method used prior to each antibody was dependent on the individual antibody and is detailed in table 2.4.

Table 2.4: Details of antibodies, their suppliers, the antigen retrieval method used on skin sections prior to their application and the working dilution.

Antibody	Supplier/ (cat#)	Antigen retrieval method: HIAR= (heat induced) Enz AR=(enzyme-induced)	Dilution
Lamin B1	Abcam (ab16048)	HIAR	1:200
YAP1	Novus Biologicals (NB110-58358)	HIAR	1:150
Keratin 10	Abcam (ab76318)	HIAR	1:500
Keratin 14	Abcam (ab181595)	HIAR	1:500
Loricrin	Abcam (ab83679)	HIAR	1:100
Collagen I	Abcam (ab34720)	Both used	1:100
Collagen III	Abcam (ab7778)	Both used	1:100
Collagen IV	Abcam (ab6586)	Enz AR	1:200
Collagen VII	Abcam (ab93350)	Enz AR	1:50
P53BP1	Cell signalling (4937S)	HIAR	1:200
Ki67 directly labelled with Alexa Fluor 488	Abcam- custom order	HIAR	1:100

Blocking solution was removed prior to application of primary antibody, and approx. 100 µl of antibody solution was pipetted onto each skin section, ensuring that the tissue was fully covered with antibody solution. Slides were then incubated in a moist staining chamber, protected from light, overnight (~16h) at 4℃. Primary antibody was then removed and slides were washed in tris-buffered saline with Tween 20 [TBS/T- 50 mM Tris-HCl pH 7.5. 150 mM NaCl, 0.01% (v/v) Tween® 20 (Sigma)] for 3x 10 min, with the buffer being changed each time and gentle agitation being used to encourage dissociation of non-specifically bound antibody.

The secondary antibody used for all primary antibodies aside from P53BP1 and Ki67 was a Goat anti-rabbit conjugated Alexa Fluor 568 (Molecular probes, Invitrogen- A11011) which was prepared at a working dilution of 1:1000 in antibody diluent with the addition of DAPI (4',6-diamidino-2-phenylindole- Sigma) at a concentration of 2mg/ml also diluted 1:1000. Slides were incubated in a moist staining chamber, protected from light, at room temperature for 1 hour. Secondary antibody was then washed away as for the primary antibody. Skin sections were then covered in Vectashield anti-fade mounting medium (Vector Laboratories, cat# H-1000) then sealed with nail polish and left to dry overnight before imaging.

2.3.5 P53BP1/Ki67 immunofluorescence double staining

Slides were prepared as detailed in sections 2.1.3-2.1.4 and subjected to HIAR and blocking of non-specific antibody binding as described in 2.3.1 and 2.3.3. The first primary antibody incubation was the Ki67 antibody (directly labelled with Alexa Fluor 488) which was prepared in antibody diluent [0.1% BSA in PBS], pipetted onto sections and incubated overnight at 4℃ in a moist staining chamber protected from light. Excess antibody was then washed away using 3x 7 min changes TBS/T under agitation. Next P53BP1 antibody prepared in antibody diluent was applied to slides and they were incubated overnight at 4℃ in a moist staining chamber. Excess antibody was then washed away using 3x 7 min changes TBS/T under agitation. Next a biotinylated Goat anti-rabbit IgG secondary antibody (Vector Laboratories- BA-1000) was prepared at a working dilution of 1:400 in antibody diluent and applied to skin sections for 30 min at room temperature. Excess anti-rabbit IgG was then washed away using 3x 7 min changes of TBS/T. Texas Red® labelled Avidin (Vector Laboratories- A-2006) prepared in PBS at a working dilution of 1:800 was then applied to the skin sections for 20 min. Excess Avidin was then washed away from slides using 3x 7 min changes of TBS/T under agitation. Excess buffer was then blotted away from slides using absorbent paper and slides were then mounted in Vectashield containing DAPI (Vector Laboratories-H-1200) then sealed with nail polish and left to dry overnight before imaging.

2.3.6 Imaging and quantitative analysis of DNA damage and cell proliferation

Slides were imaged using a Leica TCS SP5 confocal laser scanning microscope. 405 nm and 488 nm lasers were used to image DAPI and Ki67 stains respectively. A HyD (Leica) laser set to 594 nm was used to image P53BP1 staining. 5μm thick Z-stack images were captured using a 63x oil lens (NA=1.4). Pinhole diameter was optimised to 1 Airy unit and 1024 x 1024 pixel images were captured at a scan speed of 400Hz. Imaging conditions were kept constant for the entirety of the data collection between all samples. 3 images were collected for each of the four mice in each age group and 2D maximal projection images of the image stacks were collated in LAS AF software (Leica). Individual nuclei were scored according to the scoring system depicted in figure 3.3.3 –section 3.3. Data was collated in Microsoft Excel. Subsequent downstream analysis was performed in Sigmaplot v12.5 and the data was assessed for statistically significant differences using computational methods. One-way analysis of variance (ANOVA) was used as the statistical test and prior testing for equal variance between samples was performed for all age groups assessed by performing Levene's testing. Post-hoc analysis of results was performed using Holm-Sidak testing.

2.3.7 Imaging and semi-quantitative analysis of epidermal lamin B1 levels

Using a Leica TCS SP5 confocal laser scanning microscope, a 405 nm laser were used to image DAPI and a HyD (Leica) laser set to 568 nm was used to image lamin B1 staining. 5μm thick Z-stack images were captured using a 40x oil lens. Pinhole diameter was optimised to 1 Airy unit and 1024 x 1024 pixel images were captured at a scan speed of 400Hz. Imaging conditions were kept constant for the entirety of the data collection between all samples. 3 images were collected for each of the four mice in each age group and 2D maximal projection images of the image stacks were collated in LAS AF software (Leica). 2D maximally projected stacks were subsequently produced and the maximally projected images were exported as .tiff files. Subsequent analysis was completed in image J with all images being processed identically: A median filter was applied to all images using a radius of 1.5 pixels and background subtraction was also completed using a rolling ball radius of 50 pixels. Using the freehand selection tool, the epidermal region was isolated and the average integrated density (pixel intensity) within this region was measured, along with the area. For each image, the result was expressed as the average pixel intensity per unit area. Data was collated in Microsoft Excel and subsequent downstream analysis (ANOVA) was performed in Sigmaplot v12.5 as described in 2.4.6.

2.3.8 Imaging and calculation of YAP1 nuclear:cytoplasmic ratio in C57BL/6 epidermis

Mouse skin epidermis from 3 mo and 30 mo old animals was imaged as for section 2.4.7 with the 405 nm laser imaging DAPI and the HyD laser imaging YAP1 primary antibody conjugated to Alexa Fluor 568 secondary antibody. 2D maximally projected stacks were prepared in the same way as described in 2.3.7 and images were exported as tiff files with DAPI staining and YAP1 staining being exported as separate image files. Nuclear to cytoplasmic ratio values were calculated in image J. A median filter was applied to all images using a radius of 1.5 pixels. Background subtraction was also completed using a rolling ball radius of 50 pixels and all images were processed identically. The binary masking tool was used to generate templates of both nuclei (from DAPI images) and cytoplasmic regions (from YAP1 images). The image subtraction and addition functions were then used to isolate nuclear and cytoplasmic YAP1 epidermal expression. Mean pixel intensity values for YAP1 expression in epidermal nuclei and epidermal cytoplasm were then measured using histogram data. An example of image processing is shown below in figure 2.3. The nuclear to cytoplasmic ratio value was then calculated for each epidermal compartment in each image by dividing the average nuclear pixel intensity by the average cytoplasmic pixel intensity. A ratio greater than 1 indicated greater nuclear YAP compared to cytoplasmic YAP and vice versa. 6 images were taken from each mouse and two mice aged 30 mo and two mice aged 3 mo were used in the analysis.
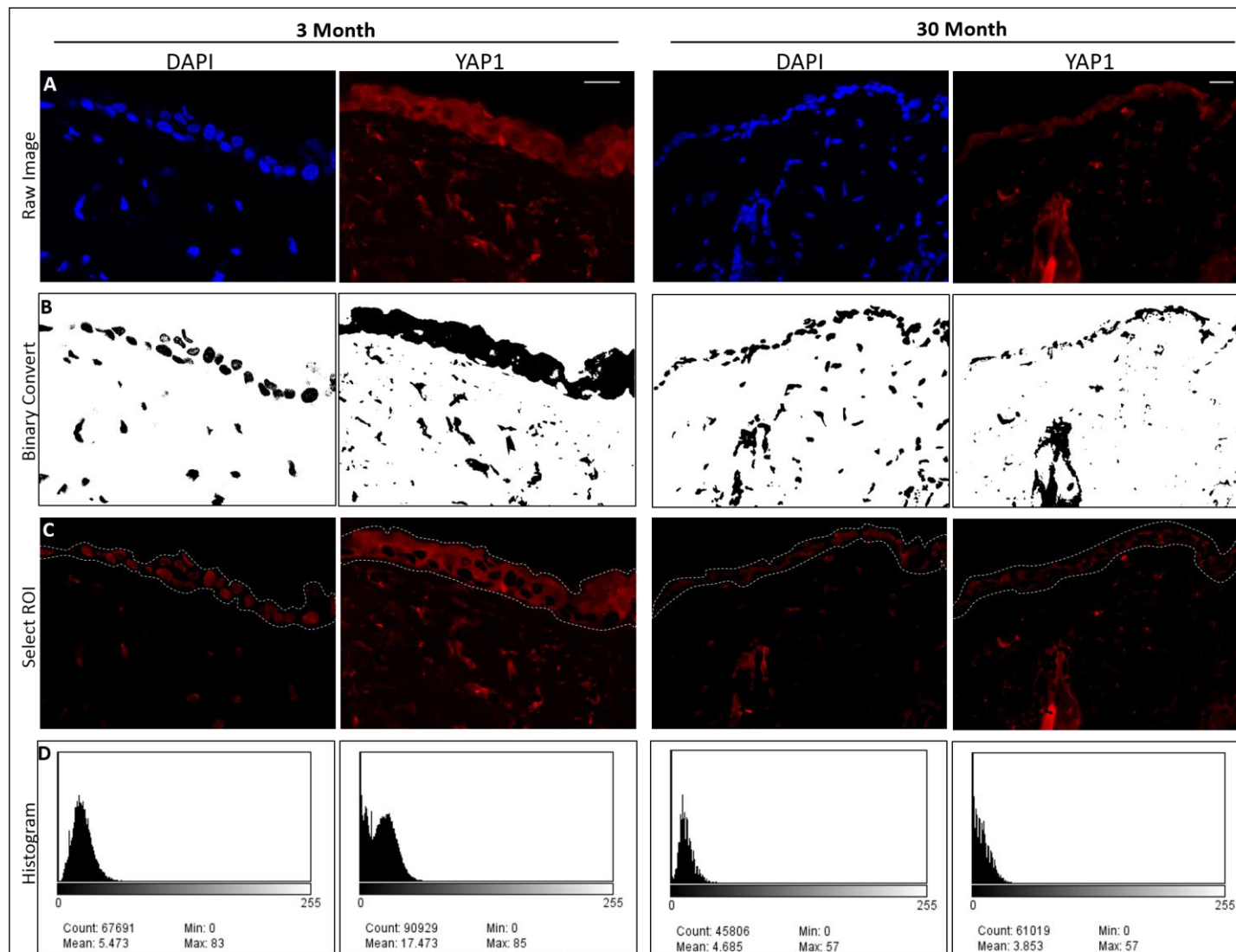
Figure 2.3: Deduction of YAP1 nuclear:cytoplasmic ratios in 3 mo and 30 mo epidermis using binary masking. ImageJ software was used to create templates of YAP1 expression (red) and nuclear material (DAPI-blue) (A,B). In order to deduce nuclear and cytoplasmic-region specific levels of YAP1 in the epidermis (C), the image calculation tool was used in ImageJ. Histogram plots generated from the pixels contained within the selections (D) allowed quantification of the levels of YAP1 present in these regions resulting in an average pixel intensity value for the nuclear and cytoplasmic regions.

2.4   Preparation of mice for EM

2.4.1   Mice

Infarct mice were provided by Gavin Richardson (Institute of genetic medicine: Newcastle University). Shortly after birth all mice were subjected to surgical ligation of the left descending artery. Mice aged 2.75 months and 23.5 months (subjected to anaesthesia) were prepared for TEM.

2.4.2   Skin tissue preparation

Mice were subjected to chemical depilation to remove excess hair. Subsequently, 5 mm x 10 mm squares of back skin were taken from mice and placed immediately in Karnovsky's double strength fixative [5% glutaraldehyde, 4% paraformaldehyde, 0.1M cacodylate buffer and 0.05% (w/v) $CaCl_2$] for 3 hr. Akis Karakesisoglou and Gavin Richardson both assisted with collection of the mouse skin samples.

The next processing steps were completed by Christine Richardson and Helen Grindley at Durham University. Samples were then processed for epoxy resin embedding and ultra-thin sections were cut using a Leica EM UC6 microtome. Sections were then mounted on copper grids and imaged using a Hitachi TEM-H7600 transmission electron microscope with assistance from Helen Grindley.

2.5   HaCaT cell culture

2.5.1   Cell line maintenance

Human keratinocyte cell line HaCaT (AddexBio, T0020001) was cultured in high glucose Dulbecco's modified Eagle's medium (DMEM, Sigma) supplemented with 10% (v/v) foetal bovine serum (FBS-Sigma), 2mM L-glutamine (Sigma) and 100 units/ml penicillin/streptomycin (Sigma). Routine culturing was performed on CELLSTAR® culture plastic (T-75cm^2 flasks- Greiner Bio-one) and cells were maintained in a humidified incubator at 37℃ in 5% CO_2.

2.5.2   Passaging of cell cultures

At 70% confluence, HaCaT cells were enzymatically passaged by removing growth media, washing adherent cells in sterile (autoclaved) versene [137mM NaCl, 2.7mM KCl, 8mM Na_2HPO_4, 1.5mM KH_2PO_4, 1.5mM EDTA pH 7.4] and incubating cells in 10% (v/v) trypsin (Lonza) in versene at 37℃ until cell detachment occurred (5-10 min). Trypsin neutralisation was performed by addition of an equal volume of complete medium before splitting cells into

several culture flasks and replenishing medium in each flask. Culture splitting was dependent on the rate of cell growth and cells were normally split in a 1:4 ratio.

2.5.3 Storage of cell culture reagents

Versene, versene with 10% trypsin and complete culture medium were stored at 4°C and heated to 37°C in a chemically treated water bath before use on cells. FBS was aliquotted and stored at -20°C and thawed before use

2.5.4 Cryopreservation of cells

Cells were cryopreserved at -150°C in 1.5ml Nunc vials (ThermoScientific). Following trypsinisation of cells as described in 2.5.2, centrifugation was performed in an Eppendorf 5810R centrifuge at 1000rpm for 4 min, with the temperature maintained at 4°C. The cell pellet was re-suspended in freezing medium (10% (v/v) dimethysulfoxide (DMSO- Sigma) and 20% (v/v) FBS (Sigma) in DMEM culture medium). Cells were frozen at a density of one 70% confluent T-75 flask per 4 ml of medium. To re-establish cultures after freezing, vials were defrosted in a water bath at 37°C before the addition of 5ml growth media in order to form a cell suspension. The suspension was then centrifuged as above and the supernatant containing DMSO was removed. The cell pellet was then re-suspended in fresh, complete culture medium and incubated in a T-25 flask to allow mono-layer re-establishment.

2.6 Immunofluorescence of cell cultures

2.6.1 Coverslip preparation

Glass coverslips with a circumference of 1cm (SLS) were prepared in 6 well plates (Greiner Bio-One) in a sterile flow cabinet. 3 coverslips were placed in each well using tweezers sterilised with ethanol. 200µl of 0.01mg/ml of Poly-D-Lysine (Sigma) was pipetted onto each coverslip ensuring that the coverslip was fully coated with solution before being left to dry in the hood for 24h.

2.6.2 Seeding of HaCaT cells

Cellular suspensions for seeding were prepared when cells were at 70% confluence. Growth flasks of cells were washed in Versene before undergoing trypsinisation and pelleting as described in section 2.5.2 and 2.5.4 above. Cells were then counted by collecting a small sample of suspension into a 1ml pipette then dropping the liquid on to the chambers of an improved Neubauer haemocytometer (Marienfeld-Superior) by capillary action. Counting grids were viewed under a Zeiss Televal 31 microscope and cells that fell within the 16 square grid

area were counted. Cells that fell on bottom and left sides of the grid were included and cells that fell on the top and right hand sides of the grid were ignored. Cells were seeded at a density of 0.5×10^6 cells per well and each well was filled with 2ml of complete DMEM medium. Cells were maintained in a 5% CO_2 humidified incubator at 37°C until they were ready for fixation.

2.6.3 Cell Fixation and processing for immunofluorescence

"Low cell density" cultures were fixed when the cells reached 50% confluence and "high cell density" cultures were fixed when cells reached 100% confluence. Medium was removed from each well of the 6 well plates before cells were washed in PBS. Remaining in the 6 well plates, coverslips with cells were incubated in 4% (w/v) Paraformaldehyde prepared in PBS (PFA-Agar Scientific) at a pH of 7.4 at 25°C on an orbital shaker for 15 moin. 500µl of PFA was used per well of each 6 well plate. Excess PFA was then removed and disposed of according to safely guidelines. The coverslips were washed for 3 x 5min in 1x PBS to remove any residual fixative. Cells were then incubated in 400µl per well of permeabilisation buffer (10% (v/v) NCS (Sigma), 0.1% (v/v) TritonX-100 (Sigma) in PBS) for 15 moin at 25°C before washing for 2x 5min in 1x PBS. To avoid non-specific anti-body binding cells were subsequently blocked in 1% PBS containing 10% NCS for 1hr on an orbital shaker at 25°C.

2.6.4 YAP1 primary antibody and secondary antibody incubations

In order to observe the staining of rabbit YAP1 primary antibody (Novus Biologicals cat# NB110-58358) in cells cultured at low and high cell density, the antibody was prepared in antibody diluent (1% (v/v) NCS in 0.1% (w/v) BSA in PBS) at a dilution of 1:150. 50µl of antibody solution was used per coverslip. Prior to antibody application, coverslips were removed from 6 well plates using sterile, fine tweezers and placed in moist, dark staining chambers prepared using absorbent paper soaked in 1% PBS covered with aluminium foil. Primary antibodies were applied using a 100µl Gilson pipette. Primary antibody was incubated overnight (~16hr) at 4°C.

Goat anti–rabbit Alexa Fluor 568 secondary antibody (Molecular probes-Invitrogen cat# A11011) was prepared in antibody diluent at a dilution of 1:1000. Additionally, DAPI (4',6-diamidino-2-phenylindole- Sigma) at a concentration of 2mg/ml was added to the antibody diluent using a 1:1000 dilution. Prior to secondary antibody incubation, coverslips were returned to clean 6 well plates for washing by 3x 5 min changes of PBS under gentle agitation. Coverslips were then removed from plates using fine tweezers and placed in moist staining chambers before addition of 50µl of secondary antibody solution containing DAPI using a pipette. Coverslips were protected from light and incubated at room temperature for 1 hr. After incubation, excess secondary antibody was washed away using 3x 5 min changes of PBS

under gentle agitation. Coverslips were then carefully blotted using absorbent paper at the edges to remove excess wash buffer before mounting.

2.6.5 Coverslip mounting and imaging

Coverslips were inverted and mounted onto glass microscope slides (Fisher) in Vectashield anti-fade mounting medium (Vector Laboratories, cat# H-1000) then sealed with nail polish and left to dry overnight before imaging. Images were taken on a Zeiss Aksioskopp 40 fluorescent microscope (Carl Zeiss GmbH, Germany) fitted with a 40x oil lens. Images were viewed and saved in the corresponding software (Zeiss Axiovision) before being exported as tiff files.

2.7 Transcriptomic analysis of female skin

Statement of Ethics: All consent for patient tissue use was obtained by Procter and Gamble, USA, in compliance with local laws and regulations. The protocol for obtaining samples was approved by an Institutional Review Board, and the participants signed informed consent documents for procurement of the tissue biopsy or surgical waste samples. A Material Transfer Agreement was subsequently drawn up to cover transfer of tissue to Durham, UK." Storage and use of the tissues at Durham University was in full compliance with codes of practice from the Human Tissue Act.

Work detailed in 2.7.1-2.7.5 was performed by members of Procter and Gamble – Cincinnati. Experiment leaders were Bob Binder (binder.rl@pg.com) Charlie Bascom (bascom.cc@pg.com) and Bob Isfort (isfort.rj@pg.com). As far as the author of this thesis is aware, full acknowledgement of all persons contributing to the work has been made.

2.7.1 Experimental design of study

The following persons contributed to the design of this study: Rosemarie Osborne, Robert L. Binder, Charles C. Bascom, Robert J. Isfort, Bradley B. Jarrold, Heather L. Rocchetta, Dionne Swift, Jay P. Tiesman and Daniel Schnell (all from Procter and Gamble).

2.7.2 Subjects

Biopsy collection, clinical execution and clinical data management was performed by Alexandra B. Kimball (Harvard University and Massachusetts General Hospital), the Dermatology resident staff (Massachusetts General Hospital), Scott M. Hartman, Debora Whittenbarger, Robert Hinkle, Joseph Kaczvinsky and Elizabeth Jewell-Motz (all from Procter and Gamble).

Subjects were female Fitzpatrick types I-III (Caucasian individuals) and were taken from age cohorts within the following decades of life: 2nd , 3rd , 4th , 5th ,6th and 7th . The subjects were verified as non-smokers and females at menopausal age were not on hormone replacement therapy (HRT). Two full thickness biopsies were collected from the arm (representative of photo-exposed condition) and the buttock (representative of photo-protected condition). One biopsy was used to generate full-thickness skin (FTS) skin biopsy samples and the other for Laser Capture Microdissection (LCM) to separate the epidermis and dermis.

2.7.3   Laser capture microdissection

For LCM biopsies were embedded in OCT (optimal cutting temperature medium) and cryo sectioned at 14µm. Typically, 4 sections were pooled from 4 mm biopsies and in some cases additional 4 sections were taken to get enough RNA for microarray chips (25 ng). Prior to LCM sections were stained with cresyl violet and Eosin Y to determine nuclei and ECM respectively. Haematoxylin was not used as a nuclear stain due to its propensity to degrade RNA. All skin structures including epidermis, dermis, hypodermis, hair follicles and sebaceous glands could now be identified and such the epidermis and dermis were isolated in the samples to create samples representing the epidermal and dermal compartments only. The 6 sample sub-sets produced following LCM, including full-thickness skin samples are shown in table 2.5.

Table 2.4: Tissue sub-sets following the LCM procedure

Photo-Protected Condition (buttock skin)	Photo-Exposed Condition (arm skin)
Photo protected dermis	Photo exposed dermis
Photo protected epidermis	Photo exposed epidermis
Photo protected full thickness skin (FTS)	Photo exposed full thickness skin (FTS)

The complete list of samples for each age group and each condition is shown in table 2.6.

Table 2.5: Number of samples collected for each age group and condition subjected to microarray analysis. The table shows how many subjects were in each age group, the mean age of the subjects in the age group and the standard deviation of the mean age.

Sample type	Number of subjects						Mean age in years						Standard Deviations					
	20s	30s	40s	50s	60s	70s	20s	30s	40s	50s	60s	70s	20s	30s	40s	50s	60s	70s
ARM Full thickness	30	24	25	26	25	25	22.4	32.1	42.5	51.8	62.2	71.6	1.5	1.5	1.2	1.5	1.5	1.5
BUTTOCK Full thickness	31	23	25	26	23	25	22.5	32.0	42.5	51.8	62.1	71.6	1.5	1.5	1.2	1.5	1.5	1.5
ARM epidermis	30	24	25	26	24	24	22.5	32.1	42.5	51.8	62.3	71.6	1.5	1.5	1.2	1.5	1.4	1.5
ARM dermis	30	24	25	25	24	24	22.5	32.1	42.5	51.8	62.3	71.6	1.5	1.5	1.2	1.5	1.4	1.5
BUTTOCK epidermis	30	22	25	26	24	25	22.5	32.2	42.5	51.8	62.3	71.6	1.5	1.5	1.2	1.5	1.4	1.5
BUTTOCK dermis	30	24	25	26	24	25	22.5	32.1	42.5	51.8	62.3	71.6	1.5	1.5	1.2	1.5	1.4	1.5

2.7.4 Preparation and processing of microarray chips

Transcriptomic analysis was performed using Affymetrix HG-U219 GeneChips (GeneTitan system) with one chip being used per sample. mRNA extraction, target cRNA synthesis, GeneChip analysis, and raw GeneChip data normalization was performed by Rachel Adams and Chelsea Combs (Procter and Gamble). Following hybridisation and washing of chips, microarray chips were scanned and the intensity calculations on the scanner pixel values were stored in CEL-files with a single representative intensity per feature. CEL-files were pre-processed by Quantile normalization and PLIER (proprietary Affymetrix algorithm) summarization using the algorithms default parameters to obtain a single signal expression value for a probe set. Normalization was completed across all of the GeneChips run in a batch.

2.7.5 Data extrapolation and quality control

GeneChip quality control, statistical analysis and summary of data (including calculations of p values and fold changes were carried out by Dionne Swift (Procter and Gamble). For each probe set, log2 transformed data were used to compare different age groups and estimate correlation between mRNA expression and age. The significance of correlation between expression and age was evaluated based on the Spearman's rank correlation. Preparation of excel documents specific for the author of this thesis, detailing both mean expression and statistical data for selected genes and data summaries were prepared by Robert L. Binder (Procter and Gamble).

2.7.6 Generation of mean expression plots

Mean expression plots for target genes of interest were prepared in excel by the author of this thesis using mean expression data from the probe sets targeting our genes of interest.

2.8 Female skin immunohistochemistry

2.8.1 Subjects

Three female subjects each were in the "young" and "old" data pools. A skin biopsy from the forearm and buttock of each female was collected by members of Procter and Gamble as detailed in 2.7.2. Skin was then fixed and processed for paraffin embedding by Procter and Gamble. Details of the ages of the female subjects are shown in table 2.7.

Table 2.6: Details of ages of female subjects. Shown in parentheses are the abbreviations used to indicate young photo-protected skin (Y-PP), old photo-protected skin (O-PP), young photo-exposed skin (Y-PE) and old photo-exposed skin (O-PE).

Young Buttock (Y-PP)	Old Buttock (O-PP)	Young Arm (Y-PE)	Old Arm (O-PE)
Young female 1= 21y	Old female 1= 60y	Young female 1= 21y	Old female 1= 60y
Young female 2= 22y	Old female 2- 64y	Young female 2= 22y	Old female 2- 64y
Young female 3= 21y	Old female 3= 65y	Young female 3= 21y	Old female 3= 65y

2.8.2 Sectioning of samples

Sections were prepared as for paraffin embedded mouse skin described in section 2.1.3. Due to the precious nature of the tissue, assistance with sectioning was provided by Dr Mathilde Roger.

2.8.3 Female skin histology

Skin sections were prepared for Haematoxylin and Eosin staining as described in 2.1.5. Herovici staining was also completed as described in 2.1.6.

2.8.4 Female skin Immunohistochemistry

Female paraffin embedded skin sections were prepared for antigen retrieval as described in 2.1.4. Antigen retrieval method was dependent on the target antigen and for collagen I, collagen IV, collagen VII, YAP1 and lamin B1 immunostaining. For these proteins, identical antigen retrieval methods, blocking for non-specific binding and antibodies were used as described in 2.3.1-2.3.4 and table 2.4 in section 2.3.4.

Additionally, human skin sections were stained with a mouse monoclonal Jol2 (anti Lamin A/C) primary antibody with details of conditions shown in table 2.8. The secondary antibody used for this staining was a Goat anti-mouse Alexa 568 IgG (Invitrogen- A-11004) used at a working dilution of 1:1000 and antibody diluents and incubation conditions for primary and secondary antibodies were completed as described for mice in 2.3.4. All slides were mounted in Vectashield mounting medium, coverslipped and edges were sealed with nail polish. Slides were left to dry overnight before imaging.

Table 2.7: Details of Jol2 antibody staining conditions

Antibody	Supplier	Antigen retrieval method:	Dilution
Jol2 (lamin A/C)	Produced in house	HIAR	1:25

2.8.5   Imaging and semi-quantitative analysis

Semi-quantitative protein analysis was performed to calculate protein amounts for the proteins in skin regions described in table 2.9. The nuclear to cytoplasmic ratio of YAP1 in epidermis was also assessed. To complete this analysis, skin from all of the female subjects listed in table 2.7 was used and 2 images each were taken from the photo-protected and photo-exposed skin samples for each of the 3 subjects in the "young" and "old" age groups.

Table 2.8: Proteins assessed in the semi-quantitative analysis of human skin and the detail of the region where the analysis was completed

Protein	Skin region assessed
Lamin B1	epidermis
Lamin A/C	epidermis
Collagen IV	Basement membrane of epidermis (not dermal vasculature)
Collagen VII	Basement membrane of epidermis
YAP1 (nuclear to cytoplasmic ratio)	epidermis

All images for analysis were taken using a Leica TCS SP5 CLSM using a 40x oil objective, and pinhole optimised to 1 airy unit. 1024 x 1024 pixel Z-stack images were captured at a scan speed of 400Hz and the z-depth for each stack was standardised at 3μm. Imaging conditions were kept constant for the young and aged photo-protected and photo-exposed samples generated for each protein of interest.

2.8.6   Lamin B1 and lamin A/C semi-quantitative analysis of protein expression in epidermis

Analysis of epidermal lamin B1 and lamin A/C expression was performed as for mouse epidermis described in 2.3.7. The average fluorescence intensity of the epidermal staining of 2 images from each skin sample (2 skin samples from 3 subjects in each condition make a total of 6 images per condition) were quantified in image J and the mean and standard deviation values for the young PP, young PE, old PP and old PE epidermal levels of lamin B1 and lamin A/C were generated computationally. Data values were collated in excel and significance between young and aged photo-exposed and young and aged photo-protected skin was assessed by un-paired t-testing in Microsoft Excel.

2.8.7   Collagen IV and collagen VII semi-quantitative analysis of protein expression in the basement membrane

Image processing using median filtering and background subtraction was performed in Image J. Semi-quantitative analysis of collagen IV and collagen VII was then calculated from the signal isolated at the basement membrane and was expressed as the average pixel intensity per

unit area of staining. Staining from 2 images from each skin sample (2 skin samples from 3 subjects in each condition make a total of 6 images per condition) were quantified and the mean and standard deviation values for the young PP, young PE, old PP and old PE collagen IV and collagen VII protein levels were generated computationally. Data values were collated in Microsoft Excel and significance between young and aged photo-exposed and young and aged photo-protected skin was assessed by un-paired t-testing in excel.

2.8.8 Mean epidermal YAP1 and Nuclear to cytoplasmic ratio of YAP1 in epidermis

Quantification of mean epidermal YAP1 was completed as for epidermal lamin B1 in mice, described in section 2.3.7. Epidermal YAP1 nuclear to cytoplasmic ratio calculations in female epidermis was performed as for mice in section 2.3.8. Data values were collated in Microsoft Excel using 2 skin samples from 3 subjects in each condition, making a total of 6 images per condition. The mean and standard deviation values for the young PP, young PE, old PP and old PE were generated computationally. The statistical significance between mean epidermal YAP1 and the mean nuclear:cytoplasmic ratio of YAP1 in young and aged photo-exposed and young and aged photo-protected skin was assessed by un-paired t-testing in Microsoft Excel.

Chapter 3: Identification of the skin ageing phenotype in C57BL/6 mice

3.1   Introduction

3.1.1   Benefits of the use of mice for ageing research

The laboratory mouse has proven to be a powerful tool in studies addressing the molecular mechanisms of ageing. Mice are ideal for biomedical research due to their relatively short lifespan, genetic tractability and varied strain availability (Vanhooren and Libert, 2013). Mouse models have been used to understand several of the factors contributing to ageing, like the role of diet, oxidative stress and genomic stability (Liao and Kennedy, 2014). Additionally, mouse models of age-related diseases like Progeria (Burtner and Kennedy, 2010) and Alzheimer's (Janus and Welzl, 2010) have been used to study these specific age-associated pathologies in more detail.

Various phenomena and mechanisms of skin aging have been verified by *in vivo* experimental data from rodent models, such as changes to the epidermal compartment during intrinsic ageing and the impact of UV exposure on dermal elastins (Hwang et al, 2011). Additionally, specific strains like hairless mice have advanced dermatological knowledge in the fields of wound healing, carcinogenesis and inflammation due the ease of process observation. Mice are also useful models for studying cutaneous aging because they eliminate problems associated with reliable sampling and effects of the environment that present confounding issues in human studies (Bhattacharyya and Thomas, 2004).

3.1.2 Mouse studies on epidermal ageing

Several previous studies looking at morphometric changes to the skin of ageing mice have been completed and in many of these, the epidermal compartment has been characterised in detail. There appears to be strain-specific differences in epidermal changes. For example, in hairless mice (Haratake et al, 1997) and in Balb/c mice (Farage et al, 2008), epidermal thinning has been observed to occur during ageing. Additionally, in the dorsal skin of CBA mice decreases in epidermal thickness and epidermal cell numbers with age were statistically significant, along with fewer pilosebaceous units being present in the skin of aged animals (Bhattacharyya and Thomas, 2004-see figure 3.1.1). However, in other strains such as C57BL/6N the number of epidermal cell layers and epidermal thickness have been shown to be constant between 1 mo and 22 mo animals, which suggests no significant change in epidermal thickness in these mice with age (Monteiro-Riviere et al, 1991). In a detailed study completed

by M.W Hill (1988) the epidermal thickness, epidermal cell density, and number of cells per mm of basement membrane were all found to decrease in C57B1/6NNia mice. However, none of these findings were statistically significant, suggesting only minor morphometric changes occurred in the epidermis of this strain during ageing.

Studies that examine the proliferative index of epidermal cells are also numerous, and have generally shown that epidermal proliferation decreases with age. In particular, this was observed in Swiss albino male mice (Cameron, IL, 1972) and C57/B16 mice (Giangreco et al, 2008). However, strain specific differences were also present in terms of changes to epidermal proliferation with age, as there was no decrease in the mitotic activity and DNA-labelling index of 20 mo Balb/c mice compared to 2 mo Balb/c mice (Farage et al, 2008). Limited data is available on epidermal cell size changes in ageing mice but Farage et al (2008) observed a decrease in cell size in aged Balb/c mice whereas Hill (1988) saw a small but non-significant increase in cell volume in C57B1/6NNia mice.
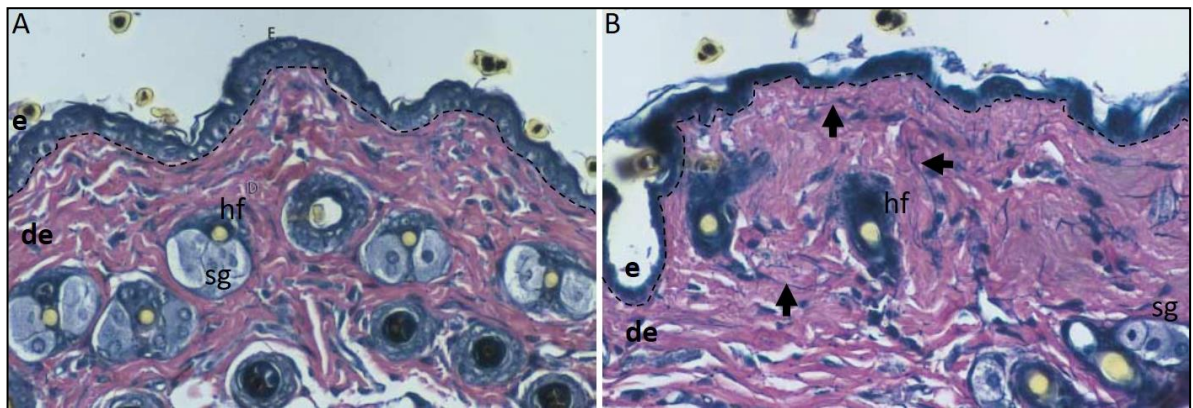
Figure 3.1.1: Images of back skin from CBA mice aged 1 mo (A) and 27 mo (B) stained with Verhoeff van Gieson stain for collagen (pink) and elastin (blue). Nuclei are stained dark purple. e=epidermis, de= dermis, hf= hair follicle, sg= sebaceous gland. Dotted line= DEJ. Original magnification x400. The authors identified epidermal thinning, fewer pilosebaceous units and an increase in elastin fibres (black arrows) in aged mice of this strain. Images from Bhattacharyya and Thomas, 2004.

3.1.3   Mouse studies on dermal ageing

The majority of studies concerning dermal ageing have been completed in rats not mice. Fornieri et al (1989) used electron microscopy to show that collagen bundles become dis-organised in aged rat dermis. They also observed a significant reduction in the percentage of collagen present in the dermis as well as atrophying of dermal cells. Collagen synthesis rates have also been shown to decline in this rodent model with age. In one study of changes in collagen synthesis and degradation in male Lewis rats between the ages of 1 and 24 months, collagen synthesis rates decreased by at least 10-fold in the 24 month animals compared to rates in 1-month old animals. Additionally, the proportion of newly synthesized collagen that was degraded in the skin was increased from 6.4% at 1 month of age to 56% at 15 months of

age, indicating modulation of both collagen synthesis and degradation mechanisms during rat skin ageing (Mays et al, 1991).

A report using hairless mice showed that total collagen synthesis in mouse skin expressed as the amount of hydroxyproline according to the wet weight was decreased by about 30% between 2 and 22 months of age. This study also found that the proportion of type I collagen to type III collagen increased with age from ~25% at 12 mo to 60% at 22 mo (Boyer et al, 1991). Giangreco et al, (2008) also reported changes to the dermal compartment with age, where they observed a decreased dermal thickness and increased subcutaneous fat layer in the back skin of aged C57/Bl6 mice (figure 3.1.2).
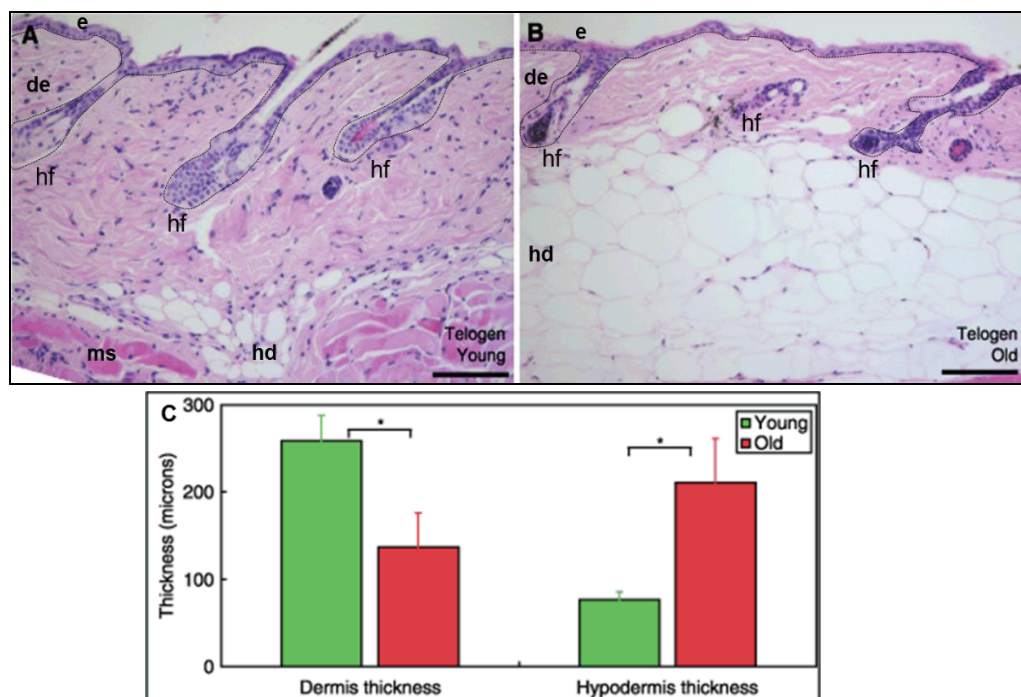
Figure 3.1.2: Age-associated changes in C57/Bl6 murine skin. (A, B) Haematoxylin-and-eosin-stained sections of young, 3 month (A) and old, 25 month (B) telogen dorsal skin. e= epidermis, de= dermis, hd= hypodermis, ms= muscle, hf= hair follicle. Dotted line =DEJ. Abnormal follicular architecture, dermal thinning, and hypodermal thickening are present in aged skin. Scale bars= 100μm. (C) Average dermis (measured from epidermis to hypodermis) and hypodermis (measured from dermis to underlying muscle) thickness in young (green) and old (red) mice. Dermal thickness significantly decreased in aged animals and hypodermal thickness increased (p< 0.05). Images from Giangreco et al, 2008.

3.1.4   Mice in Gerontological studies- Factors for consideration

Together previous reports on the epidermal and dermal studies completed on rodents show that age-related changes to the thickness and cellular content of the epidermis and ECM changes in the dermis occur with age. A clear drawback in these studies however, is a lack of systematic assessment of the same changes across multiple rodent strains. This is an issue because the mice or rats making up a single population of an in-bred strain are so genetically similar to one another that any conclusions drawn from single-strain studies provide evidence

for ageing changes in this genetic background only. Findings would therefore need to be cross-validated with other strains to identify if changes are ubiquitous to all mice (Masoro, E.J, 2000).

Additionally, no formal criterion for the defining age of a "young" or "aged" mouse has been established in the literature for several mouse strains, meaning that there is no agreement between researchers as to what constitutes a "young" or an "aged" mouse of a certain strain. Selection of suitable chronological ages for "young" and "aged" mice is made challenging by strain specific differences in lifespan, which additionally makes inter-strain comparisons in skin morphology at the same chronological age somewhat redundant.

Furthermore, there are general factors that should be considered in the design of gerontological studies using mice, such as their age, the genotype of the mouse, the financial resources available and the planned methods of data collection. As the goal of our research was to identify age-related changes, we wanted to avoid falsely mis-interpreting changes associated with early-life development or late-life disease. For our "young" age groups we therefore had mice of 3 mo and 12 mo, as they were fully developed and for our "old" age groups, we considered both 24 mo and 30 mo mice, with any mice presenting with tumours or pathological lesions as a result of old age being removed from the study. We also included 15 mo mice in our study because mice at interim life stages allow the trajectory of ageing changes over time to be studied in detail and also ensure that maturational effects that could last several months are separated from ageing effects (Nadon, N.L 2000).

In the design of gerontological studies, several animals are needed for statistically powerful observations, but the financial cost of animal maintenance increases as they continue to age. As previously identified, extremely aged animals are more likely to present with diseases that impact data quality. It is therefore more cost effective to use a population of animals that have been subjected to ageing processes, but not to the extent that the financial costs outweigh the benefits of the experiment (Miller and Nadon, 2000). This meant that although C57BL/6 mice can live up to 35 months of age in the laboratory, we decided not to use mice over the age of 30 mo in our analysis.

Finally, laboratory experiments should be carefully designed to take into account batch effects and other confounding errors. Experimental techniques should be performed on batches that include young and aged animals to ensure any differences are due to ageing, not experimental technique. Additionally, tissues should not be pooled during experimental preparations. Experimental work will have more statistical impact if the researcher is able to show age effects in several independent animals using several independent experiments than if they were to pool all the tissue and consider this a single biological replicate (Nadon, N.L 2006).

For this reason, we had 4 mice in each age group and considered data from each mouse separately in our analysis.

3.1.5 Research Objectives

Once we had selected suitable age groups and numbers of mice in which to implement our research, our objectives were to complete systematic studies that would allow us to characterise the skin ageing process in C57BL/6 skin in more detail. This would allow us to develop the information found in previous reports. We therefore aimed to:

1. Produce a morphometric characterisation of age-related changes in the epidermal and dermal compartments in the young, middle age and aged mice.

2. Use protein-based methods to identify changes to the dermal and basement membrane collagens with age.

3. Exploit electron microscopy (EM) in order to look at ultrastructural changes occurring at the dermo-epidermal junction during ageing.

4. Identify epidermal biomarkers of ageing using fluorescent immunohistochemistry.

5. Explore whether the Hippo Pathway effector YAP1 is modulated by the ageing process in the epidermis.

3.2 Morphometric assessment of intrinsic skin ageing in male C57BL/6 mice

3.2.1 Survival Curve for C57BL/6 mice

Figure 3.2.1 shows survival curves for both female and male C57BL/6J mice taken from Jackson Laboratory data [see footnote 1]. Compared to other inbred strains of mice, this strain is relatively long lived with the median lifespan being 28.9 months for females and 30.0 months for males (Yuan et al, 2009). After 15 months (m) there is a progressive decline in the percentage of mice surviving with less than 10% of males and females being alive after 35m. This suggests that the animals could show ageing phenotypes from around 15 mo to 30 mo. As very few mice are able to survive after 30 mo, it is likely that the health of any surviving mice after this time would be very poor.
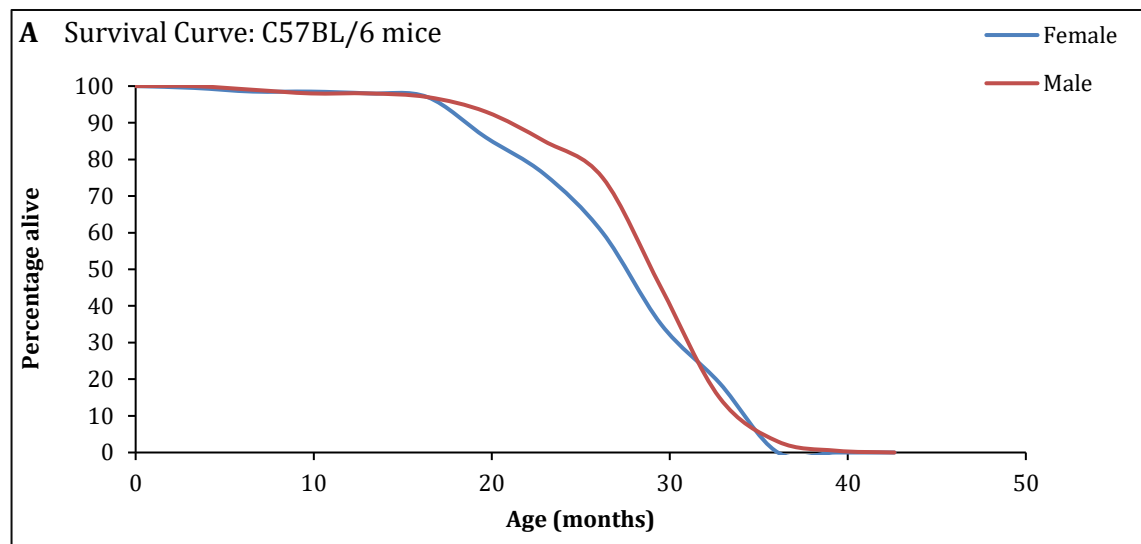
Figure 3.2.1: Representative survival curves for the C57BL/6 mouse strain adapted from the Jackson Laboratory website for male and female mice.

Taking into account the median lifespan and mortality over time for C57BL/6 males, we designed our study along the guidelines outlined in part 3.1.4 of this thesis. We therefore used young animals that had finished their development (3 mo), mice at early to middle age (12 mo and 15 mo), and aged mice (24 mo and 30 mo). The details of the mice used in our study are shown below in table 3.2.1.

Footnote 1: Graph adapted from https://www.jax.org/research-and-faculty/research-labs/the-harrison-lab/gerontology/available-data

Table 3.2.1: Details of the 5 mouse age groups used in our study

Age mouse (months-mo)	% survival (from plot)	Number used in study
3	100	4
12	99	4
15	98	4
24	78	4
30	30	4

3.2.2 Morphological characterisation of the skin of young, middle age and aged mice

To gain an understanding of how the skin presented histologically in the different age groups, sections of the skin taken from the back of each animal were stained with haematoxylin and eosin (H+E). Figure 3.2.2 shows that in the 3 mo animals (A, A'), the epidermis was several cells thick and the dermis was rich in both hair follicles and their accompanying sebaceous glands. Many cells also populated the dermal compartment, shown by the presence of several nuclei. At 12 mo (B, B'), the epidermis became thinner and was 1-2 cells thick in most regions. The dermis was still populated with several hair follicles, but the numbers of nuclei populating the dermal extracellular matrix (ECM) was reduced compared to 3 mo animals. The 15 mo skin (C, C') was similar to the 12 mo skin in terms of epidermal thickness and dermal cell numbers but by 24 mo (D, D'), the epidermis had thinned considerably (D'). At 30 mo (E, E') fewer hair follicles and cells were present in the dermal region compared to younger animals. Like the 24 mo animals, epidermal thinning was prominent (E') and in some areas of the epidermis cells were spaced further apart, leaving larger distances between the basal epidermal nuclei. These spaces were less frequent and extensive in 3 mo, 12 mo and 15 mo epidermis (black arrows D', E').

In the 3 mo animals basal epidermal (BE) nuclei were typically rounded, tightly packed, and regularly shaped (green arrowheads-A'). In the 24 mo and 30 mo animals, epidermal nuclei became less regularly arranged, less circular and had a greater variation in their size (green arrowheads- D', E').
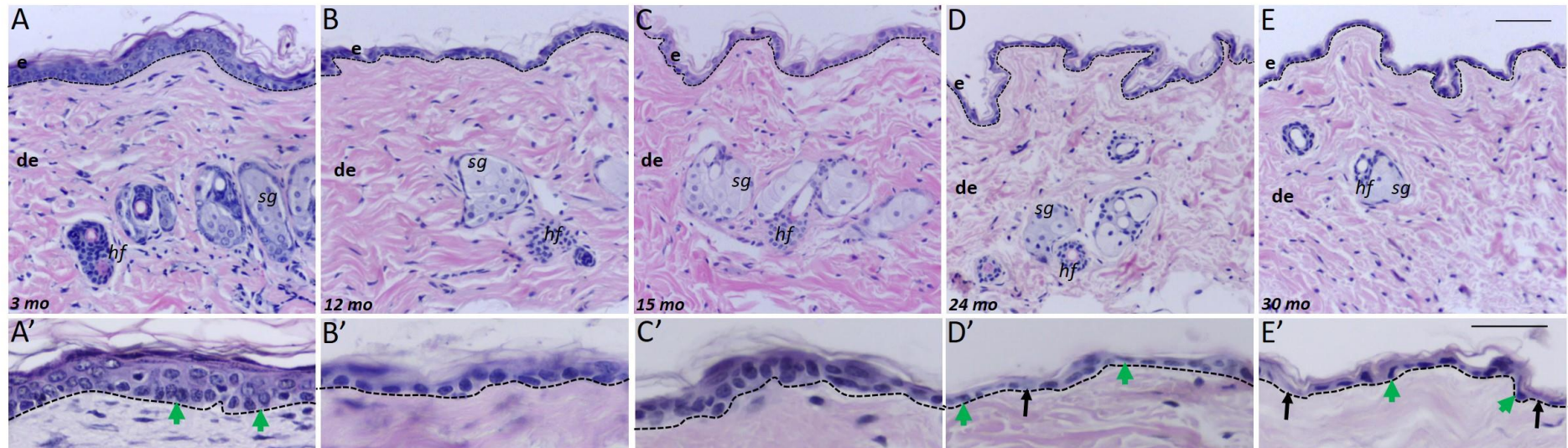
Figure 3.2.2: Low magnification representative light microscope images of H&E staining of mouse skin epidermis and dermis (A-E) taken using a 20x objective lens and high magnification images showing the epidermis, DEJ and papillary dermis (A'-E') taken using a 40x objective lens. Images are shown for mice at ages 3 months (A, A'), 12 months (B, B'), 15 months (C, C'), 24 months (D, D') and 30 months (E, E'). e= epidermis, de= dermis, hf= hair follicle, sg= sebaceous gland. Black dotted lines indicate the DEJ. Scale same for A-E. Scale bar shown in E = 100 μm. Scale same for A'-E'. Scale bar shown in E' = 50 μm. **Black** arrows show enlarged spaces between cells in the epidermis of aged animals. **Green** arrowheads show that BE nuclei become more irregular in 24 mo (D') and 30 mo (E') animals compared to 3 mo (A') animals.

3.2.3   Decline in dermal cellularity with age

As we had observed fewer nuclei in the dermal region of the aged skin samples, this was quantified to determine the extent of cellular loss in this area. In order to create un-biased analyses, we developed a grid system whereby equally spaced lines were placed perpendicular to the epidermis. Grids measuring 100 µm x 100 µm were placed to the right of the lines and the nuclei found within this area were counted.

This procedure was applied to 4 grids per image, ensuring that hair follicles and other appendages were omitted from the analysis. 4 images for each mouse in each age group were quantified, effectively meaning 16 measurements per mouse and 64 measurements per age group were taken. An example of this methodology applied to 3 mo and 30 mo skin is shown below in figure 3.2.3. An identical methodology was applied to all of the images in all of the age groups (3 mo, 12 mo, 15 mo, 24 mo and 30 mo mice). The data collected is shown in table 3.2.2 and figure 3.2.4.
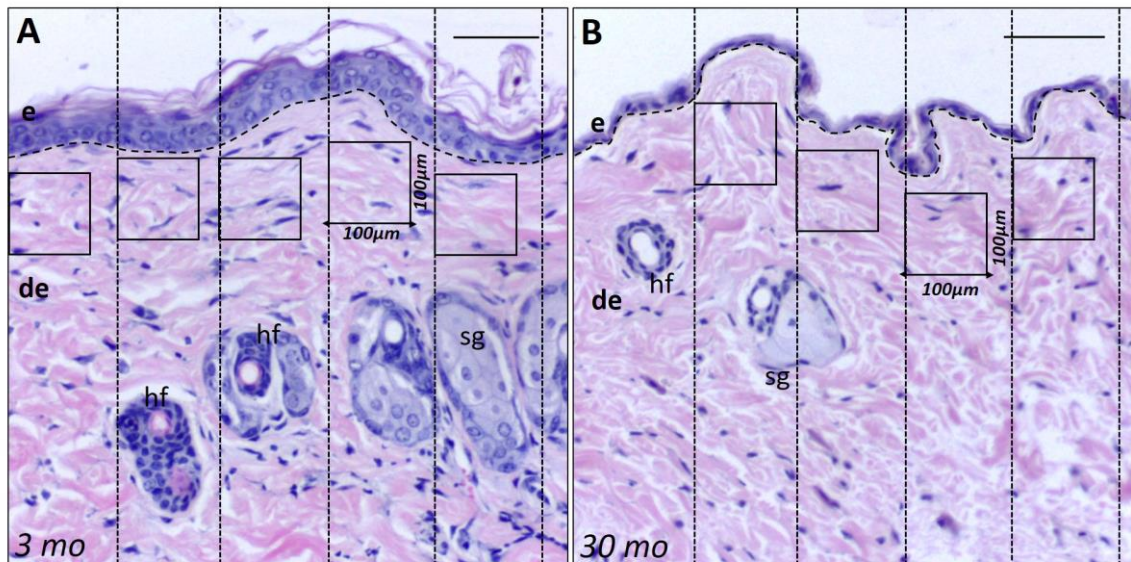
Figure 3.2.3.: Example of the grid system used to calculate the numbers of nuclei in the dermis of young (3 mo), middle aged (12 mo and 15 mo) and aged (24 mo and 30 mo) mice. A= 3 mo example, B= 30 mo examples of haematoxylin and eosin-stained skin images taken using a 20x objective lens on a light microscope. Vertical dotted lines indicate the grid system used to create un-biased points for data collection in the dermis, avoiding areas where appendages were present. Scale bar = 100 µm. Horizontal dotted line=DEJ. e= epidermis, de= dermis, hf= hair follicle, sg= sebaceous gland. Squares not to scale.

Table 3.2.2: Mean and standard deviation values for dermal cellularity in 3 mo, 12 mo, 15 mo, 24 mo and 30 mo mice

Mouse age	Mean dermal cellularity (number of cells per 10000 µm²)	Standard Deviation
3 month	19.280	8.313
12 month	10.815	3.195
15 month	13.540	1.616
24 month	10.830	3.361
30 month	8.415	1.345
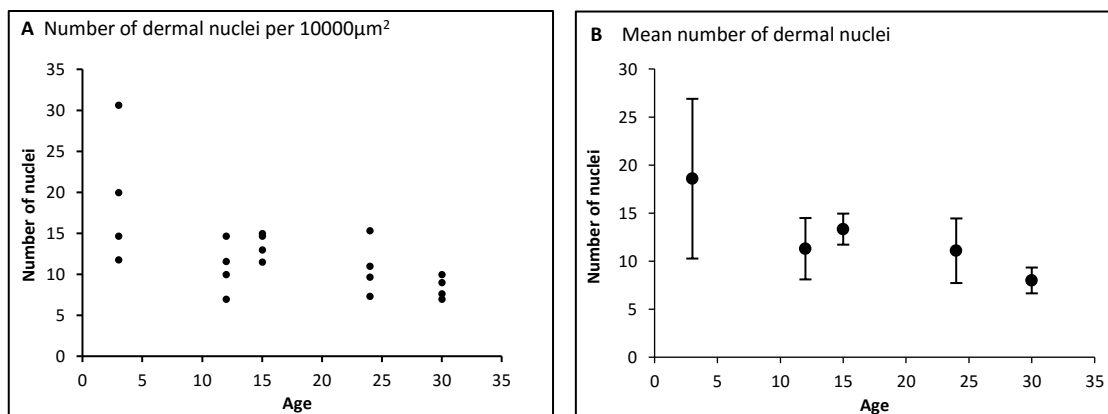
Figure 3.2.4: Counts of dermal nuclei in 3 mo, 12 mo, 15 mo, 24 mo and 30 mo mice. A= average dermal nuclei counts per 10000 μm² for each animal with each data point representing the data collected from 4 images for 1 mouse. Data point close in value show overlap in 15 mo animals. B= mean dermal nuclei per 10000 μm² in each age group. Error bars represent standard deviations calculated from the values for the 4 animals in each age group.

As table 3.2.2 and figure 3.2.4 show, the number of dermal nuclei decreased with age from 3 mo to 30 mo. At 3 mo dermal nuclei numbers were high, and varied considerably between animals. By 12 mo, fewer dermal nuclei were present in the dermis and the number of nuclei showed less variation between animals. The number of nuclei stayed approximately the same in the 12 mo, 15 mo and 24 mo animals before decreasing slightly in the 30 mo animals. By this stage, the variation in dermal nuclei numbers was very low.

One-way ANOVA was used to assess the statistical significance of dermal nuclei numbers between age groups. The ANOVA showed that the differences between the groups was statistically significant (p= 0.029). Post-hoc analysis using Holm-Sidak testing was then completed to identify between which age groups the significant differences occurred and the results are summarised in table 3.2.3. The table shows that significant differences in dermal cellularity occurred between 3 mo and 30 mo animals but none of the other age groups tested.

Table 3.2.3: Post-Hoc testing using Holm Sidak analysis. The only statistically significant difference in dermal cellularity was between 3 mo and 30 mo skin shown by green fill.

Comparison	Difference of Means	P	P<0.050
3 month vs. 30 month	10.865	0.030	Yes
3 month vs. 12 month	8.465	0.127	No
3 month vs. 24 month	8.450	0.115	No
3 month vs. 15 month	5.740	0.452	No
15 month vs. 30 month	5.125	0.527	No
15 month vs. 12 month	2.725	0.916	No
15 month vs. 24 month	2.710	0.864	No
24 month vs. 30 month	2.415	0.830	No
12 month vs. 30 month	2.400	0.696	No
24 month vs. 12 month	0.0150	0.996	No

3.2.4   Decline in epidermal cellularity with age

As we had observed in figure 3.2.2 that thinning occurred in the epidermis with age, we speculated that fewer cells would be present in the epidermis of aged animals. We therefore quantified the total number of nuclei per unit length of the epidermis. We used fluorescent images that were also collected to analyse YAP1 as the nuclear and cytoplasmic location (analyses presented later in thesis) of YAP1 in epidermal cells allowed all of the cells within the epidermal compartment to be clearly outlined. DAPI was used as a nuclear counterstain.

Nuclei from all layers of inter-follicular epidermis (IFE) were considered in this analysis and areas where hair follicles intersected with the epidermis were excluded. Figure 3.2.5 shows representative examples from 3 mo and 30 mo skin of the system used to score nuclei. The epidermal outline was identified by YAP1 staining (A, D). In the same area, nuclei were identified by DAPI staining (B, E). Counts of nuclei were made from merged images by measuring the dotted line located at the DEJ and counting the nuclei above within the epidermal boundary (individual nuclei shown by 'x'- C, F). Single channel images were used for reference when necessary- i.e. when distinguishing overlapping nuclei (white arrows- B, C, E, F).
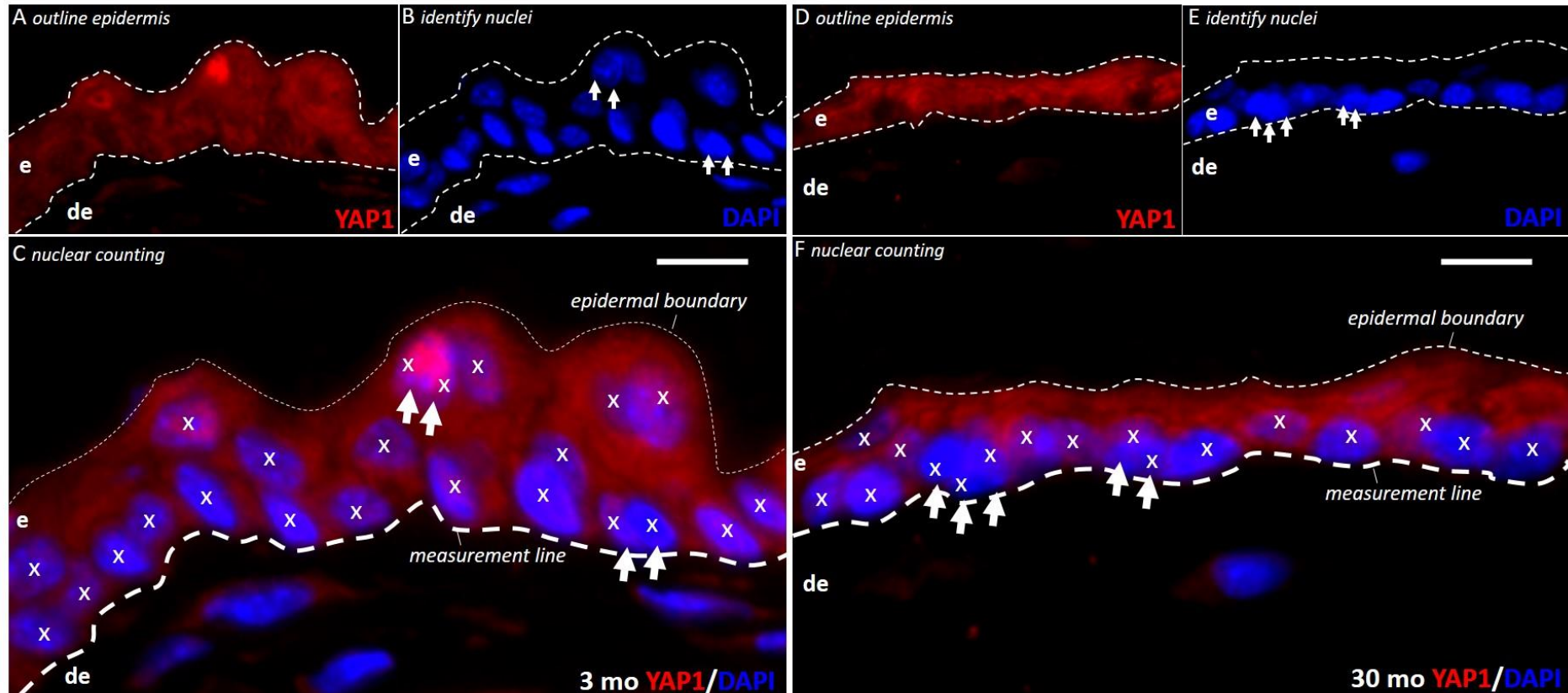
Figure 3.2.5: Representative examples of epidermal cell counting analysis using YAP1 primary antibody, Alexa 568 secondary antibody and DAPI nuclear counterstain in 3 mo (A,B,C) and 30 mo (D,E,F) mice. Images were taken using a Zeiss fluorescence microscope and 40x objective lens. e=epidermis, de= dermis, dotted line above de- DEJ, dotted line above e= epidermal boundary. A+D= YAP1 single channel, B+E= DAPI single channel, C+F=merged image. Scale bar (panel C and F) = 20 µm, and scale was identical for all images. x= denotes a single nucleus. White arrows= overlapping nuclei. Thick dotted line in C+F shows the measurement line used to measure length of epidermis. Fine dotted line shows epidermal boundary. Any cells falling outside of the two boundaries were excluded from the counts.

The methodology shown in figure 3.2.5 was applied to 6 images from each of the 4 mice in the 3 mo, 12 mo, 15 mo, 24 mo and 30 mo age groups. Results of the nuclei counted were expressed as the number of epidermal nuclei per 100 μm of the DEJ. The results of this analysis are shown in figure 3.2.6 and table 3.2.4.
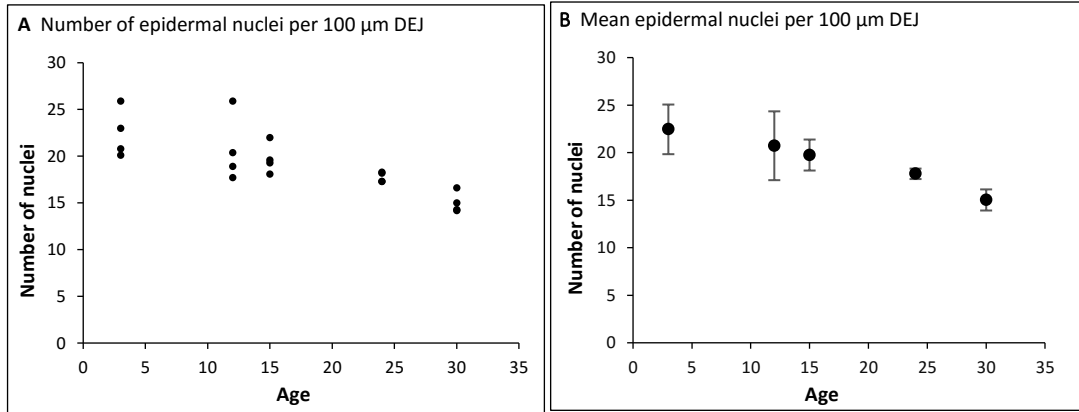
Figure 3.2.6: Counts of epidermal nuclei in 3 mo, 12 mo, 15 mo, 24 mo and 30 mo old mice per 100 μm of basement membrane. 4 mice in each age group. A= epidermal nuclei counts for each animal with each data point representing data collected from 6 images in 1 mouse. Data points close in value in 15 mo, 24 mo and 30 mo show overlap. B= mean number of nuclei per 100 μm of dermal-epidermal junction (DEJ). Error bars represent standard deviations calculated from the values for the 4 animals in each age group.

Table 3.2.4: Mean epidermal cellularity and standard deviation values for 3 mo, 12 mo, 15 mo, 24 mo and 30 mo mice.

Mouse age	Mean epidermal cellularity (number of cells per 100 μm of DEJ)	Standard Deviation
3 month	22.450	2.611
12 month	20.725	3.622
15 month	19.750	1.634
24 month	17.775	0.550
30 month	15.025	1.109

Figure 3.2.6 and table 3.2.4 show that epidermal cell numbers steadily declined with age in the mouse IFE. The greatest variation in cell numbers per 100 μm of DEJ occurred in the 3 mo and 12 mo animals. One-way ANOVA analysis on the data indicated that the differences between epidermal cell numbers in the age groups was highly significant (p= 0.003). Post-hoc analysis using Holm Sidak testing showed that this decline in cell number was highly significant between 3 mo and 30 mo animals (p=0.002) and significant between 12 mo and 30 mo animals (green fill- table 3.2.5).

Table 3.2.5: Holm-Sidak post-hoc analysis of the one way ANOVA assessing epidermal cellularity in the mouse age groups. The analysis indicates statistically significant differences occurred between 3 mo vs 30 mo and 12 mo vs 30 mo age groups.

Comparison	Difference of Means	P	P<0.050
3 month vs. 30 month	7.425	0.002	Yes
12 month vs. 30 month	5.700	0.020	Yes
15 month vs. 30 month	4.725	0.064	No
3 month vs. 24 month	4.675	0.060	No
12 month vs. 24 month	2.950	0.382	No
24 month vs. 30 month	2.750	0.400	No
3 month vs. 15 month	2.700	0.352	No
15 month vs. 24 month	1.975	0.531	No
3 month vs. 12 month	1.725	0.488	No
12 month vs. 15 month	0.975	0.540	No

To express the significant decreases in cell numbers numerically, the percentage decrease of epidermal nuclei was calculated in the 3 mo vs 30 mo and 12 mo vs 30 mo animals. Compared to the 3 mo animals, the 30 mo animals had 33.2% fewer IFE cells and compared to the 12 mo animals they had 25.5 % fewer cells. These numbers suggest that the ageing process can reduce IFE cell numbers by up to a third.

3.2.5   Loss of basal epidermal nuclei with age

The basal layer of the epidermis is the region where epidermal proliferation occurs, and is the epidermal layer where keratinocyte stem cells reside and make an active contribution to epidermal cell numbers (Charruyer et al, 2009). As we had observed the increased presence of inter-nuclear gaps between cells in the epidermis of aged skin (figure 3.2.2 D' and E') and also a loss of epidermal cellularity (figure 3.2.6 A and B), we sought to determine whether this loss was caused by a reduced cellular presence in the basal epidermal layer.

Keratinocytes are not the sole cellular population within the epidermis, as melanocytes, Merkel and Langerhans cells are also present in this region. Keratinocytes, however, form the vast majority of the cellular population, constituting over 95% of the epidermal cellular presence (Barker et al, 1991). So although we did not formally distinguish keratinocytes from other epidermal cells, it was likely that observations of cellular loss in this layer could represent depletion of at least some of the keratinocyte population residing here as they make up such a large proportion of the resident cells. To complete this analysis, we counted the number of basal epidermal nuclei interacting with the basement membrane (BM) along a certain length. We used collagen IV immunofluorescence staining to identify the BM and DAPI to identify nuclei. Figure 3.2.7 shows an example of our methodology in 3 mo and 30 mo skin.
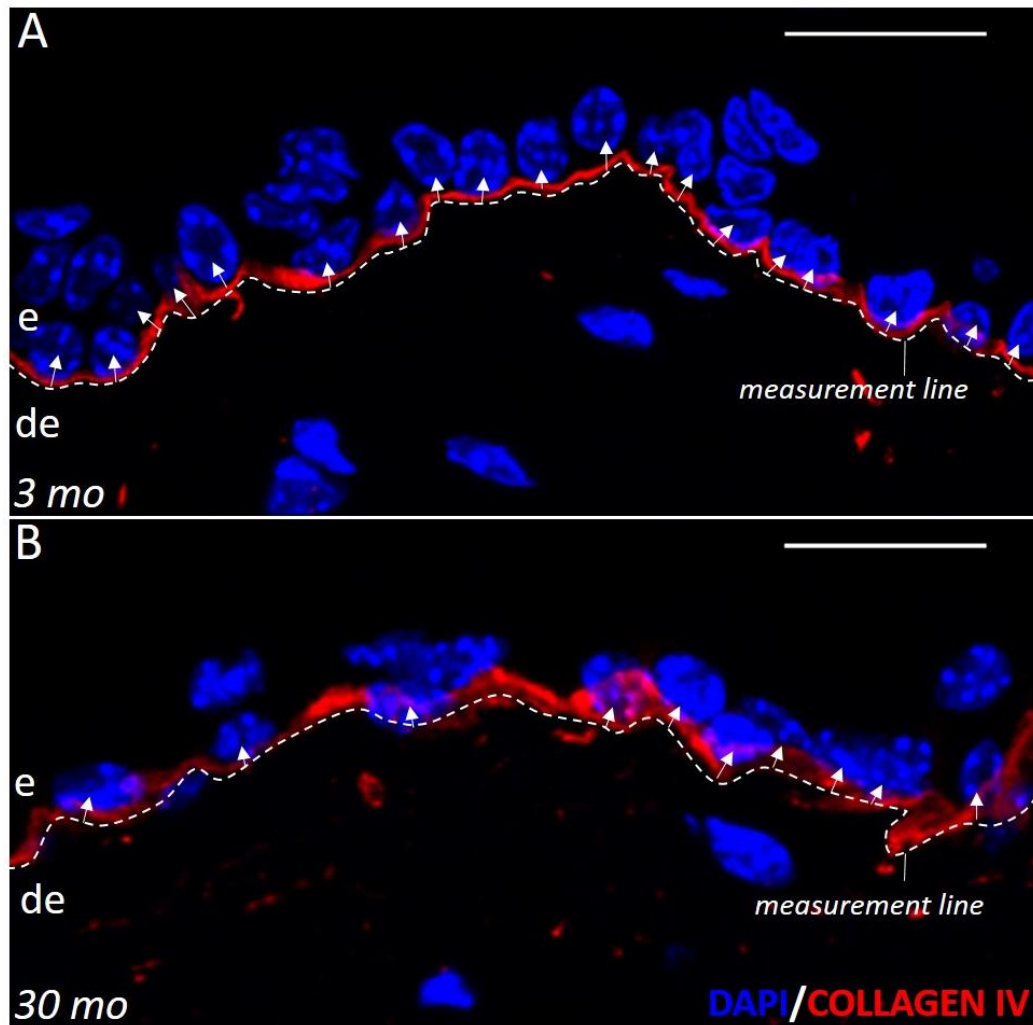
Figure 3.2.7: Example images taken using a fluorescent microscope and 40x objective lens from 3 mo (A) and 30 mo (B) mice showing how nuclei along the BM were counted. Collagen IV primary antibody indirectly conjugated to Alexa 568 secondary antibody was used to mark the BM. Nuclei were counterstained with DAPI. White dotted line at DEJ= measurement line of BM length. White arrows represent nuclei counted along the measurement line. e=epidermis, de=dermis. Scale bars= 20 μm.

Along with 3 mo and 30 mo skin, an identical methodology was applied to 12 mo, 15 mo and 24 mo age groups with 4 images being taken for each mouse using a fluorescent microscope and 40x objective lens. The entire basement membrane and nuclei in the field of view of each image were measured. Areas where hair follicles intersected with the IF epidermis were omitted. The data collected is shown in figure 3.2.8 and table 3.2.6.
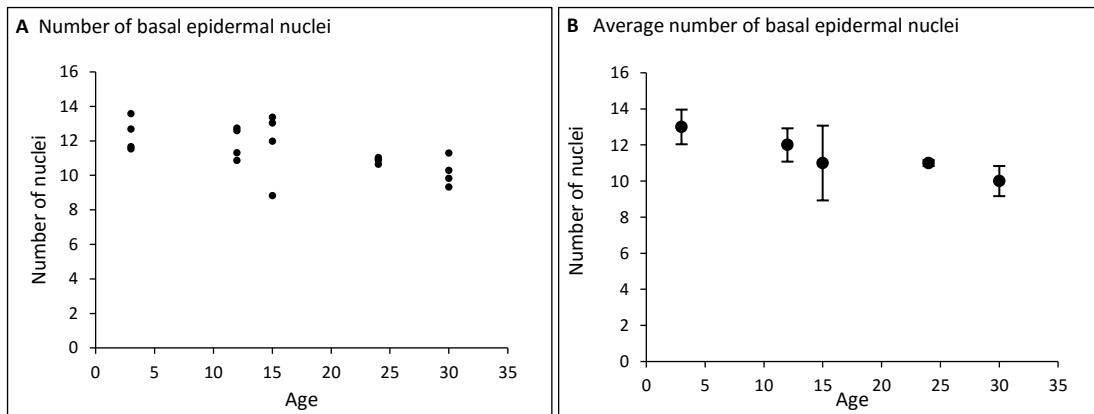
Figure 3.2.8: Number of basal epidermal cells in 3 mo, 12 mo, 15 mo, 24 mo and 30 mo old mice. 4 mice in each age group. A= plots of average number of nuclei per 100 µm of basement membrane in each mouse with each marker representing the average of 4 images. Data points close in value show overlap in 24 mo animals. B= Plots of average number of nuclei per 100 µm of basement membrane within each age group. Error bars represent standard deviations calculated from the values for the 4 animals in each age group.

Table 3.2.6: Mean basal epidermal nuclei and standard deviation values for 3 mo, 12 mo, 15 mo, 24 mo and 30 mo mice. *We observed that the variation in basal layer nuclei numbers was much higher in the 15 mo animals

Age Group	Mean number of basal layer nuclei (per 100 µm of BM)	Standard Deviation
3 month	12.383	0.961
12 month	11.893	0.923
15 month	11.820	2.072*
24 month	10.890	0.166
30 month	10.195	0.834

Figure 3.2.8 and table 3.2.6 show that the number of basal epidermal nuclei decreased with age. One-way ANOVA analysis assessing the differences between all of the age groups indicated that these observed decreases were not statistically significant (p= 0.110). However, one anomaly in the data was seen in the 15 mo animals. 3 out of the 4 animals assessed had basal layer nuclei values similar to the 3 mo and 12 mo animals and some of these values were greater than the 12 mo animals (figure 3.2.8- A). There was one 15 mo animal,which had a very low number of basal layer nuclei even smaller than the mean value generated from the 30 mo animals. This resulted in a very high standard deviation value in the 15 mo age group, which would have impacted subsequent downstream statistical testing. To account for this, we also completed an ANOVA test where the 15 mo animals were omitted from the analysis. This test did show that there were significant differences between the 3 mo, 12 mo, 24 mo and 30 mo age groups (p=0.009), which are summarised in table 3.2.7 below.

Table 3.2.7: Holm-Sidak post-hoc analysis of the one way ANOVA assessing numbers of basal epidermal nuclei in the mouse age groups with the data from 15 mo animals excluded. The analysis indicates that a statistically significant differences occurred between 3 mo vs 30 mo age groups (green fill) and that the difference between 12 mo vs 30 mo age groups was close to significance (*).

Comparison	Difference of means	P	P<0.050
3 month vs. 30 month	2.188	0.012	Yes
12 month vs. 30 month	1.697	0.051*	No
3 month vs. 24 month	1.492	0.079	No
12 month vs. 24 month	1.002	0.266	No
24 month vs. 30 month	0.695	0.419	No
3 month vs. 12 month	0.490	0.398	No

3.2.6   Epidermal thinning

As we had observed epidermal thinning with age in the mice (figure 3.2.2 A'-E'), we quantified this. We again used an un-biased approach by taking measurements at equidistant points in the epidermis. Figure 3.2.9 shows how we collected our data using an example using images of 3 mo and 30 mo skin. Measurement lines (m) were drawn at a perpendicular angle from the DEJ (dotted line) to the outermost cells of the granular layer (dotted line- upper epidermis). The stratum corneum (SC) was not included in analysis as it had been lost in the processing of some samples. This methodology was applied to 3 mo, 12 mo, 15 mo, 24 mo and 30 mo mice with 2 images for each mouse and an average of ~10 measurements taken per image. This makes a total of approximately 20 measurements per mouse and 80 per age group. The results of the analysis are shown in table 3.2.8 and figure 3.2.10.
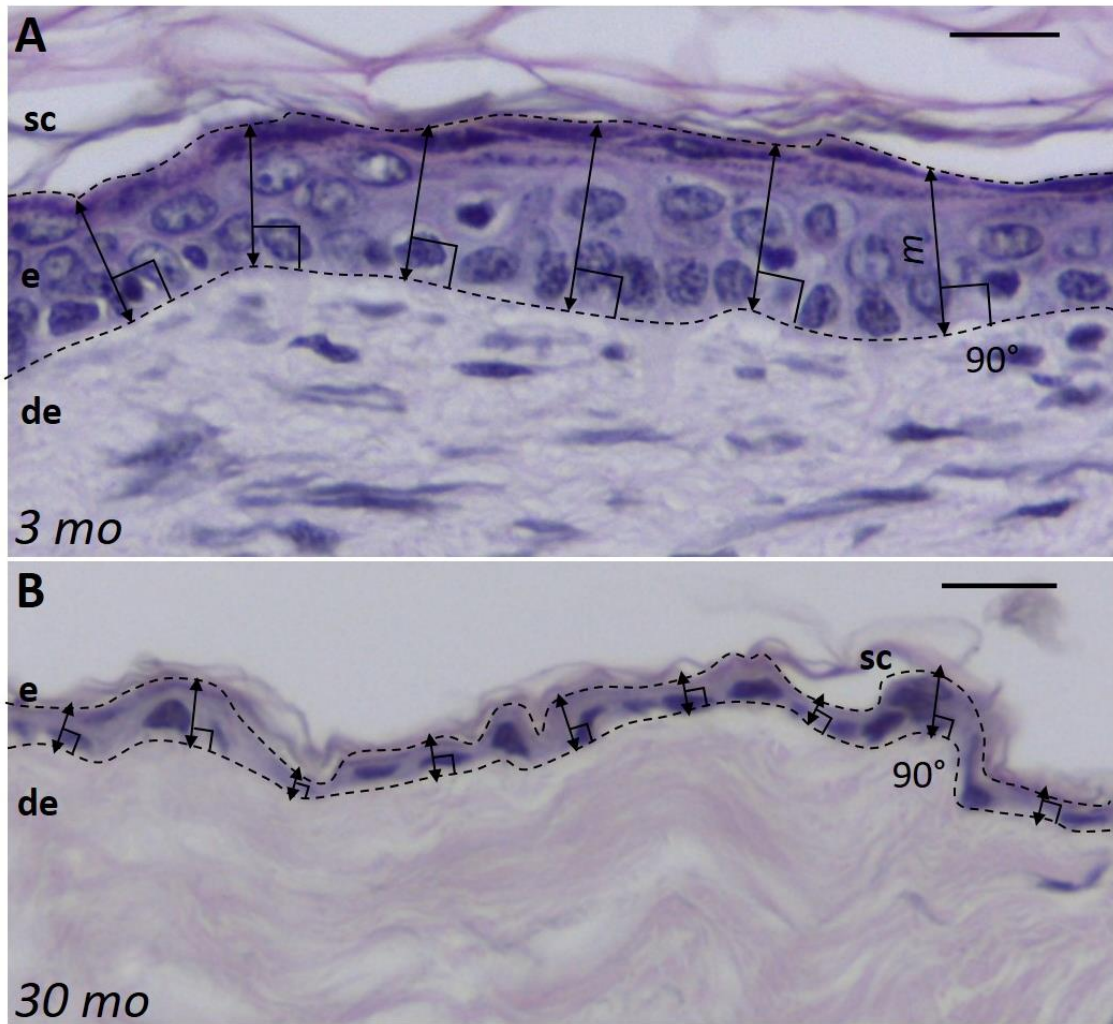
Figure 3.2.9: Representative example of data collection for epidermal thickness measurements using images of haematoxylin and eosin stained 3 mo (A) and 30 mo (B) skin taken using a light microscope and 40x objective lens. Scale bars= 20 μm. e= epidermis, de= dermis, sc= stratum corneum. Measurements (m) were made at equidistant points from the DEJ (lower dotted line) to the granular layer (upper dotted line).

Table 3.2.8: Mean IFE thickness and standard deviation values for 3 mo, 12 mo, 15 mo, 24 mo and 30 mo mice. *samples in this age group failed to show equal variance.

Age Group	Mean epidermal thickness	Standard Deviation
3 month*	17.67	5.34*
12 month	8.85	0.91
15 month	11.63	2.32
24 month	7.82	2.03
30 month	6.52	0.42
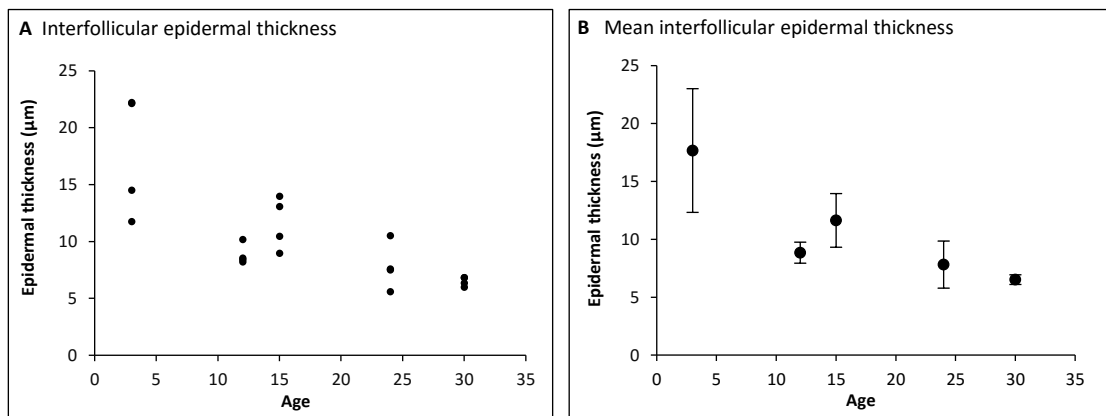
Figure 3.2.10: Epidermal thickness measurements in 3 mo, 12 mo, 15 mo, 24 mo and 30 mo mice with 4 animals per age group. A= measurements for each animal with each data point representing data collected from 2 images per mouse. Data points close in value show overlap in 3 mo, 12 mo, 24 mo and 30 mo animals. B= mean IFE thickness. Error bars represent standard deviations calculated from the values for the 4 animals in each age group.

Figure 3.2.10 and table 3.2.8 show that the mean and standard deviation values for IFE thickness in 3 mo animals was very high, indicating a large variation in epidermal thickness in these animals. Two of the animals had a very high epidermal thickness at around 22 μm (overlapping data points, A) whereas the other two 3 mo animals had a thinner epidermis. The variation in epidermal thickness in 15 mo animals was also high. Overall mean IFE thickness decreased with age from 12 mo to 30 mo. Unexpectedly, 15 mo animals had a larger mean epidermal thickness than 12 mo animals. It was also apparent that the most marked decreases in epidermal thickness occurred early on in life between 3 mo and 12 mo animals.

One way ANOVA testing involves working by the assumption that the variance in all of the populations being compared to one another are equal. Prior to ANOVA testing, data from each of the age groups within the mice is therefore subjected to Levene's testing for equal variance (Levene, 1960). Due to the dramatic skew in variation of IFE thickness shown in the 3 mo animals, the data from 3 mo animals failed to show equal variance by this test.

The hair follicle cycle (HFC) of C57BL/6 mice is known to impact epidermal thickness (Chase and Eaton, 1959). The first two hair follicle cycle's following birth are highly synchronized, and occur when the mice are approximately 4 weeks and 12 weeks old (Müller-Röver et al, 2001). It is therefore likely that some of the 3 mo animals in this study had actively cycling hair follicles. To explore this further, sections of the 3 mo animals were examined to determine rough hair follicle cycle stages in relation to the epidermal thickness. This was made possible by the fact that follicle stages in mice are histologically distinct from one another (Paus and Cotsarelis, 1999). Examples of how we classified the hair follicles in the skin of mice of various ages is shown in figure 3.2.11.

In several of the 3 mo animals we observed actively growing (anagen) hair follicles which showed enlarged structures that extended deep into the dermis (black arrows-A= longitudinal view of HF). In some cases follicles had extended into the hypodermis, and showed a large, rounded morphology (black arrows and brackets- B=transverse views of anagen follicles in 3 mo skin). In the 12 mo animals the majority of hair follicles in the mice were in telogen and they were reduced in size and length compared to the actively growing follicles seen in the 3 mo mice (C= Longitudinal view of telogen follicles in 12 mo mice). In the 15 mo mice some of the animals had catagen and late anagen follicles but the majority were in telogen and the number of anagen follicles was not as extensive or uniform as those seen in the 3 mo animals (data not shown).

In the 24 mo and 30 mo mice almost all of the hair follicles were in telogen, suggesting that few hair follicles were actively cycling in the aged mice (D= longitudinal and transverse views of telogen follicles in 30 mo mice) (black arrows and brackets, D). From these observations it appeared that the 3 mo animals had the greatest numbers of actively cycling hair follicles and when the hair follicle stage of the skin was considered alongside epidermal thickness values, it was clear that the hair follicle stage impacted epidermal thickness (table 3.2.9).
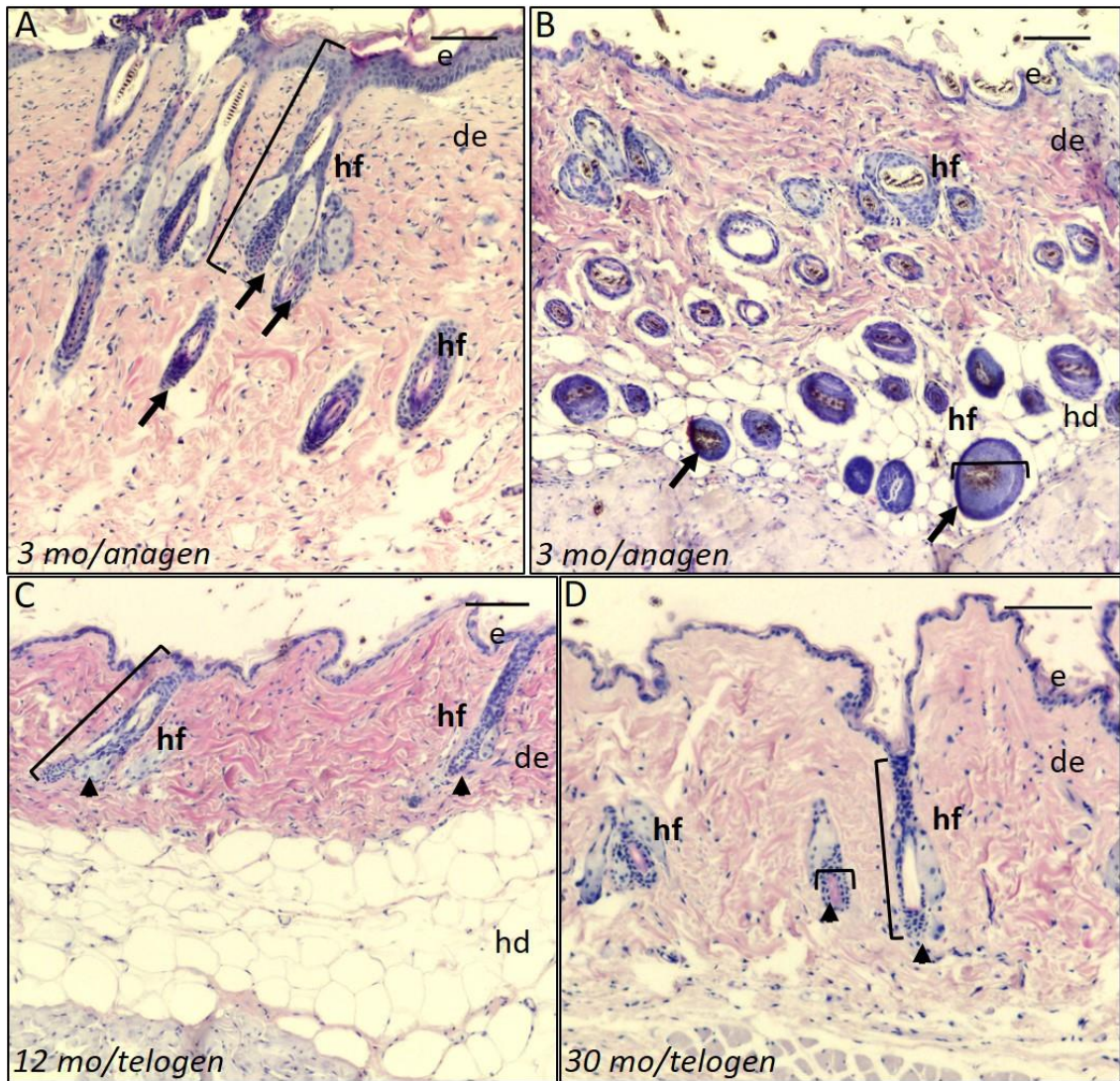
Figure 3.2.11: Classification of hair follicle staging in the skin of mice. Images A-D show Haematoxylin and Eosin staining of C57BL/6 back skin in 3 mo (A, B), 12 mo (C) and 30 mo (D) skin. Images were captured using a light microscope with 10x objective lens. A= longitudinal view of anagen follicles in 3 mo skin showing show enlarged structures that extend deep into the dermis (black arrows-A). B=Transverse views of anagen follicles in 3 mo skin show some follicles had extended into the hypodermis and show a large, rounded morphology (black arrows and brackets- B). C= longitudinal view of telogen follicles in 12 mo mice show that they are reduced in size compared to the 3 mo anagen follicles and do not extend into the hypodermis (black arrows and brackets, C). D= longitudinal and transverse views of telogen follicles in 30 mo mice showing reduced length and thickness compared to anagen follicles in 3 mo mice (black arrows and brackets, D). e=epidermis, de= dermis, hd= hypodermis, hf= hair follicle. Scale bars all 100 µm.

Table 3.2.9: Hair follicle stages of the 3 mo month mice used in this study.

Mouse ID#	Hair follicle stage	Mean epidermal thickness
H3464	Many HF in anagen. Some in catagen	22.15
4273BN	Most in anagen	22.24
42722LN	Most HF in telogen.	11.76
4273RN	Some in catagen. Some telogen	14.53

The data in table 3.2.9 indicates that the actively cycling follicles caused increased epidermal thickness, which is consistent with previous reports in mouse (Hansen et al, 1984). After 12 weeks of age, hair follicle cycles in mice become less synchronised, and occur in distinct domains across the body (Plikus et al, 2008). Hair follicle cycles also become less regular with increasing age and aged animals typically have few actively growing hair follicles (Chen et al, 2014). This suggests that the hair follicle cycle would be less of a confounding issue for data collected from later-stage animals. As our analyses from 12 mo, 15 mo, 24 mo and 30 mo skin sections showed that the majority of hair follicle's in these animals were in telogen phase, this meant that across the 12-30 mo age groups, variation in epidermal thickness was much less likely to occur due to the activity of hair follicles in the mouse skin.

The IFE thickness data from the 3 mo mice was highly variable due to the mice being in different stages of the hair follicle cycle, so it could confound the analysis of change in IFE thickness with age. This confounding factor coupled with the fact that the data from 3 mo mice did not show equal variance, meant that this age group was omitted from the subsequent one way ANOVA analysis. 12 mo animals are still relatively young, and so the assessment of change in inter-follicular epidermal thickness with age using these animals as the youngest age group was still a worthwhile analysis. Table 3.2.10 shows the results of the ANOVA, which indicated a statistically significant change occurred with age (p=0.029). Post-hoc testing showed that significant differences in IFE thickness occurred between 15 mo and 30 mo animals and 15 mo and 24 mo animals. This indicated that from our analyses, the IFE thickness significantly decreased with age between these age groups only.

Table 3.2.10: Results of ANOVA analysis and Holm-Sidak post-hoc testing for assessment of change in IFE thickness in the different age groups.

Comparison	Difference of Means	P	P<0.050
15 month vs. 30 month	4.007	0.009	Yes
15 month vs. 24 month	3.083	0.048	Yes
15 month vs. 12 month	2.118	0.225	No
12 month vs. 30 month	1.889	0.251	No
12 month vs. 24 month	0.966	0.607	No
24 month vs. 30 month	0.923	0.394	No

3.2.7   Alteration of markers of terminal differentiation in aged epidermis

Our previous observations of loss of epidermal cells in aged skin and epidermal thinning prompted us to explore the epidermal region in more detail. We therefore assessed if any changes occurred in the protein levels of specific keratinocyte cytoskeletal markers in the basal layer (keratin 14) and spinous layer (keratin 10) of the epidermis. Additionally, we looked at changes in the expression of loricrin, which is expressed in the superficial granular layers of skin and is the primary constituent (~70% of the total protein) of the cornified envelope (CE) (Nithya et al, 2015).

To confirm the specificity of our antibodies, we completed Western blotting of whole skin lysates using rabbit antibodies against K10, K14 and loricrin. Additionally, we blotted skin lysates for E-cadherin, as this cell-cell adherens junction protein is expressed by all cells in the epidermal layers of mice (Tunggal et al, 2005). Figure 3.2.12 shows the results of these blots in 3 biological replicates each of 3 mo and 30 mo animals. Bands for E-cadherin (135kDa), keratin 10 (60kDa), keratin 14 (52kDa) and loricrin (26kDa) were observed at their predicted molecular weights.

In the 3 mo and 30 mo animals, there was clear variation in the levels of E-cadherin, and particularly within the young animals. The variation in the young animals was to be expected, given that we had observed large variation in epidermal thickness in our histological analysis of 3 mo old mouse skin samples. Overall E-cadherin expression was reduced in the 30 mo animals, and in one sample detection was almost negligible. This observation is consistent with our reports of both a loss of epidermal cellularity and epidermal thinning, and indicates that the epidermal compartment forms a smaller proportion of the whole skin in aged animals.

Keratin 10 expression was only slightly reduced in the 30 mo animals compared to the 3 mo, and given that overall epidermal cellularity is reduced and the epidermis is proportionally thinner in the 30 mo animals, this suggests that cells of the spinous layer are mostly maintained in the aged epidermis despite overall cellular loss from this area. Keratin 14 expression was generally higher in the 30 mo compared to 3 mo animals, which suggests that cells of the basal layer are preferentially retained in the aged epidermis, thus making up a greater proportion of the whole epidermis in young compared to aged animals.

Loricrin protein expression was drastically decreased in all of the 30 mo biological replicates compared to the technical replicates, indicating that the main protein of the cornified envelope was reduced in the whole skin of 30 mo animals.
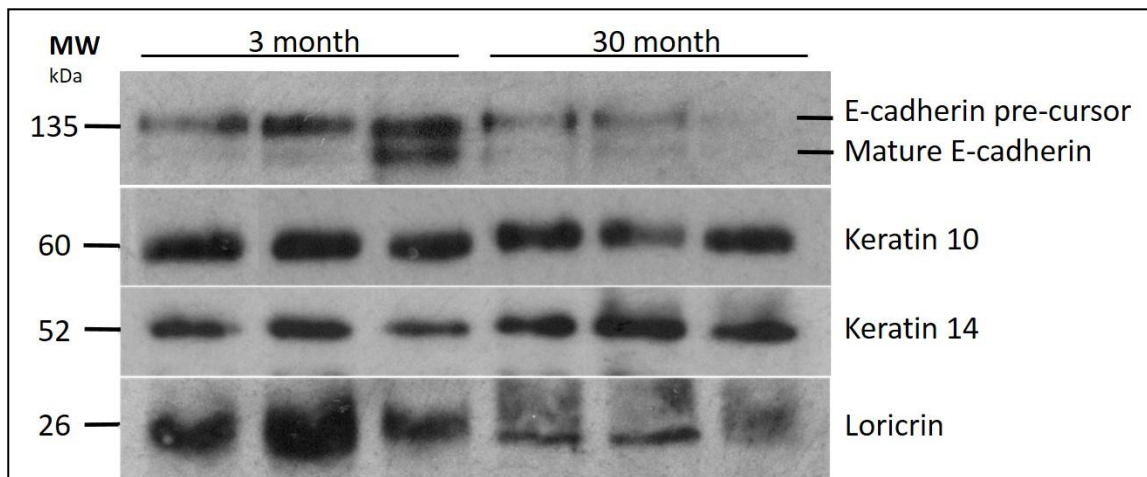
Figure 3.2.12: Protein expression of epidermal differentiation and cell junction markers in whole skin lysates of young 3 month and aged 30 month mice. 3 biological replicates each for young, and aged mice were used to complete Western blots of E-cadherin, K10, K14 and loricrin after SDS-PAGE. E-cadherin bands indicate both the precursor (upper band) and mature (lower band) form of E-cadherin (Geng et al, 2012).

As our Western blotting had indicated stoichiometric changes in the levels of epidermal differentiation proteins between 3 mo and 30 mo animals, we used fluorescence immunohistochemistry to visualize the arrangement of K14, K10 and loricrin expression in 3 mo, 12 mo, 15 mo, 24 mo and 30 mo epidermis to determine the extent of their change in expression over time. Figure 3.2.13 shows the results of the staining on paraformaldehyde-fixed, paraffin embedded mouse skin subjected to citrate-based heat-induced antigen retrieval and antibody staining with the same antibodies used in the Western blots.

Keratin 14 (K14) expression was prominent in the cells of the basal layer of epidermis from all age groups, but as the proportion of cells in the overall epidermis was reduced over time, the cells expressing K14 in the aged epidermis (D, E) occupied the majority of the cells within the epidermal compartment. This observation was consistent with our Western blotting data, as K14 expression was greater in the whole skin lysates of aged 30 mo animals compared to 3 mo because proportionally, its expression within the epidermis as a whole becomes greater with age. Additionally, the basal epidermal cells showed a change in their arrangement along the basal layer with age. In the 3 mo animals, the DAPI and K14 staining showed that the oval nuclei and surrounding cell body adopted a vertical polarity (yellow arrow, A) whereas in the 30 mo animals the nuclei had a horizontal polarity, and appeared to be spread horizontally along the basement membrane (yellow arrow, C).

Keratin 10 (K10) expression was seen in several cellular layers in the young 3 mo and 12 mo skin (yellow double arrows, A, B') but with age, its expression was reduced to a single layer in the outer epidermis (yellow double arrow, E'). Loricrin expression was prominent in the outer epidermis of 3 mo, 12 mo, 15 mo and 24 mo animals but in 30 mo skin, absence of loricrin was

seen in areas indicating that loss of this protein had occurred in some areas of the outer epidermis of the oldest 30 mo animals (yellow arrows, E''). Our observations of protein expression of K10 and loricrin here are therefore also consistent with the previous Western blots, which showed that keratin 10 expression showed a marginal reduction whereas loricrin was reduced overall in 30 mo, compared to 3 mo whole skin.
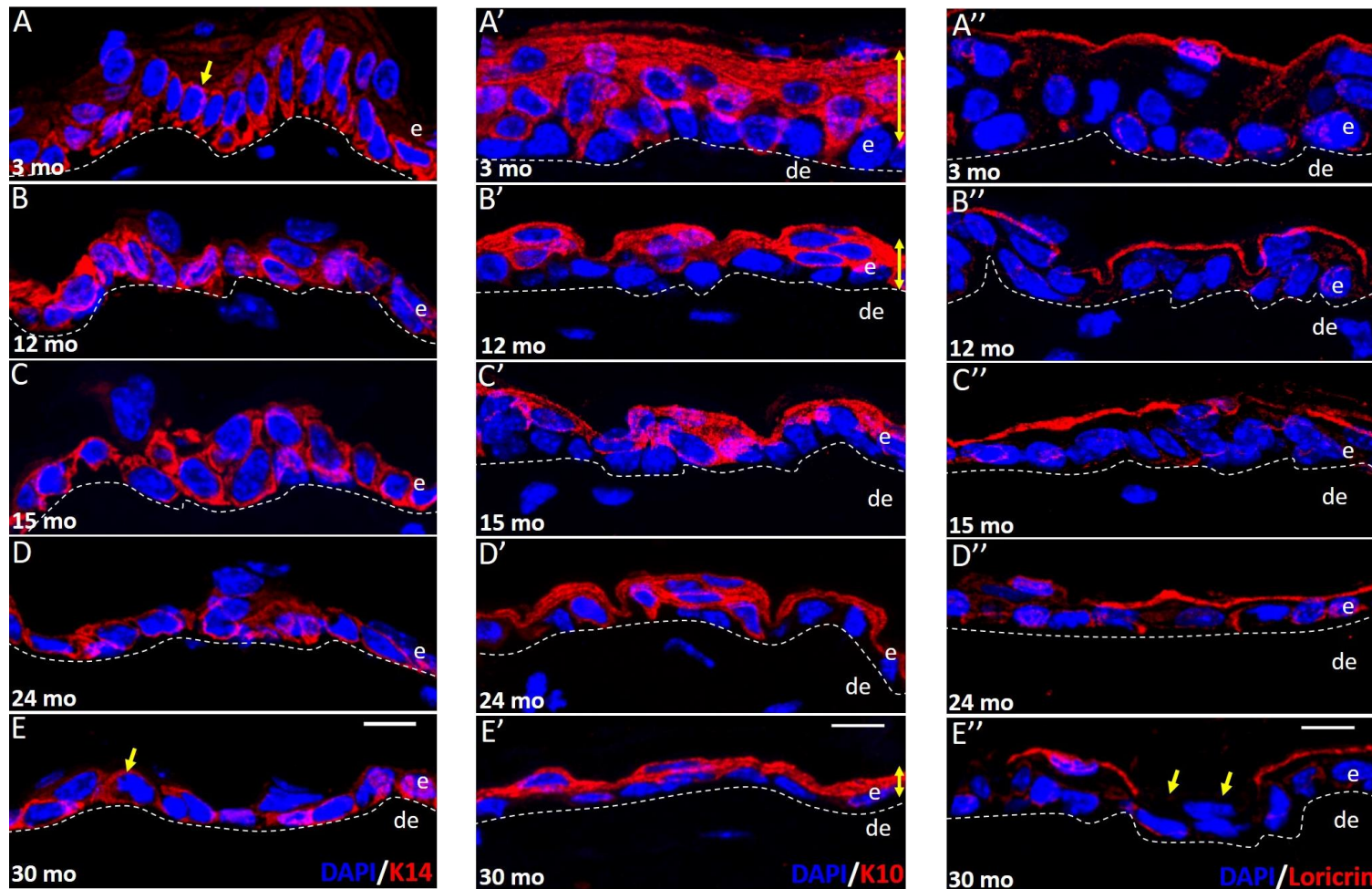
Figure 3.2.13: Immunofluorescence staining of keratinocyte differentiation expression in the epidermis of 3 mo (A, A', A''), 12 mo (B, B', B''), 15 mo (C, C', C''), 24 mo (D, D', D'') and 30 mo (E, E', E'') mice. Mouse skin sections were incubated with rabbit primary antibodies against the basal layer marker Keratin 14 (column 1), the suprabasal/spinous layer marker keratin 10 (column 2) and the cornified envelope marker loricrin (column 3). The secondary antibody for all staining was anti-rabbit Alexa 568 and nuclei were counterstained with DAPI. Slides were imaged using CLSM and a 40x objective lens. Images shown a maximum 2D projections of 5 µm z-stacks with imaging conditions optimised to 1 Airy unit. e= epidermis, de= dermis, dotted line= DEJ. Scale same for all images and scale bars shown in E, E', E'' all 10 µm. Yellow arrows in A and E show shape differences in 3 mo vs 3 mo cells. Yellow double headed arrows in A', B' and E' indicate decreasing K10 levels over time. Yellow arrows in E'' show absent loricrin expression in 30 mo skin..

3.2.8   Changes to the morphology of basal epidermal cells with age

Intrinsic ageing has been known to be associated with increased abnormality in nuclear shape in the cells of humans (Scaffidi and Mistelli et al, 2006) and model organisms like *Drosophila* (Brandt et al, 2008). As Figure 3.2.2 showed that epidermal cell nuclei become more irregular with age (3.3.2, D' and E'), and we observed a change in the orientation of cells in the basal layer using K14 and DAPI staining (Fig 3.2.13, A and E), we sought to quantify these observations. To complete our analysis, we assessed the circularity index of basal epidermal (BE) nuclei of 3 mo, 12 mo, 15 mo, 24 mo and 30 mo animals using high power Z-stack confocal images of epidermal cells, which were captured using a 63x objective lens. By imaging in the Z-dimension as well as X and Y, we were able to gain more information about the shape of nuclei in each skin section, as a greater proportion of the whole nucleus was captured. One image was used for each mouse and 10 measurements were of made of the nuclei making a total of 40 measurements per age group.

Figure 3.2.14 depicts maximally projected images of BE nuclei from 3 mo (A), 12 mo (B), 15 mo (C), 24 mo (D) and 30 mo (E) mice. In 3 mo animals, nuclei are rounded and regular in shape (yellow outline and arrow- A). Over time the nuclei become progressively flatter and more irregular. Marked cell flattening is evident in the nuclei of 24 mo and 30 mo animals (yellow outlines and arrows, D, E). Quantification of mean nuclear circularity of BE cells in each mouse (F) and each age group (G) showed that in the 3 mo and 12 mo animals, the circularity index of nuclei was similar. In the 15 mo animals it was slightly lower and in the 24 mo and 30 mo animals, it was dramatically reduced and lowest in the 30 mo animals. The mean and standard deviations for nuclear circularity index values in each age group are shown in table 3.2.11

Table 3.2.11: Mean and standard deviation BE nuclear circularity values for 3 mo, 12 mo, 15 mo, 24 mo and 30 mo mice

Age group	Mean	Standard Deviation
3 month	0.75	0.035
12 month	0.74	0.031
15 month	0.72	0.031
24 month	0.66	0.026
30 month	0.63	0.033
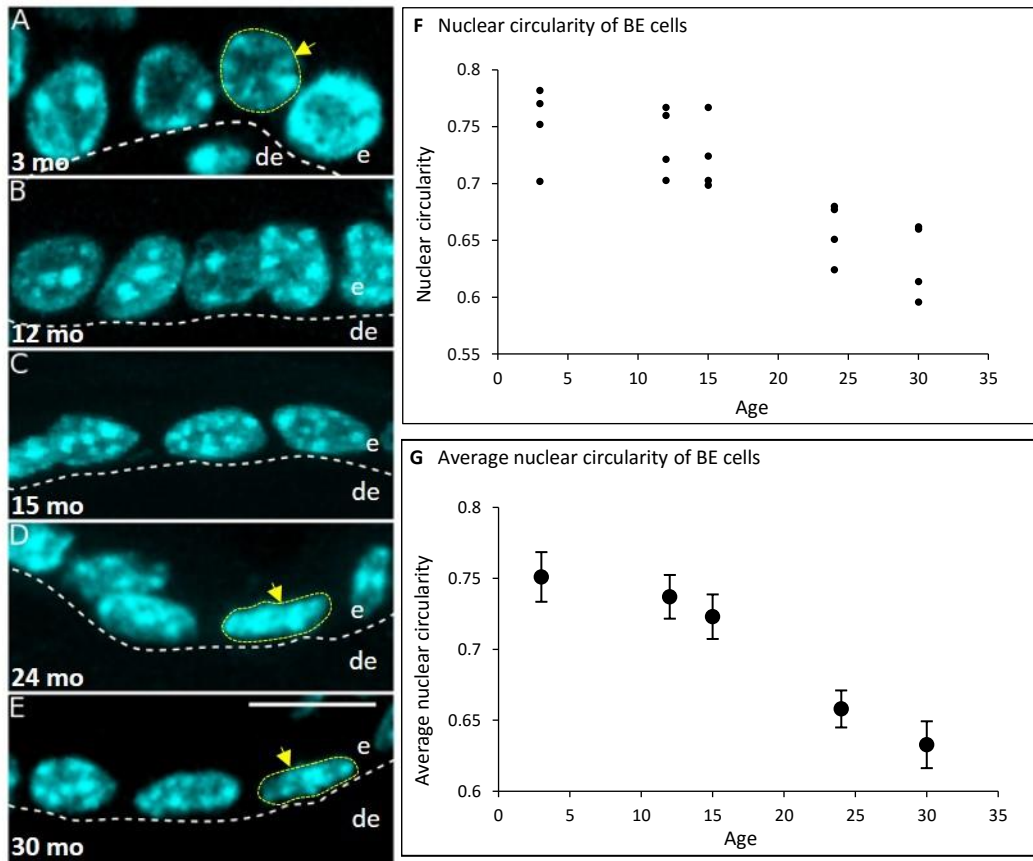
Figure 3.2.14: Morphological changes in epidermal basal nuclei with age. High magnification Z-stack images of 3 mo (A), 12 mo (B), 15 mo (C), 24 mo (D) and 30 m (E) nuclei were taken using a confocal microscope with 63x objective lens. Nuclei were visualised using DAPI. Nuclei become less circular in aged animals (yellow outlines and arrows A, D, E). White dotted lines indicate the epidermal-dermal junction in each image. e= epidermis, de= dermis. Scale the same for all images-scale bar in E=10 µm. F and G= Plots of nuclear circularity measurements in 3 mo, 12 mo, 15 mo, 24 mo and 30 mo mice. F= measurements for each animal with each data point representing data collected nuclei in one image per mouse. 15 mo, 24 mo and 30 mo data points that were close in value showed overlap. G= Average nuclear circularity for each age group. Error bars represent standard deviations calculated from the values for the 4 animals in each age group.

We assessed the statistical significance of these observations using one way ANOVA, which indicated there was a highly significant difference between age groups (p <0.0001). Post-Hoc analysis using Holm-Sidak testing showed several significant differences between the age groups as detailed in table 3.2.12. All of the significant differences occurred between 3 mo, 12 mo, and 24 mo and 30 mo age groups, which suggests that nuclear circularity significantly decreases in older compared to younger age groups.

Table 3.2.12: Holm-Sidak post-hoc testing of the ANOVA analysis for the assessment of nuclear circularity in the different age groups. Green fill indicates statistically significant differences

Comparison	Difference of Means	P	P<0.050
3 month vs. 30 month	0.119	<0.001	Yes
12 month vs. 30 month	0.105	0.003	Yes
3 month vs. 24 month	0.0936	0.006	Yes
15 month vs. 30 month	0.0903	0.007	Yes
12 month vs. 24 month	0.0797	0.017	Yes
15 month vs. 24 month	0.0651	0.052	No
3 month vs. 15 month	0.0285	0.632	No
24 month vs. 30 month	0.0252	0.621	No
12 month vs. 15 month	0.0147	0.771	No
3 month vs. 12 month	0.0138	0.545	No

3.2.9   Summary of significant morphometric changes to C57BL/6 skin with age

The morphometric changes occurring to C57BL/6 skin with age are summarized in table 3.2.13, which shows that the most significant changes with age occurred within the epidermal compartment. Loss of epidermal cellularity and a decrease in regular epidermal nuclear shape were the most highly significant changes that we tested. Decreases in dermal cellularity and epidermal thinning were also significant to a lesser extent.

Table 3.2.13: Summary of morphometric changes occurring to C57BL/6 skin with age. Green fill indicates highly significant changes (p <0.005) and yellow fill indicates significant changes (p<0.05). *= ANOVA completed with 15 mo animals being omitted from the analysis.

Factor quantified	Observed change with age	ANOVA p-value
Dermal cellularity	Rapidly decreases between 3 mo and 12 mo. Slower rate of decline 12 mo to 30 mo	0.029
Epidermal cellularity	Cell numbers decrease steadily with age.	0.003
Basal epidermal cellularity*	Cell numbers decrease slightly with age	0.009*
Epidermal thickness	Rapid decrease in thickness between 3 mo and 12 mo. Slower rate of decrease 12 mo to 30 mo	0.029
Basal cell nuclear shape	Similar circularity index in 3 mo to 15 mo animals. Decreases at 24 mo and further decreases at 30 mo	<0.0001

3.2.10 Discussion part 1: Morphometric changes have been identified in C57BL/6 skin- Future work should focus on taking measurements under standardized hair follicle cycles.

Our morphometric analysis of C57BL/6 has showed several key changes to the skin with age, but there are certain limitations in the data. One important limitation of carrying out a morphometric analysis on mice was shown by the fact that some of the 3 mo skin contained actively cycling hair follicles, which resulted in increased epidermal thickness in some of the animals.

Additionally, the presence of actively cycling follicles in the 3 mo animals was also likely to impact some of our other analyses. For example, there was a large variation in the dermal cellularity values generated from the 3 mo animals, and dermal cellularity showed a marked decrease between the 3 mo and 12 mo animals, where the difference in mean dermal cell numbers from 3 mo to 12 mo was 8.47. Although not statistically significant, this difference was much higher than the difference in means between the relatively young 12 mo animals and the aged 30 mo animals (2.40= which was also not significant). This suggests that the dramatic change in dermal cellularity between the 3 mo and 12 mo animals could be due to the presence of actively cycling follicles in the younger animals. Alternatively, it could represent a maturational effect- perhaps of the immune cell population within this area.

Whatever the reasons for this dramatic decline in dermal cellularity in between the 3 mo and 12 mo animals, we must consider it carefully in the analysis of our data. Therefore, although it is technically correct to conclude that statistically significant changes in dermal cellularity values occurred between "young" 3 mo animals and "aged" 30 mo animals, we cannot rule out the fact that the hair follicle stage or other effects in the young mice could have contributed to this significant result. Future work could look at this in more detail by confirming the identity of this dermal cell population using fibroblast and immune cell markers to determine if they are part of an immune response or are resident fibroblasts (Adam et al, 2015).

Furthermore, it is possible to synchronize the hair follicle cycles of mice using depilatory techniques like shaving (Tasseff et al, 2014). This would help to overcome the issue of studying the skin of mice at different stages in the HF cycle, as all follicles in the mice of all age groups could be synchronized to be in telogen. This would standardize comparisons between the young (3 mo-12 mo) and aged (24 mo and 30 mo) mice and ensure that any identified changes were not a result of actively cycling follicles.

Variation in measurements between animals is to be expected, but in the 15 mo age group, there was a very large variation in both epidermal thickness and numbers of basal

epidermal nuclei. This impacted some of our statistical analyses, as higher standard deviation values decreased the probability of identifying statistically significant differences between the different age groups. This variation could have occurred by chance, however, in this age group we had observed both catagen and late anagen follicles in two out of the four animals. HF cycle causes an increase in epidermal thickness, which may have accounted for the fact that significant differences in epidermal thickness between 15 mo and 30 mo animals were seen. It is therefore difficult to ascertain whether epidermal thinning with age was statistically significant due to this factor. As mentioned previously, HF follicle cycles become progressively asynchronous with age in mice (Müller-Röver et al, 2001), so with hindsight, it is clear that using techniques to standardize the HF cycle in all animals in each age group would have been optimal in order to delineate hair growth effects from ageing effects.

Despite these limitations we have observed some marked changes between young and aged animals, with many changes being identified in the epidermal compartment. The presence of dysmorphic nuclei in ageing tissues has been previously reported in human skin (Scaffidi and Misteli, 2006), but to our knowledge this is the first report of a change in nuclear shape during ageing in mouse epidermis, which indicates that it could be a biomarker of ageing epidermis in this strain of mouse.

The potential for future work in this field is vast, as our studies did not include measurements such as dermal and hypodermal thicknesses or numbers of pilosebaceous units and we therefore did not address in depth the dermal compartment or hair follicles in our morphometric analysis. Decreased dermal thickness and increased hypodermal thickness with age has been shown to occur in this strain of mice in previous reports (Giangreco et al, 2008), so future work may look to measure this over the lifespan of the mice. Furthermore, little data is available on the how the numbers of pilosebaceous units change with age in C57BL/6, so quantification of this could also form the basis of future studies.

3.2.11 Discussion part 2: Observations of differences in epidermal terminal differentiation markers in aged skin

Although no formal quantification was completed, we also observed through western blotting that the epidermal compartment, as measured by E-cadherin expression, occupies a reduced proportion of the overall skin in 30 mo animals. As E-cadherin is expressed in both the hair follicles and IFE (Young et al, 2003), this suggests that both the previously observed epidermal thinning, reduction in epidermal cellularity (from our histological analysis) and potential un-quantified changes in the numbers and structure of hair follicles that may occur in

aged skin could contribute to this overall reduction in E-cadherin protein expression in 30 mo animals.

K14 is also expressed in the keratinocytes of hair follicles (Coulombe et al, 1989), and therefore cells from hair follicles in the mouse skin lysates that we prepared for western blotting could have also contributed keratin 14 protein. This suggests that, although we observed stable k14 protein levels in the whole skin lysates between 3 mo and 30 mo animals, like for E-cadherin expression, the contribution of hair follicles cells to these protein levels in both 3 mo and 30 mo animals were not known.

K10 expression appeared marginally reduced in aged animals through both Western blotting and immunofluorescence observations and although epidermal thinning was apparent in aged animals, keratin 10 expression was still clearly displayed in suprabasal cells. The terminal differentiation marker loricrin, however, was clearly reduced in the aged skin compared to young skin. Reduced epidermal cell turnover in aged human skin has been previously reported (Grove and Kligman, 1983). In C57BL/6TgN mice, Charruyer et al (2009) have shown that the number of epidermal stem cells in young and aged animals is constant, but qualitatively, aged epidermal stem cells and transit amplifying cells have a reduced proliferative capacity, because the cell cycle is prolonged. The group found that aged transit-amplifying cells persisted for a greater period of time in the epidermis of aged animals, taking longer to differentiate. As we have observed that basal K14 expression was maintained with age, but protein expression of the terminal differentiation marker loricrin, and overall epidermal thickness was reduced, this suggests a reduction in epidermal cell turnover in the aged 30 mo animals compared to young 3 mo and 12 mo animals. As loricrin is a critical component of the skin barrier, its reduction with age suggests that the barrier function in the aged mouse skin could have been compromised. The uptake of histological stains like toluidine blue can be used to assess the integrity of the skin barrier (Indra and Leid, 2011), so a future experiment could look to measure toluidine blue uptake in young and aged mice to determine if more dye is taken up in the aged animals

Although we had 3 biological replicates in our Western blots for each of the 3 mo and 30 mo age groups, we completed only one technical replicate for the antibodies K10, K14 and loricrin. Due to our limited number of technical replicates, optimisation of the best dilutions and blotting conditions for each antibody had not been completed. We therefore did not complete semi-quantitative analysis of these proteins in western blots, as future work is needed to optimise these procedures.

Furthermore, we have yet to complete any quantitative analysis of the change in amount of k14, k10 and loricrin with age in our observations of epidermis using

immunohistochemistry. Future work should look to address this limitation. Ideally the levels of k14, k10 and loricrin could be quantified using analysis of fluorescence immunohistochemistry, with the results being expressed as the levels of these proteins as a proportion of the whole epidermis. This would allow us to standardise for the fact that the epidermis becomes thinner with age, thus allowing us to determine what proportions of the cells in the basal, spinous and granular layers are lost from the epidermis over time.

3.3   Identification of Biomarkers of epidermal ageing in C57BL/6 mice

3.3.1   Cellular Senescence occurs as part of physiological ageing

Senescent cells are morphologically distinct from healthy, proliferating cells, as they show an enlarged, flattened morphology (figure 3.3.1). Along with changes to cell shape, they undergo several transcriptional modulations, causing them to have their own secretory phenotype (known as the SASP- senescence associated secretory phenotype). Senescent cells can therefore produce and secrete large quantities of pro-inflammatory bioactive molecules such as interleukins, growth factors and matrix degrading enzymes that can impact the surrounding tissue micro-environment (Coppe et al, 2008).

In the presence of nuclear instability, induction of senescence preserves cellular fitness as it behaves as a tumour suppressor mechanism, stopping the cell from entering a "crisis" state where mitosis becomes highly un-controlled (Campisi and d'Adda di Fagagna, 2007). However, along with these longevity promoting effects, the presence of senescent cells in ageing tissues can also result in deleterious consequences (Ohtani et al, 2012), partly because cellular senescence is associated with mitochondrial dysfunction and production of ROS, which can damage DNA and protein in excess amounts (Moiseeva et al, 2009).
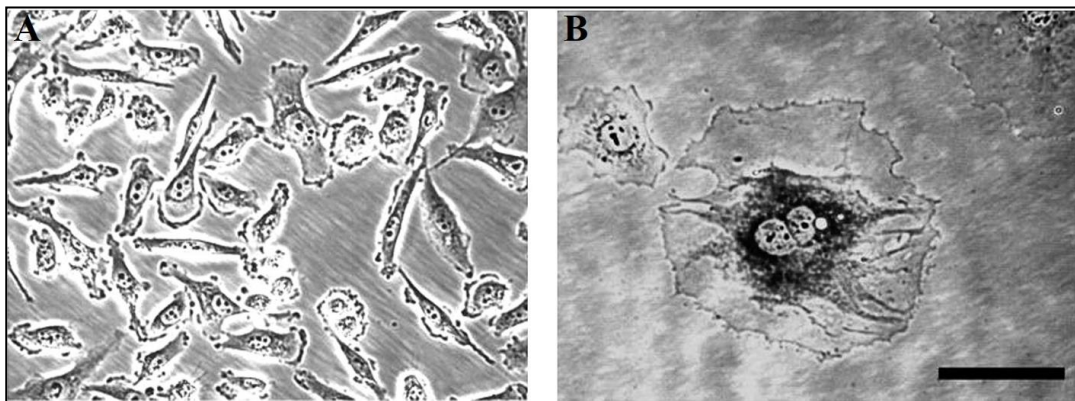
Figure 3.3.1: Senescent cells are morphologically distinct from proliferating cells. Proliferating (A) and drug-induced senescent (B) PC3 prostate cancer cells visualized under ×200 magnification using phase contrast microscopy. Senescent cells have an enlarged nucleus and cytoplasm. In this example the senescent cell is bi-nucleate, which is also a characteristic of the senescent phenotype. Scale bar = 100 μm. Image taken from Ewald et al, 2010.

3.3.2   Senescent cells cause by-stander effects to neighbouring cells

Senescent cells are known to accumulate in our tissues during physiological ageing (Jeyapalan and Sedivy, 2008) and *in vivo* studies looking at the impact of senescent cells in ageing tissues have shown that these cells cause "by-stander" effects, whereby the factors secreted from senescent cells drive neighbouring cells to become senescent (figure 3.3.2).

Nelson et al (2012) have shown that healthy fibroblasts co-cultured with senescent fibroblasts become senescent themselves due to ROS-induced DNA damage. This group also showed that senescent cells were organized in clusters in the livers of aged mice. The fact that senescent cells were not randomly arranged and occurred in distinct regions in the liver offered further evidence for a senescent cell by-stander effect.

Furthermore, a proof-of-principle publication from Baker et al (2011), directly implicated senescent cells as propagators of tissue dysfunction in an eloquent experiment involving mice. The authors generated transgenic mice whereby inducible elimination of p16[Ink4a] expressing senescent cells occurred upon drug treatment. Selective removal of these cells over the lifespan of the mice resulted in reduced age-related tissue atrophy and number of lesions. This study showed directly that the presence of senescent cells in tissues can drive an age-related decline in tissue integrity, as targeted removal of these cells over the course of the mouse lifespan dramatically improved health.
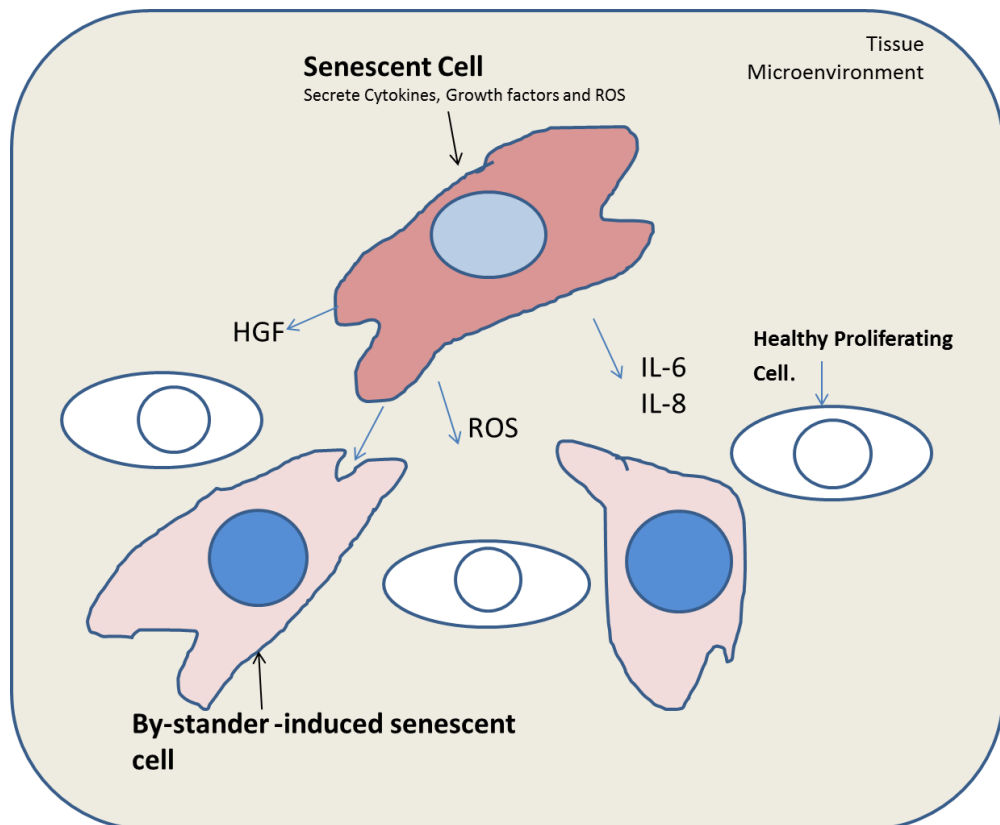
Figure 3.3.2: Senescent cell by-stander effects induce senescence in neighboring cells. A primary senescent cell (red cytoplasm, light blue nucleus) can produce and secrete molecules that induce senescence in neighboring healthy, proliferating cells (white cytoplasm and nucleus). This causes by-stander effects, which induce senescence within neighboring cells in the same tissue microenvironment (light pink cytoplasm, dark blue nucleus). Image= authors own. HGF= human growth factor, ROS= reactive oxygen species, IL6 and IL8: interleukins 6 and 8, respectively.

3.3.3 Identification of cellular senescence in C57BL/6 epidermis using DNA damage and cellular proliferation markers

From our morphometric analyses in part 3.2 it was clear that changes to the epidermal nuclei were occurring with age. Two of the most statistically robust changes were the decline in epidermal cellularity and also epidermal nuclear circularity. We therefore completed further studies that allowed us to assess nuclear stability changes over time in more detail. We hypothesized that reduced epidermal cellularity could be a result of increased cellular senescence in the aged skin resulting in reduced keratinocyte proliferation and therefore reduced cell numbers.

Giangreco et al (2008) have studied epidermal cellular proliferation during ageing in this strain of mice, where they considered the difference in Ki67 staining between "young" (2-4 m) and "aged (24-26 m) animals. They found a decrease in Ki67 between these age groups that was close to being statistically significant (p= 0.09). As their analysis did not include older 30 mo animals or animals in mid-life stages, we developed their findings by completing Ki67 analysis in our 3 mo, 12 mo, 15 mo, 24 mo and 30 mo mice to examine the change in epidermal cell proliferation over time.

Many authors have sought to quantify the presence of cellular senescence in ageing skin by using assays such as senescence-associated β-galactosidase staining, which causes a blue colour change due to the enzyme activity of β-galactosidase in senescent cells (sen-B-gal) (Dimri et al, 1995). Other groups have looked for evidence of cell cycle arrest in the form of p16^{INK4A} antibody staining as a marker of cellular senescence (Ressler et al, 2006). However, concerns have arisen as to whether β-galactosidase activity is actually causally related to senescence induction, which has lead to questioning about the efficacy of this assay in the identification of senescent cells (Lee et al, 2006). Furthermore, it is known that p16^{INK4A} antibodies are notoriously difficult to use in mouse studies, due to lack of high-quality antibody availability and also the presence of non-senescent p16^{INK4A} expressing cells confounding data analysis (Childs et al, 2015).

Solutions to these caveats have been identified by Wang et al (2009), who used DNA damage foci counting to identify senescent cells in the tissues of ageing mice *in vivo* by working on the assumption that long-lived DNA-damage foci are induced by a permanent DNA damage response which is unique to senescent cells. Although a transient DNA damage response can occur as a result of DNA repair or apoptosis, these outcomes have only a short lifespan and thus have a much lower probability of detection (d' Adda di Fagagna et al, 2003).

3.3.4 Section objectives

Our main objective going into this work was therefore to identify cellular senescence biomarkers in ageing C57BL/6 epidermal cells. In order to do so, we sought to fulfill the following objectives:

1. Assess if DNA damage accumulates in the non-proliferating cells of 3 mo, 12 mo, 15 mo, 24 mo and 30 epidermis.

2. Assess if cell proliferation changed in the 3 mo, 12 mo, 15 mo 24 mo and 30 mo epidermis

3. Given that lamin B1 expression has been shown to be decreased in aged human skin and is also modulated by senescence programmes (see thesis introduction part 1.15), we also sought to identify if lamin B1 protein levels changed in the C57BL/6 epidermis with age.

3.3.5 Assessment of cell proliferation and DNA damage levels in ageing C57BL/6 epidermis

In order to identify senescence in epidermal cells, we completed assays similar to those of Wang et al (2009) by using Ki67 and P53BP1 double labelling in mouse epidermis. We selected P53BP1 as our marker for DNA damage as this protein forms bright, distinct foci at regions of DNA damage, therefore making it a suitable marker for this analysis (Nelson et al, 2012). As the epidermis is a highly proliferative region of the skin, there was a probability that DNA damage foci present in replicating cells (such as in the presence of stalled replication forks) could confound our results. In order to overcome this, we developed a scoring system (figure 3.3.3) where we discounted cells positive for both Ki67 and P53BP1 (F- Ki67+ P53BP1+) in our DNA damage foci counts but included these cells in our counts for cell proliferation. As a result, DNA damage foci (DNA DF) were only counted if they occurred in non-proliferating cells (F- Ki67- P53BP1+) and the presence of at least one focus meant that the nucleus was scored positive.

To further improve the accuracy of our analysis, we took Z-stack confocal-laser scanning microscopy (CLSM) images where we imaged through the entire tissue section using a high power objective lens (63x). This ensured that all of the nuclear material that was probed with the antibody was present in our analysis and meant that proper co-localisation of P53BP1

foci with nuclear material was completed (see previous works of Gerashchenko and Dynlacht, 2009; Hewitt et al, 2012). 3 images were taken per animal and all nucleated cells in the epidermis were counted (approximately 100 nuclei were scored per animal).

Figure 3.3.3 shows 2-dimensional maximum intensity projected examples of 3 mo, 12 mo, 15 mo, 24 mo and 30 mo Z-stack images of epidermis double labeled with P53BP1 and Ki67 antibodies. High levels of proliferating cells were observed in the basal layer of 3 mo skin (green arrows-A) and also the presence of minor levels of DNA damage (White arrows-A). Over time DNA damage levels increased whereas cell proliferation was reduced (White arrows, C, D, E).
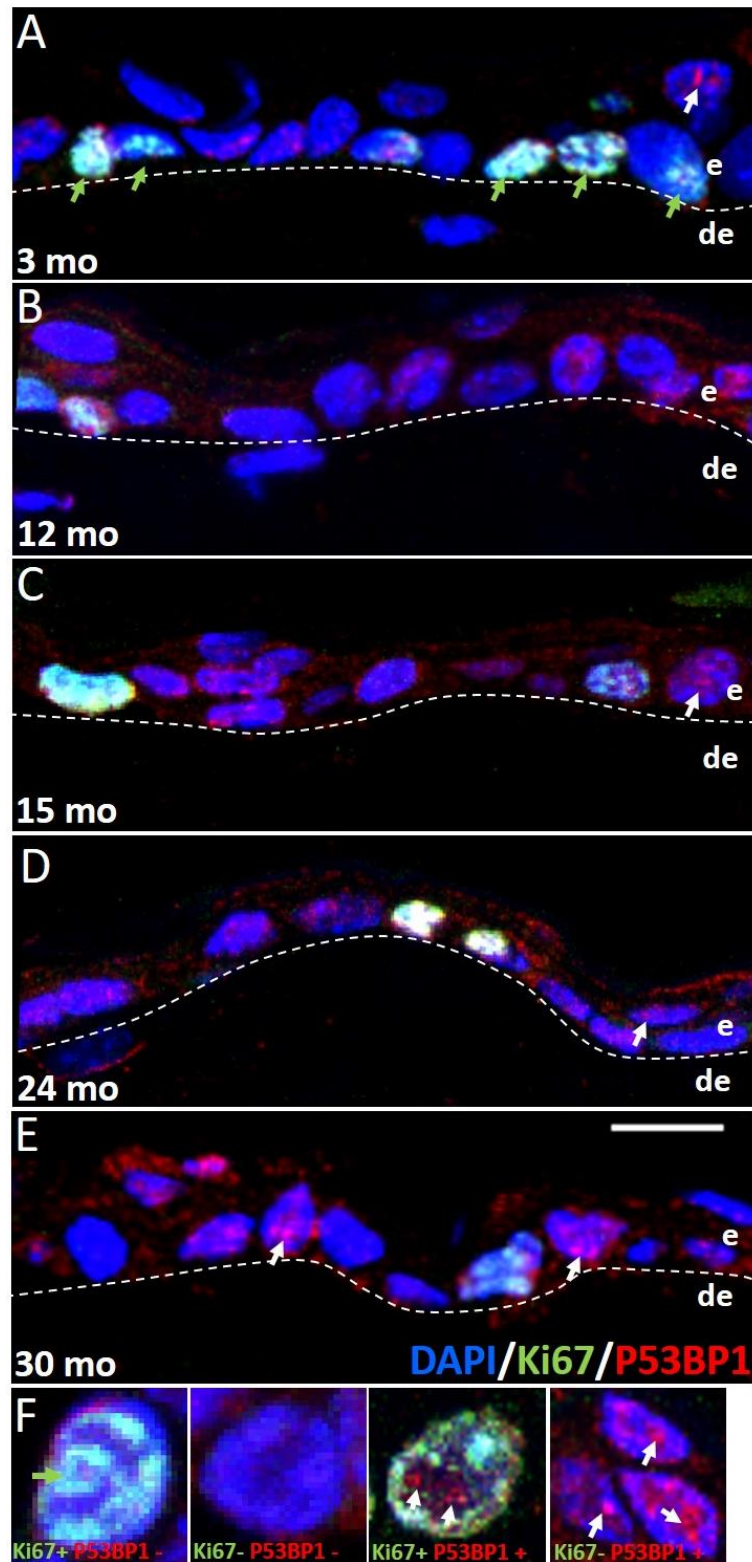
Figure 3.3.3: Immunohistochemistry of DNA DF and cellular proliferation in 3 mo (A), 12 mo (B), 15 mo (C), 24 mo (D) and 30 mo (E) epidermis. Skin was double labelled with a rabbit Ki67 antibody directly conjugated to Alexa 488 (direct label) and a biotinylated anti-rabbit P53BP1 antibody conjugated to Texas red avidin. Sections were imaged using CLSM where Z-stack images were taken using a 5 μm depth of the tissue section. F= scoring criteria for cells within the epidermis to quantify proliferating cells without DNA DF (Ki67+ P53BP1-), non-proliferating cells without DNA DF (Ki67- P53BP1-), proliferating cells with DNA DF (Ki67+ P53BP1 +) and non-proliferating cells without DNA DF (Ki67- P53BP1+). White dotted line = dermal-epidermal junction, e= epidermis, de= dermis. Scale same for images A-E and scale bar is shown in E= 10 μm. Green arrows show proliferating cells marked by Ki67 expression. White arrows show presence of DNA damage foci marked by bright spots of P53BP1 staining.

We expressed our results as percentages of P53BP1 foci-positive cells and Ki67 positive cells out of all epidermal nuclei. The results of these analyses were assimilated into plots of the percentage of DNA damage foci-positive nuclei in the epidermis of each animal (figure 3.3.4-A) and of the average percentage of DNA damage foci-positive nuclei in the epidermis of each age group (figure 3.3.4-B). Levels of cellular proliferation were shown by percentages of Ki67 positive nuclei in the epidermis of each animal (figure 3.3.4-C) and in each age group (figure 3.3.4-D). The mean and standard deviation values for DNA damage and cellular proliferation levels are also depicted numerically in table 3.3.1 (DNA damage) and table 3.3.2 (cellular proliferation).

As figure 3.3.4 A and B show, DNA damage levels were lowest in the 3 mo animals then increased progressively from 3 mo to 24 mo. After 24 mo, levels were reduced down to a level similar to that of 12 mo animals (table 3.3.1). The aged 24 mo and 30 mo animals showed the greatest variation in DNA damage levels out of all of the age groups (figure 3.3.4 B and table 3.3.1).

In the 3 mo animals cell proliferation levels were high but also variable between animals. A large drop in cellular proliferation between 3 mo and 12 mo animals was observed and following this, a minor reduction in proliferation was observed from 12 mo to 24 mo. Cell proliferation values were also variable in the 15 mo animals. Between the 24 mo and 30 mo age groups, proliferation levels increased and returned to levels similar to those observed in 12 mo animals (figure 3.3.4 D and table 3.3.2).
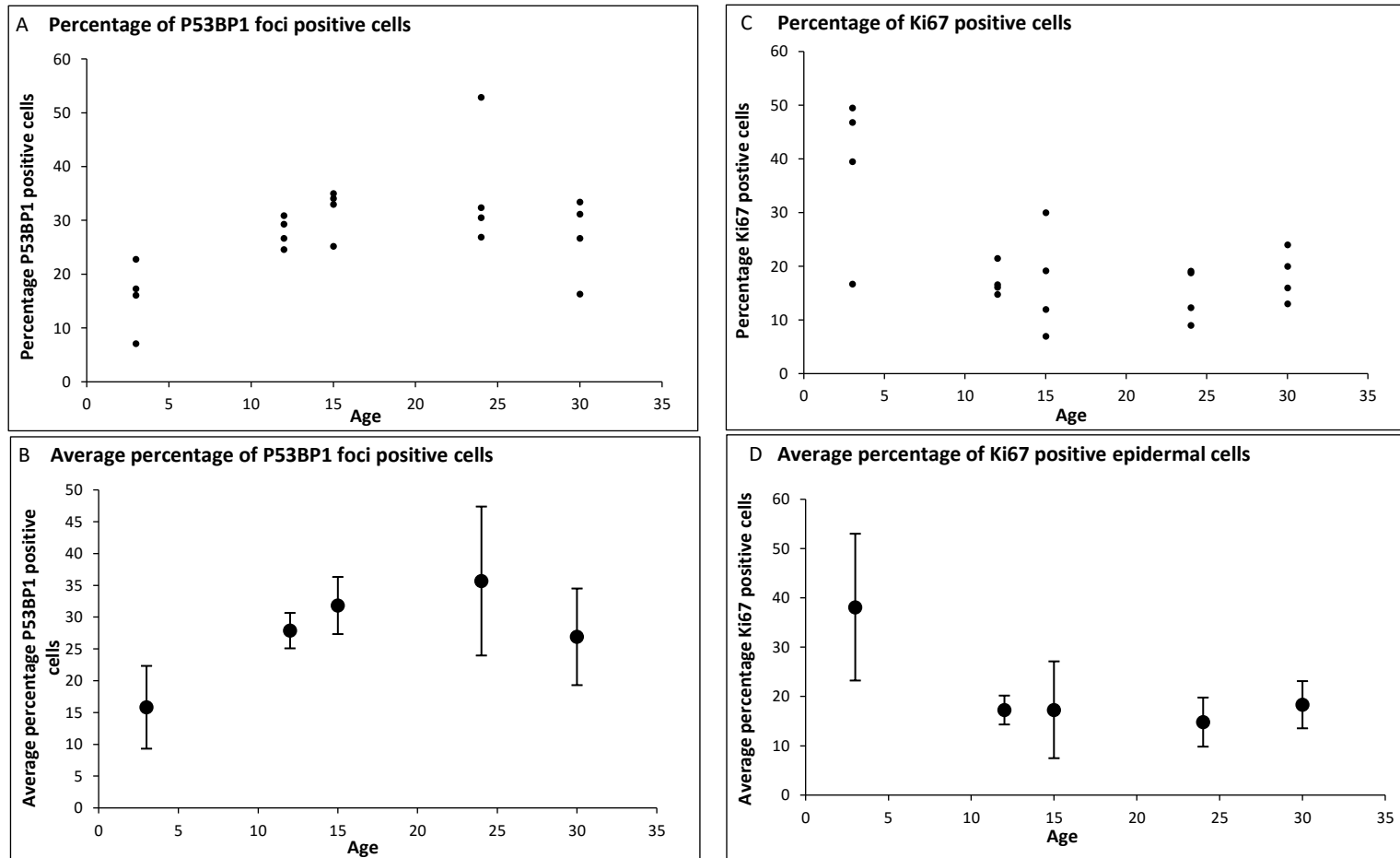
Figure 3.3.4: Quantification of DNA damage (A ,B) and cellular proliferation (C, D) in 3 mo, 12 mo, 15 mo, 24 mo and 30 mo mice. A= counts of numbers of epidermal DNA DF positive nuclei expressed as percentages of total epidermal nuclei. Each data point represents 1 animal and 4 animals were in each age group. B= average percentage of foci positive nuclei in each age group with error bars representing standard deviations calculated from each the 4 animals. C=percentage Ki67 positive cells in the epidermis of each animal, D= average percentage of Ki67 positive cells in each age group with error bars representing standard deviations calculated from all animals within the age group

Table 3.3.1 Mean and standard deviation values for the percentage of DNA damage foci (DF) positive cells in the epidermis of 3 mo, 12 mo, 15 mo, 24 mo and 30 mo mice.

Age Group	Mean percentage DNA DF positive cells	Standard Deviation
3 month	15.83	6.51
12 month	27.88	2.79
15 month	31.83	4.49
24 month	35.68	11.71
30 month	26.90	7.60

Table 3.3.2: Mean and standard deviation values for the percentage of Ki67 positive nuclei in the epidermis of 3 mo, 12 mo, 15 mo, 24 mo and 30 mo mice

Age Group	Mean percentage Ki67 positive cells	Standard Deviation
3 month	38.13	14.90
12 month	17.25	2.93
15 month	17.30	9.82
24 month	14.80	4.98
30 month	18.33	4.83

One way ANOVA was used to assess if there were significant differences in DNA damage and cell proliferation levels within the different age groups and the results showed a significant change in DNA damage levels (p=0.02) and cell proliferation (p=0.01). Post-Hoc analysis using Holm-Sidak testing was therefore subsequently employed to identify the age groups where significant differences had occurred. The results are summarized in tables 3.3.3 and 3.3.4, which indicates that significant differences in DNA damage levels occurred between 3 mo and 24 mo age groups and significant differences in cell proliferation levels occurred between 3 mo animals and all of the other age groups.

Table 3.3.3: Holm Sidak post-hoc analysis of the one way ANOVA testing differences in DNA damage levels in the epidermis of 3 mo, 12 mo, 15 mo, 24 mo and 30 mo animals. Differences in epidermal DNA damage levels were significant between the 3 mo and 24 mo age groups only (green fill)

Comparison	Difference of means	P	P<0.050
24 month vs. 3 month	19.85	0.015	Yes
15 month vs. 3 month	16.000	0.063	No
12 month vs. 3 month	12.050	0.239	No
30 month vs. 3 month	11.075	0.292	No
24 month vs. 30 month	8.775	0.499	No
24 month vs. 12 month	7.899	0.558	No
15 month vs. 30 month	4.925	0.826	No
15 month vs. 12 month	3.950	0.838	No
24 month vs. 15 month	3.850	0.715	No
12 month vs. 30 month	0.975	0.852	No

Table 3.3.4: Holm Sidak post-hoc analysis of the one way ANOVA testing differences in cellular proliferation levels in the epidermis of 3 mo, 12 mo, 15 mo, 24 mo and 30 mo mice. Differences in epidermal cellular proliferation levels were significant between the 3 mo + 24 mo, 3 mo + 12 mo, 3 mo + 15 mo and 3 mo + 30 mo age groups (green fill).

Comparison	Difference of Means	P	P<0.050
3 month vs. 24 month	23.325	0.017	Yes
3 month vs. 12 month	20.875	0.034	Yes
3 month vs. 15 month	20.825	0.031	Yes
3 month vs. 30 month	19.793	0.038	Yes
30 month vs. 24 month	3.532	0.994	No
15 month vs. 24 month	2.500	0.997	No
12 month vs. 24 month	2.450	0.991	No
30 month vs. 12 month	1.082	0.997	No
30 month vs. 15 month	1.032	0.983	No
15 month vs. 12 month	0.0500	0.994	No

This analysis therefore showed that DNA damage in the absence of cellular proliferation accumulated in the C57BL/6 epidermis during ageing, which suggests that senescent cells accumulate in this region with age. However, the oldest age group assessed, the 30 mo mice had lower DNA damage levels than 24 month mice.

Additionally, like the DNA damage levels, cellular proliferation levels were most marked between 3 mo and 24 mo mice. In the oldest age group assessed (30 mo) cellular proliferation was still significantly lower than at 3 mo, but this difference was less significant compared to the difference between 3 mo and 24 mo animals.

3.3.6   Identification of lamin B1 as a biomarker of ageing in C57BL/6 epidermis

As we had observed significant decreases in cellular proliferation in the C57BL/6 epidermis, we next asked whether, like in human skin, lamin B1 protein was also reduced in the epidermis during ageing (decreased lamin B1 in aged human skin along with decreased Ki67 expression has been shown by Dreesen et al, 2013- Figure 1.16 in intro).

To our knowledge, studies of changes to lamin B1 levels in ageing mouse epidermis have not been completed therefore, in order to identify if epidermal lamin B1 protein levels changed in mouse, we completed immunohistochemical staining on 3 mo, 12 mo, 15 mo, 24 mo and 30 mo skin sections and imaged the results using Z-stack confocal laser scanning microscopy (CLSM- figure 3.3.5). Like for our DNA damage assessments, this imaging method was preferable over others as it allowed us to capture the arrangement of lamin B1 relative to nuclear material in both the X, Y and Z planes of view, which gave us the maximum information about the organisation of lamin B1 in the epidermal nuclei of the mouse skin sections.

Figure 3.3.5 shows lamin B1 staining was strong in the basal layer of some of the cells in 3 mo animals where mostly peri-nuclear staining was observed (white arrows, A) whereas other cells were more weakly labelled in this layer. We also observed weaker lamin B1 staining in the centre of some nuclei (grey arrowheads- A, C) which could represent intra-nuclear lamin B1. Alternatively, this staining could also represent peri-nuclear lamin B1 staining on the top of nuclei given that our images were 2D maximal projections of images taken at regular intervals of a ~5 μm slice of skin tissue. There was variation in the levels of lamin B1 in the different epidermal layers, with lower expression generally being seen in suprabasal nuclei (green arrows- A, B, C). Some exceptions to this rule were observed, shown by the presence of prominent lamin B1 staining in the occasional suprabasal cell (green arrow-D).

Reduction in cell numbers over time meant that the overall numbers of lamin B1, stained nuclei decreased, but there was not a noticeable difference in the lamin B1 levels in the basal layer nuclei of 3 mo, 12 mo, 15 mo and 24 mo animals despite there being different nuclear numbers present in these age groups. Like the other age groups, there was variation in the level of lamin B1 in the basal layer nuclei in 30 mo animals. However, lamin B1 appeared reduced in this layer overall compared to the other age groups (green arrows- E).
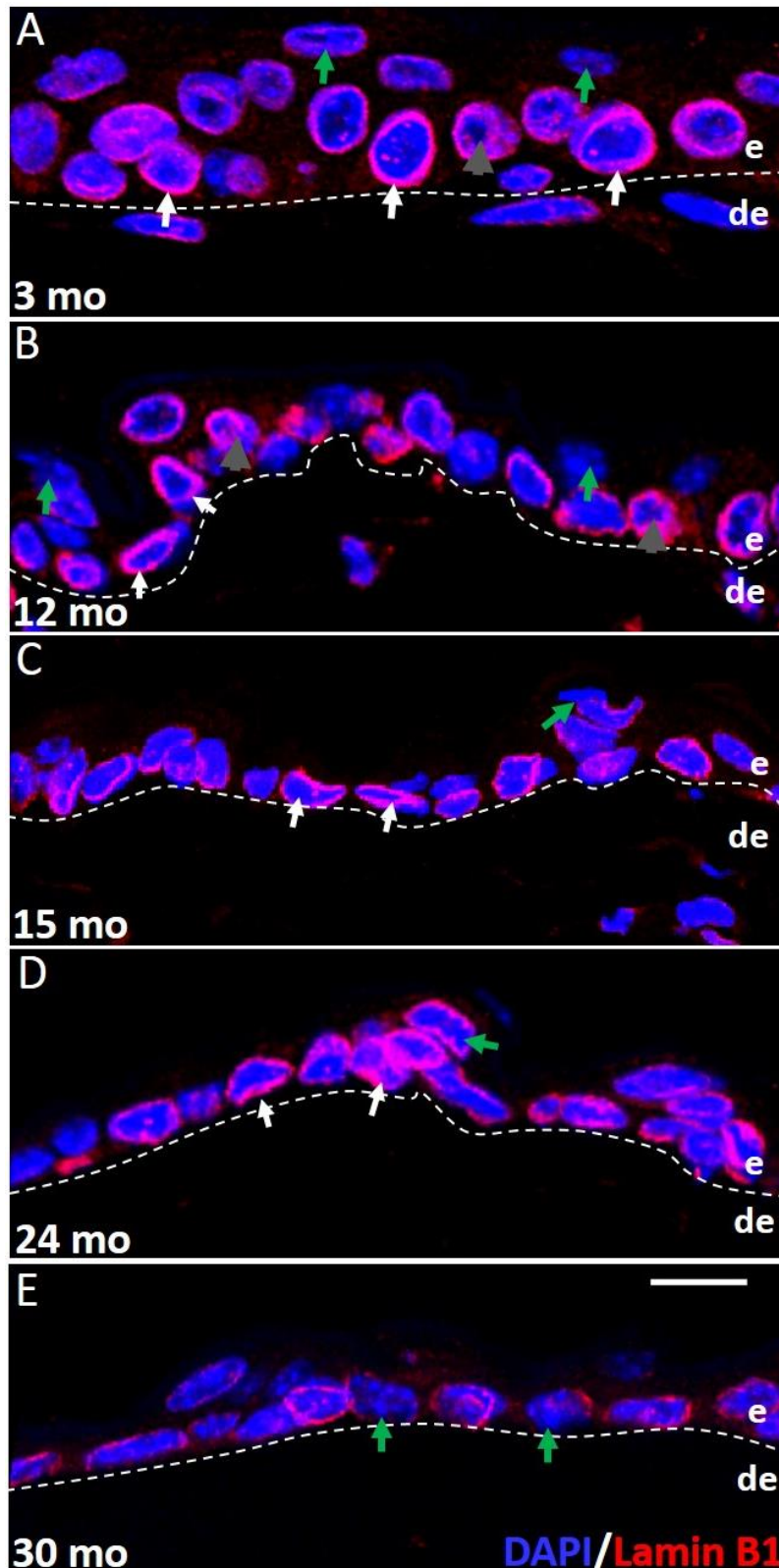
Figure 3.3.5: Immunofluorescence staining of lamin B1 in 3 mo (A),12 mo (B),15 mo (C),24 mo (D) and 30 mo (E) skin. Sections were stained with a rabbit lamin B1 primary antibody conjugated to an anti-rabbit Alexa 568 secondary antibody. Nuclei were counterstained with DAPI. Z-stack images were taken using CLSM with a 40x oil objective and the pinhole optimised to 1 airy unit. Images represent 2D maximal projections of all of the images in one 5 μm stack. e= epidermis, de= dermis, white dotted line= DEJ. White arrows represent high levels of lamin B1 in some of the nuclei in the basal epidermis. Green arrows represent low levels of lamin B1 in the nuclei of suprabasal cells and also in the basal cells of 30 mo animals. Grey arrowheads= areas where lamin B1 staining was seen in the middle of nuclei (intranuclear). Scale bar was same for all images and shown in E= 10 μm.

To analyse the average epidermal level of lamin B1 for each animal, 3 individual Z-stack confocal images with a Z-depth of 5 μm were captured for each animal in each age group. Fluorescence intensity levels of lamin B1 in all of the epidermal nuclei from the 3 images were quantified in ImageJ to give relative levels of mean epidermal lamin B1 expression for each animal (figure 3.3.6 A) and for each age group (figure 3.3.6 B, table 3.3.5). The plots of these results show that lamin B1 expression was highly variable in the 3 mo animals and in 2 of the animals epidermal lamin B1 exprssion was high (figure 3.3.6 A;- 3 mo-2.40, 2.45). This level of expression was not observed in any of the other age groups.

In the 12 mo and 15 mo animals lamin B1 was reduced and less variable. At 24 mo, variation in lamin B1 levels were high again, with animals showing relative expression levels greater than those seen at 12 mo and 15 mo (figure 3.3.6 A-24 mo-1.70, 1.23, 1.24) but also animals with lower levels of lamin B1 (0.34). At 30 mo all 4 mice had relatively low values of epidermal lamin B1 and the variation between levels was low compared to other age groups. In 2 of the 30 mo animals expression was dramatically reduced compared to the other age groups (Figure 3.3.6 A- 30 mo- 0.12, 0.08).

Overall lamin B1 expression was reduced over time. Initially, mean expression level declined markedly between 3 mo and 12 mo then stayed relatively constant between 12 mo, 15 mo and 24 mo until 30 mo where expression levels were at their lowest.
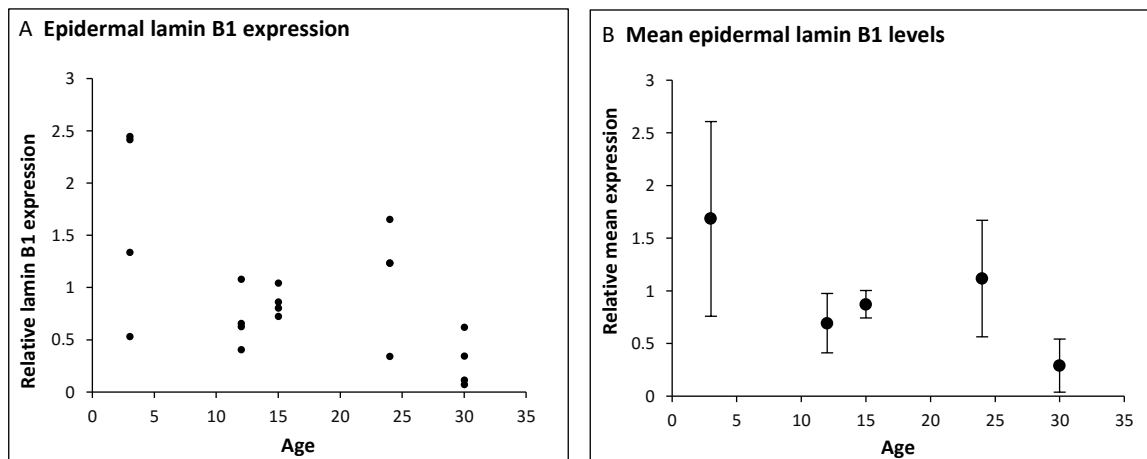
Figure 3.3.6: Quantification of mean epidermal lamin B1 levels in 3 mo, 12 mo, 15 mo, 24 mo and 30 mo mice. A= relative mean epidermal lamin B1 expression in each animal with each data point representing 1 of the 4 mice in each age group. B= mean epidermal lamin B1 in each age group. Data points close in value show overlap in 3 mo and 24 mo mice. Error bars represent standard deviations calculated from the recordings taken in all 4 animals in each age group.

Table 3.3.5: Mean and standard deviation values of epidermal lamin B1 levels in 3 mo, 12 mo, 15 mo, 24 mo and 30 mo age groups

Group Name	Mean epidermal lamin B1	Standard Deviation
3 moonth	1.683	0.924
12 month	0.693	0.282
15 month	0.873	0.130
24 month	1.117	0.553
30 month	0.290	0.252

To assess the statistical significance of these changes, differences between mean lamin B1 levels in the 5 age groups were analysed by one way ANOVA, which indicated that a significant change in lamin B1 levels occurred with age (p= 0.020). Post-hoc analysis of the ANOVA to identify which age groups showed significant differences indicated that the difference was significant between the 3 mo and 30 mo age groups only (p=0.016, table 3.3.6).

Table 3.3.6: Post-hoc analysis of the one was ANOVA using Holm-Sidak multiple comparison testing. These tests indicated that differences in mean epidermal lamin B1 were statistically significant between the 3 mo and 30 mo age groups only (green fill)

Comparison	Diff of Means	P	P<0.050
3 moonth vs. 30 month	1.393	0.016	Yes
3 moonth vs. 12 month	0.990	0.133	No
24 month vs. 30 month	0.827	0.267	No
3 moonth vs. 15 month	0.810	0.256	No
15 month vs. 30 month	0.583	0.565	No
3 moonth vs. 24 month	0.566	0.529	No
24 month vs. 12 month	0.424	0.703	No
12 month vs. 30 month	0.403	0.634	No
24 month vs. 15 month	0.244	0.762	No
15 month vs. 12 month	0.180	0.628	No

As the most significant differences were observed between 3 mo and 30 mo animals, we also assessed the change in lamin B1 in these age groups using western blotting of whole skin. We generated lysates from 3 biological replicates of 3 mo and 30 mo C576BL/6 mice. Traditional cellular loading controls such as GAPDH and β-actin proteins have both been shown to be reduced in ageing skeletal muscle (Viglesø et al, 2015), and other authors have shown that total protein quantification techniques are more reliable loading controls in the quantification of proteins in tissues from C57BL/6 mice (Eaton et al, 2013). We therefore determined equal protein loading between our skin samples by using in-gel Coomassie blue protein staining (Diezel et al, 1972), before proceeding to blot the equalized protein volumes on subsequent gels. Figure 3.3.7 shows the results of our Coomassie blue protein staining,

which indicated equal loading from an even intensity and distribution of protein bands in each lane of the gel.

Once we had determined equal loading of our protein samples, we proceeded to blotting. As western blotting of 3 mo and 30 mo C57BL/6 whole mouse skin lysates is a novel experiment that has not completed by others, we also carried out blotting of traditional loading controls to determine if they showed any variance. Figure 3.3.8 shows the results of the blots, which indicated that lamin B1 was reduced in 2 out of the 3 animals aged 30 mo in comparison to the 3 mo animals. The cellular loading controls showed similar levels to one another in 3 mo samples, but in the 30 mo samples β-actin was more highly expressed than β-tubulin and GAPDH.
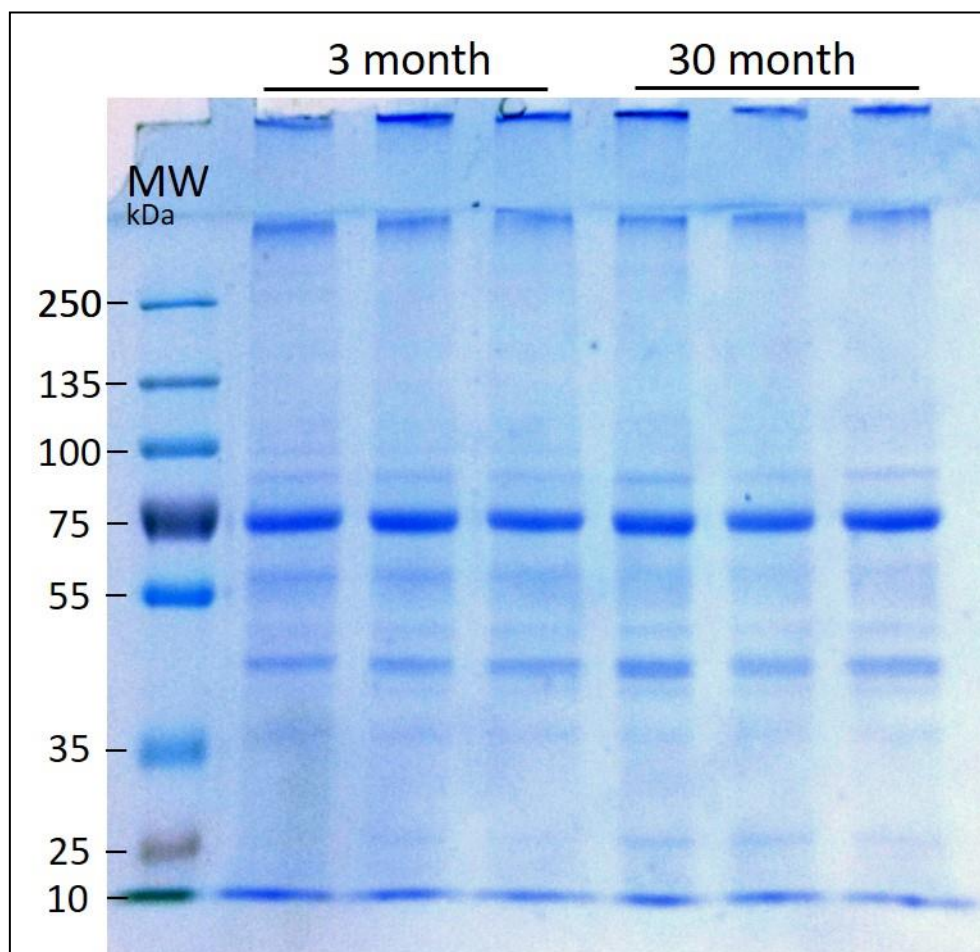
Figure 3.3.7: Coomassie blue in-gel protein staining of 3 mo and 30 mo skin lysates showing an equal amount of protein present in each lane of 3 different 3 mo animals and 3 different 30 mo animals. The presence of strong bands between ~70 kDa and ~40kDa were observed in all animals. As keratins have a molecular weights in a similar range to this and are highly abundant in the skin, these bands could represent keratin proteins (Moll et al, 2008).
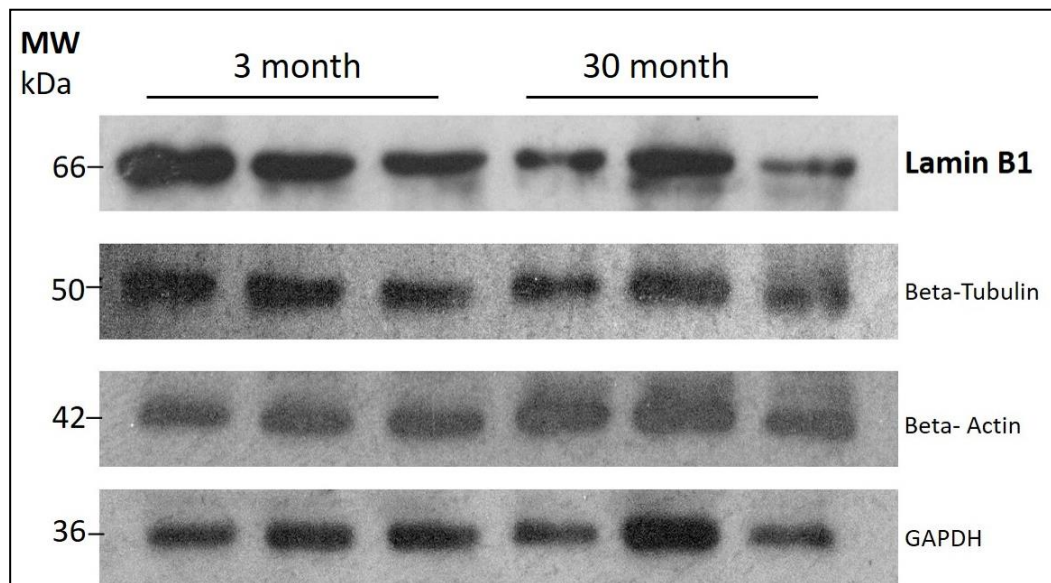
Figure 3.3.8: Western blotting of lamin B1 (66 kDa), β-tubulin (50 kDa), β-actin (42 kDa) and GAPDH (36 kDa) in 3 month and 30 month skin lysates. Lamin B1 expression was reduced in 2 of the 30 mo animals in comparison to the 3 mo animals. However, variation in levels of cellular loading controls were observed between the 30 mo samples.

3.3.7   Discussion: Lamin B1 is a biomarker of epidermal ageing in C57BL/6 mice

We have studied the impact of age on cellular proliferation, DNA damage and lamin B1 levels in the epidermis of C57BL/6 mice of various ages and observed as a trend that DNA damage increases with age whereas cellular proliferation and lamin B1 levels are reduced. Using whole skin lysates, we also observed a decrease in lamin B1 protein levels by western blot. Together these observations support the hypothesis that cellular senescence increased in the ageing mouse skin.

To our knowledge there is only one other published report that has quantified DNA damage levels in the epidermis of mice of several age groups (Schuler and Rübe, 2013) and these authors saw a significant increase in P53BP1-positive foci per cell in the inter-follicular epidermis of 24 mo old C57BL/6 mice compared to younger animals. Our data is consistent with these reports and furthermore provides additional information about DNA damage in older C57BL/6 mice, where surprisingly, we observed that DNA damage levels are reduced. According to the lifespan curve for C57BL/6 males (section 3.2 figure 3.2.1), approximately 40% of mice are able to live until age 30 mo and less than 10% are able to survive until 35m. It thus follows that by keeping animals until they are 30 mo, we are considering animals that show some selection bias towards cellular longevity and survival.

DNA repair proficiency is crucial for longevity (Vermeij et al, 2016) and longer lived species have shown up-regulated expression of DNA repair factors in comparison to shorter lived species (Mac Rae et al, 2015). The reduced levels of DNA damage we observe in our 30 mo age group may therefore represent a survivorship effect, whereby the animals that are able

to live to this age have improved DNA repair capacities compared to shorter-lived animals of the same genetic background and thus they exhibit less DNA damage. This improved repair in an identical genetic background may be the result of epigenetic mechanisms or the contribution of other factors such as feeding or exercise levels, which reduce overall cellular stress and senescence levels (Wang et al, 2010). As the epidermal cells from 30 mo mice had less DNA damage, and the induction of a DNA damage response induces cell cycle arrest (Ishikawa et al, 2006), it was perhaps un-surprising that the reduced DNA damage in 30 mo mice meant that they exhibited greater epidermal proliferation levels compared to the 24 mo animals.

Variation in cellular proliferation levels were greatest in the 3 mo animals and we had previously identified through histological staging that two of our 3 mo animals had actively cycling hair follicles whereas the other two mice in this age group had hair follicles in catagen and telogen (ie less mitotically active stages of the hair follicle cycle). Inter-follicular epidermal cells have shown an increase in proliferation during active hair follicle cycling in mice (Roy et al, 2016) and as our 3 mo epidermal data shows two animals with high levels of cell proliferation, one animal with medium levels and one animal with low levels, it might be the case that the animals with actively cycling hair follicles had greater levels of epidermal proliferation, which impacted their epidermal thickness as previously seen in section 3.2.6. We also observed a small number of actively cycling follicles in our 15 mo animals, so this may also explain why Ki67 levels in these animals were also variable compared to other age groups. As the differences between cellular proliferation levels were significant between the 3 mo animals and all other age groups tested, the presence of actively cycling hair follicles in the 3 mo animals makes it difficult to ascertain whether these observed differences are solely due to ageing, or whether the hair follicle cycle of these mice had impacted our results.

Our observed organization of lamin B1 in the epidermis of mice, with higher expression in the basal layer and reduced expression in suprabasal layers, is consistent with reports from Hanif et al (2009), who observed a similar organization in the epidermis of FVB/NCrl mice. Additionally, Oguchi and co-workers have seen similar lamin B1 arrangements in the cells of the epidermis of human skin (Oguchi et al, 2002). To our knowledge however, this is the first report of reduced lamin B1 in the epidermis of aged mice.

Reduced lamin B1 is associated with cellular senescence (Shimi et al, 2011; Freund et al, 2012, Dreesen et al, 2013), and is a potential biomarker of ageing in human epidermis (Dreesen et al, 2013). Lamin B1 is known to regulate the cell cycle through p53 dependent mechanisms (Dreesen et al, 2013) and this may potentially work through a feedback loop (Shimi et al, 2011). Therefore, reduced lamin B1 in aged tissues may be a result of reduced

cellular proliferation. One caveat to this hypothesis shown by our data is the fact that cellular proliferation levels were greater in 30 mo animals compared to 24 mo animals whereas lamin B1 expression was lower in the 30 mo animals. As the numbers of epidermal cells were lowest in the 30 mo animals, this may reflect a difference in the epidermal cell populations observed in the epidermis of 24 mo and 30 mo age groups. Although they form the majority, keratinocytes are not the only cells found in the epidermis, and it is therefore possible that the presence of melanocytes and Langerhans cells, which express different levels of lamin B1 compared to keratinocytes, could confound our analyses at the later age groups when keratinocyte cell numbers are sparse. Additionally, as lamin B1 staining was variable in the basal epidermal layer nuclei at other ages, it might be the case that these strongly-labelled cells seen in younger age groups are lost with age.

Clearly future work is needed to understand these subtle differences in relationships between cellular proliferation and lamin B1 levels in 24 mo and 30 mo mouse epidermis. The use of cell specific markers for melanocytes and Langerhans cells alonside markers for proliferation in the basal epidermis would help us to study this in more depth, as we would be able to differentiate keratinocytes from other epidermal cell populations.

Lamin B1 levels were highly variable in the 3 mo age group, with two animals showing very high expression, one medium and one relatively low. Hanif et al (2009) have identified an increase in interfollicular epidermal lamin B1 levels during active hair follicle cycling, and we speculate that active hair cycles in two of our 3 mo month mice may be driving these high expression levels. This observed variation and the conclusions drawn from our cellular proliferation data presents a clear need for hair follicle cycle standardization in all skin ageing studies completed on mice, as we are unable to say for certain that our observed decreases in lamin B1 and cellular proliferation between 3 mo and 30 mo animals are independently due to ageing. As identified in our morphometric analysis, future work could address this by using shaving methods to standardize the hair follicle cycle in mice of all age groups. Additionally, interim age groups, such as mice aged 6 months, could be added to future studies to increase the robustness of the data by confirming our observed trends at further interim age groups.

Western blotting of whole skin showed than lamin B1 was reduced in 30 mo animals compared to 3 mo animals. As identified previously, Western blotting of whole tissues in ageing studies presents several caveats in terms of suitable cellular loading controls (also covered in Li and Shen, 2013) and a comparison of young vs old mouse skin has its own individual issues. Epidermal and dermal thinning, along with reductions in the numbers of cells in the epidermal and dermal compartments reduce the overall presence of cells in aged skin, and furthermore, change the proportions of the different skin layers. This must be taken into account when

considering reductions in cellular proteins like lamin B1, as an observed reduction in this protein validated only by Western blotting of whole skin lysates could represent nothing more than a decline in nuclear numbers, and not a cell-specific reduction in lamin B1 protein.

Under some conditions routinely used loading controls could be employed to circumvent this problem, but the expression of several of these controls are not stable in ageing tissues (Viglesø et al, 2015). In our hands there was variation between the expression of the cellular loading controls β-Actin, β-tubulin and GAPDH in blots of equally loaded protein samples, so future work is needed to establish a suitable cellular loading control from these skin samples. Additionally, extra control methods along with Coomassie blue protein staining, such as staining of the membrane with Ponceau S following gel-membrane protein transfer (Romero-Calvo et al, 2010), would have increased our confidence that we had loaded equal amounts of protein between our samples.

To develop the Western blotting work completed here, an additional possible future step would be to mechanically or enzymatically separately the epidermis and dermis by using previously established methods (Maharlooei et al, 2011). Levels of lamin B1 protein could then be assessed alongside E-cadherin, which is expressed by all nucleated cells in the epidermis and does not change its expression in the skin of humans with age (Mahfouz et al, 2012). We did not address changes to lamin B1 in the dermis and therefore a marker such as vimentin could be used to identify mesenchymal cells in the dermis (Driskell et al, 2013) and identify if lamin B1 expression changes in the cells of this compartment with age along with the epidermis.

3.4 Identification of dermal and basement membrane collagen changes in aged C57BL/6 mouse skin

3.4.1 Introduction

The dermal layers in human and mouse skin are morphologically distinct, with the upper dermis, known as the papillary dermis (PD), having a looser arrangement of fine collagen III fibrils in both species. Further down in the reticular dermis (RD) collagen I fibrils, which are thicker and more tightly packed, are abundant (Lovell et al, 1987). Overall the dermis in mice is thinner compared to human skin, and proportionally, the papillary dermis is also thinner in mouse skin (Watt and Fujiwara, 2011), indicating similar, but also individual dermal characteristics between mice and humans.

As identified in the introduction to this chapter, histological changes to the collagens in the PD and RD in C57BL/6 mice with age have not been characterized in detail. In our morphometric analysis, we observed a reduction in the number of cells within the dermis with age and although we did not use specific cell identification markers, it is likely that some of these cells were fibroblasts. As fibroblast senescence and atrophy during ageing results in reduced collagen production (Varani et al, 2002), we therefore sought to understand whether the content and ratio of type I and type III collagens changed in the C57BL/6 dermis with age. Additionally, ageing of the basement membrane in C57BL/6 mice is not well characterised. We therefore sought to identify if changes occurred to the collagen proteins in this region- collagen IV and collagen VII.

To complete our analyses, we had access to formalin-fixed, paraffin embedded skin samples, whole skin snap-frozen in liquid nitrogen and skin samples prepared for transmission electron microscopy (TEM). Our objectives were therefore as follows:

3.4.2 Objectives of this section

1. Use western blotting and immunohistochemistry to identify changes in content of the dermal collagens, collagen I and collagen III in 3 mo and 30 mo animals.
2. Use immunohistochemistry to identify changes in the content and arrangement of collagens IV and VII at the basement membrane.
3. Use TEM to image ultrastructural changes at the basement membrane of young and aged animals

3.4.3 Factors for consideration in the immunostaining of dermal collagens in mice: Antibody Selection

The majority of antibodies are produced in small mammals such as mice, rats and rabbits (Wakayama et al, 2006). Commonly, monoclonal antibodies are produced in mice, but their use on mouse tissue presents a technical challenge because secondary antibodies directed against the mouse monoclonal primary antibody of interest will also detect endogenous mouse immunoglobulin in the tissue, along with the target of interest. This can result in the production of false positive data (Goodpaster and Randolph-Habecker, 2014). For this reason, we selected to complete our immunostaining for type I and type III collagens using antibodies produced in rabbits, as anti-rabbit secondary antibodies had a significantly reduced likelihood of binding non-specifically to mouse immunoglobulins present in the tissue.

A further issue with regards to identifying collagens in the dermis using immuno-histochemistry concerns the macromolecular structure of collagen fibres and their organisation in the dermal compartment. Collagen fibres are formed from the assembly of several collagen fibrils (Shoulder and Raines, 2009) and several non-collagenous molecules bind collagen fibres, such as glycosaminoglycans (Munakata et al, 1999). The natural molecular conformation of collagen, coupled with the fact it has several molecules bound to its surface in the dermal ECM, both increase the likelihood that the epitope sites for antibody binding will be masked. It could therefore be the case that, despite the presence of collagen in a tissue, antibody binding to epitope sites may not occur, leading to an absence of signal realization.

Polyclonal antibodies are typically produced in rabbits because of their convenient size, ease of handling and bleeding, relatively long life span, and adequate production of high-titer, high-affinity, precipitating antiserum (Leenaars et al, 2005). Additionally, these antibodies are able to recognize several antigenic epitopes, thus increasingly the likelihood of antibody binding to collagen antigen sites (Ivell et al, 2014). For these reasons, along with the reasons expressed above, rabbit polyclonal antibodies against collagen I and collagen III were used for our immunohistochemical studies.

3.4.4 Factors for consideration in the immunostaining of dermal collagens in mice: Use of paraffin embedded tissues

Another important consideration in the design of our experiments concerned the fact that the tissue available to us was subjected to paraformaldehyde-based fixation and was embedded in paraffin. Tissue fixation using reagents such as paraformaldehyde cause cross-linking of antigenic sites on the tissue, which obscures the presence of epitopes. This prevents antibody binding, so to overcome this, fixed and paraffin embedded tissues are typically

subjected to heat, acid or enzyme-mediated antigen retrieval methods (or a combination of the above) in order to re-expose the epitopes to allow antibody binding (Jiao et al, 1999). As different methods of antigen retrieval tend to expose antigenic sites in different ways (Shi et al, 2011), we experimented with both heat-induced antigen retrieval (HIAR) and enzymatic antigen retrieval (Enz AR) methods in order to determine the most suitable method for our collagen I and collagen III analysis.

3.4.5 Confirmation of antibody specificity and decline of collagen I and collagen III in aged mouse

Western blotting is routinely used to determine the specificity of an antibody, as the presence of a single band in a complex biological sample, at the expected molecular weight, confirms that the antibody selectively binds to its target protein (Signore and Reeder, 2011). In order to determine the specificity of our collagen I and collagen III rabbit polyclonal antibodies before proceeding to immunohistochemical analysis, we therefore completed Western blotting of whole skin lysates from 3 mo and 30 mo animals. We had 3 biological replicates for each of the 3 mo and 30 mo age groups and completed 2 technical replicates.

Additionally, we sought to determine whether our Western blotting would show us if there was any change in collagen I and collagen III protein levels with age. We therefore also determined equal protein loading between samples as part of our analysis so that we could confirm any detected differences in collagen I or collagen III were a result of genuine differences between samples and not unequal protein loading. As we had previously observed profound differences in the epidermal and dermal cellularity levels with age, conventional cellular loading controls (housekeeping genes such as GAPDH, actin, tubulin) were not a suitable method for the determination of equal protein loading in this instance, as they could result in an over-representation of protein content in the aged skin (where overall cellular levels were reduced). Instead, we considered total protein content in each sample by staining our gels with Coomassie blue, which identifies all protein bands within the sample (Chrambach et al, 1967) (See figure 3.3.7 in section 3.3.6 for representative gel image).

Once we had determined equal loading of our protein samples, we then proceeded with the Western blotting analysis of our mouse skin lysates using collagen I and collagen III antibodies. The results of the blots are shown in figure 3.4.1, which indicate that the collagen I and collagen III antibodies were specific to their targets as the detected bands were located at the predicted molecular weights for collagen I α1 (130kDa), collagen I α2 (139kDa) and collagen III α1 (138kDa).

Multiple strong banding was observed in the 3 mo samples for collagen I. Therefore, along with the bands for collagen α1 and α2, bands above these could represent heavier

collagen proteins where the collagen had polymerised or become cross-linked to other molecules. In the 30 mo samples the bands were much weaker indicating loss of collagen I α1 and collage I α2 protein. Collagen III α1 was weakly detected in the 3 mo samples in comparison to collagen I proteins in the same age group and in the 30 mo samples collagen III was barely detectable in these lysates.

The Western blotting data suggests that collagen I is more abundant in the skin compared to collagen III in both 3 mo and 30 mo animals and that both dermal collagens are reduced in aged C57BL/6 skin. However, it is important to note that these Western blots represent only the soluble fraction of dermal collagens and anything that was highly cross-linked or insoluble will not have been detected.
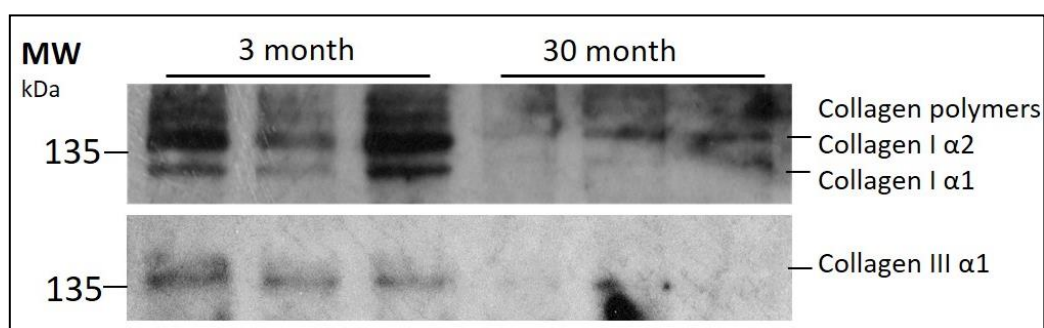
Figure 3.4.1. Dermal collagens are reduced in aged mouse skin. Western blotting of collagen I and collagen III using equal amounts of protein prepared from whole back skin lysates of mice aged 3 months and 30 months. Collagen I α1 chain (130kDa), collagen I α2 chain (139kDa), and collagen III α1 chain(138kDa) were all identified on the membrane. Note that the collagen I and III protein levels are drastically reduced in 30 mo animals compared to 3 mo animals.

3.4.6   Identification of dermal collagens in formalin-fixed, paraffin embedded mouse skin.

Our western blots indicated that the soluble fraction of collagen I and collagen III was decreased in the 3 mo and 30 mo animals. However, the blots did not give us information concerning how the collagen fibrils were arranged, or whether this reduction in soluble collagen impacted the dermal architecture of the mice.

In order to qualitatively identify how dermal collagens are reduced with age, we completed immunofluorescence on skin sections using collagen I and collagen III antibodies (details in materials and methods section 2.3). Figure 3.4.2 shows representative images of collagen I immunofluorescence in 3 mo (C, D) and 30 mo (E, F) mouse skin. In order to determine the most suitable method of antigen retrieval (AR) for antibody binding, we experimented with the use of an acidic HIAR using citrate buffer (C, E) and an Enz-AR using proteinase K enzyme in an alkaline buffer (D, F). Additionally, we completed control tissue

staining on 3 mo tissue sections subjected to HIAR (A) and Enz-AR (B) by omitting the primary antibody in the first incubation step (slides were incubated in primary antibody diluent instead). All other parts of the staining protocol were standardised between the control and primary antibody tissue sections, and the HIAR and Enz-AR tissue sections. Therefore, we could identify that any differences in staining observed would be a result of the behaviour of the primary antibody under the different AR conditions.

Comparison of the 3 mo (C) and 30 mo (E) tissues showed that the HIAR method produced a greater amount of labelling in the 30 mo skin, where this labelling was most prominent in the lower, reticular dermal area. (green arrowheads, E). Labelling of collagen was weaker in the 3 mo skin (C), and it showed a similar, but less pronounced pattern of staining with the strongest labelling being found in the reticular dermis (green arrowheads, C). Despite thorough washing, non-specific binding of large antibody molecules were present on the skin sections (white arrows, C and E), which were present on HIAR control slides in much lower numbers (white arrow, A).

Like in the HIAR, Enz-AR also showed that the greatest amounts of collagen were present in the lower, reticular dermis in 3 mo (D) and 30 mo (F) skin. However, the Enz-AR resulted in a different appearance of collagen staining compared to HIAR. This method allowed the resolution of some fine collagen I fibrils in areas; and surrounding hair follicles and other appendages they were particularly prominent (green arrowheads D, F). Using, Enz-AR, collagen I levels appeared to be similar in both the 3 mo and 30 mo skin. This method also resulted in non-specific antibody binding, which was located in the nuclei of the epidermis (white arrows D) and did not occur in control slides (B).
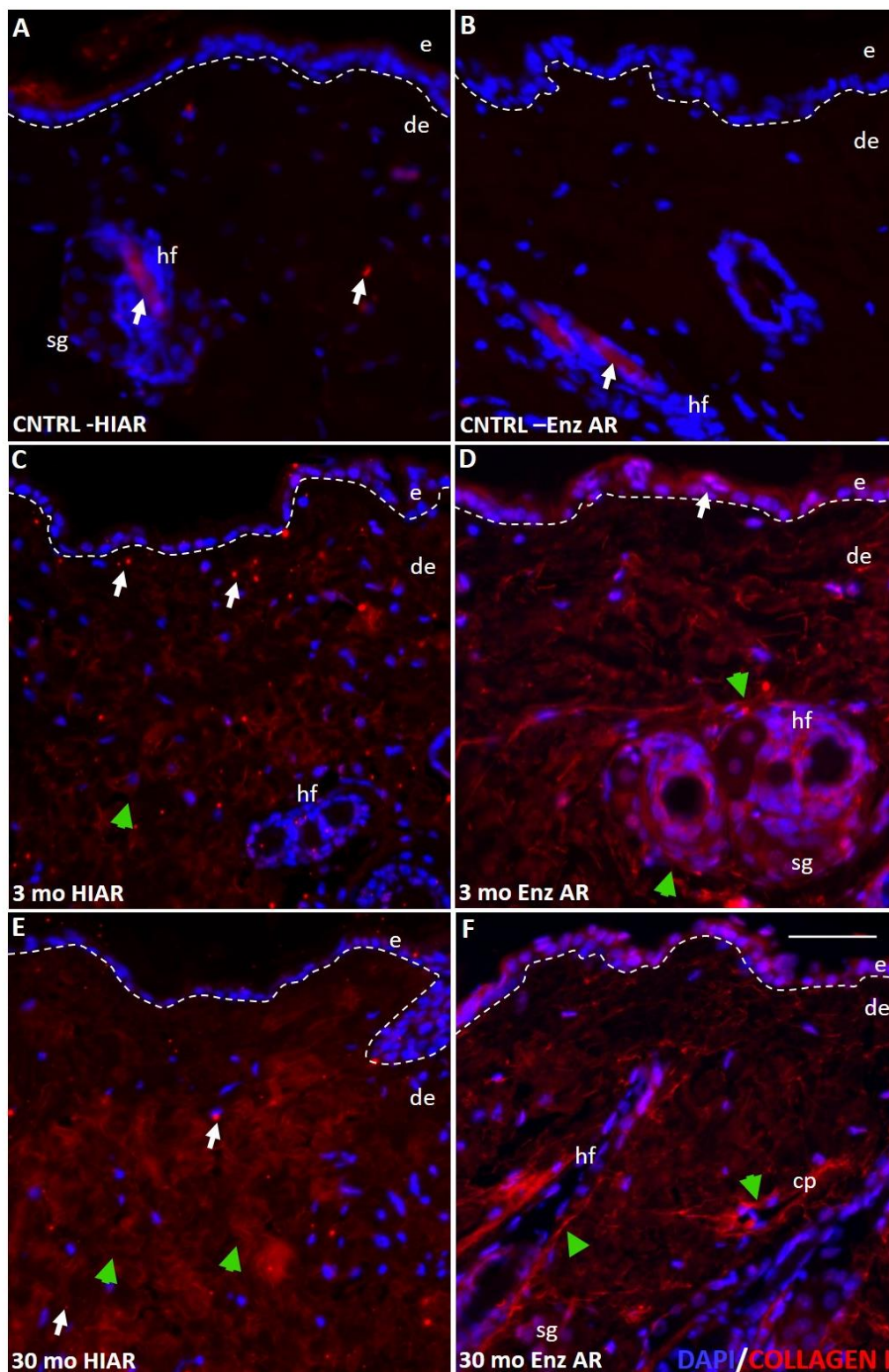
Figure 3.4.2: Optimisation of collagen I antibody staining using two different AR methods. 3 mo (C, D) and 30 mo (E, F) skin was subjected to HIAR (C, E) and Enz-AR (D, F) prior to staining with collagen I primary antibody, anti-rabbit Alexa 568 secondary antibody and DAPI nuclear counterstain. These slides were then compared to 3 mo control slides incubated with secondary antibody only (A= control subjected to HIAR), (B= control subjected to Enz-AR). All slides were imaged on a fluorescence microscope using a 20x objective lens. e= epidermis, de= dermis, hf= hair follicle, sg= sebaceous gland, cp= capillary, white dotted line= DEJ. Scale same for all 6 images, scale bar shown in F= 50 μm. White arrows show non-specific antibody binding in dermis (C, E) and nuclei (D) of HIAR and Enz-AR slides treated with primary antibody. White arrows also indicate autofluorescence of hair follicles in slides without antibody (A, B). Green arrowheads show collagen labelling in the reticular dermis (C, E) and surrounding hair follicles and capillaries (D, F).

We subsequently applied an identical methodology using a collagen III antibody and like for collagen I, the results were variable (figure 3.4.3). The HIAR method resulted in a homogenous labelling of collagen III in the dermis of 3 mo skin (A) and areas of reduced labelling in the 30 mo skin (green arrowheads, C). Large granules of antibody were non-specifically bound to the tissue (white arrows, A and C) in a similar fashion to tissue subjected to HIAR and collagen I antibody staining.

The young (B) and aged (D) skin subjected to the Enz-AR and collagen III antibody staining showed a poor signal. The signal was slightly greater in the 30 mo (D) skin and could be detected around hair follicles and other structures (green arrows, D). In the 3 mo skin the signal was barely detectable and was similar to control slides incubated with the secondary antibody only (B).
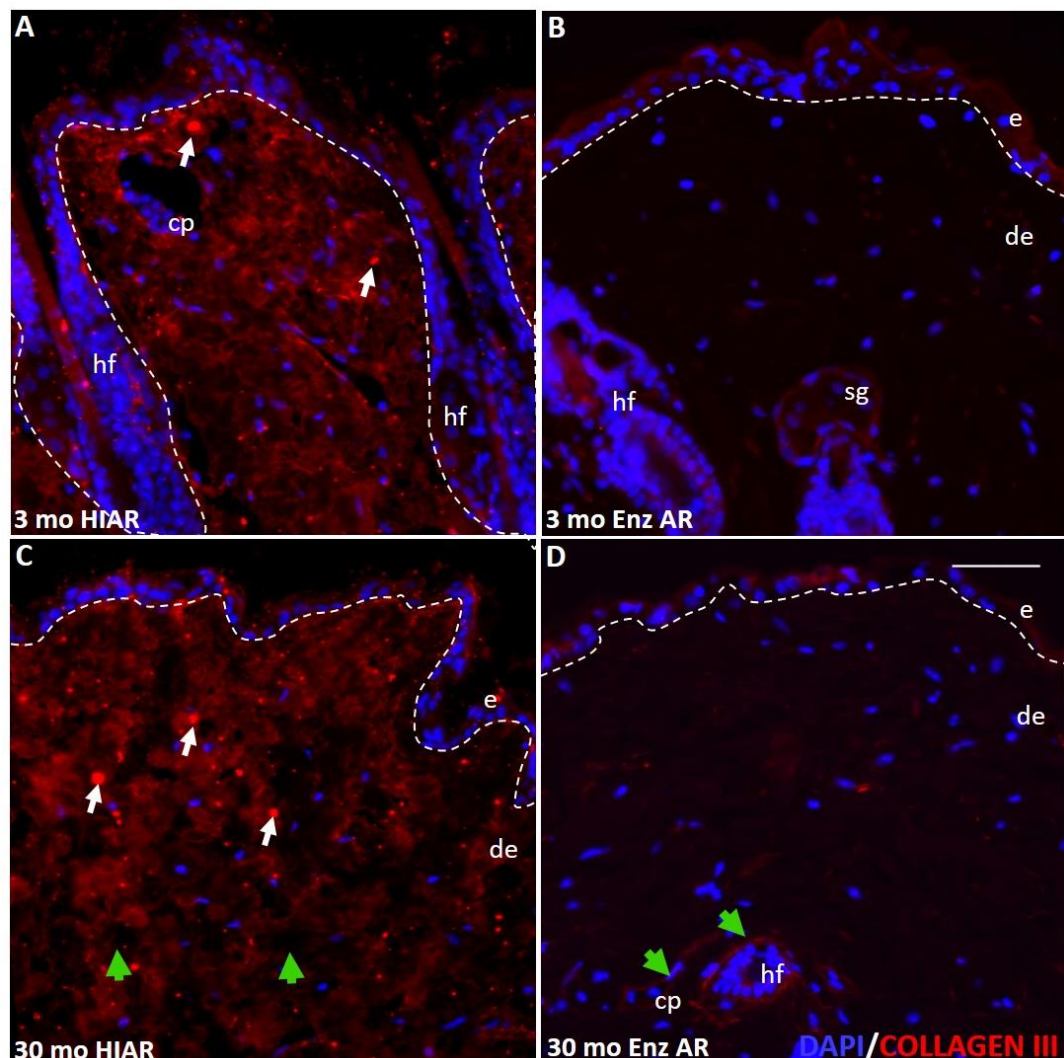
Figure 3.4.3: 3 mo (A, B) and 30 mo (C, D) skin subjected to HIAR (A, C) and Enz-AR (B, D) prior to staining with rabbit collagen III primary antibody, anti-rabbit Alexa 568 secondary antibody and DAPI nuclear counterstain. All slides were imaged using a fluorescence microscope and 20x objective. e= epidermis, de= dermis, hf= hair follicle, sg= sebaceous gland, cp= capillary. White dotted line= DEJ. Scale same for all 4 images, scale bar shown in D= 50 µm. White arrows show non-specific antibody binding (A, C). Green arrowheads show collagen labelling in the reticular dermis (C) and surrounding hair follicles and capillaries (D).

Altogether, immunostaining of collagen I and collagen III presented variable results. For the staining using the collagen I antibody, the HIAR showed greater staining levels of collagen I in the 30 mo skin whereas for the Enz-AR, similar levels were observed in both 3 mo and 30 mo skin. For the staining using the collagen III antibody, the HIAR produced a strong equal signal in 3 mo and 30 mo skin whereas the Enz-AR produced a weak signal in both 3 mo and 30 mo skin that was slightly increased in the 30 mo skin. Additionally, both AR methods and antibodies resulted in non-specific binding in different areas of the skin sections.

These immunofluorescence results conflict with our Western blotting data that shows that collagen I and collagen III levels decrease in 30 mo skin compared to 3 mo skin. Together these observations suggest that, despite exploring different AR methods, the immunofluorescence-staining for the dermal collagens produced sub-optimal results and for this reason we decided to explore alternative staining methods.

Although it was possible to try other methods of antigen retrieval or purchase different antibodies, this would have resulted in both a high financial and time investment. Alternatively, we decided to try methods that did not rely on unmasking of antigenic site and high-quality antibody binding. Polychrome histological stains are able to differentiate cellular structures from the surrounding ECM and several stains are highly specific for certain ECM structures such as collagens and elastins (Kazlouskaya et al, 2013). Histological staining involves the use of dye molecules, which typically are much smaller in size compared to antibodies. For example, the typical MW of an anti-mouse IgG is 150kDa [footnote 1] whereas a molecule of acid fuchsin dye display a molecular weight of 0.585 kDa[footnote 2]. Dye molecules can therefore be over 250 times smaller than antibodies. This is advantageous when one considers the structures of collagen molecules, as a dye molecule is more likely to be able to penetrate the small gaps between closely cross-linked fibrils compared to an antibody.

Additionally, dye molecules bind ECM structures due to being attracted to charged amino acids on their surfaces whereas antibody molecules rely on the presence of an epitope for binding. Collagens are rich in basic amino acids, which easily attract negatively charged dye molecules as they are protonated and therefore overall are positively charged (Motta and Ruggeri, 1984). Due to aforementioned issues regarding the potential for antibodies to bind collagens in a highly variable manner, exploring use of dyes that are selective and sensitive to the presence of collagen was a logical future step.

Footnote 1:(http://www.agrisera.com/en/info/molecular-weight-and-isoelectric-point-of-various-immunoglobulins.html.
Footnote 2: (https://pubchem.ncbi.nlm.nih.gov/compound/5464362).

The Van Gieson stain uses acid fuchsin dye (despite the name the overall charge of this dye in staining solution is negative and it therefore has a high affinity for collagen) in the presence of picric acid to distinguish collagen from other ECM material (Prentø, P, 1993). A variation on the Van Gieson stain is the Herovici polypichrome stain, which used picro acid fuchsin and picro aniline blue to differentiate young and mature collagens (Lillie et al, 1980). The stain has been used to show that the papillary dermis, and in particular the site at the DEJ is rich in young, type III collagen fibrils (Fitzgerald et al, 1996) and also to demonstrate the structural differences in the dermal compartment of mouse and human skin (Watt and Fujiwara, 2011). These previous reports have demonstrated that the Herovici stain is able to resolve type I and type III collagen along with nuclei and other dermal structures, indicating that it could be a useful method for distinguishing changes to the dermal collagens in the C57BL/6 skin with age.

A detailed example of how the Herovici stain presented in the dermal compartment of young mouse skin is shown in figure 3.4.4, which indicates that the stain was able to successfully differentiate between type I and type III collagens in the dermal region and showed a high resolution of collagen fibres. Furthermore, unlike the antibody staining for collagen, the staining showed little non-specific binding in either the dermal compartment or in epidermal nuclei. As the Herovici stain resolved the young and mature dermal collagens without non-specific binding and did not result in highly variable staining levels like the fluorescent immunohistochemistry, we therefore applied the technique on our 3 mo, 12 mo, 15 mo, 24 mo and 30 mo mouse skin samples in order to determine changes to the dermal collagens with age.
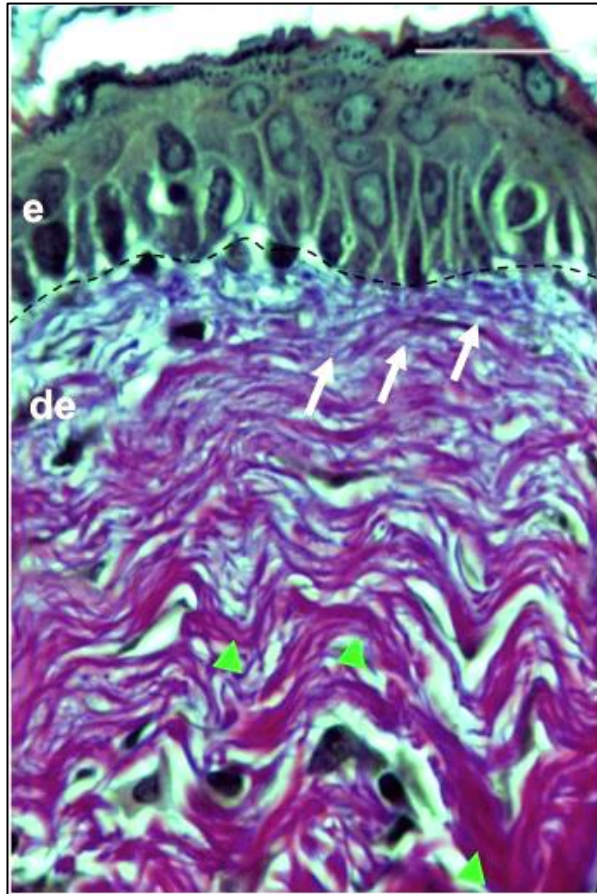
Figure 3.4.4: An example of Herovici staining in 3 mo (young) skin. Epidermal and dermal nuclei are stained blue/black. Young type III collagen is stained blue and mature type I collagen is stained magenta. Image taken using a light microscope and 40x objective. White arrows indicate the presence of fine, blue coloured collagen III fibrils in the upper dermis and green arrows show thick bundles of pink (collagen I) and blue-stained collagen fibres in the lower dermis. Black dotted line indicates DEJ. e= epidermis, de= dermis. Scale bar= 20 μm.

Figure 3.4.5 shows representative, low magnification images of Herovici stains of the epidermis and dermis of 3 mo-30 mo mice. At 3 mo, young collagen (i.e. collagen III) is abundant in the papillary dermis (PD), shown by the presence of fine blue and magenta stained fibrils running parallel to the DEJ (black arrows, A). Similarly, many thick, mature collagen I fibrils are present (green arrowhead, A) in the reticular dermis (RD). In the 12 mo skin, some of the young collagen III in the PD region is lost, shown by a reduction in the band of fine, blue fibril staining in the PD, indicating that the PD could be reduced in thickness compared to the 3 mo skin (black arrows, B). At 15 mo the PD remained similar in structure to the 12 mo skin, but there was some loss of mature collagen I in the lower RD (green arrowheads, C). The 24 mo skin was similar to the 15 mo skin with a thin band of fine collagen fibrils, some of which stained blue, running parallel to the DEJ in the PD (black arrow, D) and the presence of thicker magenta collagen bundles in the RD (green arrowhead, D). By 30 mo there was a noticeable loss of type I and type III collagen in the PD, with few blue fibres present and sparse bundles of magenta stained fibres remaining in some areas (black arrows, E). In the RD of 30 mo skin,

thinning of magenta-coloured mature collagen bundles was also observed and they appeared to take on a sparser arrangement compared to younger animals (green arrowheads, E).
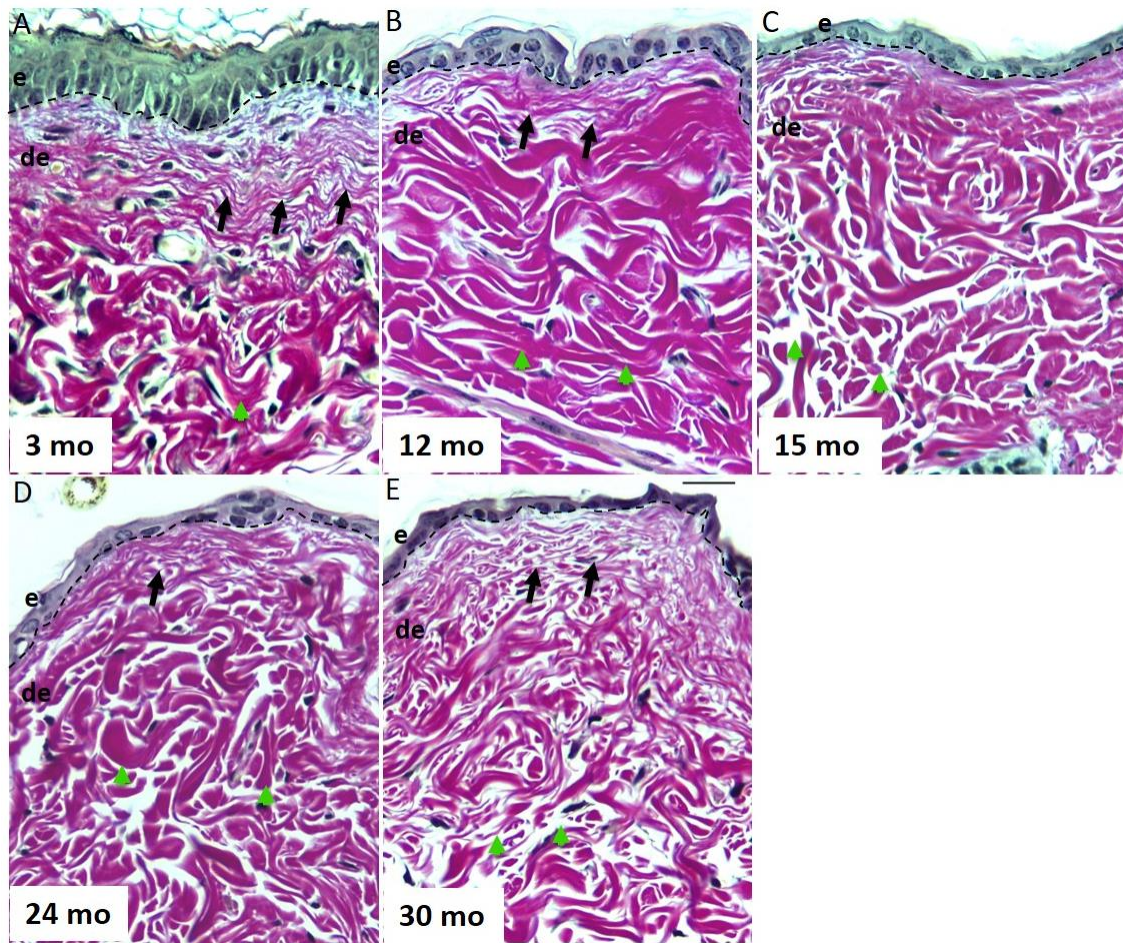
Figure 3.4.5: Herovici staining in 3 mo (A), 12 mo (B), 15 mo (C), 24 mo (D) and 30 mo (E) skin. Nuclei are stained blue/black, young, type III collagen is stained blue and mature, type I collagen is stained magenta. Images were taken using a light microscope and 20x objective. e-epidermis, de= dermis, black dotted line= DEJ. Scale same for all images and scale bar shown in E= 50 µm. Black arrows (A, B, D) represent fine collagen fibrils in the PD, which are reduced in number in 30 mo animals (E). Green arrowheads represent thick collagen bundles (A, B, C, D) in the reticular dermis that are lost in number with age and become thinner at 30 mo (green arrowheads, E).

In order to observe the papillary dermis (PD) and the arrangement of collagen at the DEJ in more detail, we used a 100X oil objective to image skin. Figure 3.4.6 shows the arrangement of collagen staining in the PD and at the DEJ of 3 mo (A), 12 mo (B), 15 mo (C), 24 mo, (D) and 30 mo (E) mice. At 3 mo the papillary dermis and the DEJ were rich in fine, collagen III fibrils (stained blue, black arrows, A). In deeper dermal areas there was a mixture of pink and blue fibre staining, suggesting the presence of both type I and type III collagen (green arrowheads, A). Although reduced in number, many fine collagen fibrils were also present in the papillary dermis of 12 mo and 15 mo animals (black arrows, B and C). Additionally, some of the fibrils were less blue and more magenta in colour, suggesting the presence of more mature, type I collagen in this region compared to the 3 mo skin. There was a reduction in number of

blue and magenta collagen fibrils in the PD of 24 mo and 30 mo skin, where very few young

collagen fibrils were present in the PD. In the 30 mo there was a sparse arrangement of

collagen I in the PD (green arrowheads, E) and type I and type III collagen loss at the DEJ was

prominent (black arrows, E).
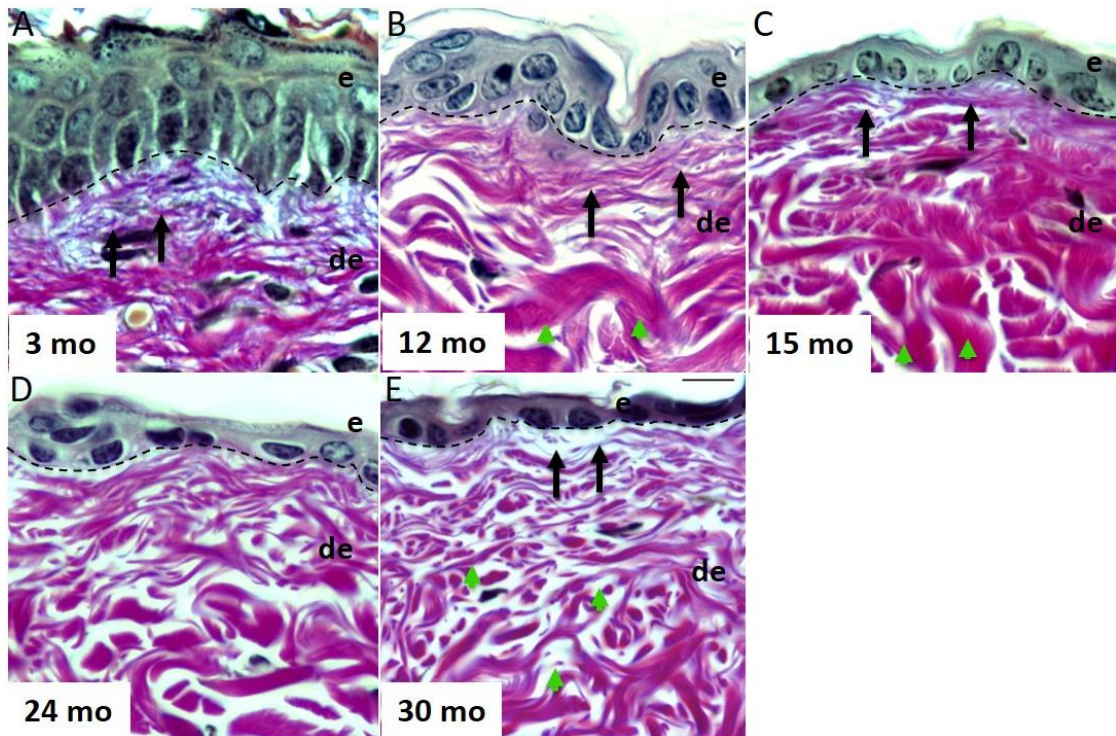
Figure 3.4.6: High magnification examples of Herovici staining in the PD and at the DEJ in 3 mo (A), 12 mo (B), 15 mo (C), 24 mo (D) and 30 mo (E) skin. Nuclei are stained blue/black, young, type III collagen is stained blue and mature, type I collagen is stained magenta. Images taken using a light microscope and 100x oil objective. e-epidermis, de= dermis, black dotted line= DEJ. Scale same for all images and scale bar shown in E= 10 μm. Black arrows (A, B, C) represent fine collagen fibrils in the PD. Green arrowheads (A, B, C) represent thick type I collagen bundles. Green arrowheads (E), represent thin type I collagen bundles. Black arrows (E) show collagen loss at the DEJ.

Overall, the Herovici staining showed that collagen I and collagen III were lost from the

dermis with age. It appeared that there was a dramatic loss of young type III collagen in the

papillary dermis and at the DEJ between 3 mo and 12 mo mice that could be a maturational

and therefore not an ageing-associated effect. However, type III collagens levels also declined

from 12 mo to 30 mo in this region, and by 30 mo, type III collagen levels were significantly

reduced in the PD and at the DEJ. This suggests that collagen III is lost in the PD of C57BL/6

mice during ageing. Collagen I levels also declined in both the PD and RD during ageing, but this

effect only became marked in the 30 mo animals. Collagen I loss did not appear to occur

specifically from one region, suggesting that over time intrinsic ageing causes a global loss in

mature, type I collagen from the dermis of C57BL/6 mice.

3.4.7 Identification of basement membrane (BM) changes in the C57BL/6 mouse skin with age

Several changes to the two epidermal BM collagens have been identified in aged human skin, including loss of collagen IV and VII (Langton et al, 2016), and fewer collagen VII anchoring fibrils at the DEJ (Craven et al, 1997), but relatively little is known about changes to the BM in ageing mouse skin. We therefore sought to identify if the epidermal basement membrane is modulated by ageing processes in C57BL/6 mice by using immunohistochemistry against type IV and type VII collagens. We also studied ultrastructural changes at the DEJ using transmission electron microscopy (TEM).

3.4.8 Collagen IV expression is altered in the epidermal BM of aged mice

As mentioned in the introduction of this thesis, collagen IV is the main protein found in the *lamina densa*, the lower part of the BM. In order to identify if collagen IV protein expression is changed in the basement membrane during ageing, we completed collagen IV immunohistochemistry on 3 mo and 30 mo mouse skin and imaged the results using confocal laser scanning microscopy (CLSM). Figure 3.4.7 shows representative 2D maximum projection z-stack images of 3 mo (A) and 30 mo (B) paraformaldehyde-fixed, paraffin embedded skin sections stained with a rabbit polyclonal collagen IV antibody following enzymatic antigen retrieval.

There was no apparent change in collagen IV levels, but the difference in organisation of collagen IV at the basement membrane of aged mice was marked. In the 3 mo mice, collagen IV protein expression was seen in a thin, dense band under the basal epidermal nuclei (presumably marking the lamina densa), whereas in the 30 mo animals it appeared thickened in areas (white arrows, B) and in other areas the staining was more diffuse compared to 3 mo skin (green arrows, B). We quantified the thickness of the collagen IV staining at the DEJ in 3 mo and 30 mo animals by taking perpendicular measurements across the band of collagen staining seen in this region. Examples of how we made these measurements are shown in figure 3.4.7 (A' = 3 mo, B'= 30 mo). Using a 100x oil objective and a fluorescent microscope, we captured 5images from each mouse and took 10 measurements at regular intervals in each image. 4 animals were present in each of the 3 mo and 30 mo age groups.
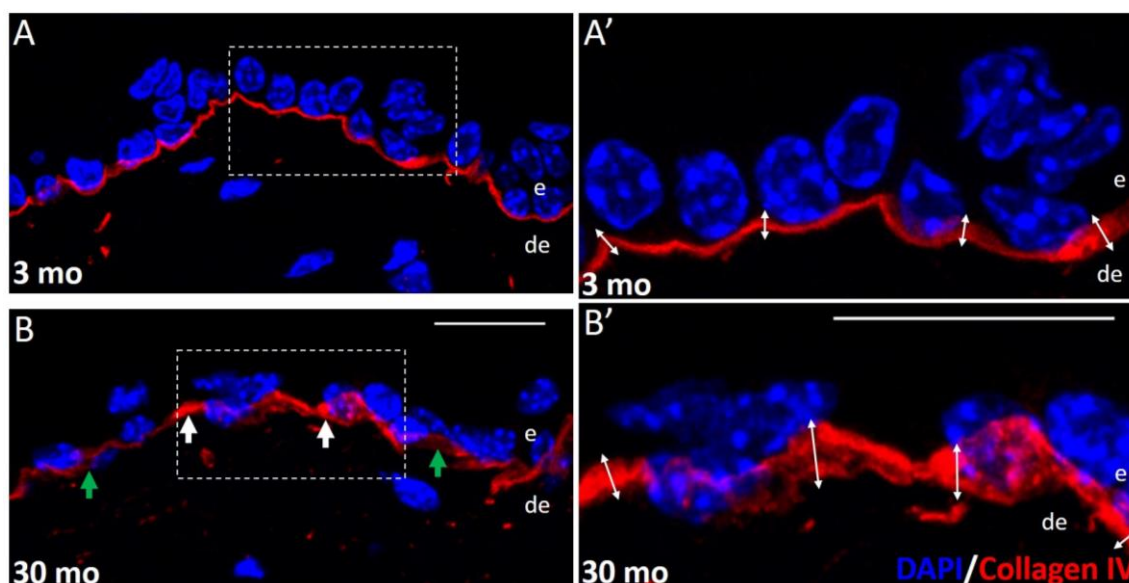
Figure 3.4.7: Analysis of change collagen IV protein levels and arrangement in 3 mo (A, A') and 30 mo (B, B') skin. C57BL/6 back skin was stained with a rabbit polyclonal collagen IV primary antibody then anti-rabbit Alexa 568 secondary antibody with DAPI nuclear counterstain. Images were captured using CLSM and a 63x oil lens. Representative examples of collagen IV staining in 3 mo (A) and 30 mo (B) skin are shown. A' and B' show magnified images of the two white dotted rectangles in A and B. White double-headed arrows (A' and B') show example measurements taken of collagen IV thickness at the DEJ. e= epidermis, de= dermis. Scale same for A and B, Scale same for A' and B'. Both scale bars shown in B, B' are 20 µm. White arrows (B) show thickening of the band of collagen IV in the BM of 30 mo animals. Green arrows (B) show diffuse collagen IV staining in 30 mo animals.

The results of our quantifications are shown below in figure 3.4.8, which depicts the thickness of collagen IV protein expression in the BM of 3 mo "young" and 30 mo "aged" mice. Figure 3.4.8 A shows the measurements of collagen IV/lamina densa thicknesses in the images taken from each of the 4 mice in each age group. The measurements from each mouse are represented by a colour coding system, with a different colour for each mouse (yellow, green, black and red). A shows that the majority of 3 mo measurements gave a BM thickness of around 1.25µm (several overlapping data points in this region) with a few outliers present. In the aged animals however, there was a huge level of variation in the average BM thickness, with one animal (black dots) having a relatively thin BM with little variation in thickness but other animals (red, yellow and green dots) showing high levels of variation in their mean BM thickness as measured by collagen IV expression. Figure 3.4.8 B shows the average BM thickness in the 3 mo "young" compared to 30 mo "aged" mice. There was a clear increase in the mean thickness of the BM marked by collagen IV in this area. We assessed the statistical significance of this difference using an un-paired t-test. This test showed that the difference in mean thickness between 3 mo and 30 mo animals was highly significant ($p < 2 \times 10^{-4}$).
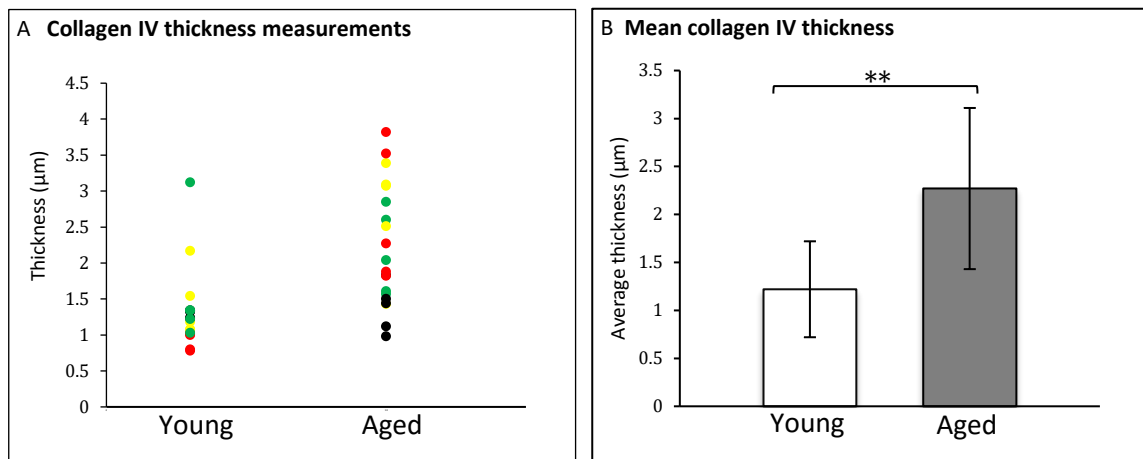
Figure 3.4.8: A The average BM thickness of young 3 mo vs aged 30 mo animals. Measurements from 4 animals were used for each age group and individual data points represent the average BM thickness in a single image taken from an animal. The 4 different mice in each age group are colour coded: red, yellow, green and black. B The mean BM thicknesses in young and aged mice as measured by collagen IV staining. Error bars represent standard deviations for each age category. Un-paired t-testing showed that the difference in mean BM thickness as measured by collagen IV staining was statistically significant

3.4.9   Loss of collagen VII from the basement membrane with age

Collagen VII expression at the BM was also assessed by immunohistochemical staining in 3 mo and 30 mo mice. As figure 3.4.9 shows, a thin line of collagen VII expression staining at the BM was observed in 3 mo animals along with some non-specific antibody binding in the stratum corneum (green arrows, A'). In the 30 mo animals, collagen VII expression at the basement membrane was negligible, indicating that expression was dramatically reduced in the aged 30 mo animals.
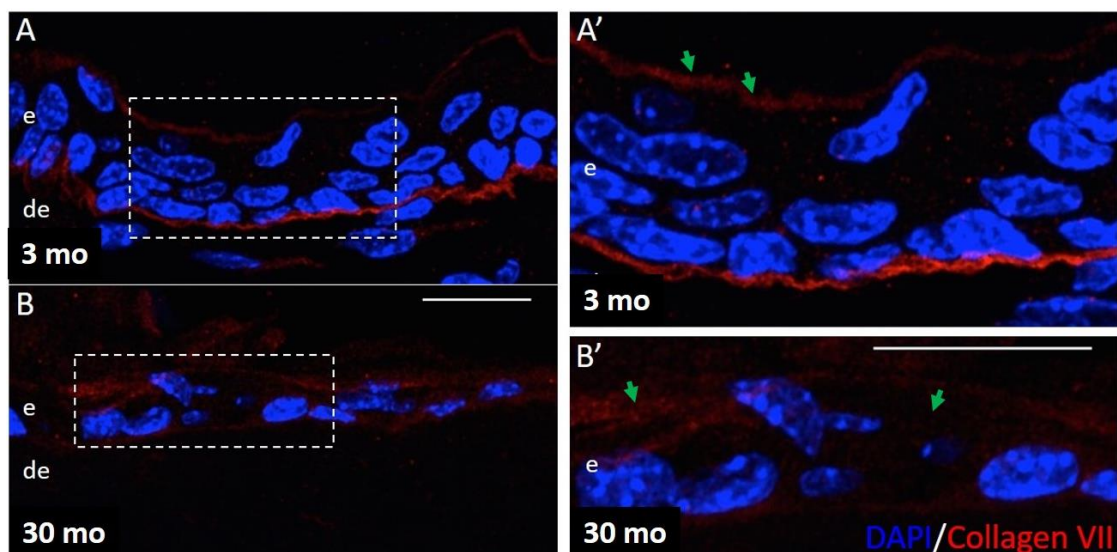
Figure 3.4.9: Immunofluorescence staining of collagen VII in 3 mo (A, A') and 30 mo (B, B') animals. Staining was completed using a rabbit collagen VII primary antibody coupled to Alexa 568 anti-rabbit secondary antibody with DAPI nuclear counterstain. Slides were imaged using CLSM and 40x objective lens. A'(3 mo) and B'(30 mo) show magnified images of the two white dotted rectangles in A and B. Scale the same for A+B and same for A'+B', both scale bars= 20 μm. Green arrowheads represent non-specific binding of the antibody in the stratum corneum.

3.4.10 Ultrastructural changes at the basement membrane in aged mice

As we had observed both a loss of collagen VII and abnormal BM architecture through collagen IV immunofluorescence in the 30 mo mouse skin, we sought to understand what ultra-structural changes were occurring at the basement membrane in young (3.75 mo) vs aged (23.5 mo) mice. We therefore employed the use of transmission electron microscopy (TEM) to study changes in this area in greater detail. Figure 3.4.10 shows example micrographs of young (A) and aged (B, C) C57BL/6 skin at the DEJ.

As the figure shows, the basement membrane was flat and uniform in thickness in young skin. Hemidesmosomes on the cell surface were regularly spaced (black arrowheads), without gaps between the basal cell cytoplasm and the BM. In the young skin collagen fibrils resident in the papillary dermis (PD) were regularly arranged in parallel bundles that were tightly packed (black arrow, A).

In the aged skin, the BM was typically less well defined and was more irregular in shape (black arrow, C). Additionally, the hemidesmosomes on the surface of basal keratinocytes were no longer regularly spaced along the BM and appeared more varied in shape (black arrowheads, C). In some areas, gaps were present between the cell cytoplasm and the basement membrane in aged skin (black arrows, B) that were not seen in younger tissues. Compared to the young tissue, the organisation of collagen fibrils in the papillary dermis (PD-C) was haphazard and collagen fibril loss was evident at the DEJ under the basement membrane (under black dotted line, B). It therefore appeared that the ultrastructural architecture of the BM and the collagen fibrils residing in the papillary dermis were modified with age.
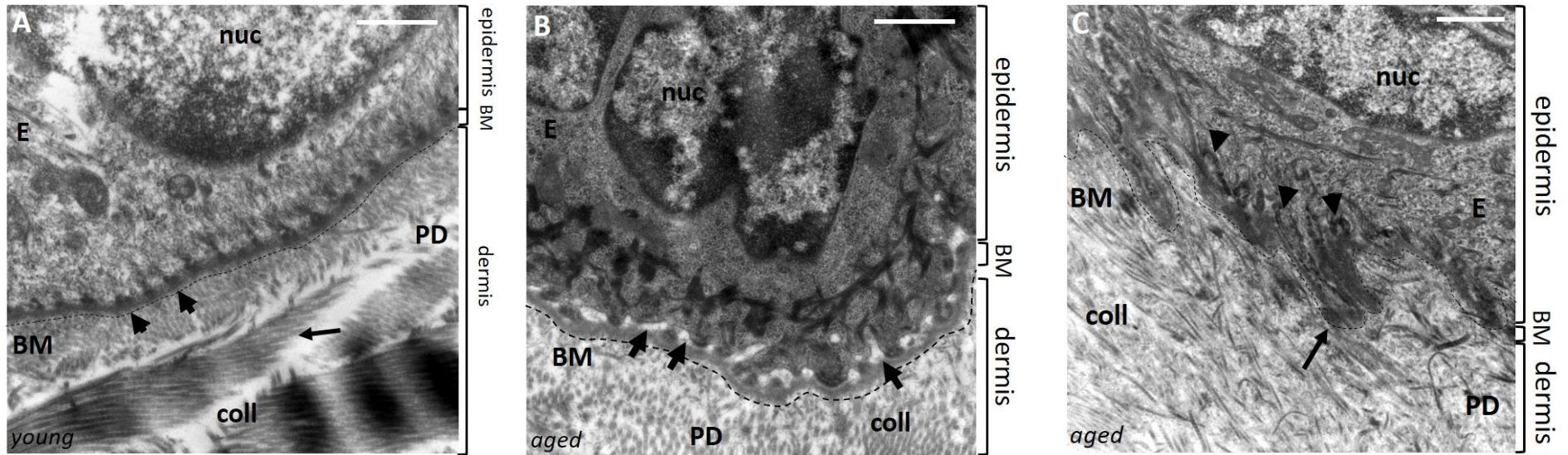
Figure 3.4.10: An ultrastructural comparison of the basement membrane in "young" (3.75 mo-A) and "aged" (23.5 mo-B, C) mice. Back skin from post-natal, left-ventricular infarct-induced mice (see materials and methods for more detail) was fixed in Karnovsky's fixative, sectioned for TEM and imaged using a Hitachi H7600 TEM at high magnification. Shown in all 3 images are E= epidermis, PD= papillary dermis, BM- basement membrane, nuc= nucleus, coll= collagen. Black arrowheads in A, C show hemidesmosome arrangement. Black arrowheads in B show gaps between cell cytoplasm and BM. Arrow in A= regularly arranged, dense collagen fibrils. Arrow in C= thickening and disorganisation of the BM in aged animals.

3.4.11 Discussion: Basement membrane and dermal collagen changes in aged mouse skin are similar to intrinsically aged human skin

The data presented in this section has explored the changes to the dermal and basement membrane (BM) collagens with age. Additionally, ultrastructural observations of the arrangement of young and aged skin at the DEJ have been made.

Our analysis has shown that the dermal collagens, collagen I and collagen III, are lost during the intrinsic ageing process in C57BL/6 mice and furthermore, these changes appeared to differ depending on the region of the dermis. In the papillary dermis, a marked loss of collagen III occurred between 3 mo and 12 mo mice, which could be representative of a maturational effect in these animals. Similar observations have been made in humans, as a quantification of the ratio of type I to type III collagen showed that in foetal skin, collagen I and collagen III are expressed in an ~1:1 ratio whereas in adolescent skin, there is 2.27 times more collagen I compared to collagen III (Cheng et al, 2011), indicating that decline in collagen III occurs in the skin of youthful humans as well as mice.

Over time we observed that collagen III levels continued to decline from the papillary dermis in ageing mice, suggesting that this is an ageing as well as maturational effect. Indeed, studies on intrinsically aged human skin have also shown similar, where between adolescent and elderly skin, type III collagen was lost at a greater rate than type I in the dermis (type I/III changed from 2.27±0.13 in adolescent to 2.97±0.40 in elderly- Cheng et al, 2011).

In the reticular dermis, where mature, collagen I was predominant in all age groups, levels were relatively stable from 3 mo to 24 mo but decreases in this protein were apparent in Herovici staining of skin from the aged 30 mo animals, which was also confirmed by Western blot analysis. In intrinsically aged human skin, changes in collagen levels only become apparent after the 8th decade of life (El-Domyati et al, 2002). This suggests that both human skin and C57BL/6 mouse skin show a similar trajectory of change in dermal collagen content during intrinsic ageing, with effects only becoming noticeable at very late stages in life in both models. Quantification of collagen changes in several other rodent models have shown dramatic decreases in the collagen content of aged animals, where other authors have shown that synthesis rates of dermal collagens in male lewis rats decreases 10 fold in 1m compared to 24 mo animals (Mays et al, 1991). In the skin of hairless mice, Boyer et al (1991), calculated a 30% decrease in total collagen content between mice aged 2m and 22m.

To our knowledge only one study has quantified the change in collagen levels with age in the C57BL/6 strain. Sayama et al (2010) used a Sircol™ colorimetric collagen assay to compare collagen content in the skin of 11 wk (2.75 mo) and 16 wk (4 mo) animals. This group found a significant decrease in collagen levels between the younger and older animals (510 ±

44.8 µg/ml in 16 wk animals compared to 672±56.7 µg/ml in 11 wk animals, p <0.05). This study was limited in the sense that it detected changes between age groups that are not far apart in age in terms of the mean lifespan of this strain of mouse (a difference of 1.25 mo is not a significant period of time in an animal that can live for up to 35 mo) and therefore our report of decreased collagen I and III between 3 mo and 30 mo mice is more significant in identifying age-related loss of collagen from the dermis in this strain with age. Our work, however, is limited by a lack of quantitative analysis of these observed collagen losses. Future efforts should look to develop our findings by completing densitometry on both biological and technical replicates of Western blots from 3 mo and 30 mo C57BL/6 skin samples to provide a semi-quantitative evaluation of changes to collagen I and collagen III protein levels with age. Additionally, quantitative collagen assays, such as measurement of hydroxyproline residues can even be completed in paraffin embedded tissues (Schwartz et al, 1985), which would allow us to express these changes in collagen levels in young vs aged skin in numerical terms.

Collagen loss also occurred at the BM, where collagen VII levels were markedly declined in aged 30 mo compared to young 3 mo mice. The paucity of data available on protein-based changes in the BM of ageing mice makes our observation novel, and it is consistent with data from intrinsically aged human skin that has shown a decline in collagen VII (Langton et al, 2016). Interestingly, collagen IV loss was not visible in this region, which may reflect the insensitivity of our immunohistochemical technique, as collagen IV is highly abundant in this region, and therefore a small change in amount of this protein would need a sensitive technique to be detected. Alternatively, this observation may be genuine, which would mean that changes to collagen IV in ageing mouse skin are different to human skin, where Langton et al, 2016 have shown a decrease in collagen IV protein in this region with age. What was clear however, from both this collagen IV immunofluorescence and from our TEM studies, was that the thickness of the basement membrane increases and shows greater variance with age, which was also observed by Vázquez et al, 1996 during intrinsic ageing in female human skin. Additionally, other reports have shown similar in the BM's of aged human corneal epithelia, which indicates that BM thickening may not be an age-associated effect that is confined to the skin only (Alvarado et al, 1983).

At the ultrastructural level, we observed that the BM becomes increasingly more disorganised with age, with striking loss of regular hemi-desmosome arrangement and the BM itself taking on a corrugated (bumpy) appearance. TEM studies from photo-aged human skin have shown re-duplication of the lamina densa in this region (Amano, S. 2009), which was not a regular occurrence in our intrinsically aged mouse skin, suggesting that this feature may not occur during intrinsic skin ageing. One important caveat to mention from our TEM analysis was

the fact that the data collected was completed on mice that had a compromised cardiac output, where a left-ventricular infarct had been induced after birth. Future studies should therefore determine that the observed ultra-structural differences in the young and aged mice occur in additional control animals.

Despite several attempts we were unable to identify collagen IV and collagen VII in our whole skin lysates through Western blot and were therefore unable to complete a semi-quantitative analysis of protein levels in 3 mo and 30 mo skin through this technique. It is challenging to de-lineate whether this was a result of poor antibody performance under blotting conditions or whether protein abundance in the whole skin sample was too low for obvious detection. This suggests that a different approach would be needed to perform quantitative evaluation of the change in levels of these proteins with age. This could be assessed by quantifying fluorescence intensity in this region in immunohistochemical stainings from young and aged mice.

Ultrastructurally, our TEM data revealed profound changes in BM architecture with age and one of the most prominent changes appeared to be occurring in the hemidesmosomes. Future work could look to quantify changes in their spacing along the BM with age. Additionally, the increased disorganisation of the basal lamina in this area caused the BM to appear much less flat in nature. To determine the extent at which this occurs with age, the length of BM per unit area in the skin could be measured to determine if this increases with age.

3.5   Identification of YAP1 modulation in aged C57BL/6 epidermis

3.5.1   Introduction and objectives

In our aged mice, we have observed several changes in the skin properties of aged animals that prompted us to inspect a change in the levels and localisation of YAP1. They are outlined bullet points below:

1. **Epidermal cell proliferation changes**

Cell proliferation is decreased in epidermis of young (3 mo and 12 mo) compared to aged (24 mo and 30 mo) animals. As YAP1 regulates epidermal cell proliferation, the changes we observe could reflect differences in YAP1 expression levels and its localisation in young compared to aged skin.

2. **Changes to dermal ECM with age**

We saw several changes to the dermal ECM, in the form of loss of collagen I and collagen III from the dermis, and in particular, collagen III loss at the papillary dermis (PD) and a decrease in the thickness of the PD with age. The PD in human skin is softer than the reticular dermis (RD) (Achterberg et al, 2014) and overall, dermal ageing is associated with an increase in tissue stiffness (Pawlaczyk et al, 2013). The changes we observe in our aged mouse skin therefore suggest (although do not directly prove) that the dermal compartment may change its biomechanical properties with age. As YAP1 is responsive to the biomechanical properties of the tissue microenvironment, these observed changes may modulate its expression and subcellular distribution in the epidermal cells, which are situated above the dermal compartment.

3. **Loss of basement membrane organization**

We have shown a loss of collagen VII at the DEJ of aged mice, coupled with an increasingly disorganized BM architecture seen by collagen IV labelling and ultrastructural studies. These changes could impact the mechanical properties of the BM and in a similar way to dermal collagen changes, modulate YAP1 biology in basal epidermal keratinocytes.

4. **Basal cell flattening in aged epidermis**

At low cell density, when cells become flattened, YAP1 is typically localised to the nucleus whereas at high cell density, when cells are rounded and tightly packed, YAP1 localises to the cytoplasm (Wada et al, 2011). Furthermore, in the developing lens, YAP1 is crucial for maintaining the apical-basal polarity of lens epithelial cells, and in its absence, cells become disorganised and flattened (Song et al, 2014). In aged mouse epidermis, we have shown that

both the density of cells in the basal layer and their nuclear shape, undergoes a prominent change. We therefore wanted to know, given that both cell-shape and cell-density changes have been shown to modulate YAP1 localisation in previous reports, if this contributed to a change in YAP1 in the aged mouse epidermis.

The above changes, and their potential to regulate the localisation of the Hippo pathway effector YAP1 in aged skin, therefore prompted us to investigate YAP1 in more detail. Our objectives in this section were therefore:

1) Use immunohistochemistry to assess the level and arrangement of YAP1 in C57BL/6 mouse skin of various ages.
2) Identify if there is a difference in the amount of nuclear YAP compared to cytoplasmic YAP in young vs aged epidermis.

3.5.2 Validation of YAP1 antibody

Reports of expression of YAP1 in mouse embryonic skin and neonatal mouse have been previously published (Silvis et al, 2011; Zhang et al, 2011; Schlegelmilch et al, 2011), but studies of its expression in aged skin have not been completed. We therefore completed immunofluorescence staining of YAP1 in skin sections taken from 3 mo, 12 mo, 15 mo, 24 mo and 30 mo animals. Beforehand, we confirmed the sensitivity of our antibody by completing immunofluorescence on HaCaT cells cultured at low and high cell density and Western blotting in whole skin lysates. Figure 3.5.1 shows the results of the immunofluorescence staining, which showed that YAP1 was predominantly localised to the cytoplasm in cells cultured at a high density (white arrows, A) and was predominantly localised to the nucleus in cells cultured at a low density (white arrows, B). The suggested that the antibody identified differential modulation of YAP1 depending on cell density, thus showing it behaved in a manner consistent with previous reports (Wada et al, 2011; Piccolo et al, 2014).

Figure 3.5.2 shows Western blotting of 3 mo and 30 mo whole skin lysates using the same antibody. Faint bands of protein were seen at the predicted molecular weight for YAP1 (65kDa). As this antibody showed protein bands present in whole skin at the correct molecular weight, and demonstrated predicted re-localisation of YAP1 in cells cultured at low and high cell density, we therefore deemed it suitable for immunohistochemical staining.
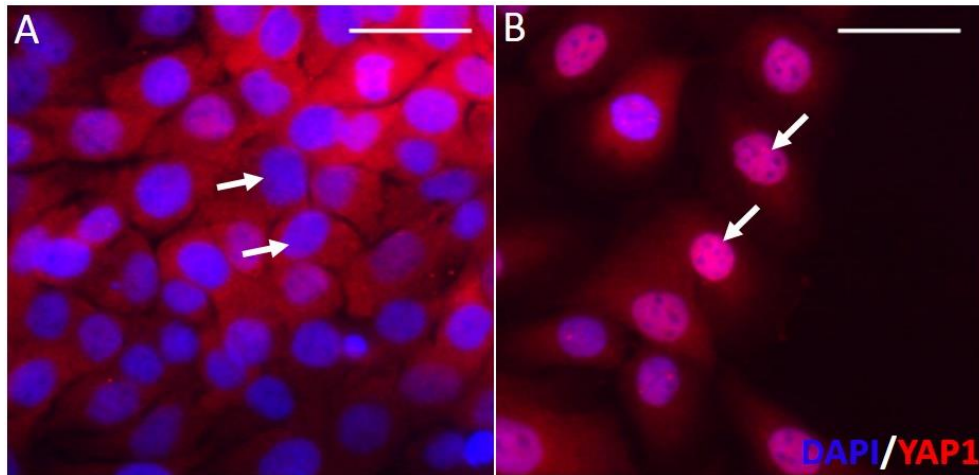
Figure 3.5.1: Expression of YAP1 in HaCaT cells cultured at high (A) and low (B) cell density. HaCaT cells were cultured on poly-D-lysine coated glass coverslips prior to fixation and staining with an anti-rabbit YAP1 antibody, Alexa 568 secondary antibody and DAPI nuclear counterstain. At high cell density, YAP1 was mostly absent from the nucleus (white arrows, A) whereas at low cell density YAP1 was abundant in the nucleus (white arrows, B). Scale bars= 20 µm.
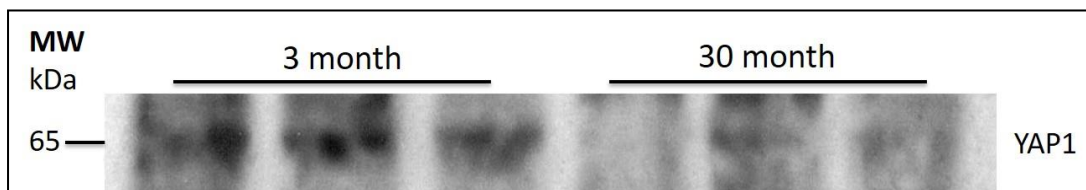
Figure 3.5.2: Expression of YAP1 in young and aged whole skin lysates confirmed by Western blot. Equal protein levels of lysates from three mice aged 3 months and three mice aged 30 months were subjected to gel electrophoresis and immunoblotting. Bands were seen at the correct molecular weight for YAP1, suggesting specificity of the antibody.

3.5.3   Expression of YAP1 in young, middle age and aged mouse skin

We stained 3 mo, 12 mo, 15 mo, 24 mo and 30 mo mouse skin with the anti YAP1 antibody, and then used confocal laser scanning microscopy (CSLM) to take Z-stack images of our results. By capturing images in both the X, Y and Z planes, we were able to obtain maximum information concerning the nuclear and cytoplasmic location of YAP1 in the tissue sections. Results of our staining and imaging is shown below in figure 3.5.3, which depicts 2D maximally-projected images of the Z-stacks, showing the arrangement of YAP1 in the cells of the epidermal and dermal regions. In the epidermis, YAP1 localisation was variable and we noted high levels of nuclear staining in the granular layer of the epidermis in areas (white arrows in epidermis- A, C, E). In the basal layer, YAP1 localisation was also variable where some cells had predominantly nuclear YAP and others had cytoplasmic YAP. In the dermis, cells with both nuclear YAP (N-yap- A, D, E) and cytoplasmic YAP (C-yap-A, C, D, E) were present in tissues from all age groups.

Figure 3.5.4 presents magnified images of YAP1 staining in the epidermal region of 3 mo, 12 mo, 15 mo, 24 mo and 30 mo mice. In the basal layer of 3 mo animals, we observed YAP1 nuclear staining (green arrows, 3.5.4 A) and also cytoplasmic staining. In the basal layer of 12 mo and 15 mo animals, nuclear YAP in the basal epidermal layer appeared reduced (3.5.4 B, also 3.5.3 C). In the 24 mo and 30 mo animals, nuclear YAP1 in the basal layer was observed in many of the cells (Green arrows- 3.5.4 D, 3.5.3 E). In the outer epidermal layers, punctuate nuclear YAP was present in many of the cells in 3 mo, 12 mo, and 15 mo animals (White arrows, 3.4.4 A, 3.5.3 B and C), which was seen to a lesser extent in 24 mo and 30 mo epidermis.
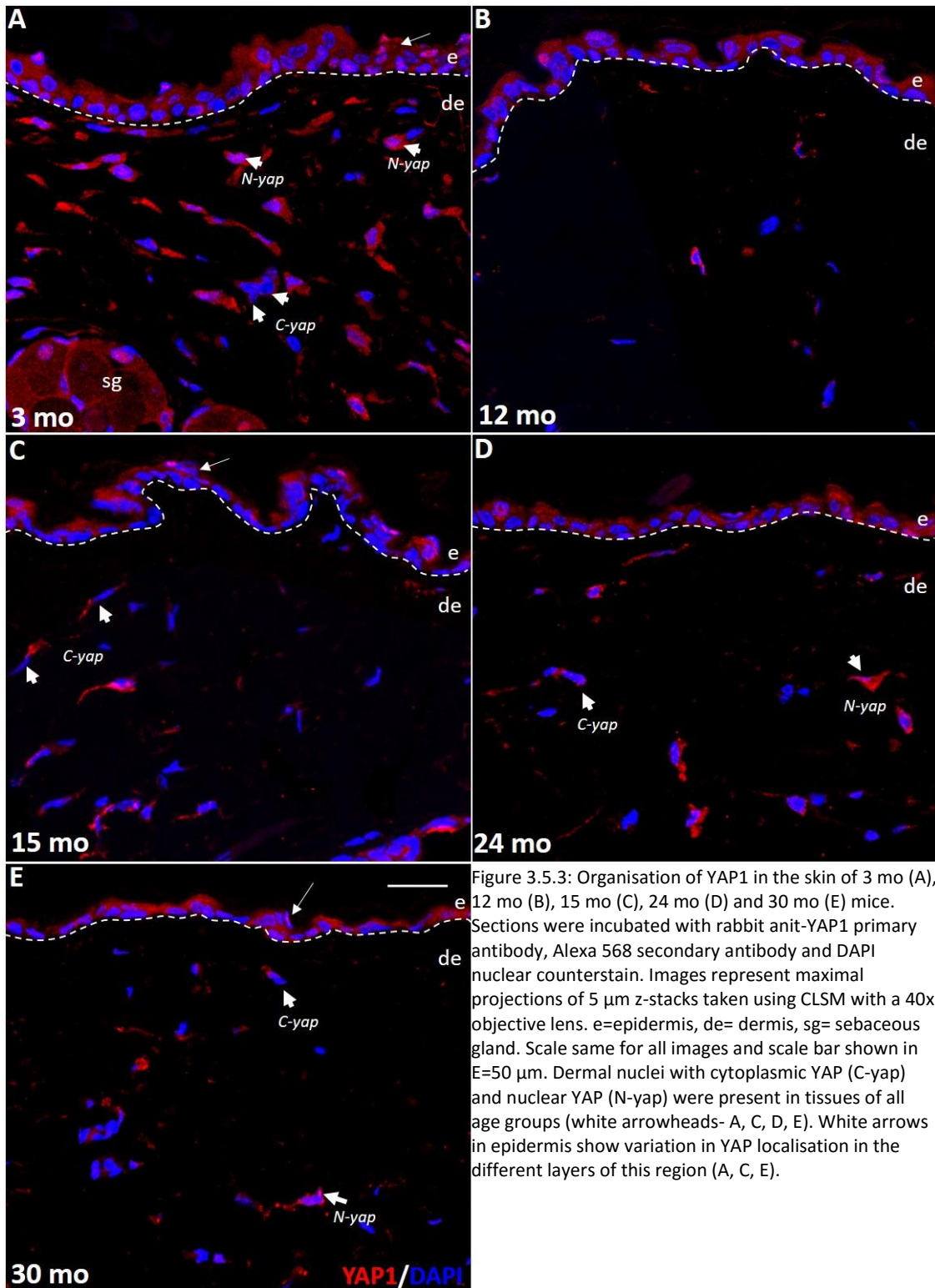
Figure 3.5.3: Organisation of YAP1 in the skin of 3 mo (A), 12 mo (B), 15 mo (C), 24 mo (D) and 30 mo (E) mice. Sections were incubated with rabbit anit-YAP1 primary antibody, Alexa 568 secondary antibody and DAPI nuclear counterstain. Images represent maximal projections of 5 µm z-stacks taken using CLSM with a 40x objective lens. e=epidermis, de= dermis, sg= sebaceous gland. Scale same for all images and scale bar shown in E=50 µm. Dermal nuclei with cytoplasmic YAP (C-yap) and nuclear YAP (N-yap) were present in tissues of all age groups (white arrowheads- A, C, D, E). White arrows in epidermis show variation in YAP localisation in the different layers of this region (A, C, E).
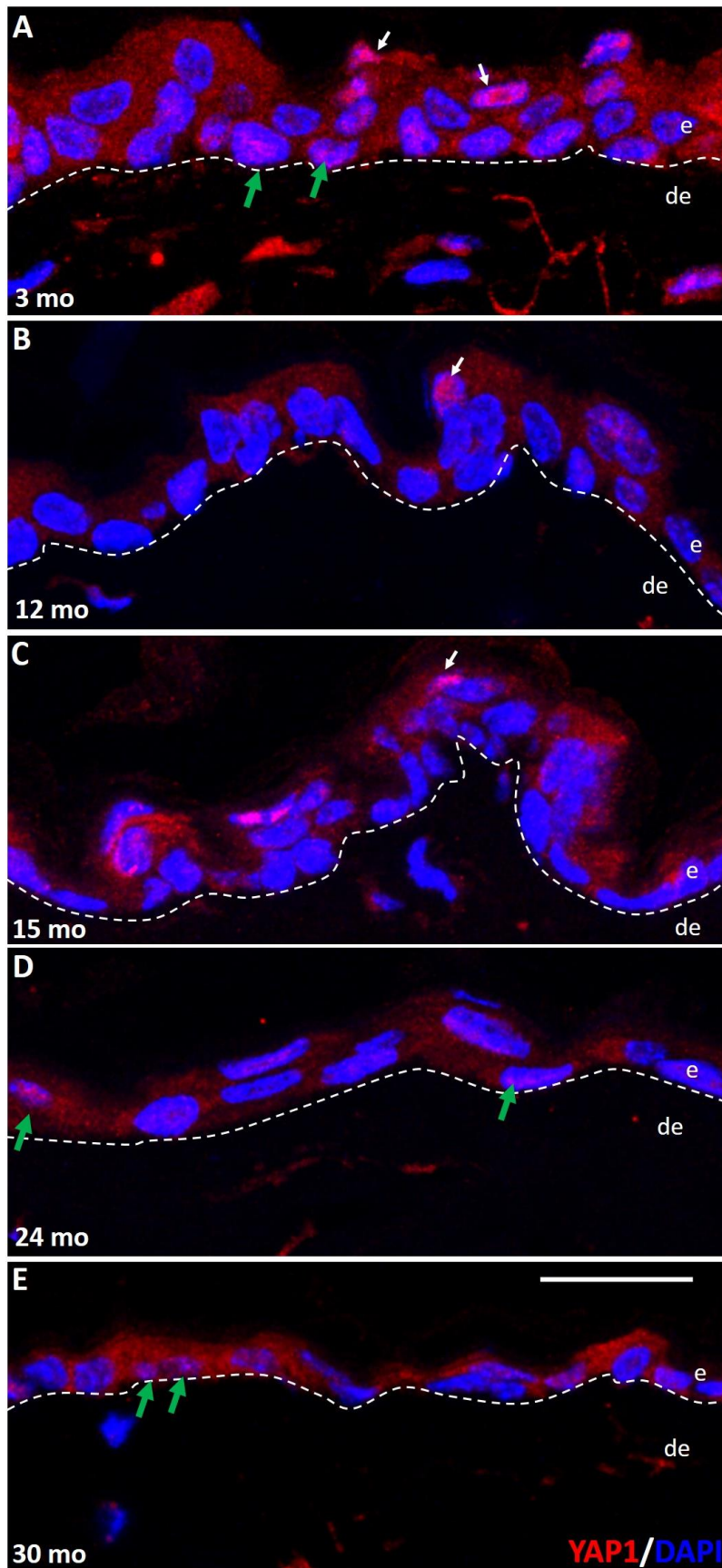
Figure 3.5.4: Localisation of YAP1 in epidermis of 3 mo (A), 12 mo (B), 15 mo (C), 24 mo (D) and 30 mo (E) skin. Sections were prepared and imaged as for figure 3.5.3. e=epidermis, de= dermis. Scale same for all images and scale bar shown in E=20 μm. YAP1 staining in some cells of the upper epidermis showed intense, nuclear YAP staining (white arrows, A, B, C). In the basal epidermal layer YAP1 localisation was variable with some cells showing nuclear YAP (green arrows A, D, E) whereas in other regions YAP was cytoplasmic.

3.5.4 The nuclear to cytoplasmic ratio of YAP1 is altered in aged epidermis

Given our observations of differential localisation of YAP1 in the different layers of young and aged epidermis, we sought to investigate whether the localisation of nuclear YAP1 changed in the resident epidermal cells with age. We therefore calculated the nuclear to cytoplasmic ratio of YAP1 in epidermal nuclei from 6 representative images taken from 2 mice aged 3 mo and 2 aged 30 mo. Previous authors have used binary masking techniques to calculate the nuclear to cytoplasmic ratio of cellular transcription factors such as NF-κB (Fujihara et al, 2002; Noursadeghi et al, 2008). We used a similar approach to isolate nuclear YAP1 from cytoplasmic YAP1 in the epidermis of images from 3 mo and 30 mo mice (details in materials and methods part 2.3.8).

To capture the entire slice of the epidermis in each tissue section we imaged, we took Z-stack images prepared as described in figure 3.5.3, using a 63x oil objective lens and imaging conditions optimised to 1 Airy unit. Figure 3.5.5 shows the results of the analysis, which indicated that the nuclear to cytoplasmic ratio in young 3 mo animals was close to 1, therefore suggesting equal distribution overall of YAP1 in the cytoplasm and nuclei of the cells of the whole epidermis in this age group. In the 30 mo animals however, the average nuclear to cytoplasmic ratio value was 1.2, indicating a greater amount of nuclear YAP1 compared to cytoplasmic YAP1 in this age group. To determine if this change was statistically significant, an un-paired t-test was completed on the data, and the result indicated that the difference in the epidermal nuclear to cytoplasmic ratio of YAP1 in 3 mo compared to 30 mo was statistically significant ($p=0.009$).
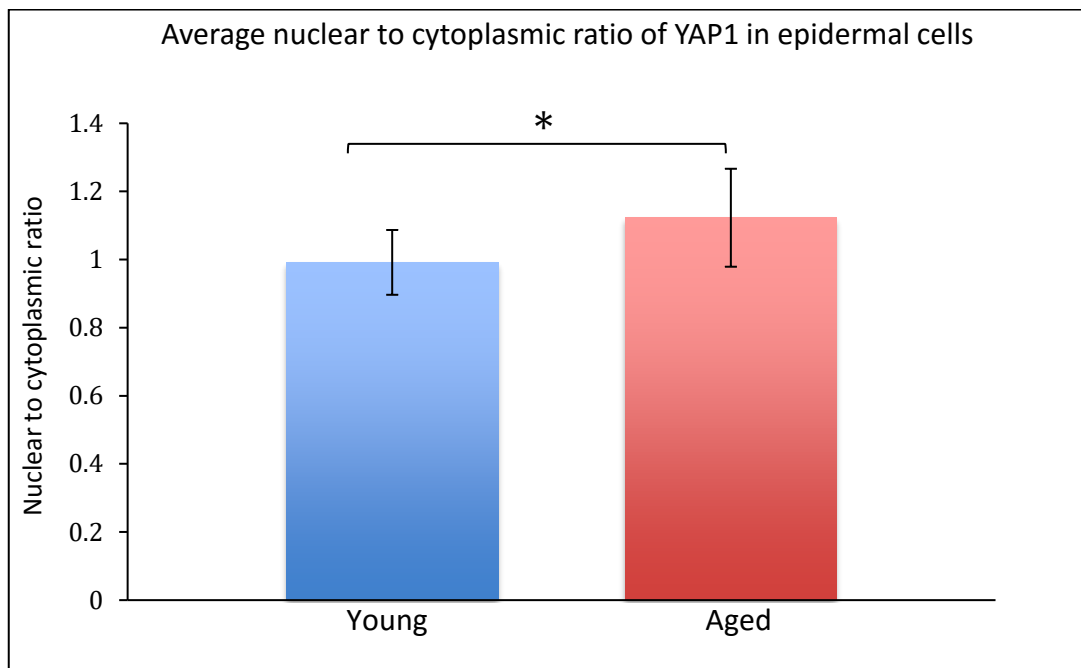
Figure 3.5.5: Analysis of the nuclear to cytoplasmic ratio of YAP1 in the epidermis of young (3 mo) compared to aged (30 mo) mice. Measurements were taken from 6 images each from 2 mice in each age group using CLSM. Difference in the mean nuclear to cytoplasmic ratio in the 2 age groups was assessed by un-paired t-testing and shown to be statistically significant (p=0.009).

3.5.5   Discussion: Increased nuclear localization of YAP1 in aged epidermis

The data presented here demonstrated validation of the use of a rabbit polyclonal YAP1 antibody in order to produce novel staining of YAP1 in C57BL/6 mice of several age groups. Our analysis has shown that YAP1 localisation is changed in the cells of the epidermis of aged mice, where an increase in nuclear-localised YAP1 occurs. There are several reasons why more nuclear YAP1 may be present in the epidermis of aged animals compared to young animals. Nuclear-localised YAP1 drives epidermal cell proliferation in the basal epidermis (Zhang et al, 2011). We have observed that a dramatic loss of cells occurs in the epidermal compartment between 3 mo and 30 mo animals and from staining of undifferentiated (K14) and differentiated (K10, loricrin) cells in both 3 mo and 30 mo animals, it appears that basal epidermal cells (K14 positive) are maintained in 30 mo epidermis whereas terminally differentiated cell numbers are reduced compared to young epidermis. This was previously indicated by a loss of the terminal differentiation marker loricrin in aged skin (see section 3.2.7).

If it is the case that basal epidermal nuclei make up a greater proportion of the whole epidermis in aged animals as we have observed, this would mean that the most proliferative compartment of the epidermis is maintained during ageing. As YAP1 drives proliferation, and aged epidermal SC's spend a greater amount of time in the cell cycle compared to young (Charruyer et al, 2009), the increased nuclear YAP1 calculated from our data here concerning

the overall epidermis in young and aged mice may reflect this change in the proportions of the k14 positive epidermal cells present in young compared to aged skin. A future experiment to validate this would be to analyse the nuclear to cytoplasmic ratio of the cells isolated in the basal epidermis *only* of 3 mo and 30 mo skin, by completing dual immunofluorescence of K14 and YAP1. This would allow us to more accurately de-lineate the contribution of the basal epidermal cells to this change observed in YAP1 nuclear localisation with age.

Additionally, many of the cells in the outer epidermis had intense nuclear YAP1 staining in the 3 mo, 12 mo and 15 mo animals. This was seen to a lesser extent in 24 mo and 30 mo animals. As cells in this layer are undergoing several changes in order to form the cornified envelope, future research could look to understand if YAP1 plays a role in the flattening and programmed apoptosis known to occur in these cells to allow them to form the stratum corneum (Simpson et al, 2011). As a difference in the numbers of these cells is purely observational at present, future efforts to quantify the difference in their number in young and aged animals would also provide more information about a potential change in their numbers with age.

Along with potential changes to YAP1 localisation due to proliferation-based reasons, the increased nuclear localisation of YAP in the aged epidermis could also be a result of mechanical changes occurring to the skin. Several methods are available to calculate the stiffness (Young's modulus) of skin *in vivo* (reviewed in Liang and Boppart, 2010*)* and at present, no data is available indicating quantitatively how the skin of C57BL/6 mice changes with age*.* Future studies should therefore look to draw parallels between the stiffness of the epidermis and underlying dermis in young compared to aged animals of this strain to determine how this contributes to the differences in observed YAP1 nuclear localisation in the cells of the epidermis. As the fibroblasts of the dermis are a relatively quiescent cellular population in comparison to the keratinocytes of the epidermis, there is a potential that they are differentially responsive to both changes in the mechanical properties of aged dermis and proliferative cues. Future studies should therefore look to study this cellular population in more detail.

Chapter 4: Transcriptomic and proteomic analyses of a multi-decadal cohort of photo-protected and photo-exposed female skin tissues.

4.1   Introduction

Chapter 3 explored the use of C57BL/6 mice in the study of skin ageing and several key conclusions were drawn. To briefly summarise the key findings:

- Several morphometric changes occurred in the tissue including loss of epidermal and dermal cells, epidermal thinning and epidermal cell flattening.

- The primary dermal ECM constituents: The type I and type III collagens were lost with age resulting in a more loosely structured dermal matrix

- Loss of youthful basement membrane architecture was shown by collagen VII loss. There was also alteration in the architecture of the aged BM shown by electron microscopy and collagen IV staining.

- Loss of epidermal nuclear stability in the form of lamin B1 loss, reduced cellular proliferation and increased DNA damage occurred.

- An increase in the nuclear localisation of the Hippo Pathway effector YAP1 in the epidermal cells was observed.

4.1.1   Drawbacks of using mice in skin ageing research

The use of model organisms like mice in ageing research offers several benefits as described in section 3.1.1. There are however, drawbacks to be considered. The mouse and human genomes are highly similar in terms of their DNA content (Emes et al, 2003). However, there are differences between the gene expression patterns seen in immune response, metabolism and stress response mechanisms in mice compared to humans (Cheng et al, 2014). The roles of stress (Haigis and Yankner,2010) and metabolism (Barzilai et al, 2012) are highly implicated in ageing biology as they both contribute to cellular longevity mechanisms (Davalli et al, 2016). It thus follows that having genetic differences in these critical processes could impose limitations on the extent that murine ageing processes are able to model ageing in humans.

The structure of mouse and human skin is also different. Human skin has a thicker epidermis and dermis with sparsely arranged hair follicles whereas in the mouse, hair follicles are densely packed. The primary protective layer in murine skin is the dense covering of hair found on the skin surface whereas for human skin, the stratum corneum plays this role (Younis

et al, 2014). There are also differences between the epidermal and dermal immune cell sub-populations in mouse and human skin. For example, murine epidermis houses dendritic epidermal T cells (DETCs) that are not present in the human epidermis (Pasparakis et al, 2014). The difference in structure and immune cell populations in mouse and human skin raises the possibility that they will be subjected to different ageing mechanisms. As one of the objectives of this thesis is to understand human skin ageing alongside murine skin ageing, this provides further motivation to validate age-related changes found in mice in humans. Completing this objective will also enable us to determine to what extent the C57BL/6 male mouse can be used as a model of female human skin ageing. As male and female mammals demonstrate skin-specific differences in steroid hormone profiles (Stevenson and Thornton, 2007), cross-matching results from our studies will allow us to identify potential age-related changes that occur independently of these hormonal differences.

4.1.2   Alternative ageing tools: 3D in vitro skin equivalent (SE) models

As a more accessible, and ethical alternative to model organism use, several *in vitro* 3D models using human cells from both young and aged donors have been developed (Janson et al, 2013; Dos Santos et al, 2015; Diekmann et al, 2016). These models have allowed the study of intrinsic ageing (Janson et al, 2013) along with allowing the mimicry of photo-aging to an extent through the use of irradiation (Armento et al, 2015). *In vitro* SE models have also accelerated the development of therapeutics as they provide a controlled environment for study of compounds that can attenuate the ageing process, such as phytochemical photo-protectants (Evans-Johnson et al, 2013). *In vitro* skin ageing studies have therefore become a powerful tool for ageing biologists looking to study the molecular mechanisms behind skin ageing and for finding ways to ameliorate the aged skin phenotype.

However, there are limitations to use of 3D cultures, with one of the fundamental issues being that skin equivalents are relatively short-lived compared to human skin *in vivo* (Dos Santos et al, 2015). It is also difficult to mimic natural extrinsic ageing processes *in vitro*, as it is difficult to artificially replicate the sporadic nature of un-controlled, low-level doses of UVA and UVB irradiation found in natural sun light, along with other environmental insults that occur in daily life (Naylor et al, 2011). Furthermore, 3D in vitro skin cultures rarely contain all of the different skin cells and adnexal structures found in human skin *in vivo*, like hair follicles. The majority of *in vitro* skin equivalents are based on keratinocytes and fibroblasts only, and therefore they provide a simplified model of human skin.

4.1.3 Humans as ageing models

Human tissues are difficult to obtain due to the need for strict guidelines involving ethical approval, patient consent and careful use of samples (Seppet et al 2011). Several factors must be considered in the design of experiments using human tissues. For example, human ageing has been shown to be heterogeneous in terms of displayed age-related phenotypes (Mitnitski et al, 2016). This has been seen in studies observing the ageing of identical twins who despite having the same DNA, are able to show different age-related phenotypes (Steves et al, 2012). Additionally, current research emphasizes that there is a distinction between lifespan and "healthspan", meaning that ageing is highly multi-factorial, and chronological age alone cannot measure the ageing process (Bansal et al, 2015). Statistically speaking therefore, in ageing studies, one must account for the fact that there could be increased phenotypic variation in age-matched individuals within a given population with increasing age. Sample sizes must therefore be large enough to account for this potential increase in variation if one wishes to express their findings in statistical terms (Halsey et al, 2015).

As already mentioned, ageing is multifactorial, which presents problems in ageing research as the impact of diet, exercise and stress can heavily influence the ageing process (Mody et al, 2008). Additionally, it is well known that the role of gender is crucial in causing a differential in the trajectory of male and female ageing, which has been shown to be markedly different in terms of disease presentation and the timing of senescence (Franceschi et al, 2000). These limitations show that great care must be taken when considering the design of an experiment using human tissues. However, once these factors are taken into account, the use of human tissues in ageing studies allows us to observe first-hand how our bodies are impacted by the ageing process, which can offer the most direct route to further understanding of ageing mechanisms (Seppet et al, 2011). For this reason, their use is sometimes preferable to *in vitro* 3D culture models and other animal models, because these tools only offer mimicry of natural human ageing.

4.1.4 "Skinomics" emerges as a research tool

Genomic studies are becoming increasingly more prevalent in ageing biology research (Kaeberlein, M. 2006). Additionally, with the continued development of more powerful "omics" technologies, such as genome wide association studies (GWAS) (Newman et al, 2010), it has become feasible to comprehensively understand changes to the whole genome with age in several human tissues and organs. With reference to the skin, "skinomics" technology is a rapidly developing field where genetic tools, like DNA microarrays and RNA sequencing, can be used to study age-related changes (Younis et al, 2015).

Several biologists believe that DNA microarrays offer a powerful platform in order to deduce changes to gene networks with age (Benech and Patatian, 2014). Studies have identified changes to expression of general age-associated genes such as those that contribute to immune-response and metabolic pathways and also more specifically for the skin, ECM and protease genes (Lener et al, 2006). Two studies have independently identified Wnt signaling as being down-regulated with age in the skin of both males and females (Makrantonaki et al, 2012) and in the skin of a cohort of females (Glass et al, 2013). This pathway controls progenitor cell proliferation and asymmetric cell division, which are crucial processes in skin biology (Lim and Nusse, 2013). Studies looking at transcriptional changes during intrinsic versus photo-ageing are sparse, but one publication suggests that many of the changes occurring during photo-ageing are similar to intrinsic ageing but tend to be more severe (Robinson et al, 2009).

4.1.6 Microarray analysis of our genes of interest during intrinsic and extrinsic ageing

We have identified that microarrays are powerful tools for studying transcriptional changes during ageing but the way that they are used depends heavily on the hypotheses being tested and the individual goals of the researcher (Naidoo et al, 2005). Our goals concerned the identification of differentially expressed genes during female skin ageing. Our target genes of interest were the dermal and basement membrane collagens, nuclear lamins and Hippo pathway components. As we had access to tissue from photo-protected and photo-exposed skin sites, we were also able to assess whether intrinsic or "chronological ageing" caused different transcriptional changes over time compared to extrinsic or "photo-ageing".

In order to identify differentially expressed genes, Spearman's rank correlation was used. This statistical testing method allowed us to assess to what degree gene expression changes (the first variable) changed in relation to the age of the subject (the second variable). Unlike other methods like Pearson's correlation testing, Spearman's correlation allows the assessment of the change in non-linear relationships. This is important for studies concerning biological ageing as it is a complex dynamic process (Higgins, J, 2002), with many gene expression changes not necessarily following a linear relationship (Cao et al, 2013).

4.1.7 Quantifying significant gene expression changes in our microarray data

There are several different ways to assess significance of the transcriptional changes occurring in microarray data. Computational methods such as ANOVA and SAM (Jeffery et al, 2006) can be used to calculate lists of differentially expressed genes from raw microarray data.

However, it is accepted that different statistical testing methods vary in their ability to identify differentially expressed genes (Jeanmougin et al, 2010). With our method, we have pre-selected in advance which genes are of interest, and subsequently considered the extent that their expression changes with age.

Along with our genes of interest, the microarray experiments completed assessed the differential expression of hundreds of other genes. Like other microarray experiments, our data is therefore subject to the high false discovery rate (FDR) that comes with multiple-testing experiments. The Bonferroni correction method (Nadon and Shoemaker, 2002) was used to overcome this problem. This correction method computes the possibility of a significant p-value occurring by chance in a large data-set and thus generates a q-value, which indicates the likelihood of the implied p-value being a false-positive or type I error (Benjamini et al, 2001).

Two key issues in the use of microarray technology are the ability for RNA molecules to non-specifically bind to probe-sets on microarray chips and also to the chip itself. To account for the former problem, mis-matched probes, which are highly similar in nucleotide sequence to the specific probes, aside from (typically) a single base pair are also present on the chip. The signal generated from transcripts binding to these mis-matched probes compared to the specific probes is used to control for non-specific mRNA hybridisation. To account for the latter problem, the background signal from the chip itself is measured and the value removed from subsequent downstream analyses (Schuster et al, 2007).

As well as completing these data processing steps, we looked at the behaviour of each individual probe sets over time, by plotting the data of the mean expression taken from all of the female subjects at each decade. In this way, probe sets that targeted the same gene, but that behaved differently to one another could be identified and those that did not show any modulation with age could be eliminated from further analyses. We identified differentially modulated probe sets with robust changes during ageing as those which had a significant change from the 2nd to 7th decade. These probe sets had $p \leq 0.05$ and $q \leq 0.05$ in our statistical assessment by rank correllation.

Our microarray experimental design used laser capture microdissection (LCD) to isolate epidermal and dermal compartments free from appendages as part of our analyses. This increases the likelihood of picking up significant changes to genes specific to the dermis, like the genes encoding collagen I and collagen III fibrils and those that have been more highly implicated to play a role in the epidermis, like YAP1 (see thesis introduction for further information). Additionally, we assessed gene expression changes in full thickness skin, which also had appendages such as hair follicles and sweat glands present. Having full thickness data

alongside separate epidermal and dermal compartment data allowed us to compare compartment-specific changes to whole-skin changes with age.

4.1.8 Validating transcriptional changes at the protein level

mRNA molecules are known to be highly un-stable. They are easily subject to degradation and require several post-transcriptional processes to occur, including efficient translation, in order to create their encoded protein (Plotkin, J.B., 2010). Furthermore, the correlation between mRNA presence and protein presence is not a linear relationship. In fact, only 1.9% of the human genome accounts for the mRNA variants that encode functional proteins (Int Human Genome Seq Consortium, 2004). The earlier principles of molecular biology worked on the rule that genomic DNA encodes the templates for mRNA which serve as protein-coding molecules (Hombach and Kretz, 2013). Many exceptions to this rule have now been identified, and it is becoming commonly accepted that non-coding RNA's such as lncRNA's (long non-coding RNA's), miRNA's (micro-RNA's), rRNA's (ribosomal RNA's) and other variants have their own distinct roles in cellular biology and gene expression (Matera et al, 2007).

Additionally, mRNA transcripts can also be subject to alternative splicing mechanisms. This impacts their proteomic fate as an alternatively spliced mRNA transcript can theoretically yield several different protein isoforms, which may be distinct in their structure and function (Graveley, B. R. 2001). Alternative splicing mechanisms, coupled with the action of non-coding RNA's indicate the complexity of gene transcription, and show that mRNA presence represents only partial evidence for functional cellular changes. To compound matters, the cellular ageing process has been shown to be associated with less efficient mRNA splicing and maturation, which in turn leads to the decreased likelihood of proper protein formation (Harries et al, 2011). For these reasons it was important to determine if any transcriptional changes we observed also caused changes in cellular protein levels.

The sub-cellular localisation of proteins like the transcription factor YAP1 are of biological relevance. The nuclear presence of YAP1 places it in close proximity to chromatin, where it can bind an activate transcription of its target genes (Marti et al, 2015). Likewise, the lamin proteins form a meshwork under the inner nuclear membrane (INM) in healthy cellular conditions and can be mis-localised in diseased states, such as in cancers (Hutchison, C.J, 2002). For these reasons proteomic tools like immuno-histochemical staining (IHC) of human skin tissues can be advantageous, as they allow us to visualise both the levels and localisation of our proteins of interest. We therefore exploited the benefits of IHC using human skin samples taken from both photo-protected and photo-exposed sites of young and aged female subjects in order to analyse the expression of our target genes of interest at the protein level.

4.1.9 Histological presentation of our female skin samples

Before we began subsequent experiments, we observed the histological presentation of photo-exposed and photo-protected skin from young and old females using haematoxylin and eosin staining. Representative examples of the skin is shown below in figure 4.1.1. As the figure shows, both the young photo-protected (A) and young photo-exposed (B) skin had an epidermis (e) of similar thickness and prominent pink eosin staining in the dermis (de). In the old photo-protected skin (C), the epidermis was similar to the young skin, but there appeared to be less pink eosin staining in the dermis (de). In the old photo-exposed skin (D) the epidermis was thinner compared to the young photo-exposed skin and less pink staining was present in the dermis. Additionally, prominent melanin colouration (black arrows- D) was observed in the basal epidermal layer. As eosin is non-specific protein stains for both cytoplasm and extracellular matrix components, decreased eosin staining in the old skin suggests that the ECM protein levels decreased with age in the old photo-protected and old photo-exposed skin
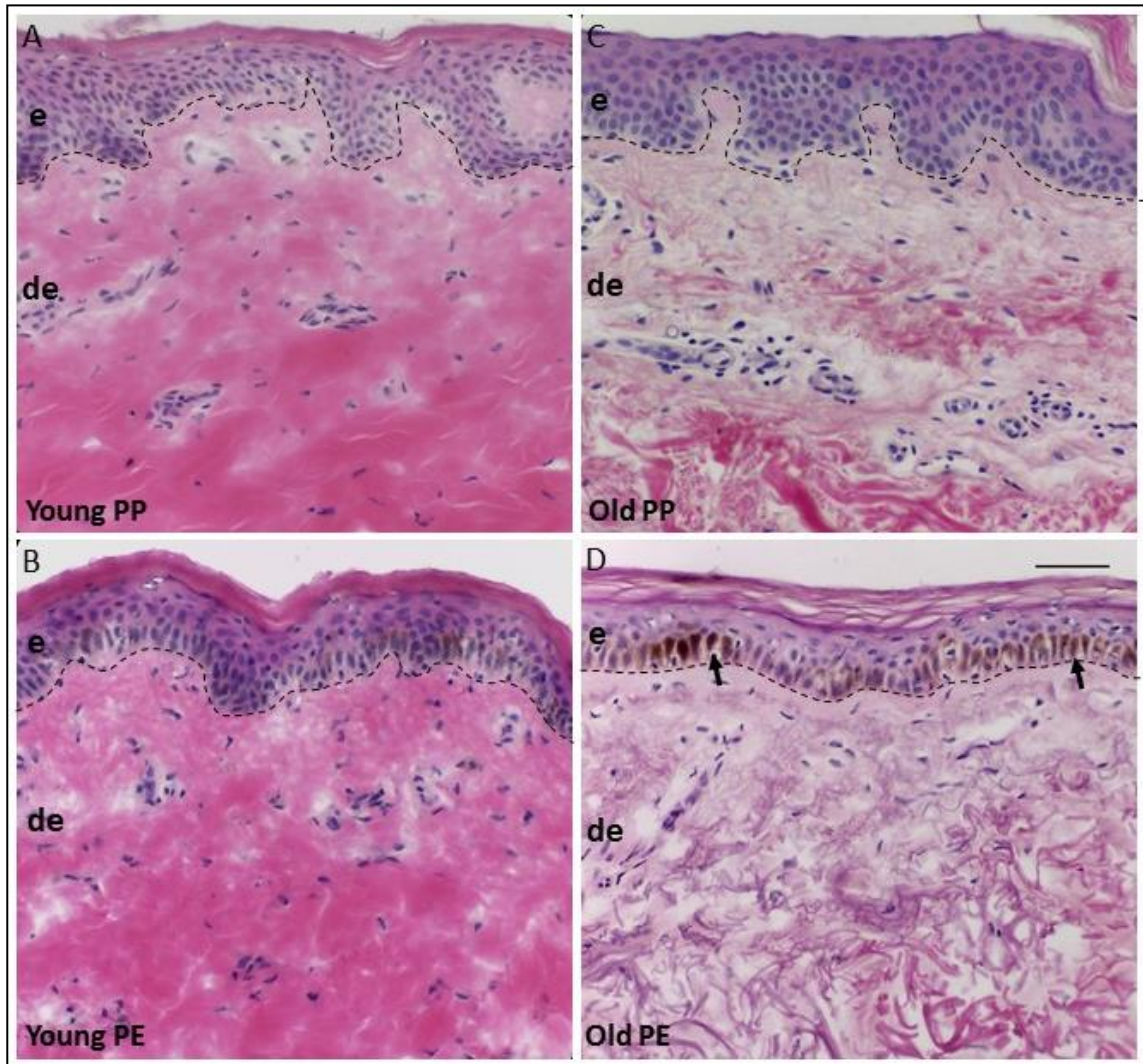
Figure 4.1.1: Haematoxylin and Eosin staining of human skin sections of young (22y) photo-protected (PP-A) and photo-exposed (PE-B) skin along with old (60y) photo-protected (PP-C) and old photo-exposed (PE-D) skin. Sections were imaged on a light microscope using a 20x objective lens. e=epidermis, de= dermis, black dotted line= DEJ. Scale same for all images and scale bar shown in D= 100 μm. Black arrows in D show the presence of prominent melanin pigmentation in the basal epidermis of old photo-exposed skin.

4.1.10 Objectives

The objectives of this work were to identify transcriptional changes in the dermal collagen genes, the basement membrane collagen genes, genes of the nuclear lamina and the Hippo pathway effector YAP1. We also sought to validate identified transcriptional changes at the protein level, and where appropriate, determine age-associated changes in protein localization and arrangement. More detailed accounts of all objectives are given at the beginning of each results section within this chapter.

4.2. Identification of transcriptomic and proteomic changes to dermal collagens in ageing female skin

4.2.1 Introduction and Objectives

Intrinsic and photo-ageing are associated with collagen fragmentation by proteolytic enzymes, water loss and fibroblast senescence. Together these processes, along with modifications to other dermal ECM constituents (Watson et al, 2014) contribute to the aged dermal phenotype.

The mechanisms of intrinsic and photo-ageing share both common and distinct modalities. Photo-ageing results in a more marked degradation of the dermal components due to the potent damaging effects of UVA and UVB rays. Dermal atrophy in intrinsic ageing can be attributed to the decreased production of collagen due to fibroblast senescence along with increased degradation of the collagens already present by MMPs (Varani et al, 2002). The collagen fibrils become fragmented and are no longer able to support their resident fibroblasts, which collapse and lose their normal mechanical properties. The collapsed fibroblasts produce less collagen and more collagen-degrading enzymes and hence the net effect is a loss of dermal collagen, which subsequently perpetuates this cycle (Fisher et al, 2008).

During extrinsic ageing the processes of intrinsic ageing are compounded by the presence of excessive ROS, which are produced as a result of UVR (ultra-violet ray) exposure (Poljsak and Dahmane, 2012). UVR themselves are direct protein and nucleic acid damaging agents. They cause defects to DNA such as dimerization of nucleic acid bases, mutagenic C-> G transversions and lesions such as 8-oxo-Gua. Free radical formation as a result of ROS can also cause protein cross-linking and aggregation (Pattison and Davies, 2006). Both the aforementioned direct damage to DNA and in-direct damage to protein occurs within the dermal matrix and impacts the resident fibroblasts. In response to ROS, damaged fibroblasts undergo senescence and apoptosis, which depletes the dermal population of healthy, ECM producing cells (Watson et al, 2014). Due to the additional damage from UVR, age-matched intrinsic and extrinsically aged skin thus commonly present with differing phenotypes, with a more severe phenotype being seen in photo-aged skin (Naylor et al, 2011).

The plethora of literature concerning intrinsic and extrinsic dermal ageing indicates that this aspect of skin ageing biology is well studied, but this is the first detailed study of the change in dermal collagen transcription in a female ageing population over a series of time-points. Having access to tissue of both young, pre-menopausal and post-menopausal females offers a fascinating insight into the impact of age-associated hormonal changes on dermal

collagen transcription. As HRT (hormone replacement therapy) was an exclusion criterion in the study, the transcriptomic changes identified concern natural hormonal changes only. The objectives are therefore to:

1) Identify the impact of ageing on collagen I and collagen III transcription in the dermal and full thickness skin (FTS) compartments of photo-exposed and photo-protected skin. As our interest concerns fibroblast transcription only, and fibroblasts are the primary synthesizers of type I and type III collagens (Lemons et al, 2010), the epidermal compartment was omitted from the analysis.

2) Use immune-based histological staining techniques to validate the mRNA changes at the protein level.

4.2.2   Age-related decline in dermal collagen transcription is attenuated after menopause.

To determine the change in collagen I and collagen III mRNA levels during intrinsic and photo-ageing, biopsies from female subjects were prepared as described in section 2.7- materials and methods. There were separate probe sets used to target the two alpha chains of the two collagen I genes- *COL1A1* and *COL1A2*, which encode the α1 and α2 chains respectively (source: Genecards.org). The difference in the mean signal expression levels of the two alpha chains was high, and suprisingly the mean expression of *COL1A2* was far greater than *COL1A1* although there are thought to be twice as many α1 chains making up collagen I fibrils compared to α2 chains (McBride et al, 1997). This may be due to the fact that the *COL1A2* gene has a greater number of mRNA variants that do not appear to encode protein isoforms in comparison to *COL1A1* (see table 4.2.1, info: AceView). This means that several of the *COL1A2* mRNAs binding to targets could be non-coding mRNAs. To account for large differences in mean expression, the levels of *COL1A1* and *COL1A2* transcripts were presented separately. The probe sets used to target *COL1A1, COL1A2* and *COL3A1,* along with details regarding the mRNA variants, protein isoforms and molecular collagen structures, are summarised in table 4.2.1 below:

Table 4.2.1: Details of the dermal collagen genes, numbers of known mRNA variants and protein isoforms (information online from AceView). Also shown are the molecular structures and microarray probe set identities of dermal collagens. (Information on collagen molecular structure from Mienaltowski and Birk, 2014)

Dermal collagen type	Genes	mRNA variants	Protein isoforms	Molecular Structure (s)	Probe sets
Collagen I	*COL1A1*	12 (10 alternatively spliced, 2 un-spliced)	11	**α1(I)$_2$** α2(I) *α1(I)$_3$ (present in development, cancer and fibrosis- Han et al, 2009. Modulation with age not known)	11760635_at 11746872_a_at 11715352_x_at 11715350_a_at 11715351_at
Collagen I	*COL1A2*	22 (15 alternatively spliced, 7 un-spliced)	13	α1(I)$_2$ **α2(I)**	11715355_at 11753294_a_at 11715354_a_at 11715356_x_at 11753295_x_at 11715353_s_at
Collagen III	*COL3A1*	10 (6 alternatively spliced, 4 un-spliced)	6	**α1(III)$_3$**	11715414_x_at 11715415_a_at 11744379_a_at 11744380_s_at 11758342_s_at

The results of the microarray analyses using the probe sets presented in table 4.2.1 with RNA prepared from the female subjects in this study are presented below. Mean mRNA levels generated for each decade from age 20 to 70 are shown for dermal and FTS samples. As detailed in the introduction to this chapter, a formatting system (each individual probe set is colour coded) has been used to depict statistically significant changes. The level of signal expression for each probe set within each age group indicates the mean level of mRNA that bound to that probe set from all of the subjects.

COL1A1 and COL1A2 mRNA expression: Dermal compartment only

A COL1A1 mRNA PP dermis

Legend:
- 11760635_at COL1A1
- 11746872_a_at COL1A1
- 11715352_x_at COL1A1
- 11715350_a_at COL1A1
- 11715351_at COL1A1

B COL1A1 mRNA PE dermis

Legend:
- 11760635_at COL1A1
- 11746872_a_at COL1A1
- 11715352_x_at COL1A1
- 11715350_a_at COL1A1
- 11715351_at COL1A1

C COL1A2 mRNA PP dermis

Legend:
- 11715355_at COL1A2
- 11753294_a_at COL1A2
- 11715354_a_at COL1A2
- 11715356_x_at COL1A2
- 11753295_x_at COL1A2
- 11715353_s_at COL1A2

D COL1A2 mRNA PE dermis

Legend:
- 11715355_at COL1A2
- 11753294_a_at COL1A2
- 11715354_a_at COL1A2
- 11715356_x_at COL1A2
- 11753295_x_at COL1A2
- 11715353_s_at COL1A2

Figure 4.2.1: Microarray analysis of mRNA levels of *COL1A1* and *COL1A2* in PP (A,C) and PE (B,D) dermis of individuals aged 20, 30, 40, 50, 60 and 70. Plots A-D show the change in mean signal expression of mRNA levels from the 2nd to 7th decade. The legends in the right hand corner of the page depicts the colour and format applied to each of the 5 probe sets for *COL1A1* (A,B) and 6 probe sets from *COL1A2* (C,D). Thin dotted lines show probe sets that did not significantly change in expression level with age. Thin uniform lines show probes that significantly change with age ($p \leq 0.05$). Thick uniform lines show probe sets that had a highly significant change with age ($p \leq 0.05 + q \leq 0.05$).

COL1A1 and _COL1A2_ mRNA expression: Full thickness skin
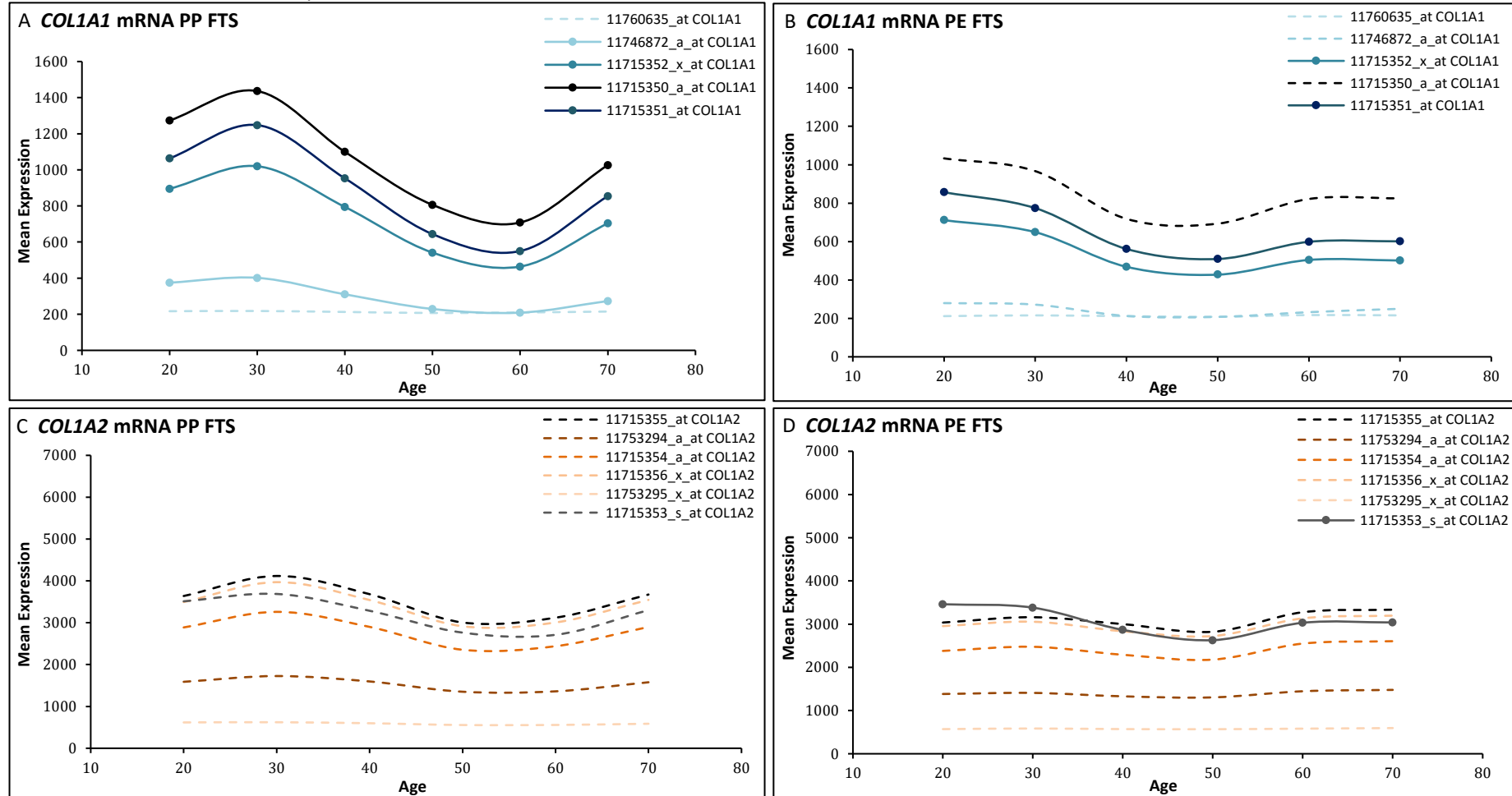
Figure 4.2.2: Microarray analysis of mRNA levels of COL1A1 and COL1A2 in PP (A,C) and PE (B,D) FTS of individuals aged 20, 30, 40, 50, 60 and 70. Plots A-D show the change in mean signal expression of mRNA levels from the 2nd to 7th decade. The legends in the right hand corner of the page depicts the colour and format applied to each of the 5 probe sets for COL1A1 (A,B) and 6 probe sets from COL1A2 (C,D). Thin dotted lines show probe sets that did not significantly change in expression level with age. Thin uniform lines show probes that significantly change with age (p ≤ 0.05). Thick uniform lines show probe sets that had a highly significant change with age (p ≤ 0.05 + q ≤ 0.05).

COL3A1 mRNA expression: dermal compartment and FTS
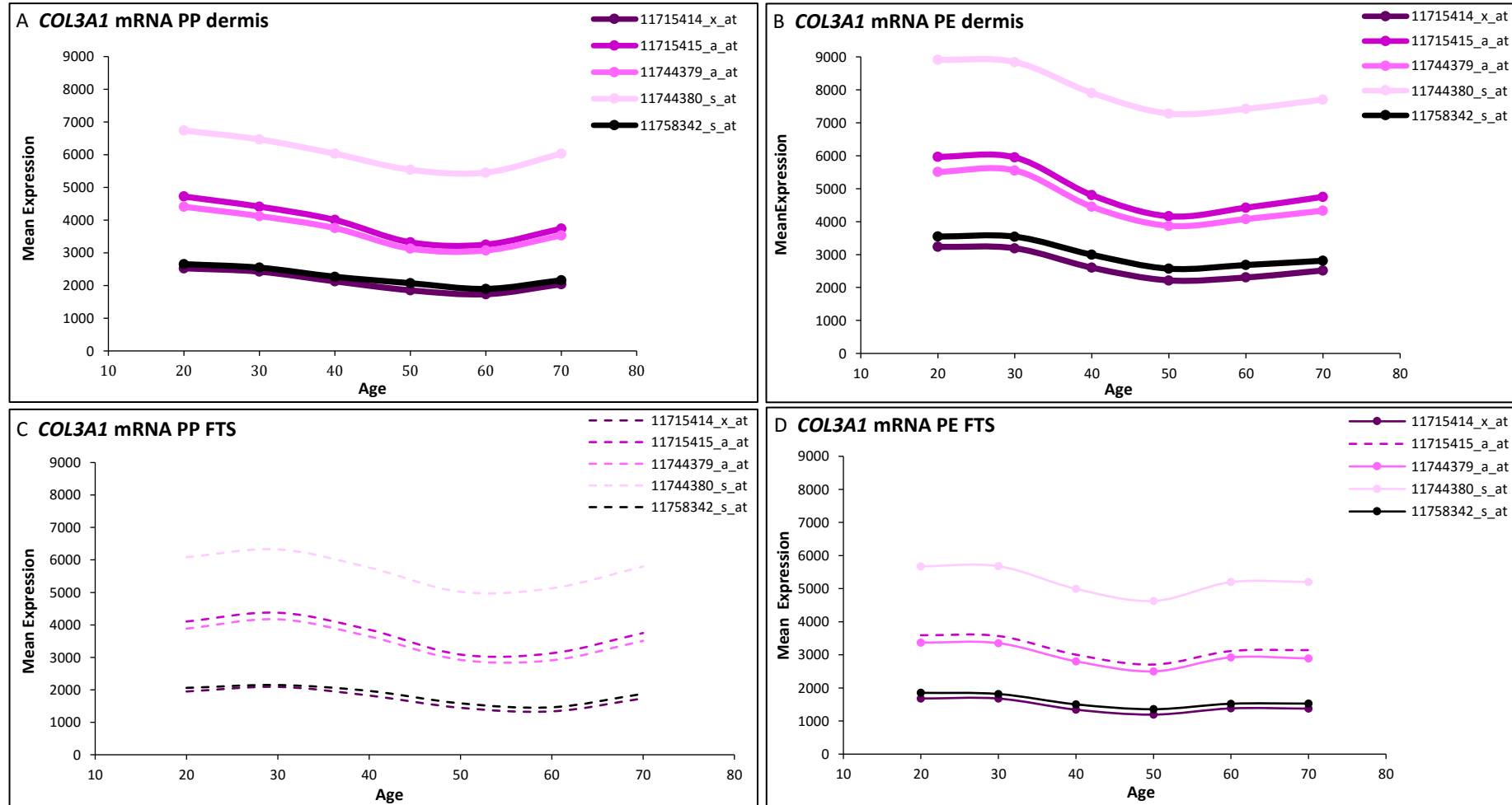
Figure: 4.2.3: Plots of the change in mean signal expression of mRNA levels from the _COL3A1_ gene as analysed by microarray in PP and PE dermis (A,B) and FTS (C,D) of individuals of ages 20, 30, 40, 50, 60 and 70. Plots A-D show the change in mean signal expression of mRNA levels from the 2nd to 7th decade .The legends in the right hand corner of the page depicts the colour and format applied to each of the 5 probe sets. Thin dotted lines show probe sets that did not significantly change in expression level with age. Thin uniform lines show probes that significantly change with age ($p \leq 0.05$). Thick uniform lines show probe sets that had a highly significant change with age ($p \leq 0.05$ + $q \leq 0.05$).

With regards to figures 4.2.1 and 4.2.2, which depict the plots of probe sets targeting *COL1A1* and *COL1A2* mRNAs in PP and PE dermal and FTS compartments, it was observed that overall, the mean expression of *COL1A1* and *COL1A2* mRNAs declined with age in both the PP and PE dermis and FTS. In the dermis, this decline was attenuated at roughly age 55, where mRNA levels then increased in late life. The observed increases did not restore collagen mRNA levels to those observed in the younger decades (20's and 30's). This increase was most marked in the PP dermis (figure 4.2.1 A and C) and was more marked for *COL1A1* mRNA at these latter stages in comparison to *COL1A2.* In the PE dermis *COL1A1* (figure 4.2.1 B) and *COL1A2* (figure 4.2.1 D) mRNA levels also increased between the 5th and 7th decade but to a reduced extent in comparison to the PP skin.

Figure 4.2.3 depicts the plots of probe sets targeting *COL3A1* mRNAs and like for the collagen I genes, the mean expression levels of the probe sets in both the PP dermis (figure 4.2.3 A) and the PE dermis (figure 4.2.3 B) decreased until ~age 55 then mean expression levels began to increase again into the 6th and 7th decade. Like for *COL1A1* and *COL1A2* mRNA's, the increases were not robust enough to prevent a decrease in *COL3A1* mRNA levels overall from the 2nd to 7th decade. This observation was slightly more marked in the dermal compartment of the PP skin compared to the PE skin (figure 4.2.3 A).

Altogether, figures 4.2.1-4.2.3 therefore show that the *COL1A1, COL1A2* and *COL3A1* mRNA's shared a unique change in their mean expression levels over time, with levels declining until middle age, then increasing in the latter decades. These late life transcriptional increases however, did not restore mRNA levels to those observed in the 2nd and 3rd decades. This meant that statistically, ageing overall was associated with a decline in dermal collagen mRNA levels. The details of our analyses concerning *COL1A1, COL1A2* and *COL1A3* mRNA levels during intrinsic and photo-ageing are summarised in tables 4.2.2-4.2.4 below.

Table 4.2.**2**: Summary of changes to statistically significant probe sets for *COL1A1* mRNA levels during intrinsic and photo-ageing. The PE and PP compartments that showed the most significant changes are highlighted in orange (PE skin) and blue (PP skin).

Skin sample/condition	Signal expression range of statistically significant probe sets (to nearest 100). *Δn=* difference between the highest mean expression and lowest.	Number of probes statistically correlating with age and in which direction (+ for up, - for down). Numbers in parentheses indicate the number of these probes that also had q ≤ 0.05.
Photo-protected (PP) dermis	**200-1200** *(Δ1000)*	**-4** (1)
Photo-exposed (PE) dermis	**200-1300** *(Δ1100)*	**-4** (4)
Photo-protected FTS (PP)	**200-1500** *(Δ1300)*	**-4** (0)
Photo-exposed FTS (PE)	**400-800** *(Δ400)*	**-2** (0)

Table 4.2.3: Summary of changes to statistically significant probe sets for *COL1A2* mRNA levels during intrinsic and photo-ageing. The PE and PP compartments that showed the most significant changes are highlighted in orange (PE skin) and blue (PP skin).

Skin sample/condition	Signal expression range of statistically significant probes (to nearest 500). *Δn=* difference between the highest mean expression and lowest.	Number of probes statistically correlating with age and in which direction (+ for up, - for down). Numbers in parentheses indicate the number of these probes that also had q ≤ 0.05.
Photo-protected (PP) dermis	**500-4500** *(Δ4000)*	**-6** (0)
Photo-exposed (PE) dermis	**2000-6000** *(Δ4000)*	**-5** (3)
Photo-protected FTS (PP)	**NP**	**NP**
Photo-exposed FTS (PE)	**3000-3500** *(Δ3000)*	**-1** (0)

Table 4.2.4: Summary of changes to statistically significant probe sets for *COL3A1* mRNA during intrinsic and photo-ageing. The PE and PP compartments that showed the most significant changes are highlighted in orange (PE skin) and blue (PP skin).

Skin sample/condition	Signal expression range of statistically significant probes (to nearest 500). *Δn=* difference between the highest mean expression and lowest.	Number of probes statistically correlating with age and in which direction (+ for up, - for down). Numbers in parentheses indicate the number of these probes that also had q ≤ 0.05.
Photo-protected (PP) dermis	**2000-6500** *(Δ4500)*	**-5** (5)
Photo-exposed (PE) dermis	**2500-9000** *(Δ6500)*	**-5** (5)
Photo-protected FTS (PP)	**NP**	**NP**
Photo-exposed FTS (PE)	**1500-5500** *(Δ4000)*	**-4** (0)

Table 4.2.2, which details significant changes to *COL1A1* mRNA levels with age, shows that in the dermal compartment, signal expression ranges for the probe sets were similar in PP and PE skin. There were also the same number of statistically significantly changing probes,

although this significance was more marked in the PE skin, where all of the changes in mean expression had significant P and Q values. In the FTS, there were more instances of high mean expression levels and a greater range of mean expression levels in the PP skin compared to the PE skin. There were also more significant changes with age in the PP FTS (mean expression levels significantly changed in 4 probe sets) compared to the PE FTS (mean expression levels significantly changed in only 2 probe sets).

Table 4.2.3 shows that *COL1A2* mRNA levels were higher in the PE dermis compared to the PP dermis, although the signal expression range of the probe sets in each condition were similar (*Δ4000)*. There were similar numbers of probe sets with significantly decreasing mean expression levels in the PP and PE dermis for *COL1A2*. However, as the decline in mean expression of 3 probe sets in the PE skin had statistically significant Q values as well as P values, this suggests *COL1A2* mRNA decreases could be more marked in the PE skin. In the FTS, few significant changes with age were present, with only one probe set significantly decreasing its mean expression with age in the PE FTS.

Table 4.2.4 indicates that *COL3A1* mRNA levels were generally higher in the PE skin compared to the PP skin in the dermis. Both the PE and PP dermis showed robust changes in mean *COL3A1* expression with age, with all 5 probe sets showing a decline in mean expression that was highly significant ($p \leq 0.05$; $q \leq 0.05$). In the FTS significant changes occurred only in the PE skin. Mean expression levels of the significantly changing probe sets in the FTS were lower in comparison to the PE dermis and the decreases were less significant.

Overall the tables detailing changes to *COL1A1*, *COL1A2* and *COL3A1* mRNA levels show that the dermal compartment was the source of the most significant mRNA changes. This was logical given that the genes studied here are transcribed by cellular populations within the dermal compartment only and not the epidermis or adnexal skin structures present in the FTS. Additionally, photo-ageing caused a more robust decline in dermal collagen mRNA levels compared to intrinsic ageing. This was shown by the greater numbers of probe sets that showed both significant P and Q values for mRNA changes in all 3 dermal collagen genes in the PE skin compared to the PP skin. Furthermore, significant changes to the dermal collagen genes in the FTS occurred mostly in the PE and not the PP skin. In the presence of epidermal and adnexal skin structure mRNA, the overall level of collagen mRNA would be diluted. Therefore, the fact that significant changes were still detected in the PE FTS but not the PP FTS suggests the changes in mean expression were more robust in the PE skin.

4.2.3 Herovici staining: A versatile alternative to identifying protein expression changes to dermal collagens with age

Collagen fibrils undergo several post-translational modifications including modification to amino acid residues and assembly of pro-collagen chains into triple helices (Koivunen et al, 2005). Additionally, the net presence of collagens within the dermis is dependent on the balance between their production and degradation by resident proteases (Fisher et al, 2008). As several processes must occur following collagen gene transcription in order for production of mature collagen fibrils, it thus follows that the cellular presence of collagen mRNA presents only partial evidence for its manifestation at the protein level. These are important facts to consider in the study of functional protein changes to ageing tissues

Immuno-histochemical validation of collagen I levels was therefore subsequently carried out on female young and aged skin sections using a rabbit polyclonal collagen I antibody (ab 34710) and a citrate based antigen retrieval protocol (details: section 2.8.4-Materials and Methods). Figure 4.2.4 shows the resulting immuno-staining, which had weak Collagen I immuno-labelling regardless of skin age and biopsy site and non-specific binding in the stratum corneum (SC) of the young skin biopsies and the aged buttock skin (white arrows C, D, E). The antibody binding present in the SC is most probably due to the action of the primary collagen I antibody, as sections from both young and aged tissue that were incubated in secondary antibody only (figure 4.2.4 A, B) do not show this non-specific binding.

We had already observed in-consistent staining results using collagen I and III antibodies in mouse skin, and there are several reasons why binding of collagen "specific" antibodies in paraffin-embedded tissues shows a poor performance. Collagen antibodies can be highly cross-reactive, so unambiguous identification of collagen I and collagen III in the dermis may be difficult to achieve (Buchwalow et al, 2011). Furthermore, the presence of proteoglycans and other ECM ground substances, which have a high affinity for collagen, may mask antigenic sites, preventing complete reaction of the antibody with all of its target sites. Additionally, the production of the collagen antibodies themselves is challenging as one must remove all of the tightly-bound, non-collagenous proteins from the collagens themselves in order to isolate the antigens needed to produce pure, specific antibodies (Montes and Junqueira, 1991).

Figure 4.2.5 shows a comparison between collagen I immunostaining and Herovici staining in human skin. The resolution of nuclei using Weigerts' iron haematoxylin and DAPI are similar, but there is a clear difference in the dermal collagen labelling in the dye-stained samples compared to the antibody stained samples. The Herovici stain shows superior collagen labelling compared to the collagen I antibody we assessed and bands of collagen fibrils could

clearly be depicted (black arrows, figure 4.2.5 A) that were not observed in antibody staining. Due to the superior collagen fibril resolution offered by the Herovici stain, we completed subsequent analysis on changes to the levels and arrangement of the dermal collagens in intrinsically aged and photo-aged skin using this dye-based method.
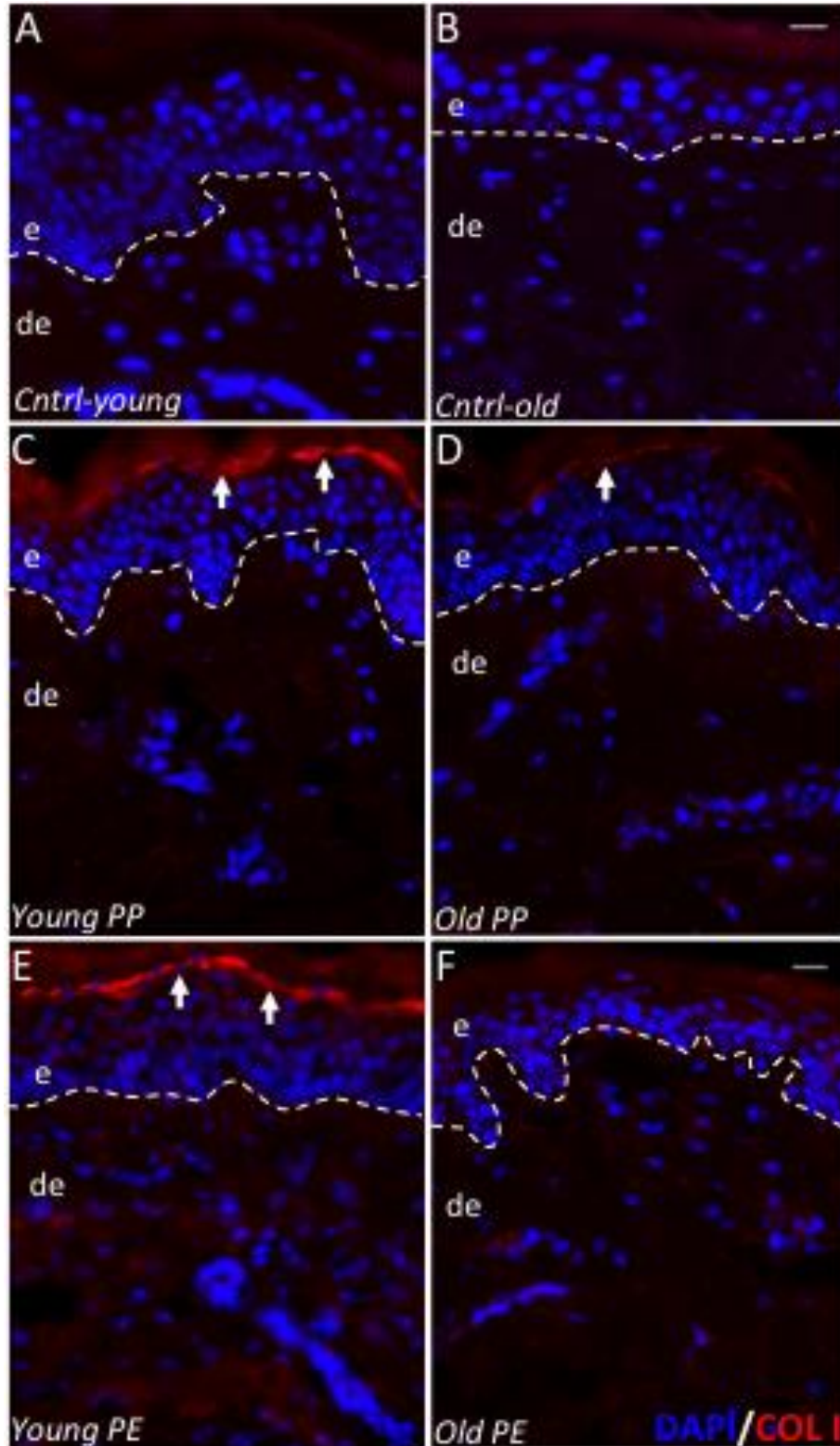
Figure 4.2.4: Immunofluorescence staining of type I collagen in 22y buttock (C), 22y forearm (E), 64y buttock (D) and 64y forearm (F). Also shown are control sections of 22y buttock (A) and 22y forearm (B). The primary antibody (Rabbit polyclonal anti-collagen I) was bound to Alexa 568 secondary antibody with DAPI used to counterstain epidermal and dermal nuclei in C-F. In the control sections the primary antibody was omitted from the staining but all other procedures were the same. All images were taken on a fluorescence microscope with a 20x objective lens. White dotted line= DEJ. e=epidermis, de=dermis. Scale the same for A and B and shown in B=20 μm. Scale the same for C-F and shown in F= 50 μm. White arrows show non-specific binding in the stratum corneum of C, D and E.
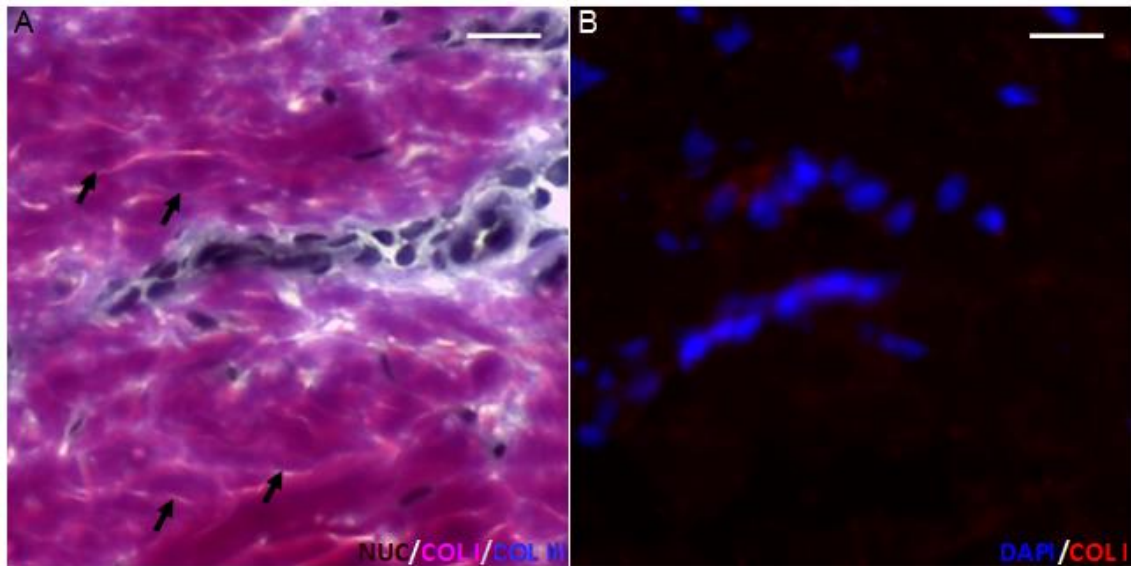
Figure 4.2.5: Direct comparison of Collagen staining in 20y buttock skin using a Herovici stain with Weigerts Iron Haematoxylin nuclear stain (A) and collagen I immunostaining with the same staining procedure as seen in figure 4.2.4.(B). In the Herovici stain nuclei are stained blue/black, young type III collagen is stained blue and mature type I collagen is stained magenta. Scale bars= 20 μm. Labelling of collagen bundles using the Herovici stain offers a much greater source of information regarding collagen fibril density and arrangement. Labelling of collagen fibril bands are shown by black arrows.

Although it is widely accepted that collagen is lost from the dermis with age, there are inconsistencies in the literature with regards as to whether type I or type III collagen is lost to a greater extent with some authors reporting greater loss of type I collagen (Lovell et al, 1987; Oikarinen, A. 1990) and others reporting that type III collagen is pre-dominantly lost (Rong et al, 2008; Cheng et al, 2011). Our mRNA data has shown robust decreases in the transcription of both collagen I and collagen III genes during intrinsic and photo-ageing, which suggests that both collagens decrease during female skin ageing. We sought to address this inconsistency at the protein level by using Herovici staining to look at the levels of type I and type III collagens in young and aged PP and PE skin.

4.2.4 Differential colouration of the dermal layers by Herovici staining and identification of age-related changes

Figure 4.2.6 shows a paraffin-embedded skin section taken from young arm skin subjected to Herovici staining and it was observed that the ratio and arrangement of the collagen fibrils varied in the different dermal layers. At the DEJ and in the papillary dermis, type III collagen was predominant, with many blue interwoven fibrils (dark blue arrowheads). In the upper reticular dermis, type I and type III collagens were present in a meshwork composed of both fine (black arrowheads) and thick (white arrows) collagen bundles. Fine collagen bundles

had more blue staining and were particularly prominent surrounding appendages within the skin (black arrowheads) whereas the thick collagen bundles were stained a deep pink. In the lower reticular dermis the staining was predominantly pink, suggesting the presence of more mature, type I collagen fibrils. The fibrils were in a densely packed arrangement, forming thick bundles in contact with one another (white arrows).
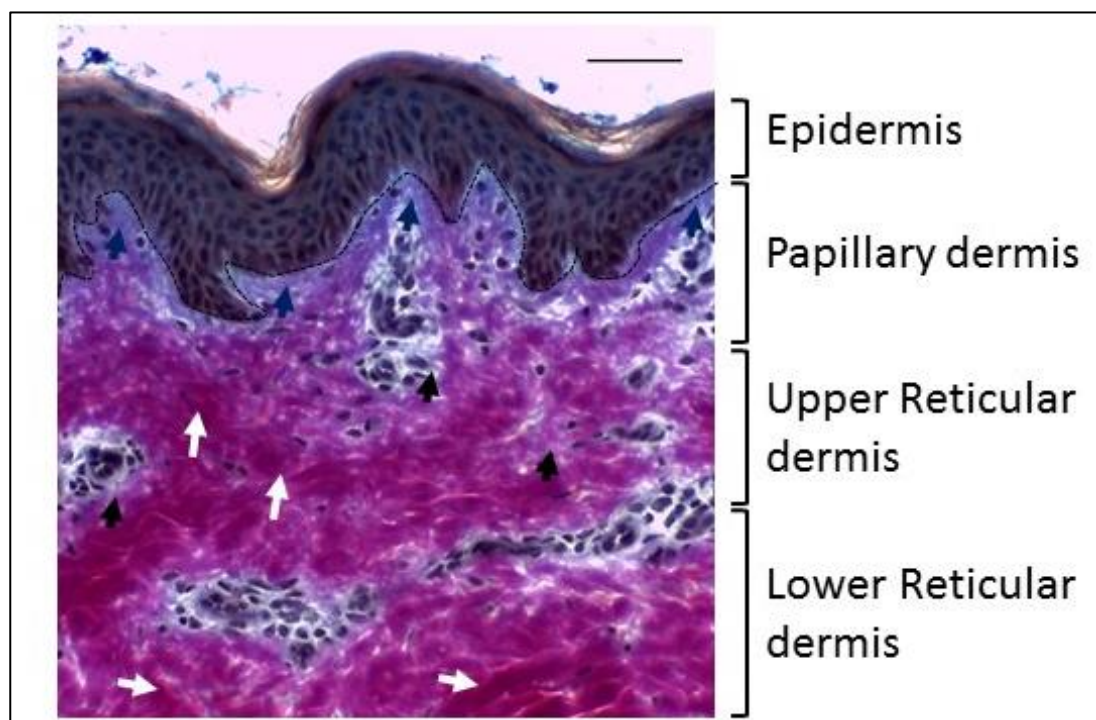
Figure 4.2.6: Schematic of the change of colour in Herovici staining in the various epidermal and dermal layers in 20y buttock skin. Nuclei are stained blue/black, type III (young) collagen= blue, type I (mature) collagen = magenta. Black dotted line= DEJ. Scale bar= 50 µm. Dark blue arrowheads indicate high levels of type III collagen at the DEJ. Black arrowheads= loosely arranged type III collagen at the site of adnexal skin structures in the papillary and upper reticular dermis. White arrows= densely packed regions of type I collagen in the upper and lower reticular dermis.
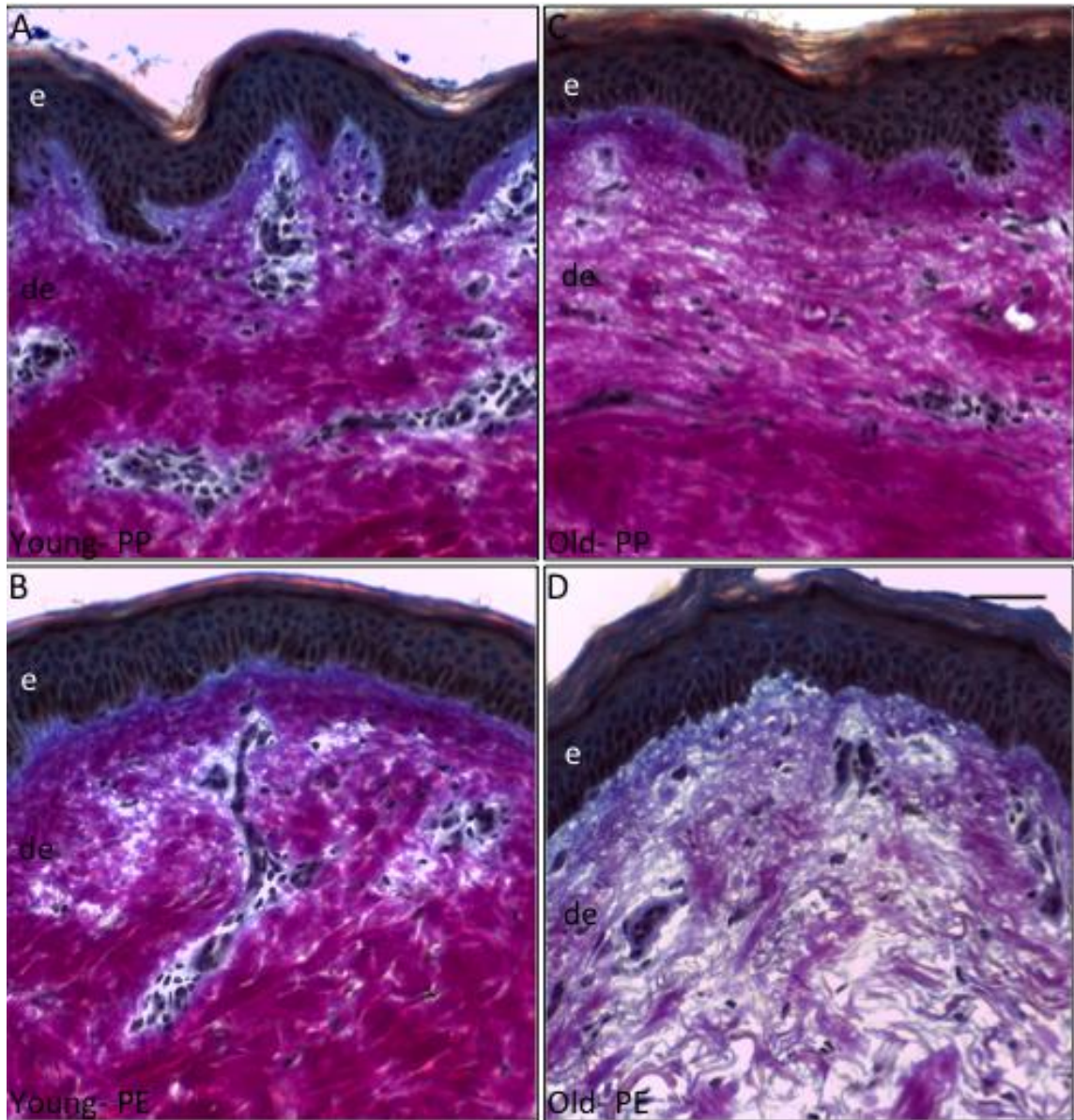
Figure 4.2.7: Low magnification images taken using a light microscope and 20x objective lens of epidermis and dermis of 20y buttock (A), 20y arm (B), 60y buttock (C) and 60y arm (D) stained with Herovici's polychrome reagent which selectively stains type I (mature) collagen magenta, type III (young) collagen blue and nuclei blue/black. Images A-D have the same scale shown in D (Scale Bar= 50 μm), e= epidermis, de= dermis.
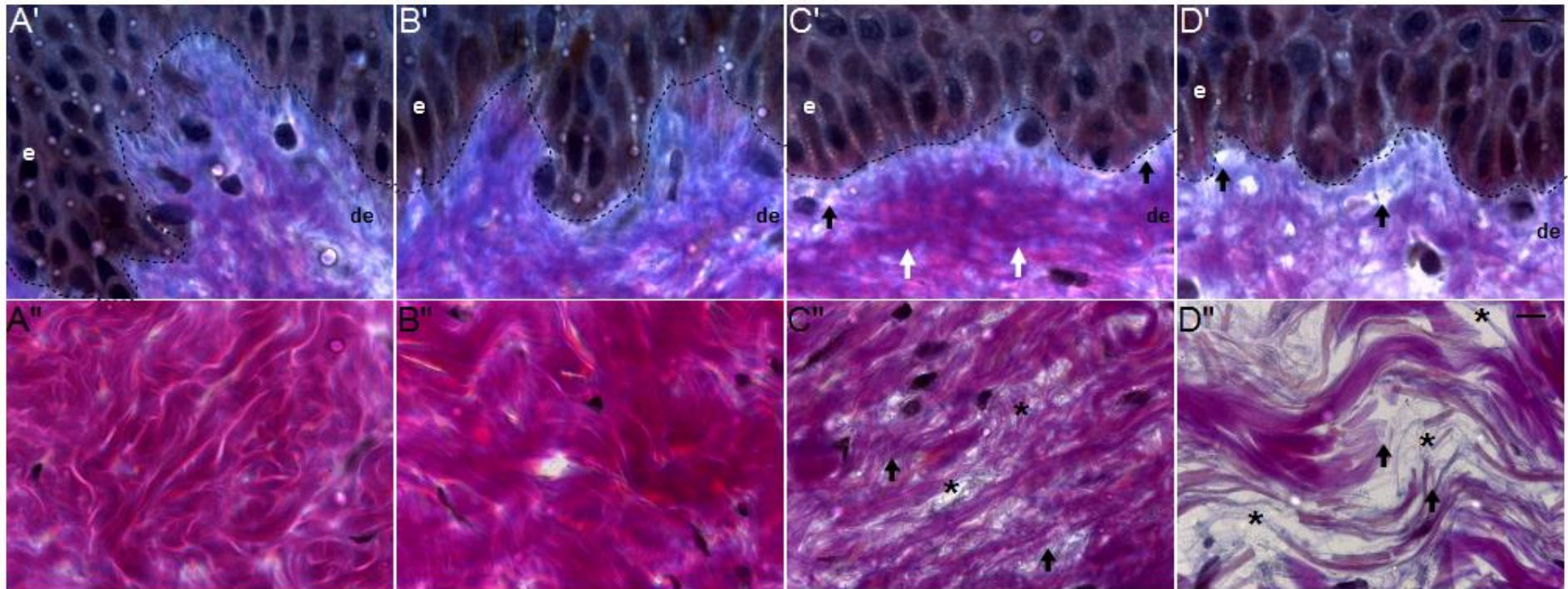
Figure 4.2.8: High magnification images of Herovici staining taken using a light microscope and 100x oil objective lens showing type I (magenta) and type III (blue) collagen fibril arrangement at the DEJ (A'-D') and in the upper reticular dermis (A''-D'') of 20y buttock (A', A''), 20y arm (B,B''), 60y buttock (C', C'') and 60y arm (D',D''). Nuclei have been stained with Weigerts' iron haematoxylin (blue/black). Black arrows in C', D' indicate type III collagen loss at DEJ. Black arrows in C'' show loss of type I collagen in the reticular dermis. Black arrows in D'' indicate collagen fibril fragmentation in reticular dermis. Asterisks in C''and D'' show the presence of gaps in the collagen meshwork in the upper reticular dermis. Scale for images A'-D' is shown in D'= 10 μm. Scale for images A''-D'' is shown in D''= 10 μm. Dotted lines in A'-D'= DEJ.

In figure 4.2.7, the arrangement of type III collagen fibrils in both 20y buttock (A) and arm (B) dermis is similar to the description above for figure 4.2.6, with areas of type III collagen (blue staining) concentrated under the DEJ, in the papillary dermis, and surrounding adnexal skin structures. Type I collagen staining (pink) was also similar in the young arm and buttock dermis, with densely packed, pink-coloured, mature collagen being present mostly in the reticular layers but also to some extent in the papillary dermis.

In the 60y buttock skin (Figure 4.2.7 C), the band of blue type III collagen under the DEJ was thinner compared to the 20y skin and loss of collagen III at the DEJ was obvious at a high magnification (black arrowheads, 4.2.8-C'). Collagen I staining was maintained in the upper papillary dermis of the PP aged skin (white arrowheads 4.2.8-C'). Further down in the reticular dermis of 60y buttock skin the collagen I bundles were thinner and more sparsely arranged than in the young skin (black arrows, 4.2.8- C'') and some small gaps were apparent in areas (asterisks, C''). The most predominant losses of collagen from the PP aged skin therefore came from collagen III loss in the papillary dermis and collagen I loss from reticular dermis.

In the 60y arm skin (Figure 4.2.7 D) collagen loss was extremely pronounced in all layers of the dermis (D). At the DEJ, type III collagen fibril loss caused gaps in the collagen meshwork (black arrowheads, D') and there was a marked loss of the pink type I fibril staining that was previously observed in the papillary dermis of the young arm skin. Blue, type III collagen staining was still present in this region, but appeared to be at a lower level in comparison to the young PE skin. In the upper and lower reticular dermis pronounced collagen I loss had occurred, leaving a loosely arranged collagen fibril network that was composed of both type I and type III collagens. The network was poorly structured in comparison to the young arm skin, and had several gaps (asterisks- D'') along with significant fibril fragmentation (black arrowheads, D''). The staining observed in the aged PE skin suggests that dramatic loss of both type I and type III collagens had occurred within the dermis. As more blue staining remains in comparison to pink staining, it is possible that the loss of collagen I was more marked than collagen III.

4.2.5 Discussion: A novel identification of transcriptional changes to dermal collagens following menopause.

To our knowledge a systematic report on changes to dermal collagen mRNA levels with age in Caucasian females has not been published. Here we show that overall, ageing causes a decrease in *COL1A1*, *COL1A2* and *COL3A1* mRNA levels with these effects being more marked in the PE skin. However, our plots of the change in mean expression of mRNA at each decade of age from 20-70 years showed a more complicated relationship across the dermal collagen genes. Collagen I and III mRNA levels decreased with advancing age but this decline was

attenuated at menopausal age and mRNA levels increased in late life. This identification of collagen transcription increases in elderly female dermis has not been shown to our knowledge, as it is commonly accepted that menopause causes decreased collagen synthesis in the skin (Brincat et al, 2005; Hall and Phillips, 2005).

The increases in collagen mRNA levels occurred after the age of 55 and given that the average age for female menopause in developed countries is 51.4 years (Henderson et al, 2008), the observed increases were most likely occurring after menopause in the majority of the female cohort. As estrogen levels decline following menopause, and estrogen signaling induces collagen synthesis (Stevenson and Thornton, 2007), it is unlikely that the transcriptional increases observed are a result of estrogen signaling.

The ageing process is heavily associated with increased inflammation (Franceschi and Campisi, 2014), and inflammatory markers like NF-kB can drive excess collagen production in ageing tissues (Brack et al, 2007). It could therefore be the case that the increased presence of inflammatory factors in aged skin is driving this collagen transcription. Another possibility is that a compensatory mechanism is occurring, whereby fibroblasts respond to age-related collagen decline and loss of youthful dermal architecture by producing more ECM mRNA's in order to restore the quality of the dermal ECM. The molecular mechanisms behind these late-stage mRNA level increases should be the goal behind future research.

Additionally, until the same genes are studied in males aged 40 to 70 and in subjects with other ethnic backgrounds, it will not be known whether the effects we observe are related to female menopause only, or are restricted to ageing processes in Caucasian subjects. Furthermore, we did not make any statistically valid, comparative changes to quantify to what extent *COL1A1, COL1A2* and *COL3A1* mRNA increased in elderly subjects in comparison to middle age subjects. This means that although late-life transcriptional increases of dermal collagen genes have been observed, the extent of their importance has not been expressed in statistical terms. These limitations could also be addressed with future work.

At the protein level, collagen I and III loss in PP and PE dermis of aged skin was apparent. Furthermore, like at the mRNA level, protein decline was particularly marked in PE skin. Losses of collagen III from the DEJ of PP and PE skin were observed, but perhaps the most marked change to dermal collagens was a loss of collagen I during photo-ageing. Collagen I gives connective tissues tensile strength, and within the skin this collagen in particular allows our skin to cope with mechanical loading (Shoulders and Raines, 2009). We observed a loss of collagen I from the dermis during both intrinsic and photo-ageing, which suggests that the ability of this area to withstand mechanical loading could be compromised over time. As outlined in the main introduction, ageing causes increased levels of collagen-degrading MMP's

to be present in the dermis over time, which causes a perturbation of the balance between collagen production and degradation (Naylor et al, 2011). Collagen proteins have long half-lives, lasting several months (Gineyts et al, 2000) and their turnover decreases with age due to age-induced decreases in fibroblast numbers and synthetic capacity (Farage et al, 2013). Reduced collagen turnover rates, coupled with metalloproteinase digestion over time, could be responsible for the collagen degradation observed in the aged skin.

Recent research has shown that dermal collagen fragmentation has deleterious consequences for the resident fibroblasts, as it disrupts healthy cytoskeletal architecture, causing them to collapse (Fisher et al, 2008). This results in an increase in MMP-1 expression through an induction of the stress signaling transcription factor c-Jun. A positive feedback loop is established whereby elevated MMP-1 levels drive collagen degradation and further fibroblast collapse (Qin et al, 2014a). ROS are also potent inducers of c-Jun signaling and elevation of cellular ROS can decrease type I collagen transcription through this pathway (Qin et al, 2014b). As mentioned previously, ROS levels are elevated during both intrinsic (Poljšak et al, 2012) and photo-ageing (Farage et al, 2013), and it is widely accepted that ROS and MMP-1 levels tend to be elevated in photo-aged skin (Naylor et al, 2011). It is therefore possible that the c-Jun-induced MMP-1 levels are elevated in photo-aged skin in comparison to intrinsically aged skin, causing a more marked collagen I loss.

Much less well studied however, is the potential for ROS to directly fragment the collagens themselves. A publication by Watson et al (2013) proposed that direct dermal collagen fibril damage induced by ROS are actually limited. Instead, they believe that damage to other ECM proteins such as fibronectin and elastic fibre-associated fibrillin plays a more pertinent role in the UVR-induced pathogenesis of dermal photo-ageing. The causative mechanisms behind ROS induced-protein damage during skin ageing remain somewhat poorly defined but what is clear however, is that extrinsic ageing caused a more robust decrease in type I collagen levels in comparison to intrinsic ageing.

In our hands, the study of declining collagen levels in human skin using immunohistochemistry presented technical challenges. We overcame these challenges to some extent by using Herovici staining and were able to identify several benefits of this staining protocol over the use of collagen antibodies. Aside from its improved resolution of dermal collagen levels, Herovici staining offers several benefits over the use of collagen antibodies, which have been summarized in table 4.2.5. However, explosive reagents such as picric acid, which form part of the dye preparation, must be used with extreme caution. Additionally, the protein-based studies completed using this reagent were limited in their quantitative nature. Future work should look to address these limitations by employing alternative methods of

measuring dermal collagen levels. It is possible that collagen antibodies may perform better in methods that do not involve tissue fixation, which is known to mask antigenic sites (Dapson, R.W. 2007). Semi-quantitative protein based methods such as Western blotting, do not require tissue fixation and could therefore be pursued. Alternatively, the histological dyes used in the Herovici procedure, like acid fuchsin, can behave as fluorochromes (Hals, E, 1977). If it is possible to differentially excite the methyl blue and acid fuchsin dyes, which label collagen III and collagen I respectively during the procedure, semi-quantitative evaluation of type I and type III collagens could take place using fluorescence microscopy.

Table 4.2.5: Factors to be considered concerning the use of the Herovici stain as a replacement for collagen I and collagen III antibodies

Factor	Herovici Polychrome Stain	Collagen I antibody
Degree of molecule binding	High. We observed strong staining in the dermal region. The acidic dye molecules used in the Herovici stain (methyl blue and acid fuchsin) have a high affinity for many of the basic amino acids present on type I and type III collagen fibrils (Motta and Ruggeri, 1984).	Low- Staining in the dermal compartment was weak and non-specific binding was present in the stratum corneum. Collagen molecules are highly cross-linked to one another and form close associations that could prevent antibodies from reaching amino acid targets (Shoulders and Raines, 2009).
Specificity of molecule binding	Correct binding of dye molecules to their targets requires that stringent attention be paid to incubation times and tissue washes in order to prevent non-specific dye binding. In order to create differential type I and type III collagen binding, the presence of picric acid is thought to displace dye molecules from non-specifically-bound areas so they remain bound to collagen only. The differences in the composition and arrangement of type I and type III collagen molecules allows a differential affinity of type III collagen for methyl blue and Type I collagen for acid fuchsin (LLewylln, B 2008). This information suggests the reagent is specific if incubation times are followed correctly.	Antibodies are produced from animals immunised against a specific target protein sequence and thus in their purified form, should be highly specific (Leenars et al, 2005). However, we showed empirically that non-specific binding occurs in the stratum corneum of human skin and also saw inconsistent results from use of the collagen I antibody in mouse skin.
Time required	Comparably short- staining can be completed in one afternoon.	Need for visualisation with fluorescently conjugated secondary antibody and overnight incubation of primary antibody means experiment takes 24 hours minimum.
Expense	Dye reagents and acids can be purchased at a fraction of the cost compared to antibodies.	Primary and secondary antibodies must be purchased which cost several hundreds of pounds
Harm to the environment	Picric acid is a high-level irritant and is explosive. It must be used with extreme caution	Antibody production involves the use of animals. According to the National Centre for the Replacement, Refinement & Reduction of Animals in Research (NC3Rs), use of animals in biomedical research should be avoided if alternatives are available (Kilkenny et al, 2010). From an ethical standpoint Herovici staining is a preferable method.

4.3   Transcriptomic and Proteomic changes to basement membrane collagens in human photo-protected and photo-exposed skin with age

4.3.1   Introduction

Collagens IV and VII are two specialised ECM proteins found in the basement membrane at the dermal-epidermal junction (DEJ). Collagen IV forms a mesh-like network of filaments in the lamina densa, which provides a support for the adherence of other BM proteins such as laminins (Poschl et al, 2004). Collagen VII filaments form anchoring fibrils that join the BM to the underlying dermis and together the two collagens promote structural integrity and mechanical stability at the DEJ (Keene et al, 1987; Aumailley et al, 1996). Collagen VII filaments are composed of 3 identical alpha chains encoded for by the *COL7A1* gene (www.genecards.org) whereas collagen IV filaments are made up of several different alpha sub-units depending on the hetero-trimer identity of the collagen IV molecule. Each chain is encoded for by its own gene and the collagen IV gene family consists of 6 genes (*COL4A1, COL4A2, COL4A3, COL4A4, COL4A5 and COL4A6*) encoding the alpha chains known as $\alpha 1(IV)$ through to $\alpha 6(IV)$. Collagen IV alpha chains assemble into 3 distinct hetero-trimers: $[\alpha 1(IV)]_2\alpha 2$, $\alpha 3(IV)$, $\alpha 4(IV)$, $\alpha 5(IV)$ and $[\alpha 5(IV)]_2\alpha 6$, which are found in unique arrangements depending on the tissue location and architecture (Behrens et al, 2012).

$[\alpha 1(IV)]_2\alpha 2$ and $[\alpha 5(IV)]_2\alpha 6$ are the two molecules found in varying proportions within skin tissue, whereas the $\alpha 3(IV)\alpha 4(IV)\alpha 5(IV)$ is absent, except from within the dermal vasculature (Hasegawa et al, 2007; Saito et al, 2000). The two skin-specific collagen IV hetero-trimers are found in the epidermal BM, the BM's of skin appendages and lining the dermal vasculature. Their regional-specific expression levels are detailed in table 4.3.1 below:

Table 4.3.1: Distribution of type IV collagen heterotrimers in skin and its appendages (table information taken from Hasegawa et al (2007)). +++= high expression, ++= medium expression, +=low expression, - = absent expression

Basement membrane/skin region	Collagen IV molecule		
	$[\alpha 1(IV)]_2\alpha 2$	$\alpha 3(IV)\alpha 4(IV)\alpha 5(IV)$	$[\alpha 5(IV)]_2\alpha 6$
Epidermal epithelium	+++	-	+++
Eccrine sweat gland- secretory portion	+++	-	+
Eccrine sweat gland- ductal portion	+	-	+++
Sebaceous gland	++	-	+++
Arrector pili muscle of hair	+++	-	++
Hair follicle sheath	++	-	+++
Dermal vasculature	++	++	++

Previous publications have detailed changes to collagen IV mRNA and protein with age in both photo-exposed and photo-protected conditions. Several publications showed a decrease in collagen IV protein content at the DEJ in both intrinsically aged (Vazquez et al, 1996; Langton et al, 2016) and photo-aged (Contet-Audonneau et al, 1999; Le Varlet et al, 1998) skin. In many of these publications the authors also implicated structural changes at the DEJ with age including rete ridge loss, DEJ flattening (Langton et al; 2016) and basement membrane thickening (Vazquez et al, 1996). These findings all suggest, but do not prove, a correlation between declining collagen IV expression and a loss of normal DEJ integrity.

Protein changes with age at the DEJ are not unique to collagen IV however, as several authors have reported a decline in collagen VII in photo-protected (Langton et al, 2016) and photo-exposed (Naylor et al, 2011; Contet-Audonneau et al, 1999) skin with age. Transcriptional changes to basement membrane (BM) components with age have also shown that collagen VII expression declines at the mRNA level (Craven et al, 1997; Langton et al, 2016) whereas some evidence indicates that collagen IV mRNA levels increase with intrinsic ageing (Langton et al, 2016; Vasquez et al, 1996). Langton et al (2016) looked at the changes in protein levels of several other BM markers in intrinsically aged skin and reported decreases in collagen XVII, integrin β4 and laminin-332 as well as collagens IV and VII.

The studies that have been completed so far on changes to the levels of collagen IV and VII mRNA and protein with age are limited by the number of subjects (Langton et al: n=3; Craven et al: n=10 for collagen VII mRNA) and gender (Langton et al= males only; Craven et al= males and females mixed). Specifically, basement membrane protein changes in females during intrinsic and photo-ageing have not been studied in depth. Herein, the data presented in this results section constructs on what has already been discovered in several ways:

4.3.2 Novel concepts in our data

1) Statistical power

At the time of writing, this is the first study of its kind to have considered 5 separate age groups with a subject number of n ≥ 22 for participants in their 20's, 30's, 40's, 50's, 60's and 70's. The standard deviations in age range for each cohort do not exceed 1.5 and the high numbers of participants in our study improved the probability of un-covering statistically valid, genuine results. This is because, in statistical terms, the sample mean we generate from our population is likely to reflect the population mean (i.e. females undergoing intrinsic and photo-ageing (Halsey et al, 2015).

2) Transcript analysis of all genes within each collagen gene family

By looking at changes in the transcript levels of all the alpha chains encoded for by collagen gene families with multiple different alpha chains (like collagen IV) we can detect chain-specific transcriptional differences. This has not been done before and is important because only certain alpha chains of collagen IV are expressed at high levels in the skin (see table 4.3.1).

3) Laser capture microdissection (LCD) compartmentalisation analyses

By using LCD to isolate epidermal and dermal compartments free from appendages the likelihood of picking up transcriptional changes specific to the dermis and to the epidermis are increased. Given that both keratinocytes and fibroblasts are able to produce collagen IV and collagen VII mRNA it will also be interesting to look at potential differences to the changes in mRNA levels with age in these two different cell types of the epidermis and dermis. Furthermore, having full thickness data along with the separate epidermal and dermal compartments will allow us to compare compartment-specific changes to whole-skin changes. Additionally, the FTS will allow us to take into account how adnexal skin structures such as hair follicles contribute to the mRNA present (as well as the epidermis and dermis).

4.3.3   Objectives

The objectives of this section are therefore:

1) Identify transcriptional changes to collagen IV and collagen VII mRNA in separate epidermal and dermal compartments as well as full thickness skin (FTS) during intrinsic ageing and photo-ageing in female subjects.

2) Determine how both intrinsic and photo-ageing impact collagen IV and collagen VII protein levels in female subjects using immunohistochemistry.

3) Consider if the levels and arrangement of collagen IV and VII at the DEJ in intrinsically aged female skin show a similar change with age compared to C57BL/6 mice.

4.3.4   Collagen IV and VII transcriptomic analysis

Subject selection and sample preparation for mRNA analysis was performed as described in section 2.7- Materials and Methods. For collagen IV transcript analysis, several probe-sets specific to each gene encoding each alpha chain sub-unit were used as detailed in

the table below. For collagen VII transcript analysis a single probe set targeting *COL7A1* mRNA transcripts was used. Details of the probe sets are summarised below in table 4.3.2.

Table 4.3.2: Details of probe sets used in the microarray design for the Collagen IV gene family and the *COL7A1* gene. Also detailed are the known mRNA transcript variants for the gene and also the number of known protein isoforms. Transcript variant and protein isoform information (columns 4 and 5 in the table) were taken from AceView online: (https://www.ncbi.nlm.nih.gov/ieb/research/acembly/)

Collagen gene	Alpha chain encoded for by gene transcript	Number of probe sets designed to bind transcripts in this study	mRNA transcript variants	Known isoforms
COL4A1	α1	**3** 11716639_a_at 11760558_at 11716638_s_at	11	5
COL4A2	α2	**3** 11715453_a_at 11715452_s_at 11715451_a_at	18	10
COL4A3	α3	**2** 11735153_a_at 11735154_a_at	12	7
COL4A4	α4	**2** 11725266_at 11725265_at	6	4
COL4A5	α5	**3** 11760523_at 11724094_a_at 11757903_s_at	13	10
COL4A6	α6	**7** 11725910_a_at 11759994_a_at 11751888_x_at 11751893_a_at 11750015_a_at 11751887_a_at 11741797_a_at	12	10
COL7A1	α1	**1** 11721705_at	30	25

Due to the high number of probe sets for collagen IV, a thresholding approach was applied to eliminate probe sets that had low mean expression levels from the analysis. A cut-off value of 100 was applied and hence any probe set showing a mean expression value of ≤100 at age 20 was removed from the analysis. The value 100 was chosen because the majority of

probes at this level or below showed negligible change to their expression levels with age and likely represented background signal or non-specific binding of mRNA (Seo and Hoffman, 2006).

Once this threshold had been applied probe sets targeting *COL4A1, COL4A2, COL4A5* and *COL4A6* mRNA's but not *COL4A3* and *COL4A4* remained. Plots of the change in mean mRNA levels for the thresholded probe-sets with age in the different skin compartments are shown in figures 4.3.2-4.3.4, where a formatting system (see figure 4.3.1) has been used to depict statistically significant changes. The level of signal expression for each probe set within each age group indicates the mean level of mRNA that bound to that probe set from all of the subjects. For collagen IV mRNAs, the probe sets targeting each individual alpha chain have been colour coded. Dermal and epidermal compartments were analysed separately along with full thickness skin for both photo-protected (PP) and photo-exposed (PE) conditions.
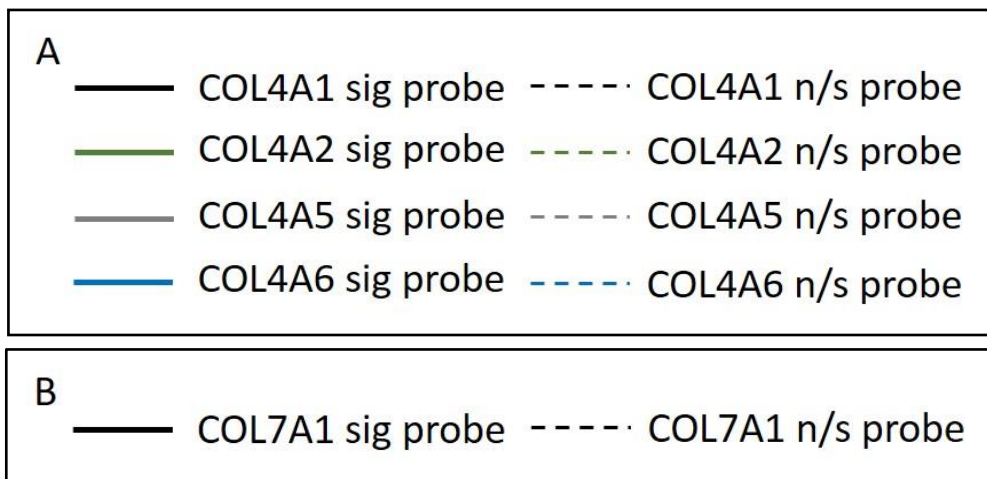
Figure 4.3.1: Formatting system assigned to the probe sets used to analyse the different mRNA transcripts from the collagen IV gene family (A) and the single probe set used to analyse transcripts from the *COL7A1* gene (B). n/s = non-significant.

Collagen IV and VII mRNA levels: Dermal Compartment only
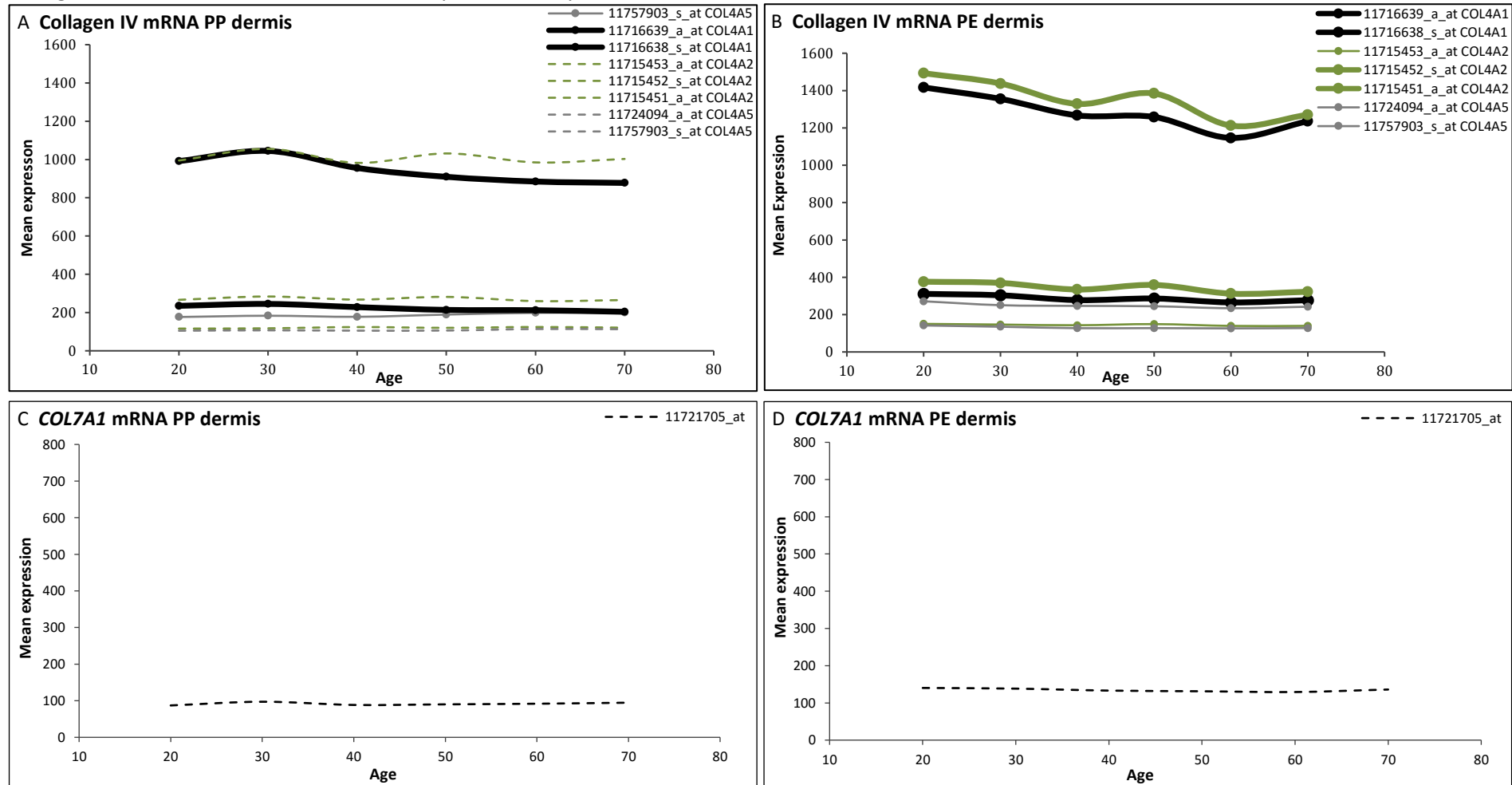
Figure 4.3.2: Microarray analysis of mRNA levels for basement membrane collagens IV and VII in PP (A, C) and PE (B, D) dermis of individuals aged 20, 30, 40, 50, 60 and 70. Plots A-D show the change in mean signal expression of mRNA levels from the 2nd to 7th decade. The different colours depict the probe sets targeting *COL4A1* (black), *COL4A2* (green), *COL4A5* (grey), *COL4A6* (blue) and *COL7A1* (black) mRNAs as shown in figure 4.3.1. Thin dotted lines show probe sets that did not significantly change in expression level with age. Thin uniform lines show probes that significantly change with age (p ≤ 0.05). Thick uniform lines show probe sets that had a highly significant change with age (p ≤ 0.05; q ≤ 0.05).

Collagen IV and VII mRNA levels: Epidermal Compartment only
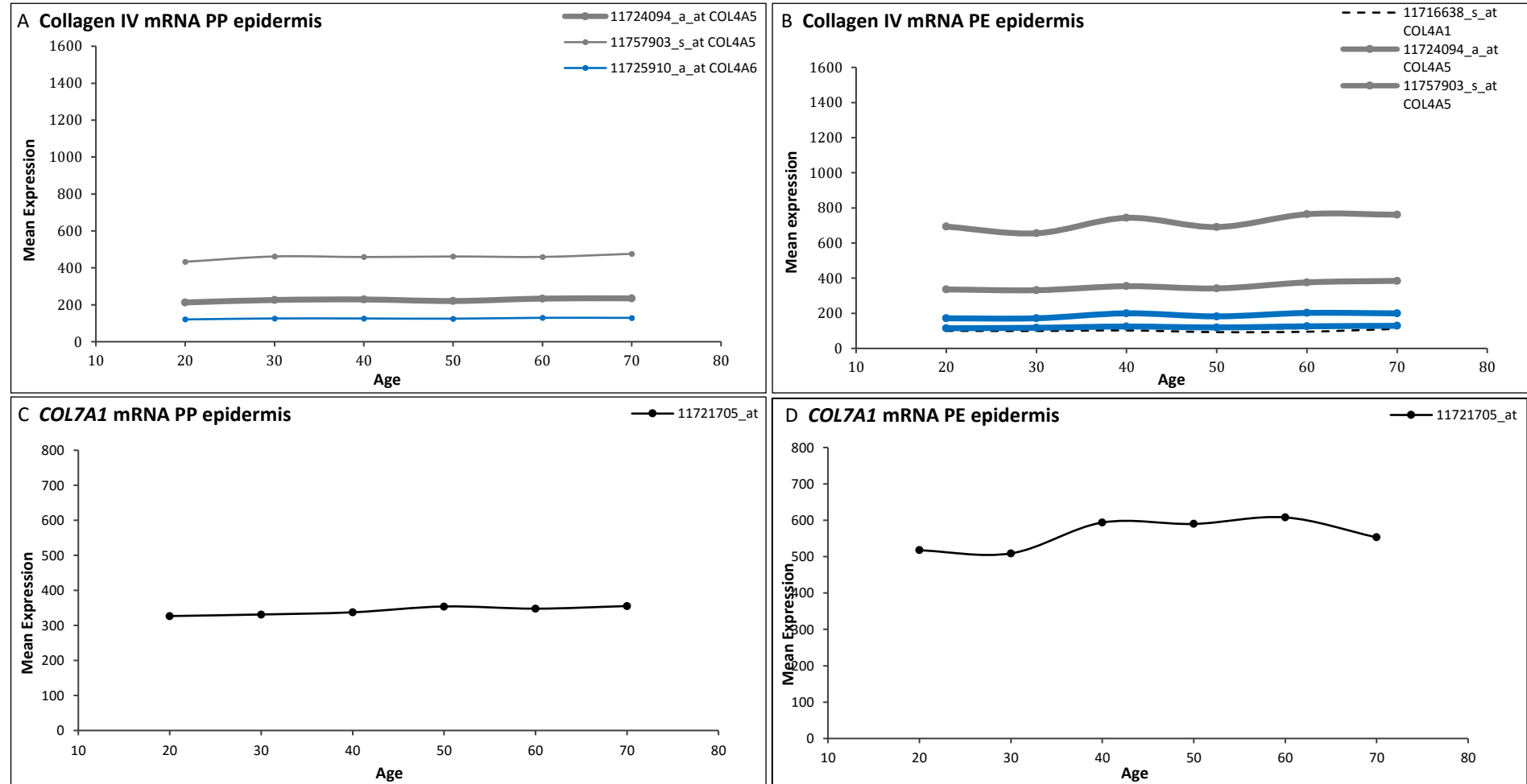
Figure 4.3.3: Microarray analysis of mRNA levels for basement membrane collagens IV and VII in PP (A,C) and PE (B,D) epidermis of individuals aged 20, 30, 40, 50, 60 and 70. Plots A-D show the change in mean signal expression of mRNA levels from the 2nd to 7th decade. The different colours depict the probe sets targeting *COL4A1* (black), *COL4A2* (green), *COL4A5* (grey), *COL4A6* (blue) and *COL7A1* (black) mRNAs as shown in Figure 1. Thin dotted lines show probe sets that did not significantly change in expression level with age. Thin uniform lines show probes that significantly change with age (p ≤ 0.05). Thick uniform lines show probe sets that had a highly significant change with age (p ≤ 0.05; q ≤ 0.05).

Collagen IV and collagen VII mRNA levels: Full-thickness skin
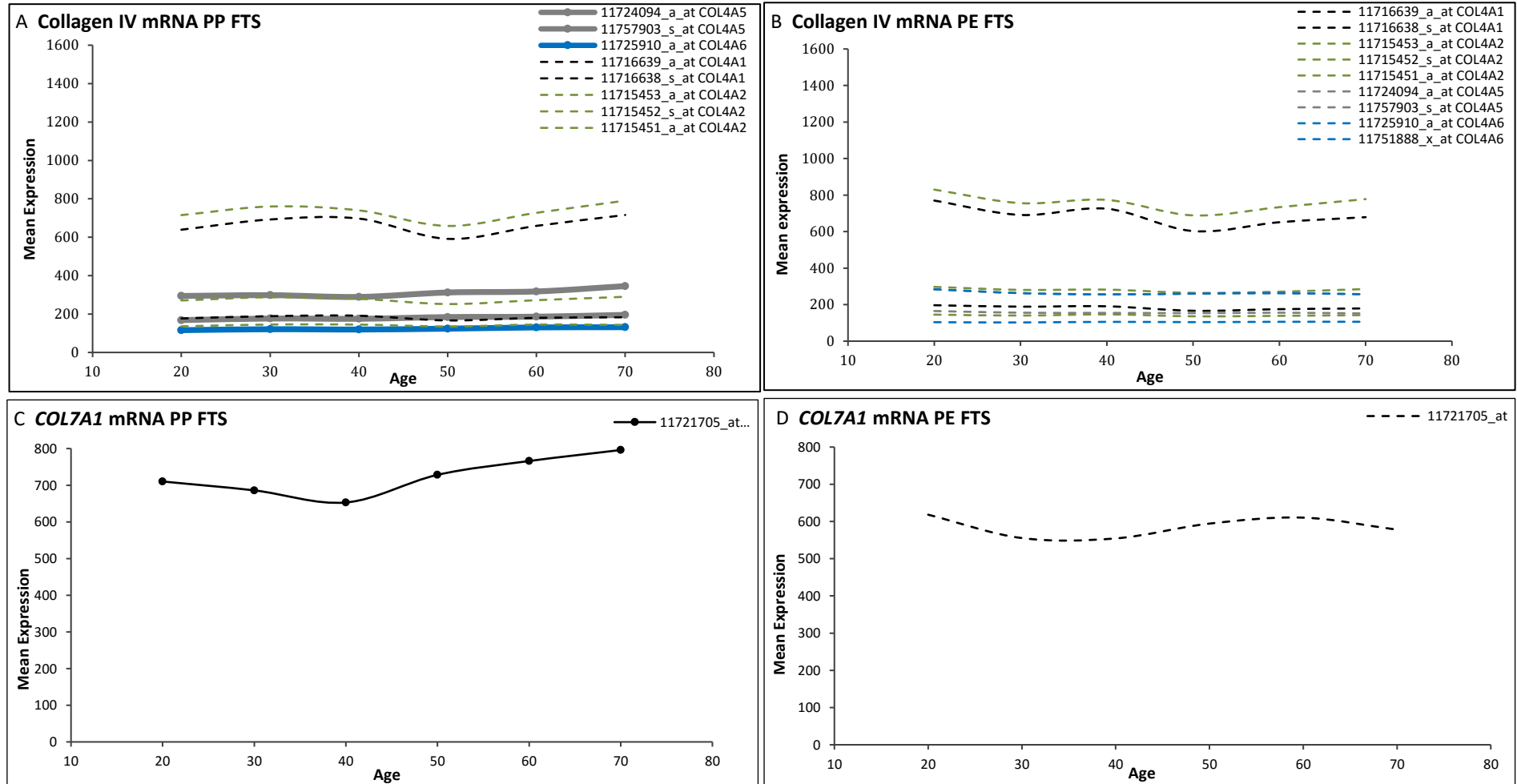
Figure 4.3.4: Microarray analysis of mRNA levels for basement membrane collagens IV and VII in PP (A,C) and PE (B,D) FTS of individuals aged 20, 30, 40, 50, 60 and 70. Plots A-D show the change in mean signal expression of mRNA levels from the 2nd to 7th decade. The different colours depict the probe sets targeting *COL4A1* (black), *COL4A2* (green), *COL4A5* (grey), *COL4A6* (blue) and *COL7A1* (black) mRNAs as shown in Figure 1. Thin dotted lines show probe sets that did not significantly change in expression level with age. Thin uniform lines show probes that significantly change with age (p ≤ 0.05). Thick uniform lines show probe sets that had a highly significant change with age (p ≤ 0.05; q ≤ 0.05)..

4.3.5   Age-related changes in collagen IV mRNA levels

For collagen IV mRNA, the different probe set expression levels and arrangements formed a distinctive pattern within the different skin compartments. In the PP (figure 4.3.2 A) and PE (figure 4.3.2 B) dermis, the two probe sets 11716638_s_at (black) and 11715452_s_at (green) which bound *COL4A1* and *COL4A2* mRNA respectively, showed the highest levels of mRNA binding. These two probes also showed the greatest change in their mean expression levels with age in the PE dermis. The dermis showed the greatest variation in probe set expression levels of all the compartments, with some probes having a mean expression level of ~1500 units and others ~100 units.

In the epidermis the probe sets were less variable in their mean expression levels compared to the dermis. However, like in the dermis, the probe sets which showed the highest level of mean expression at age 20 were also the ones that showed the greatest change with age. This occurred in both PP (figure 4.3.3 A) and PE (figure 4.3.3 B) skin. These probes were 11757903_s_at and 11724094_a_at, which both bound to *COL4A5* mRNA.

The two probe sets which had showed high levels of mean expression and changes with age in the PP and PE dermis (11716638_s_at and 11715452_s_at which bound *COL4A1* and *COL4A2* mRNA) also had the greatest mean expression in the PP (figure 4.3.4 A) and PE (figure 4.3.4 B) FTS. However, their level of mean expression here was reduced and did not significantly change with age. This may be because they could have been at more concentrated levels in the isolated dermal compartment instead of the FTS where the epidermal compartment and skin appendages are also present. Generally, more significant changes were yielded from the isolated epidermal and dermal compartments compared to the FTS, with each compartment showing the most robust changes to different collagen IV genes. In the dermis the most marked changes were occurring to *COL4A1* and *COL4A2* mRNA levels whereas in the epidermis *COL4A5* and *COL4A6* levels changed most dramatically.

4.3.6   Age related changes in collagen VII mRNA levels.

In the separate epidermal and dermal compartments, collagen VII mRNA levels showed the most significant changes in the PP (figure 4.3.3 C) and PE epidermis (figure 4.3.3 D). In the PP and PE dermis (figure 4.3.2 C and D), probe set binding was low and yielded no significant age-related changes. In the FTS, collagen VII mRNA increased with age(Figure 4.3.3 C) but in the PE FTS the mRNA level did not change (figure 4.3.4 D). Together this data suggests that the epidermal compartment was the main source of age-related changes to collagen VII mRNA as this is where significant changes to *COL7A1* mRNA levels occurred during both intrinsic and photo-ageing.

4.3.7 Summary of age-related modulation of collagen IV and collagen VII mRNA.

The information gathered from the plots in 4.3.6 was put into summary tables found below

Table 4.3.2: Details of statistically significant changes to collagen IV in each compartment. Orange fill indicates the compartment with the most significant changes in PE skin and blue fill indicates the PP skin. * PP dermis showed 2x *COL4A1* probe-sets increasing in expression and 1x *COL4A5* probe set decreasing in expression

Skin sample/condition	Signal expression range of statistically significant probes (to nearest 100)	Number of upregulated (+) or downregulated (-) probes statistically correlating with age with p ≤ 0.05. (numbers in parentheses indicate the number of these probes that also had q ≤ 0.05)
Photo-protected (PP) dermis	200-1000	**-2** (2) **+1** (0)*
Photo-exposed (PE) dermis	100-1500	**-7** (4)
Photo-protected (PP) epidermis	100-400	**+3** (1)
Photo-exposed (PE) epidermis	100-700	**+4** (4)
Photo-protected FTS (PP)	100-300	**+3** (3)
Photo-exposed FTS (PE)	NP	NP

Table 4.3.3: Details of the alpha chain identity and probe set ID for significant probes within each skin compartment.

Skin sample/condition	α-chain identity of *highly* significant probes (P≤0.05, Q≤0.05)	α-chain identity of significant probes (P≤0.05, Q≥0.05)
Photo-protected (PP) dermis	**α1** 11716638_s_at **α1** 11716639_a_at	**α5** 11715453_a_at
Photo-exposed (PE) dermis	**α1** 11716638_s_at **α1** 11716639_a_at **α2** 11715451_a_at **α2** 11715452_s_at	**α2** 11715453_a_at **α5** 11724094_a_at **α5** 11757903_s_at
Photo-protected (PP) epidermis	**α5** 11724094_a_at	**α5** 11757903_s_at **α6** 11725910_a_at
Photo-exposed (PE) epidermis	**α5** 11724094_a_at **α5** 11757903_s_at **α6** 11725910_a_at **α6** 11751888_x_at	NP
Photo-protected FTS (PP)	**α5** 11724094_a_at **α5** 11757903_s_at **α6** 11725910_a_at	NP
Photo-exposed FTS (PE)	NP	NP

Table 4.3.3 shows that there were differential changes to the mRNA levels for collagen IV in the epidermal and dermal compartments of PP and PE skin. Collagen IV mRNA levels increased in the epidermal compartment and decreased in the dermal compartment during both intrinsic and photo-ageing. The majority of the transcriptional changes in the PP and PE

dermal compartments were a result of decreasing *COL4A1* and *COL4A2* mRNA and there were more significantly changing probe sets in the PE dermis compared to the PP dermis.

In the epidermal compartment *COL4A5* and *COL4A6* transcription increased in the PP and PE skin. Like in the dermis, there were more significantly changing probes in the PE condition. The separate epidermal and dermal compartments therefore showed different changes to collagen IV alpha chain transcription with age. In the dermis decreased transcription of mRNAs encoding the alpha chains that form the heterotrimer $[\alpha1(IV)]_2\alpha2$ occurred with age. In the epidermis mRNAs encoding the alpha chains for the heterotrimer $[\alpha5(IV)]_2\alpha6$ increased. Both the transcriptional decreases in the dermis and increases in the epidermis were more marked in the PE skin compared to the PP skin, suggesting photo-ageing modulated collagen IV gene transcription to a greater extent than intrinsic ageing.

In the FTS samples fewer significant changes to the probe set expression levels were present compared to the epidermis and dermis in isolation. Despite a greater number of significantly changing probe sets in the separate epidermal and dermal compartments in the PE skin compared to the PP skin, there were more significant changes in the PP FTS compared to the PE FTS. In the PP FTS three probe sets significantly changed expression levels with age whereas in the PE FTS none of the probe sets showed age-related changes.

Collagen VII mRNA levels (see table 4.3.4) showed the most robust changes in the epidermis, where mRNA expression increased in both intrinsically aged and photo-aged tissue. This increase was also statistically significant in the PP FTS. The probe set for *COL7A1* did not show any highly significant changes with age demonstrated by the observation that there were no instances where $P \leq 0.05$ and $Q \leq 0.05$.

Table 4.3.4: Details of statistically significant changes to collagen VII in each compartment. Orange fill indicates the compartment with the most significant changes in PE skin and blue fill indicates the PP skin.

Skin sample/condition	Signal expression range of statistically significant probe (to nearest 100)	Number of upregulated (+) or downregulated (-) probes statistically correlating with age with p ≤ 0.05. (numbers in parentheses indicate the number of these probes that also had q ≤ 0.05)
Photo-protected (PP) dermis	NP	NP
Photo-exposed (PE) dermis	NP	NP
Photo-protected (PP) epidermis	300-400	**+1** (0)
Photo-exposed (PE) epidermis	500-600	**+1** (0)
Photo-protected FTS (PP)	600-800	**+1** (0)
Photo-exposed FTS (PE)	NP	NP

A summary of the main changes to collagen IV and collage VII mRNA levels with age is shown below in table 4.3.5

Table 4.3.5: Summary changes of activity for the individual genes encoding for collagen IV alpha chains and the collagen VII alpha chain

Condition	collagen IV	collagen VII
Photo-ageing	*COL4A5, COL4A6* ↑ (epidermis) *COL4A1, COL4A2* ↓ (dermis)	↑ epidermis
Intrinsic ageing	*COL4A5, COL4A6* ↑ (epidermis) *COL4A1, COL4A2* ↓ (dermis)	↑ epidermis

4.3.8 Basement membrane collagen protein expression is lost with age

The change in collagen IV and collagen VII protein expression was studied by performing fluorescent immunohistochemistry on human skin using collagen IV and collagen VII primary antibodies (details in 2.8.4- materials and methods). The collagen IV antibody used was specific to the αI chain encoded for by the *COL4A1* gene, therefore future references to "collagen IV" protein refer to α1 chain of collagen IV

Figure 4.3.5 shows representative examples of collagen IV (αI) staining in skin samples from PP and PE young and aged skin. In all skin samples collagen IV was located as previously described in aforementioned publications: at the basement membrane and lining the hair follicles, sweat glands, sebaceous glands and dermal vasculature. The levels of collagen IV were similar in the young PP (4.3.5 A, A') and PE (4.3.5 B, B') skin where a strong, wavy band of collagen IV was found at the DEJ. Thick, smooth Collagen IV labelling was also present in the dermal capillaries (white arrowheads 4.3.5 A, B, C) (some non-specific antibody binding was also present in the dermis). Collagen IV expression levels did not change in the PP aged (4.3.5 C, C') skin but were dramatically reduced in the aged PE skin (4.3.5 D, D'), which had a thinner, less intense band of collagen IV labelling located at the DEJ (green arrowheads- D') compared to the other samples.
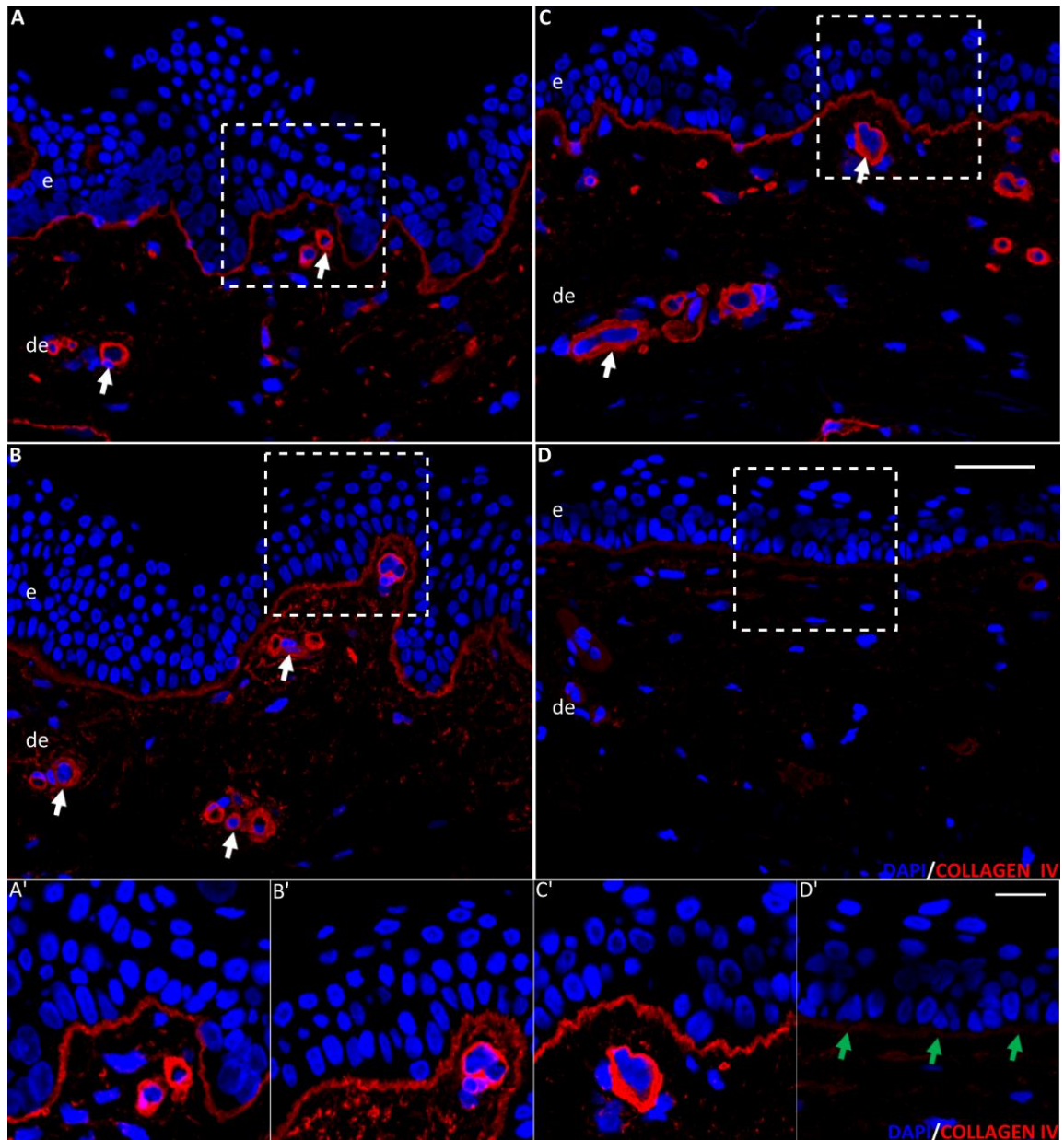
Figure 4.3.5: Representative low and high power images of photo-protected young (A, A') and old (C, C') and photo-exposed young (B, B') and old (D,D') epidermis (e) and dermis (de) stained with an Alexa 568-conjugated collagen IV antibody with DAPI nuclear counterstain. All sections were imaged on a confocal microscope using a 40x oil objective. Scale bar (low power images A-D) = 50 μm (Shown in D), (high power images A'-D'= 10 μm (Shown in D'). Dotted squares in A-D mark the corresponding magnified region in A'-D'. Prominent labelling of dermal vasculature was observed in A, B and C (white arrowheads). Green arrowheads indicate loss of collagen IV in PE aged skin.
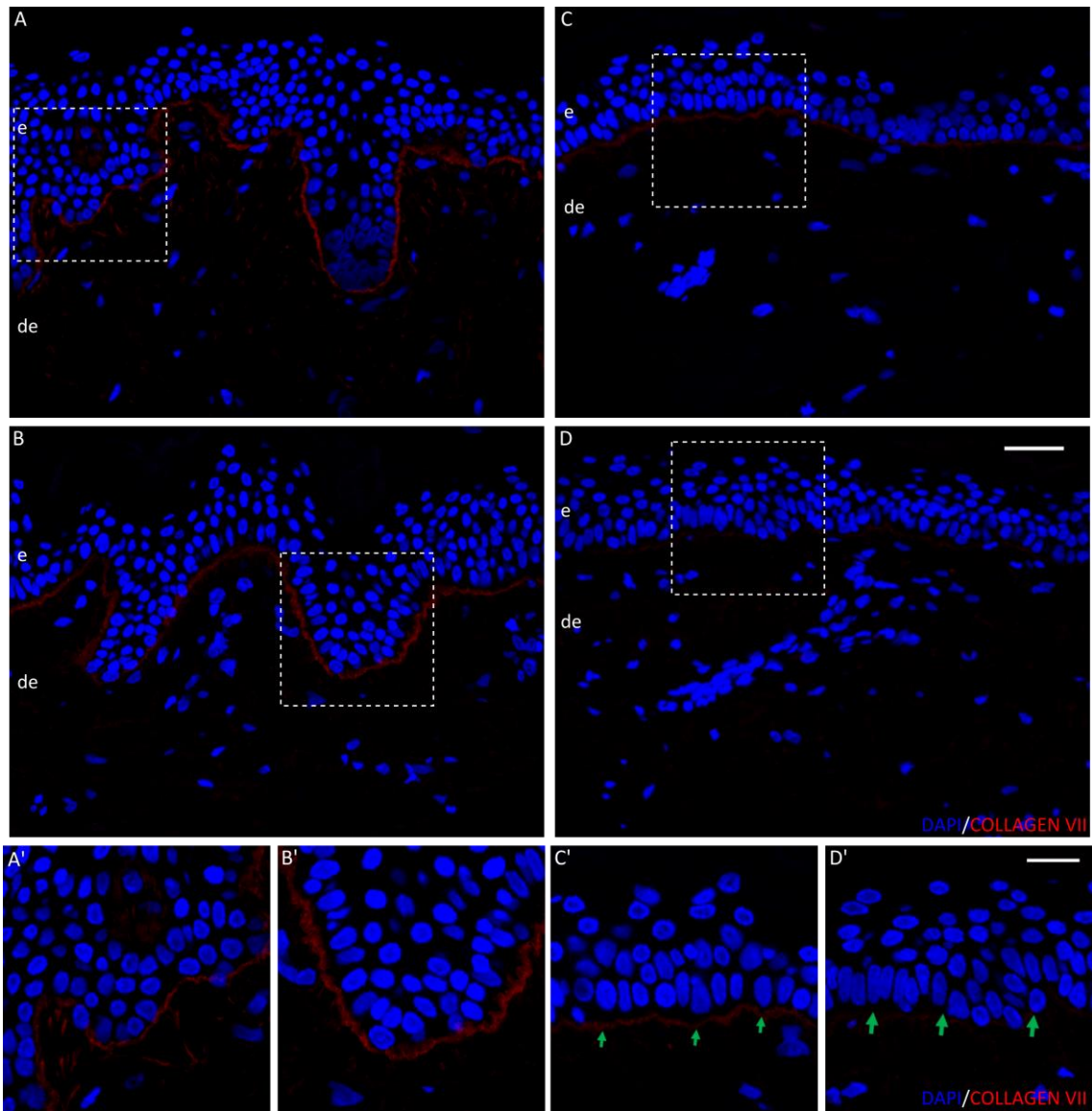
Figure 4.3.6: Representative low and high power images of photo-protected young (A, A') and old (C, C') and photo-exposed young (B, B') and old (D, D') epidermis (e) and dermis (de) stained with a collagen VII primary antibody, Alexa 568-secondary antibody with DAPI nuclear counterstain. Scale bar (low power images A-D) = 50 μm shown in D, (high power images A'-D') = 10 um shown in D'.Dotted squares in A-D mark the corresponding magnified region in A'-D'. Small green arrows in C' indicate loss of Collagen VII labelling at the DEJ. Larger arrows in D' represent more dramatic collagen VII loss.

Despite more high powered imaging settings, collagen VII immunofluorescence (figure 4.3.6) in the young age groups was less intense than age-matched collagen IV expression from the same biopsy site. This was expected given that collagen IV is thought to be more abundant than collagen VII at the DEJ (Kalluri, R, 2003). Collagen VII staining was located exclusively at the DEJ where labelling was wavy and continuous at the site of the BM. In the aged PP skin (4.3.6 C, C'), the thickness of the Collagen VII band appeared the same but the staining was less intense (green arrows, C') compared to the young counterpart (A, A'). In the young (B, B') vs aged (D, D') PE skin the thickness of the collagen VII band was reduced along with a dramatic decrease

in intensity of expression (large green arrows D'). Labelling was so limited in the old PE skin that the collagen VII no longer formed a continuous line at the DEJ.

Differences in the protein expression of collagen IV and collagen VII at the DEJ of young versus aged skin were quantified by assessing the mean expression levels in the PP and PE epidermis of young (n=3) and old (n=3) subjects. Details of the analyses to generate the levels of fluorescence intensity (FI) for each condition can be found in 2.8.7- Materials and Methods.
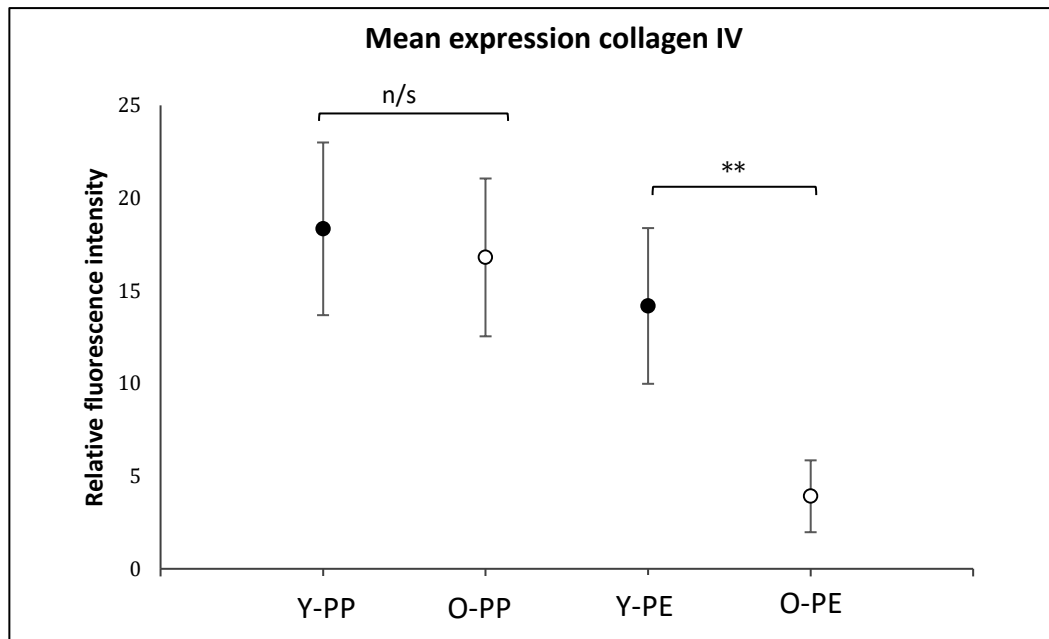
Figure 4.3.7: Mean expression levels of collagen IV protein at the DEJ of PP and PE biopsies of young (Y) and old (O) subjects. The subjects making up the data pool are detailed in the start of the chapter. Each individual data point represents the mean pixel intensity of all of the fields taken from forearm and buttock of young (21-22y) and old (60-65y) subjects. Y-PP= young photo-protected, O-PP= old photo-protected, Y-PE = young photo-exposed, O-PE= old photo-exposed. Error bars represent standard deviations calculated from the mean pixel intensity values for all of the fields imaged within each condition. Un-paired t-testing indicated that the change in expression with intrinsic ageing was not significant (n/s) but was highly significant with photo-ageing (**).
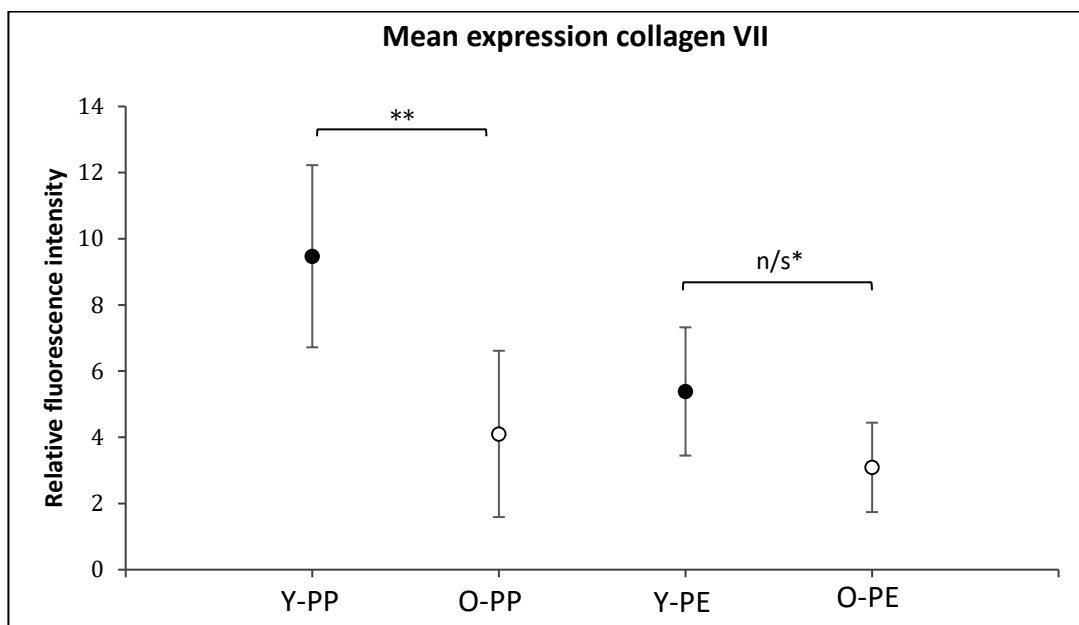
Figure 4.3.8: Mean expression levels of collagen VII protein at the DEJ of PP and PE biopsies of young (Y) and old (O) subjects. The subjects making up the data pool are detailed in the start of the chapter. Each individual data point represents the mean pixel intensity of all of the fields taken from forearm and buttock of young (21-22y) and old (60-65y) subjects. Y-PP= young photo-protected, O-PP= old photo-protected, Y-PE = young photo-exposed, O-PE= old photo-exposed. Error bars represent standard deviations calculated from the mean pixel intensity values for all of the fields imaged within each condition. Un-paired t-testing indicated that the change in expression with intrinsic ageing was highly significant (**). The change in expression with photo-ageing was close to significance- indicated by n/s*.

Figures 4.3.7 and 4.3.8 detail the change in mean protein expression of collagen IV and collagen VII young and old PP and PE skin. There was a small, non-significant, decrease in collagen IV expression in the PP aged skin and a marked decrease in aged PE skin. Collagen VII levels decreased during both intrinsic and photo-ageing with this being more marked in the PP skin. The results of the protein expression analyses are summarised below in tables 4.3.6 and 4.3.7.

Table 4.3.6: Mean expression values of collagen IV and VII at the DEJ as calculated by the average fluorescence intensity in the different skin biopsy samples. Green fill indicates a decrease with age whereas orange fill indicates an increase with age. The numbers in brackets show the relative increase or decrease with age. Numbers in brackets indicate the change in expression with age.

Skin sample/ condition	Mean collagen IV expression (accurate to 1 decimal place)	Mean collagen VII expression (accurate to 1 decimal place)
PP- young (buttock)	18.3	9.5
PP- old (buttock)	16.8 (-1.5)	4.1 (-5.4)
PE- young (forearm)	14.2	5.4
PE- old (forearm)	3.9 (-10.3)	3.1 (-2.3)

Table 4.3.7: Summary of the p-values generated from statistical testing. Green fill represents the most significant results from all of the analyses.

Epidermal sample/ condition	T-test p value: change in mean collagen IV level.	T-test p value: change in mean collagen VII level.
PP- young (buttock) PP- old (buttock)	PP young vs old 0.44	PP young vs old 0.003
PE- young (forearm) PE- old (forearm)	PE young vs old 3.8×10^{-5}	PE young vs old 0.08

4.3.9 Discussion: Novel identification of transcriptional changes in the collagen IV alpha chain genes with age

The objectives of this section were to look at how the mRNA and protein levels of collagen IV and collagen VII changed in both intrinsically aged and photo-aged female skin. At the mRNA level, there was a general trend for the collagen IV transcripts to show differential changes with age depending on their alpha chain identity. This presented as decreased *COL4A1* and *COL4A2* mRNA transcripts present in the dermis and increased *COL4A5* and *COL4A6* transcripts present in the epidermis. The 6 collagen IV genes are clustered into pairs due to their chromosomal location and transcriptional activity. [*COL4A1* and *COL4A2*] and [*COL4A5* and *COL4A6*] are gene pairs which have a highly unusual head-to-head orientation on opposite gene strands within the same chromosomal region. The gene pairs share a bi-functional promoter as well as enhancer elements (Sund et al, 2005). It is therefore logical that the two gene pairs would group together in terms of statistically significant transcriptional changes to age given that their activity is coupled, with transcription occurring from the same region under the same promoter.

Basement membranes are specialized ECM's that determine the polarity of basal keratinocytes. Basal epidermal stem cells (Epi SC's) adhere to the BM via integrins, which are trans-membrane proteins present on the Epi SC surface which modulate signalling involved in cell proliferation and motility (Choi et al, 2015). Stem cell homeostasis is maintained by cross-talk between Epi SC's and the underlying basement membrane structure. Additionally, it is thought that both the mechanical integrity and the protein composition of the BM regulate this communication (Brizzi et al, 2012). Both intrinsic and UV ageing are associated with increased levels of collagen-degrading enzymes such as Matrix Metallo-Proteinases (MMP's) and in particular, MMP-2 and MMP-9 degrade collagens IV and VII. Loss of type IV and VII collagens dramatically impacts the BM architecture and as a result negatively impacts the Epi SC niche (Panich et al, 2016).

Collagen IV α1 and α2 chains are expressed in the BM's of both epidermal epithelia and dermal vasculature whereas α5 and α6 chains are restricted to epithelial BM's only. The significant decreases in *COL4A1* and *COL4A2* mRNA we observed in the dermis could represent a decline in the presence of dermal vasculature in this region which has been shown to occur with age (Gunin et al, 2015). Given the aforementioned impact of ageing on the BM architecture and stem cell niche, the increases in α5 and α6 chain transcription, particularly within the PE epidermis, may represent a compensatory transcriptional mechanism. Replenishing the dramatic loss of collagen IV protein that was observed to occur with age could help to maintain the integrity of the Epi SC niche. This may also be the case for collagen VII, which showed increase in epidermal mRNA levels in both intrinsically aged and photo-aged tissues.

Despite this putative compensatory transcriptional increase of collagen IV and collagen VII mRNAs during ageing, both of these components decreased at the protein level in both aged PP and PE skin. This suggests that the synthesis of the BM collagens was lower than their degradation in the aged skin, either as a potential result of poorer collagen protein translation and assembly at the BM or increased degradation by proteases. In the PP skin, the collagen IV decline was not statistically significant whereas in the PE skin dramatic collagen IV loss occurred at the DEJ. Collagen VII decline at the protein level was significant in the PP aged skin and very close to conventional significance in the PE skin. Unexpectedly, collagen VII levels in the young PE skin were considerably lower than in the PP counterpart. This finding could represent either a structural difference in terms of collagen VII content at the BM of forearm and buttock skin or potential premature degradation of DEJ structures. Premature collagen VII loss has been shown to occur in photo-exposed skin of relatively young, 30 year old females, in previous reports (Amano, S 2010).

Altogether ageing decreased the levels of the BM collagens at the DEJ. There was a minor, non-significant loss of collagen IV during intrinsic ageing, suggesting that collagen IV levels are retained during this process. This is in agreement with our studies using young and aged C57BL/6 mouse tissues. Collagen VII loss was marked during intrinsic ageing, which we have also observed in mouse. This suggests that the protein changes to collagens IV and VII at the DEJ are similar in intrinsically aged mouse and human skin.

For the first time we have shown that modulation of collagen IV expression at the transcriptional level with age was different for the genes encoding the collagen IV alpha chains. However, as the immunostaining completed here was specific to the α1 chain of collagen IV, an important future step in this research would be to use other alpha-chain specific antibodies. This would allow us to determine if, like at the mRNA level, the decreases in collagen IV protein

we observed occurred to other alpha chains aside from α1. This would give further insight into the protein changes occurring at the BM during intrinsic and photo-ageing.

4.4 Investigation of mRNA and protein changes in the nuclear lamina during intrinsic and photo-ageing.

4.4.1 Introduction Lamin protein organisation in normal skin

Immuno-histochemical studies of lamins A, C, B1 and B2 in the skin of normal subjects show a distinctive pattern of expression in the different skin layers, which are summarised in table 4.4.1. Generally, A-type lamins are expressed at high levels in the upper epidermal layers and in dermal fibroblasts, while low expression levels are exhibited by cells belonging to the basal epidermal layer. B-type lamins are highly expressed in the basal epidermis and in melanocytes and Langerhans cells. In the upper epidermis lamin B1 expression is reduced compared to the basal layer. B-type lamins are expressed at much lower levels in the dermal fibroblasts compared to the epidermal region. Table 4.4.1 shows that the levels of A- and B-type lamins within different compartments of the skin and their constituent cellular populations is variable, and it is thought that high levels of lamin B1 mark proliferating cells (Broers et al, 1997).

There is conflict in the literature regarding the levels of B-type lamins in dermal fibroblasts (marked with * in table 4.4.1). Oguchi et al, (2002) and Broers et al, (1997) show that lamin B1 is absent from dermal fibroblasts whereas lamin B2 is present at a medium level whereas information from the Human Protein Atlas (http://www.proteinatlas.org/) indicates that lamin B1 levels are high and lamin B2 levels are low.

Table 4.4.1: Using the combined information from the publications Libotte et al, 2005, Tilli et al, 2003, Oguchi et al, 2002 and Broers et al, 1997 and the online Human Protein Atlas, levels of the different A and B-type lamins in skin cells are summarised. ++ (dark green) indicates high level, + (light green) indicates medium level, +/- (grey) indicates weak expression or only some cells labelled, - (white) indicates no expression, N/A information not available. Asterisk's (*) mark conflicting reports of levels.

Skin Compartment	lamin A	lamin C	lamin A/C	lamin B1	lamin B2
Basal layer	-	+	+	++	++
Spinous layer	++	++	++	+	+
Granular layer	++	++	++	+/-	+
Dermal fibroblast	+	+	+	+/-*	+/-*
Melanocyte	N/A	N/A	+	++	+
Langerhans cell	N/A	N/A	+	++	+/-

4.4.2 Objectives of this section

From reviewing the literature concerning lamins in skin development, oxidative defence and ageing biology (see main thesis intro parts 1.13-1.18) it appears that a systematic genomic and proteomic approach to answer the question of what happens to the levels and organisation of the A-type and B-type lamins in both intrinsic and extrinsic skin ageing had not been addressed. As lamin B1 and lamin A/C are the most heavily implicated in both skin ageing and development these two proteins were studied in depth. The objectives of the data presented were to:

1. Use microarray data of human tissue to identify age-related (intrinsic ageing) transcriptional changes to the *LMNA* and *LMNB1* genes.

2. Use microarray and protein data to assess whether photo-ageing causes a differential change to *LMNA* and *LMNB1* mRNA and protein levels with age compared to intrinsic ageing.

3. Complete Immuno-histochemical staining on human skin sections in order to assess if lamin B1 and lamin A/C protein levels and organisation changed during intrinsic and extrinsic ageing.

4.4.3 Identification of transcriptional changes to the *LMNA* and *LMNB1* genes with age

In order to fulfil the aims of objective's 1 and 2, changes in transcriptional activity of the *LMNA* and *LMNB1* genes was assessed in female subjects from ages 20-70. The Affymetrix microarray chip uses multiple probe sets for each gene in order to detect alternatively spliced gene products and to increase the probability of effective mRNA binding. There were 7 probe sets designed to target mRNA transcripts from the *LMNA* gene, which is known to produce 22 alternatively spliced mRNA variants, 19 of which putatively encode proteins.[Footnote 1] 5 probe-sets targeted *LMNB*1 mRNA, which has 10 mRNA splice variants, 7 of which putatively encode proteins.[Footnote 2]

Plots of the change in mean mRNA levels for each probe-set with age in the different skin compartments are shown in figures 4.4.1-4.4.3, where a formatting system (each individual probe set is colour coded) has been used to depict statistically significant changes. The level of signal expression for each probe set within each age group indicates the mean level of mRNA that bound to that probe set from all of the subjects.

1: http://www.ncbi.nlm.nih.gov/IEB/Research/Acembly/av.cgi?db=human&c=Gene&l=LMNA
2: http://www.ncbi.nlm.nih.gov/IEB/Research/Acembly/av.cgi?db=human&c=Gene&l=LMNB1)

LMNA and LMNB1 mRNA expression: Dermal compartment only
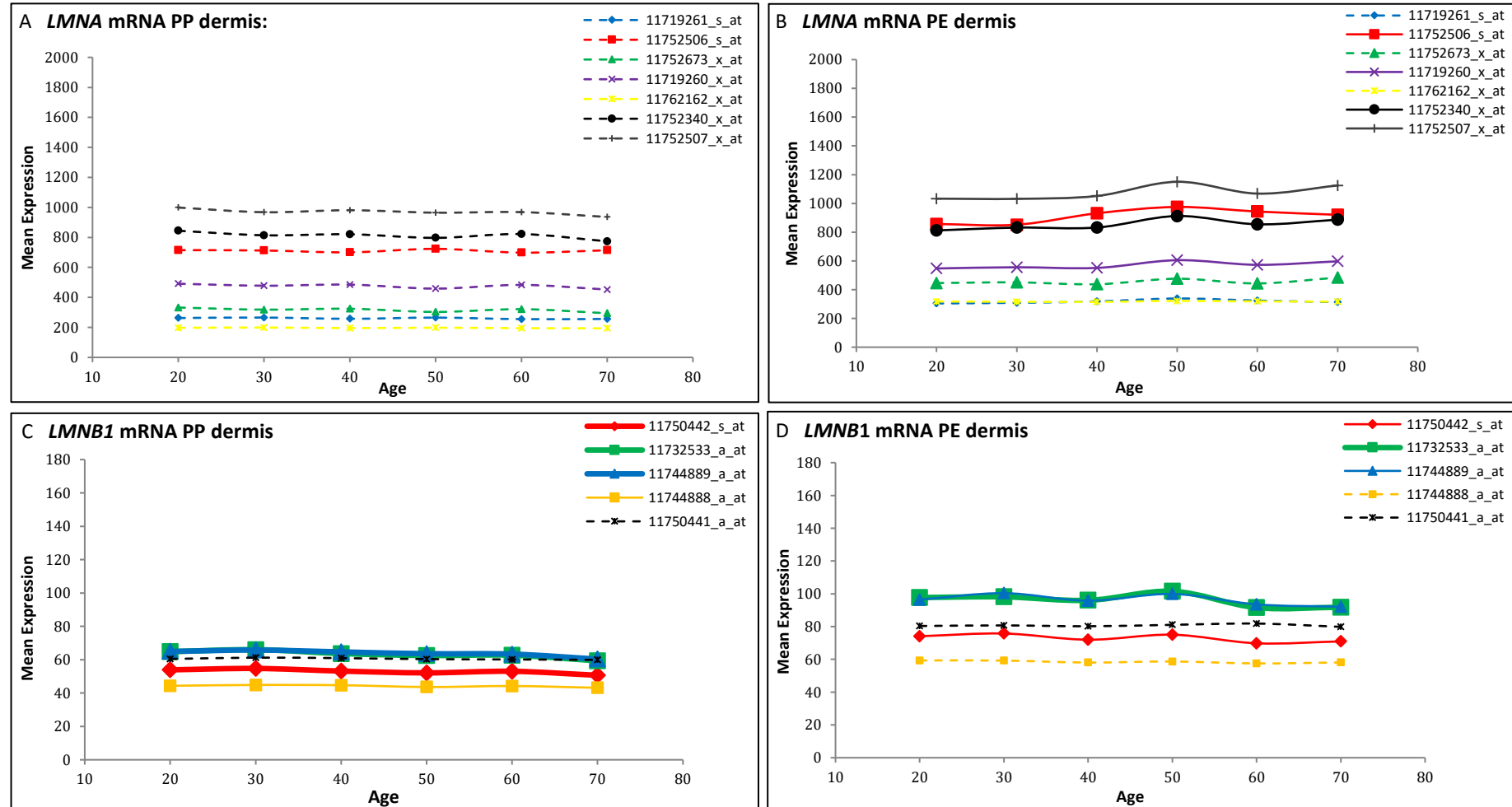
Figure 4.4.1: Microarray analysis of *LMNA* and *LMNB1* in PP (A, C) and PE (B, D) dermis of individuals of ages 20, 30, 40, 50, 60 and 70. Plots A-D show the change in mean signal expression of mRNA levels from the 2nd to 7th decade. The legends in the right hand corner of the page depict the colour and format applied to each of the 7 probe sets for *LMNA* and 5 probe sets for *LMNB1*. Thin dotted lines show probe sets that did not significantly change in expression level with age. Thin uniform lines show probes that significantly change with age (p ≤ 0.05). Thick uniform lines show probe sets that had a highly significant change with age (p ≤ 0.05; q ≤ 0.05).

LMNA and _LMNB1_ mRNA expression: Epidermal compartment only
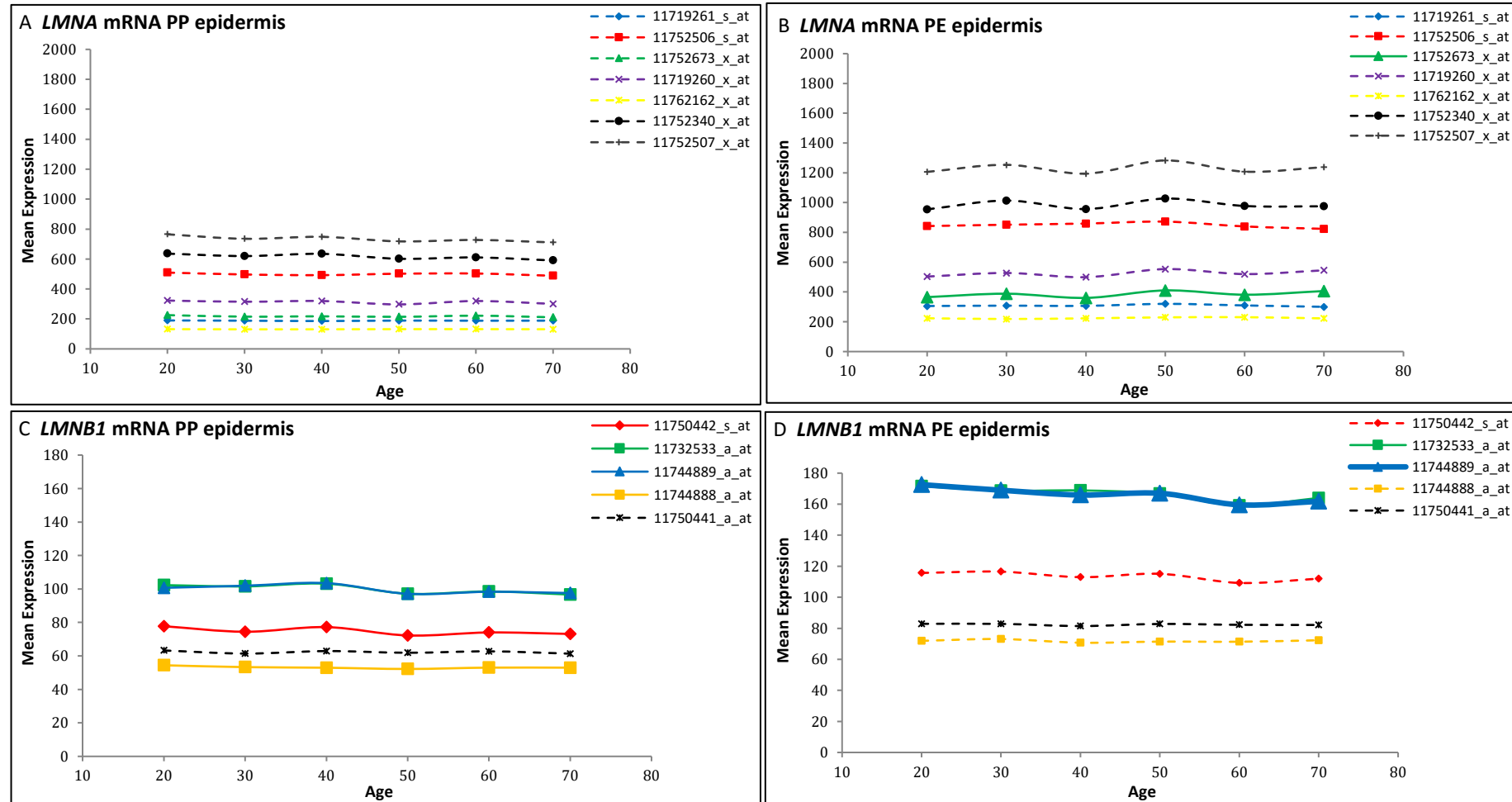
Figure 4.4.2: Microarray analysis of LMNA and LMNB1 in PP (A,C) and PE (B,D) epidermis of individuals of ages 20, 30, 40, 50, 60 and 70. Plots A-D show the change in mean signal expression of mRNA levels from the 2nd to 7th decade. The legends in the right hand corner of the page depict the colour and format applied to each of the 7 probe sets for LMNA and 5 probe sets for LMNB1. Thin dotted lines show probe sets that did not significantly change in expression level with age. Thin uniform lines show probes that significantly change with age (p ≤ 0.05). Thick uniform lines show probe sets that had a highly significant change with age (p ≤ 0.05; q ≤ 0.05).

<u>LMNA and LMNB1 mRNA expression: Full Thickness Skin</u>

Figure 4.4.3: Microarray analysis of *LMNA* and *LMNB1* in PP (A,C) and PE (B,D) FTS of individuals of ages 20, 30, 40, 50, 60 and 70. Plots A-D show the change in mean signal expression of mRNA levels from the 2nd to 7th decade. The legends in the right hand corner of the page depict the colour and format applied to each of the 7 probe sets for *LMNA* and 5 probe sets for *LMNB1*. Thin dotted lines show probe sets that did not significantly change in expression level with age. Thin uniform lines show probes that significantly change with age ($p \leq 0.05$). Thick uniform lines show probe sets that had a highly significant change with age ($p \leq 0.05$; $q \leq 0.05$). In the plot showing *LMNB1* levels in PE FTS (D) the probe sets 11744889_a_at and 11732533_a_at overlap leaving the latter obscured from view in the graph.

4.4.4 Intrinsic and photo-ageing alter *LMNA* and *LMNB1* transcription

Figures 4.4.1-4.4.3 show that there was variation in the mean signal expression levels, and their change with age, in the different probe sets targeting the same gene. For the probe sets targeting the *LMNA* mRNA, this variation was greatest in the FTS samples (figure 4.4.3 A and B) where the lowest level of expression was shown by the probe 11762162_x_at (light yellow ~200 units) and the highest by 11752507_x_at (grey ~1800 units) giving a difference of Δ1600 units. The probe sets targeting *LMNB1* mRNA also showed variability but this was less marked, with a difference in the highest (11732533_a_at-green, 170 units) and lowest (1174488_a_at-yellow, 70 units) probe expression values being Δ100 in the PE epidermis (figure 4.4.2 D). Between the two genes, the measured mRNA levels were consistently higher in the probe sets targeting *LMNA* mRNA, but this could be due to the fact there were more probe sets for *LMNA* compared to *LMNB1* and therefore there could be more mRNA binding due to the increased number of targets.

Generally, higher levels of mean expression and hence mRNA binding tended to occur in the same probe sets in the different skin compartments for each gene. The probe sets that had the highest levels of initial mean expression at age 20 were also the ones that were most likely to statistically significantly increase or decrease their expression level with age and conversely, low initial mean signal expression in a probe set generally meant that it showed little significant change to mean mRNA expression levels with age. For example probe set 11752507_x_at (shown in grey) targeting *LMNA* mRNA was the most highly expressed probe in all skin compartments and also showed significant changes with age in the PP and PE FTS and PE dermis, whereas probe set 11762162_x_at (shown in yellow) showed the lowest mRNA expression levels and no significant changes in expression with age. It is therefore likely that highly expressed probes are those that show specific binding from the target gene transcripts and depict most accurately the changes occurring with age. Probes with low expression levels and no significant changes with age could be representative of non-specific "off target" mRNA binding and therefore were eliminated from further analytical consideration (table 4.4.2).

The classifications used to assess significant changes to mRNA levels with age were the P and Q values generated from Pearson's Rank Correlation tests completed on the data (details in chapter 2-section 2.7.5), with the most robust changes being identified as those that had both significant P and Q values. The number of probes that significantly changed expression levels with age for each gene thus provides a parameter of the extent of significant *LMNA* and *LMNB1* transcriptional changes with age and these values are summarised in the tables below:

Table 4.4.2: Summary of statistically significant changes to *LMNA* mRNA levels in the different skin compartments under intrinsic and photo-ageing conditions. The PE and PP compartments that showed the most significant changes are highlighted in orange (PE skin) and blue (PP skin). NP= no significant probes in the compartment. Signal expression range data values have been rounded to the nearest whole 100 for simplicity.

Skin sample/condition	Signal expression range of statistically significant probes	Number of upregulated (+) or downregulated (-) probes statistically correlating with age with p ≤ 0.05 (numbers in parentheses indicate the number of these probes that also had q ≤ 0.05)
Photo-protected (PP) dermis	NP	NP
Photo-exposed (PE) dermis	500-1100	**+4** (0)
Photo-protected (PP) epidermis	NP	NP
Photo-exposed (PE) epidermis	300-400	**+1** (0)
Photo-protected FTS (PP)	300-1700	**-6** *(4)*
Photo-exposed FTS (PE)	300-1800	**+6** (6)

Table 4.4.3: Summary of statistically significant changes to *LMNB1* mRNA levels in the different skin compartments under intrinsic and photo-ageing conditions. The PE and PP compartments that showed the most significant changes are highlighted in orange (PE skin) and blue (PP skin). NP= no significant probes in the compartment. Signal expression range data values have been rounded to the nearest whole 10 for simplicity.

Skin sample/condition	Signal expression range of statistically significant probes	Number of upregulated (+) or downregulated (-) probes statistically correlating with age with p ≤ 0.05 (numbers in parentheses indicate the number of these probes that also had q ≤ 0.05)
Photo-protected (PP) dermis	40-70	**-4** (3)
Photo-exposed (PE) dermis	70-100	**-3** (1)
Photo-protected (PP) epidermis	50-110	**-4** (0)
Photo-exposed (PE) epidermis	160-180	**-2** (1)
Photo-protected FTS (PP)	60-80	-3 (0)
Photo-exposed FTS (PE)	60-80	-2 (2)

As seen in table 4.4.2, *LMNA* mRNA decreased with age in the PP skin and increased with age in PE skin. The separate PP epidermal and dermal compartments showed no significant changes to *LMNA* mRNA with age but the decrease in *LMNA* mRNA in the PP FTS was highly significant, with 6/7 probes significantly decreasing mRNA expression level with age. The increases in *LMNA* mRNA in PE skin were consistent across the epidermal, dermal and FTS with the greatest changes occurring in the FTS.

Table 4.4.3 shows that *LMNB1* mRNA decreased with age in both the PP and PE skin with the total number of significantly down-regulated probes from the epidermis, dermis and FTS combined being greater in the PP (11 probes total) compared to the PE (7 probes total) skin. This suggests that a more robust decrease in transcription to *LMNB1* occurred in the intrinsically aged skin compared to the photo-aged skin. The highest mean expression levels of *LMNB1* mRNA were seen in the epidermal compartments, which one might expect as they are very cell rich and the lamins are nuclear envelope proteins. However, loss of *LMNB1* mRNA levels with age were most robust in the dermal compartments of PP and PE skin as shown by orange and blue highlighting in the table.

The distribution of significantly changing probe sets in the epidermis, dermis and FTS was different for *LMNA* and *LMNB1* probes. For *LMNB1*, the numbers of significantly changing probe sets were well spread across the different epidermal, dermal and FTS compartments in both the PP and PE skin. On the other hand, the *LMNA* probe sets showed the most significant changes in the FTS skin during intrinsic and photo-ageing, with only minor changes occurring in the separate epidermal and dermal compartments The main changes occurring to *LMNA* and *LMNB1* mRNA levels with age are summarised in table 4.4.4:

Table 4.4.4: Summary changes to *LMNA* and *LMNB*1 mRNA during intrinsic and photo-ageing in human skin

Skin Condition	LMNA	LMNB1
Photo-ageing	↑	↓
Intrinsic ageing	↓	↓

4.4.5   Lamin A/C protein expression is maintained during skin ageing, while lamin B1 protein decreases

For reasons alluded to in the introduction of this chapter (section 4.1.8), the mRNA changes observed in *LMNA* and *LMNB1* were validated at the protein level. Previous reports have detailed the organisation and levels of nuclear lamins in skin taken from breast and abdomen (Tilli et al, 2003) but to our knowledge skin from young and aged photo-exposed sites had not been studied.

Figure 4.4.4 shows lamin A/C expression in young (22y) and aged (64y) skin samples taken from the buttock (sun-protected) and forearm (sun-exposed) of the same individual. In the epidermal layers of the young tissue (A= buttock, B=arm) lamin A/C organisation was similar, with most cells showing lamin A/C labelling. In the suprabasal layers expression levels were highest, with cells showing the uniform ring-like pattern typical of nuclear lamina staining. In the basal epidermis lamin A/C staining was heterogeneous, with some cells showing medium

levels of expression (white arrowheads- A' and B') and others appeared to be more weakly labelled (green arrowheads- A' and B'). These observations are consistent with a previous report (Broers et al 1997). As Tilli et al (2003) have shown lamin A is absent from the basal layer whereas lamin C is present it may be the case that the basal layer staining observed here using the Jol2 antibody is picking up predominantly lamin C in this region. Some cells in the dermis of young arm and buttock skin showed strong labelling of lamin A/C (white arrowheads, A) whereas in others staining was reduced or absent (green arrowheads, A). The heterogeneity of staining in this region could be representative of the different cell types present in the dermis, as dermal fibroblasts stain strongly for lamin A/C whereas lymphoid cells have low lamin A/C and high lamin B1 (Broers et al, 1997).

Lamin A/C expression was maintained in the aged buttock (C) and forearm (D), particularly in the cells above the basal layer where ring-like labelling of the majority of nuclei remained strong. The heterogeneity in levels of lamin A/C observed in the cells of the basal epidermis of young tissue (As depicted by white and green arrowheads in A' and C') became more marked with age, causing the basal epidermis in PP and PE aged skin to be populated by cells with strong lamin A/C staining (white arrowheads, C, D, C',D') and also cells with weak staining (green arrowheads, C,D,C',D'). The epidermal layer thinned considerably with age in both arm and buttock skin and also showed a loss of rete ridges (fine white arrows A,B showing rete ridges, lost in C,D). The strong lamin A/C staining seen in the suprabasal layers of the young PP and PE epidermis was maintained with age, aside from a few cells in the upper epidermis that showed a reduction in lamin A/C in aged PP aged skin (green arrowheads in upper epidermis, C,C'). In the dermis labelling of lamin A/C was similar in the aged skin compared to the young skin, with similar levels of lamin A/C positive and negative cells being observed in both intrinsically aged and photo-aged skin in comparison to their younger counterparts.
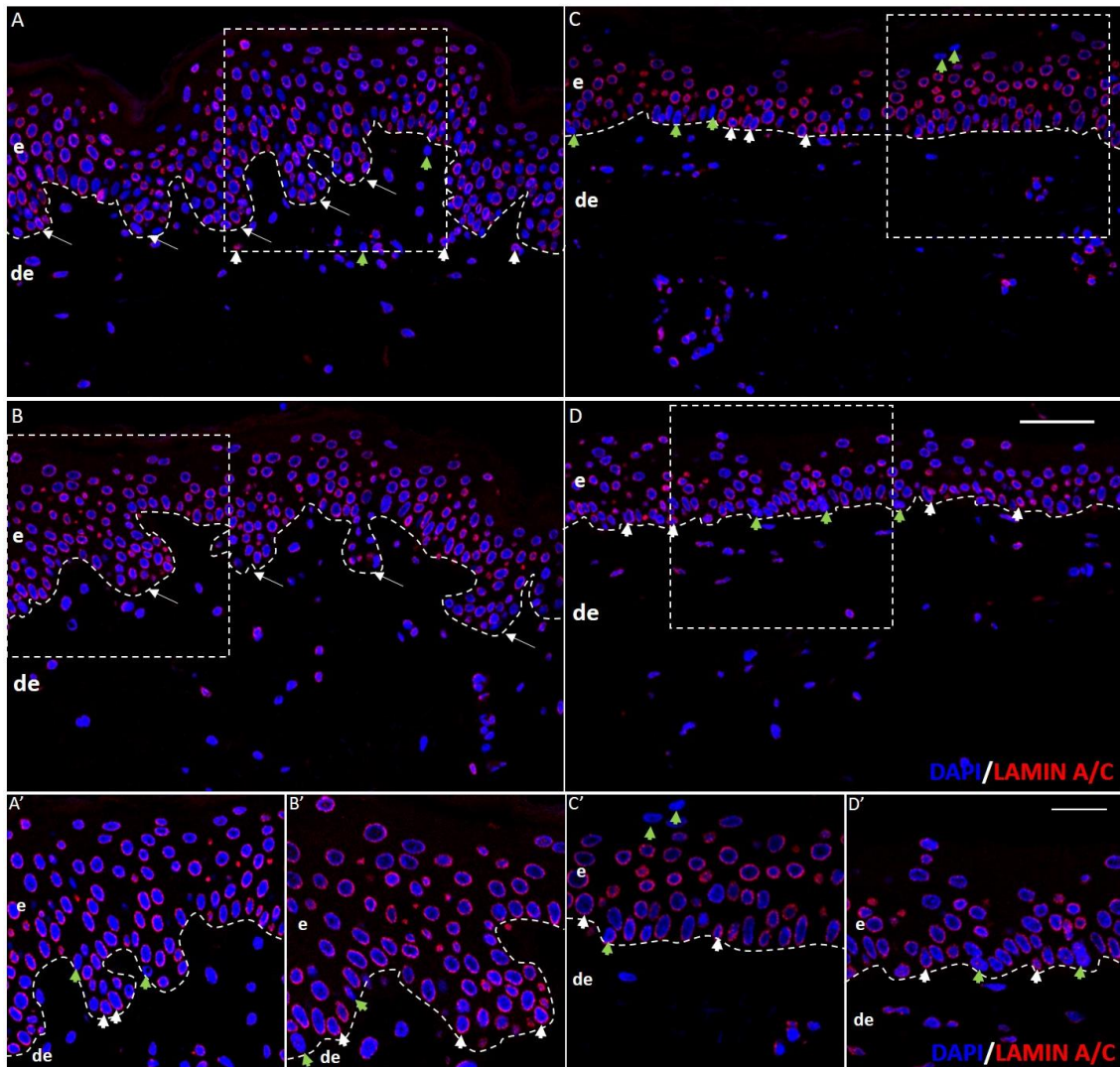
Figure 4.4.4: Immunofluorescence examination of lamin A/C expression using low (A-D) and high (A'-D') magnification confocal microscopy. Images of 22y buttock (A,A') and forearm (B,B') and 64 year buttock (C,C') and forearm (D,D') were stained with Jol2 primary antibody (detects both lamin A and lamin C isoforms) and anti-mouse Alexa 568 secondary antibody with DAPI counterstain for nuclei. Images A-D show epidermal and dermal regions. Images A'-D' show a magnified portion of the epidermis, which is marked with an asterisk in the corresponding low mag image. e= epidermis, de=dermis, dotted line= dermal-epidermal junction, scale bar (A-D same scale) = 50 µm shown in D, scale bar (A'D' same scale) =20 µm shown in D'. White arrowheads show examples of cells with high lamin A/C expression and green arrowheads show examples of cells with weak/absent lamin A/C expression. Long white arrows at the DEJ in A,B mark rete ridges.

Figure 4.4.5 documents lamin B1 staining in the PP buttock and PE arm from the same young and old individuals seen in figure 4.4.4. In the young tissue lamin B1 expression in the epidermis was heterogeneous in the basal layer, with some cells staining strongly (white arrowheads A', B') whereas in others lamin B1 expression was reduced (green arrowheads A', B'). In the suprabasal layers the majority of cells had strong lamin B1 labelling. In the upper epidermis staining was reduced (green arrowheads, A',B'). These observations are consistent with previous reports by Broers et al (1997). Most of the dermal cells were un-labelled aside from some cells making up appendages within the skin (white arrowheads, C, D) and the occasional dermal cell in isolation, which could be a putative immune cell (white arrowheads,

D). The lamin B1 labelling observed in the dermis also matches the previous reports of Broers et al, 1997; Tilli et al, 2003; Oguchi et al, 2002 but not the information provided on the Human Protein Atlas.

Due to the heterogeneity of cellular populations found in the dermal compartment, use of fibroblast specific markers such as CD34 (Driskell et al, 2013) or TE-7 (Goodpaster et al, 2008) would need to be used in co-staining experiments to definitively confirm that low/absent lamin B1 marks dermal fibroblasts. In the aged skin samples lamin B1 expression appeared reduced in both the forearm (D,D') and buttock (C,C') skin. This reduction occurred primarily in the basal epidermal layer where the majority of cells in both PP and PE skin were weakly stained (Green arrowheads, C',D'). In the suprabasal layers of PP aged epidermis lamin B1 levels were similar to young epidermis, and labelling remained strong. The levels of lamin B1 in the outermost epidermal layers were consistently low in the young and aged skin.
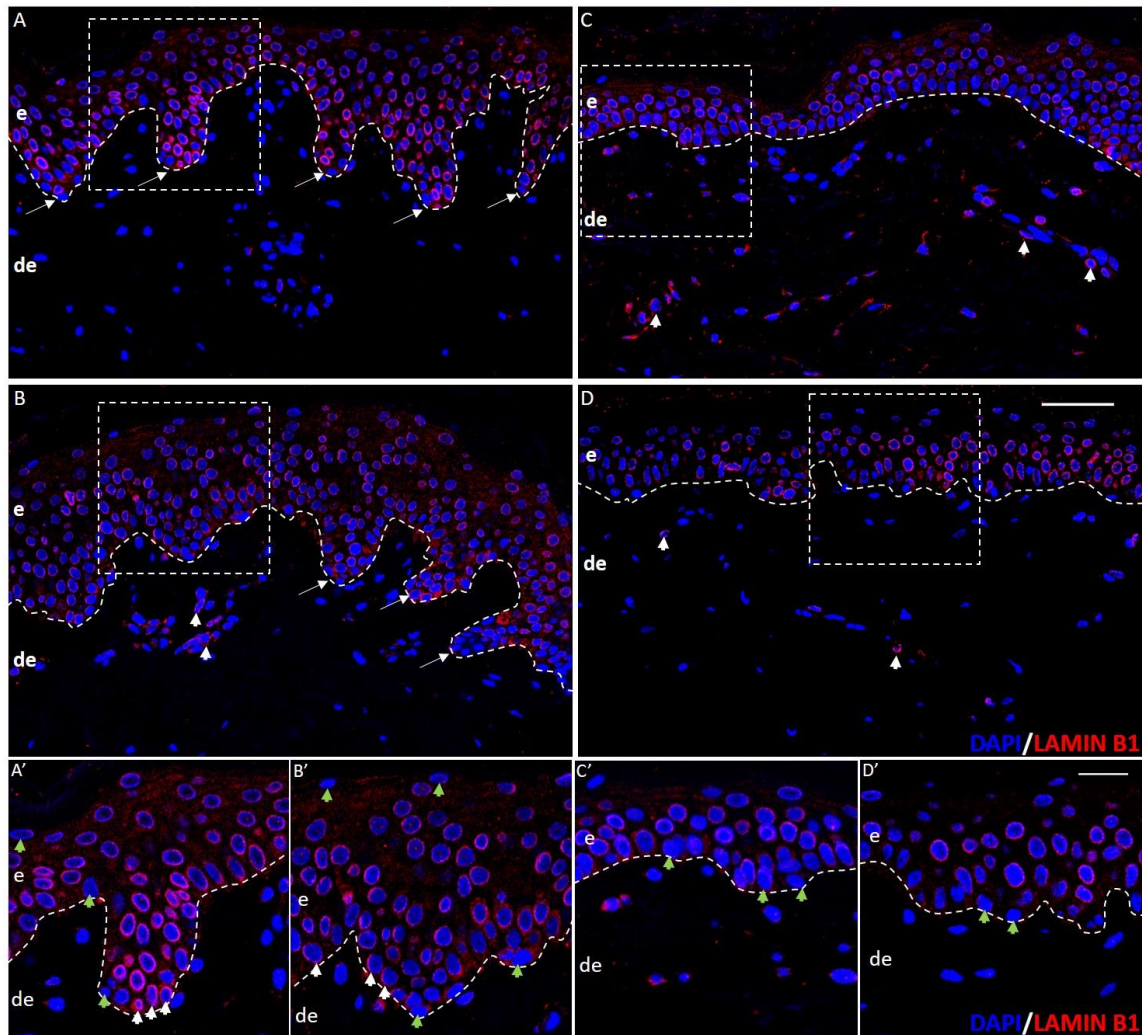
Figure 4.4.5: Immunofluorescence examination of lamin B1 expression using low (A-D) and high (A'-D') magnification confocal microscopy. Images of 22y buttock (A, A') and forearm (B, B') and 64 year buttock (C, C') and forearm (D,D') stained with anti-rabbit lamin B1 primary antibody and anti-rabbit Alexa 568 secondary antibody with DAPI counterstain for nuclei. Images A-D show epidermal and dermal regions. Images A'-D' show a magnified portion of the epidermis which is marked with an asterisk in the low mag images. e= epidermis, de=dermis, dotted line= dermal-epidermal junction, (A-D same scale) = 50 μm shown in D, scale bar (A'D' same scale) =20 μm shown in D'. White arrowheads show examples of cells with high lamin B1 expression and green arrowheads show examples of cells with weak/absent lamin B1 expression. Long white arrows at the DEJ in A,B mark rete ridges.

4.4.6 Photo-exposure in the epidermal compartment causes the greatest change in lamin A/C and lamin B1 protein levels

To compare differences in the protein expression of lamin B1 and lamin A/C in the young versus aged skin the mean expression levels in the PP and PE epidermis of young (n=3) and old (n=3) subjects was quantified. Details of the analyses to generate the levels of fluorescence intensity (FI) for each condition and information on the subjects making up the data pool can be found in section 2.8.1 of materials and methods.

As there are several cellular sub-populations with different levels of lamin expression present within the dermis, the epidermis in isolation was chosen for this analysis as it has the

least variability in cellular populations, with over 95% of the cells present in this region being keratinocytes (Thingnes et al, 2012).

Uncovering statistically significant differences to lamin B1 cellular levels with age in the dermal region would require more samples that the 3 available in this study in order to account for the increased cellular variation in this region as well as the use of appropriate markers of dermal cell sub-populations. Figure 4.4.6 shows the mean expression levels of lamin A/C in the epidermis of young and old PP (buttock biopsy) and young and old PE (forearm biopsy) skin.
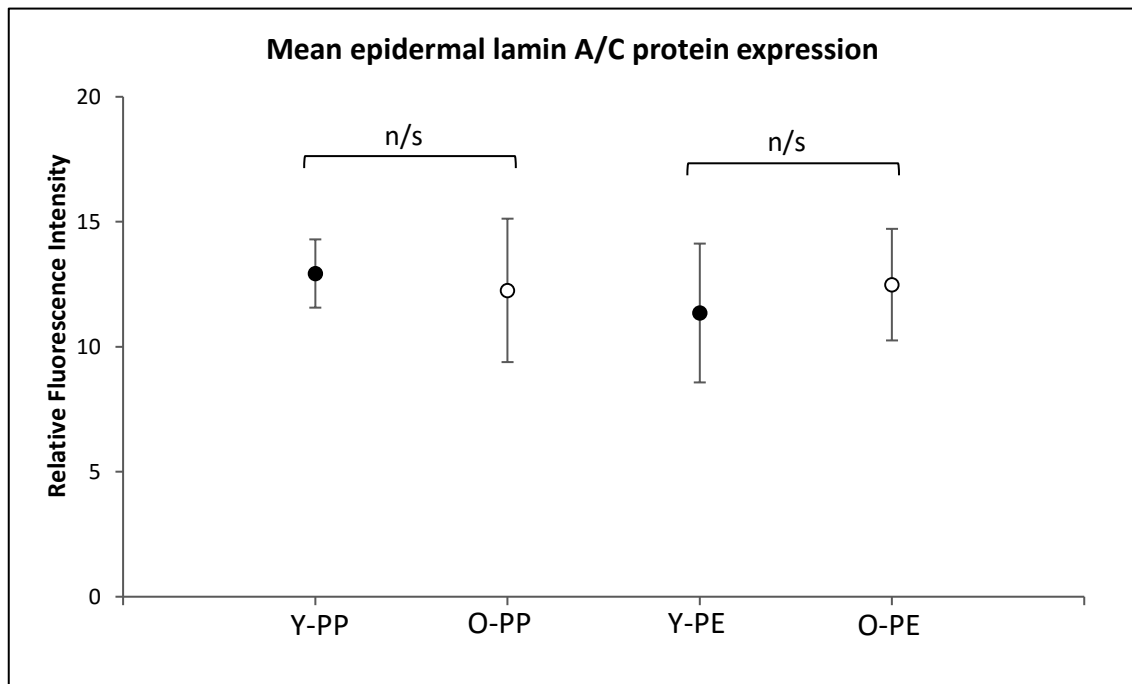
Figure 4.4.6: Mean expression levels of lamin A/C protein in the epidermis of PP and PE biopsies of young (Y) and old (O) subjects. Each individual data point represents the mean pixel intensity of all of the fields taken from forearm and buttock of young (21-22y) and old (60-65y) subjects. Y-PP= young photo-protected, O-PP= old photo-protected, Y-PE = young photo-exposed, O-PE= old photo-exposed. Error bars represent standard deviations calculated from the mean pixel intensity values for all of the fields imaged within each condition. Un-paired t-testing indicated that the change in expression with age in either condition was not significant.

As shown in figure 4.4.6, the mean level of lamin A/C expression showed a minor, non-significant decrease with age in the PP skin and a slightly more robust but still non-significant increase in the PE skin. Although the changes were not statistically significant, they did mirror the changes that were occurring at the mRNA level.
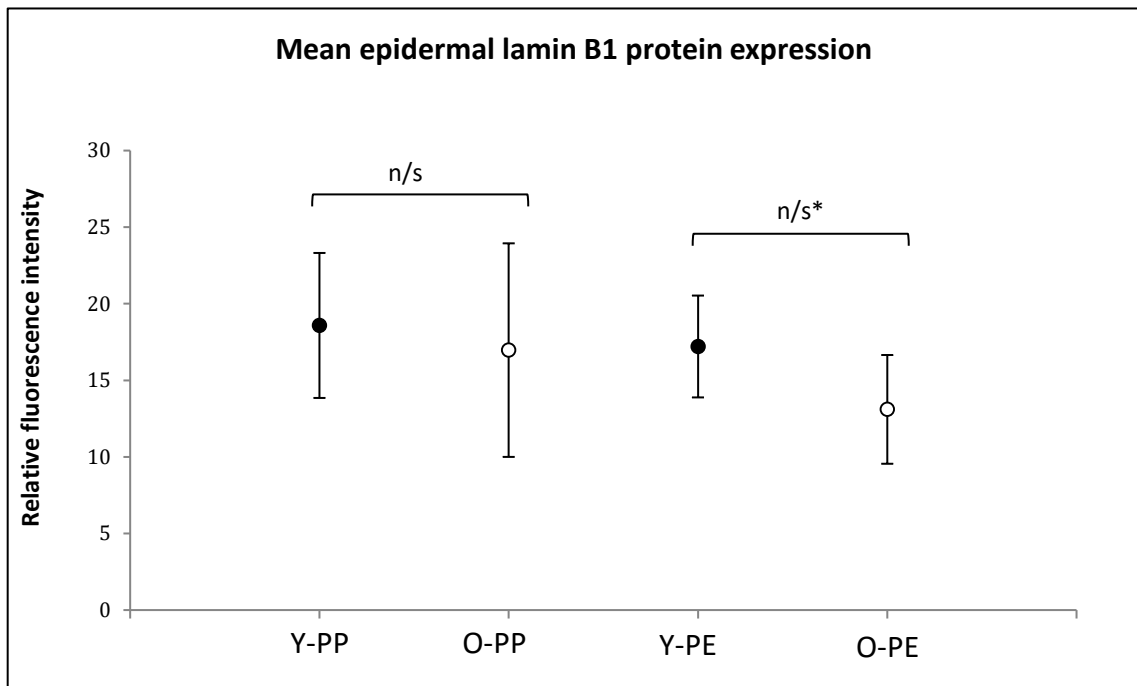
Figure 4.4.7: Mean expression levels of lamin B1 protein in the epidermis of PP and PE biopsies of young (Y) and old (O) subjects. Each individual data point represents the mean pixel intensity of all of the fields taken from forearm and buttock of young (21-22y) and old (60-65y) subjects. Y-PP= young photo-protected, O-PP= old photo-protected, Y-PE = young photo-exposed, O-PE= old photo-exposed. Error bars represent standard deviations calculated from the mean pixel intensity values for all of the fields imaged within each condition. Un-paired t-testing indicated that the change in expression with age in either condition was not significant. n/s* indicates that the difference was close to conventional significance.

As shown in figure 4.4.7, there was a small but non-significant decrease in lamin B1 expression with age in the PP skin whereas in the PE skin the decrease with age was greater and extremely close to being statistically significant. These changes match the decline in mRNA levels in lamin B1 with age but the decrease in lamin B1 was more marked in PE skin at the protein level whereas at the transcriptional level the decreases were more robust in the PP skin. The results of the fluorescence quantification experiments are summarised in tables 4.4.5 and 4.4.6.

Table 4.4.5 details mean expression values for lamin A/C and lamin B1. As laser settings were changed to optimise the imaging conditions for lamin A/C and lamin B1 separately, the levels of the two different proteins cannot be compared to one another. Comparisons of the same protein within the different biopsy samples however can be made, as settings were kept constant between samples stained for the same protein in order to detect age-related differences.

Table 4.4.5: Mean epidermal expression levels of lamin A/C and lamin B1 as calculated by the average fluorescence intensity in the different skin biopsy samples. Green fill indicates a decrease with age whereas orange fill indicates an increase with age. The numbers in parentheses show the relative increase or decrease with age.

Epidermal sample/ condition	Mean lamin A/C expression (accurate to 1 decimal place)	Mean lamin B1 expression (accurate to 1 decimal place)
PP- young (buttock)	12.9	18.6
PP- old (buttock)	12.3 (-0.7)	17.0 (-1.6)
PE- young (forearm)	11.4	17.2
PE- old (forearm)	12.5 (+1.1)	13.1 (-4.1)

Un-paired t-testing was used to assess the statistical significance of the differences in mean lamin A/C and mean lamin B1 epidermal protein levels between young and aged PP epidermis and then a separate test for young and aged PE epidermis. The p-values generated from these tests are summarised below in table 4.4.6

Table 4.4.6: Summary of the p-values generated from statistical testing. Green fill represents the most significant results from all of the analyses.

Epidermal sample/ condition	T-test p value: change in mean lamin A/C level.	T-test p value: change in mean lamin B1 level
PP- young (buttock)	PP young vs old	PP young vs old
PP- old (buttock)	0.45	0.65
PE- young (forearm)	PE young vs old	PE young vs old
PE- old (forearm)	0.45	0.06

As table 4.4.6 shows, most of the changes to lamin A/C and lamin B1 with age were not significant. The decrease observed in lamin B1 expression in the PE aged skin (p = 0.06) was extremely close to being significant by conventional standards ($p \leq 0.05$).

4.4.7 Discussion: Lamin B1 and lamin A/C show robust transcriptional changes with age which are mirrored to a lesser extent at the protein level.

The investigation of transcriptional and protein changes in lamin A/C and lamin B1 in PP and PE skin with age has uncovered several key trends. At the mRNA level lamin A/C expression decreased with intrinsic ageing and increased with photo-ageing whereas lamin B1 mRNA decreased in intrinsically aged and photo-aged skin. At the protein level these changes

followed the same pattern but from the quantification completed, appeared to be less robust. The only change validated at the protein level that approached statistical significance was the decrease in lamin B1 in PE skin.

Our mRNA data yielded robust results, but inconsistencies were present, such as the fact there was no significant differences in mRNA levels of *LMNA* in the separate PP epidermal and dermal compartments with age but robust *LMNA* mRNA decreases were observed in the PP FTS samples. One may expect to see at least minor changes in the separate epidermal and dermal compartments given that they constitute the majority of human skin (ie the FTS). However, the FTS samples contained adnexal skin structures such as hair follicles and sweat glands not present in the isolated epidermis and dermis and furthermore, the samples used in the microarrays were also prepared differently. The FTS samples yielded enough mRNA to avoid an RNA amplification step whereas the epidermis and dermis, when isolated by LCD, did not. These factors could be responsible for the inconsistencies seen because the presence of the cells in the adnexal structures and the differences in RNA processing could cause the RNA pool in the FTS to be different from the epidermis or dermis. The fact that the changes with age in both the PP and PE FTS were so marked gives significant evidence for changes to *LMNA* gene expression in human skin despite these inconsistencies in the separate epidermal and dermal compartments.

Lamins are intermediate filaments, and several studies using Fluorescence Recovery After Photobleaching (FRAP) analysis *in vitro* have indicated that they have a low protein turnover rate in interphase cells (Broers et al, 1999; Moir et al, 2000; Daigle et al, 2001). It is thought that turnover rates last several days (Daigle et al, 2001) and that A-type lamins form more stable, long-lived nuclear complexes than B-type (Moir et al, 2000). The possible weak correlation between mRNA and protein levels coupled with the high stability of lamin proteins seen at the cellular level may explain why there is a discrepancy between mRNA and protein changes, as un-stable mRNA's could represent more transient changes.

There were differences in the experimental design between the separate mRNA and protein measurement experiments. The subjects contributing to the mRNA studies were much greater in number, with at least 20 samples from different individuals used to generate the mean expression data within each age group. For the protein studies, only 3 subjects for each age group and condition were analysed and hence the probability of finding statistically significant changes are limited unless the change with age is extremely marked and the variation between subjects is minimal. Additionally, there was variation in the lamin A/C and lamin B1 protein levels between subjects, particularly in the PP aged skin. There will be considerable genetic variation in the subjects used for this study and furthermore, the ageing

process is associated with an increased heterogeneity in the efficiency of transcriptional and translational processes between subjects (Bahar et al, 2006). This could account for the increased diversity seen in the lamin B1 protein levels in PP aged epidermis. With more samples from different subjects and more specific measurements, it could be the case that the marginal changes seen with age could become more pronounced. For example, epidermal changes to lamin B1 appeared most pronounced in the basal layer, so scoring lamin B1 levels in the separate layers of the epidermis instead of calculating whole epidermal expression could reveal more significant changes with age. To increase the accuracy of determining differences to lamin expression in the different epidermal layers with age keratinocyte markers specific to the basal, spinous and granular layers could also be used to mark these specific epidermal cell populations.

The reduction in sample size and genetic variability in the intrinsically aged human skin used in this study may also explain why there was not a more robust trend between the significant decline in lamin B1 seen in the aged C57BL/6 mice epidermis in section 3.3.6 and the intrinsically aged human epidermis here.

Despite lack of clear change at the protein level, intrinsic and photo-ageing processes did appear to modulate *LMNA* and *LMNB1* transcription, with *LMNB1* mRNA levels decreasing during both intrinsic and photo-ageing. As alluded to earlier, B-type lamins have roles in cellular proliferation, chromosomal stability and their expression is modulated during senescence (Dreesen et al, 2013). In tissues that have been irradiated as a means of inducing premature ageing, lamin B1 mRNA and protein levels decline due to the induction of tumour suppressor pathways p53 and pRb as a result of cellular DNA damage. It is widely accepted that DNA damage accumulates in intrinsically aged mammalian tissues (Wang et al, 2009; Jeyapalan et al, 2007) and although not systematically proven to our knowledge, it is likely to also occur in ageing human epidermis. Aged human epidermis has less cellular proliferation than young (Gilhar et al, 2004), so the decline in *LMNB1* mRNA with age we observed may represent slowed cellular proliferation as a result of increasing levels of DNA damage, preventing cell cycle progression (Manju et al, 2006).

Furthermore, p53 and pRb are key modulators of DNA Damage response and cell cycle arrest pathways (Li et al, 2013) and direct stimulation of human cells through either p53 or pRb signalling has been shown to trigger lamin B1 loss and cellular senescence (Freund et al, 2012). The decline in *LMNB1* transcription here could therefore represent increased senescence due to increased DNA damage in the ageing tissues through p53 and pRb dependent mechanisms. Further studies looking at DNA damage, cell proliferation, p53 and pRb levels in young vs aged keratinocytes would contribute more evidence towards this hypothesis.

Intrinsic ageing also reduced *LMNA* transcription, which could represent epidermal atrophy, leading to fewer cells within the skin overall and therefore a depleted mRNA pool in the aged samples.

UVR (Ultra-Violet Rays) are potent nucleotide damaging agents and a plethora of studies have implicated increased UVR, found to penetrate the skin with sunlight exposure, as inducers of cellular damage and ageing (Panich et al, 2016). It is commonly accepted that intrinsic and extrinsic ageing have both distinct and common patho-mechanisms (Gilchrest, B.A. 2013) and reduced genomic stability with age is common to both. Telomere attrition occurs due to multiple rounds of cell division in intrinsic ageing. Compounded with this in photo-ageing is the induction of DNA breaks, lesions and other forms of damage due to ionising radiation (Gilchrest et al, 2009). Genomic damage induces p53 signalling (Reinhardt and Schumacher, 2012) so the fact that lamin B1 decline was more marked in the photo-exposed, aged epidermis could again potentially be indicative of increased DNA damage in this compartment causing increased p53 or pRb signalling which are known to negatively impact *LMNB1* mRNA stability (Freund et al, 2012).

Our lamin A/C data in photo-aged skin matches previous studies, who have shown increases in *LMNA* mRNA and lamin A/C protein in skin from aged individuals (Marji et al, 2010). Unlike our study, this study data was generated from skin biopsies of male and female photo-protected and photo-exposed skin pooled together, with several fewer samples used. Observed epidermal cellular increases in A-type lamin expression in PE skin with age may occur for several reasons. Lamin A is important in cellular DNA damage response mechanisms, where it stabilizes the response protein 53BP1, preventing abnormal localisation and proteasomal degradation (Redwood et al, 2011). Futhermore, the lamina also maintains the positional stability of reparative foci (Mahen et al, 2013) and it is believed to be important in replication fork stability during repair of DNA through non-homologous end joining (Singh et al, 2013). As mentioned previously, it also plays roles in cellular tolerance to ROS, and without proper levels of lamin A, cells undergo premature senescence under oxidative stress. Photo-ageing is the result of exposure to UVR, which induces both DNA damage and increased cellular ROS (Naylor et al, 2011). Increased *LMNA* transcription and lamin A/C protein expression during photo-ageing may therefore be representative of increased cellular defence mechanisms, in order to improve cellular tolerance to ROS and also to maintain DNA repair efficiency.

Aged skin is associated with biomechanical changes (Simpson et al, 2011) and skin stiffness is shown to increase in both intrinsically and extrinsically aged tissues (Smalls et al, 2006). Skin is subject to mechanical stress throughout our lifespan and cellular lamin A protein levels have been shown to positively correlate with the levels of stiffness and mechanical stress

load exhibited by various tissues in mouse (Swift et al, 2013). The increase in *LMNA* mRNA and lamin A/C protein in photo-aged skin could therefore also possibly represent a change in the cellular mechanics of epidermal keratinocytes with age, where tissue stiffening could induce *LMNA* gene expression and protein production in response to this biomechanical change.

The Jol2 antibody used in these studies is able to detect lamin A, lamin C and progerin (Shackleton et al, 2005) so this study did not show specifically whether increased lamin A/C was due to specific increases in one of these 3 proteins. Future studies using more specific antibodies would allow us to confirm whether epidermal and dermal increases in lamin A do mark hypothesized increases in tissue stiffness and furthermore, an antibody specific to progerin would allow us to uncover if and where this protein accumulates in intrinsically aged and photo-aged skin.

4.5 A transcriptomic and proteomic assessment of YAP1 during intrinsic and photo-ageing in human skin.

4.5.1 Objectives of this section

The studies covered in section 1.19 of the main introduction to this thesis indicate that the majority of work concerning the role of YAP1 in skin biology has focused on how the Hippo pathway regulates mouse skin development and homeostasis. However, the potential for the Hippo Pathway to be modulated by the ageing process in the skin of humans has not been studied in detail.

Our previous data shows reduced epidermal proliferation in aged C57BL/6 mice which appears to manifest as epidermal thinning. Furthermore, we have observed flattening of basal keratinocytes and a lower level of loricrin expression in the outermost epidermal layers of aged skin. Interestingly many of these observations, which together imply that epidermal cellular proliferation and turnover is lost with age, mimic the phenotype Schlegelmilch et al (2011) observed in their epidermal-specific YAP1 knock out mice.

In our studies looking at YAP1 protein in mouse epidermis using fluorescent immunohistochemistry, we have observed a significant increase in nuclear YAP1 levels with age in young (3 month) vs old (30 month) mice. These observations implicate that YAP1 could be modulated by the ageing process in mammalian epidermis. The objectives of the data presented here regarding the Hippo pathway and ageing human skin were therefore to:

1. Identify transcriptional changes to *YAP1* with age in epidermal and dermal compartments along with full thickness skin (FTS) using microarrays and furthermore determine any differences between intrinsically aged and photo-aged human skin.

2. To our knowledge, there is only one published report showing the organisation of YAP1 in human skin (As a publication from Elbediwy et al, 2016 used information from the Human Protein Atlas this is technically the only source). Furthermore, any potential change to the amount of YAP1 protein during intrinsic and photo-ageing is not known. Fluorescent immunohistochemistry was therefore used to quantify the level of YAP1 protein in young and aged epidermis

3. YAP1 transcription factor activity is highly dependent on its sub-cellular localisation (see section 1.19-1.22 of thesis introduction) and in order to in induce transcription of its target genes, it must locate to the nucleus. We therefore quantified changes to nuclear YAP1 levels, by assessing if there was a change in the nuclear to cytoplasmic

ratio- N:C of YAP1 in young vs aged tissues. Like in our mouse studies of epidermal YAP1, an increase in the nuclear:cytoplasmic ratio would indicate a higher level of nuclear YAP1 and potentially increased activation of YAP1 target genes.

4.5.2   Identification of *YAP1* transcriptional changes with age

In order to fulfil the aims of objective 1, changes in transcriptional activity of *YAP1* was assessed in female subjects at ages 20, 30, 40, 50, 60 and 70. The Affymetrix U219 array plate had 8 different probe sets designed to target *YAP1* mRNA transcripts and the *YAP1* gene is known to produce 15 mRNA variants (10 alternatively spliced and 5 un-spliced). 11 mRNA variants putatively encode proteins (source- footnote 1), indicating that a high number of cellular transcripts are able to produce functional proteins. Plots of the change in mean mRNA levels for each probe-set with age in the different skin compartments are shown in figures 4.5.1 and 4.5.2, where a formatting system (each individual probe set is colour coded) has been used to depict statistically significant changes. The level of signal expression for each probe set within each age group indicates the mean level of mRNA that bound to that probe set from all of the subjects.

There was a clear trend in the mean expression levels of the 8 different probe sets across the skin compartments. The probe sets 11717920_a_at (red), 11717921_x_at (green), 11717923_s_at (yellow) and 11740548_a_at (grey) were expressed at high levels in all compartments and showed the most dramatic changes in mean expression levels with age. 11717922_a_at (blue), 11717924_a_at (purple), 11717925_s_at (black) and 11746496_a_at (brown), were expressed at much lower levels and showed minor differences in their change of expression with age. It is likely that the design of the latter 4 probes did not allow optimal mRNA binding, given their consistently low expression levels in all compartments.

Although it is possible that these probe-sets represented low, steady-state mRNA levels of some transcripts over time, the objective was to identify the probe sets that did change during ageing, so they did not form part of further analyses. To depict this on each plot a threshold line, shown by a black double-ended arrow, has marked the boundary of the lowest expression level considered to produce significant changes with age. In further descriptions the 4 probe sets that had mean expression levels above the threshold (11717920_a_at (red), 11717921_x_at (green), 11717923_s_at (yellow) and 11740548_a_at (grey)) will be described as "*AT*-probe sets" ie above-threshold probe-sets.

Footnote 1: https://www.ncbi.nlm.nih.gov/ieb/research/acembly/

YAP1 mRNA expression: Dermal and Epidermal compartments
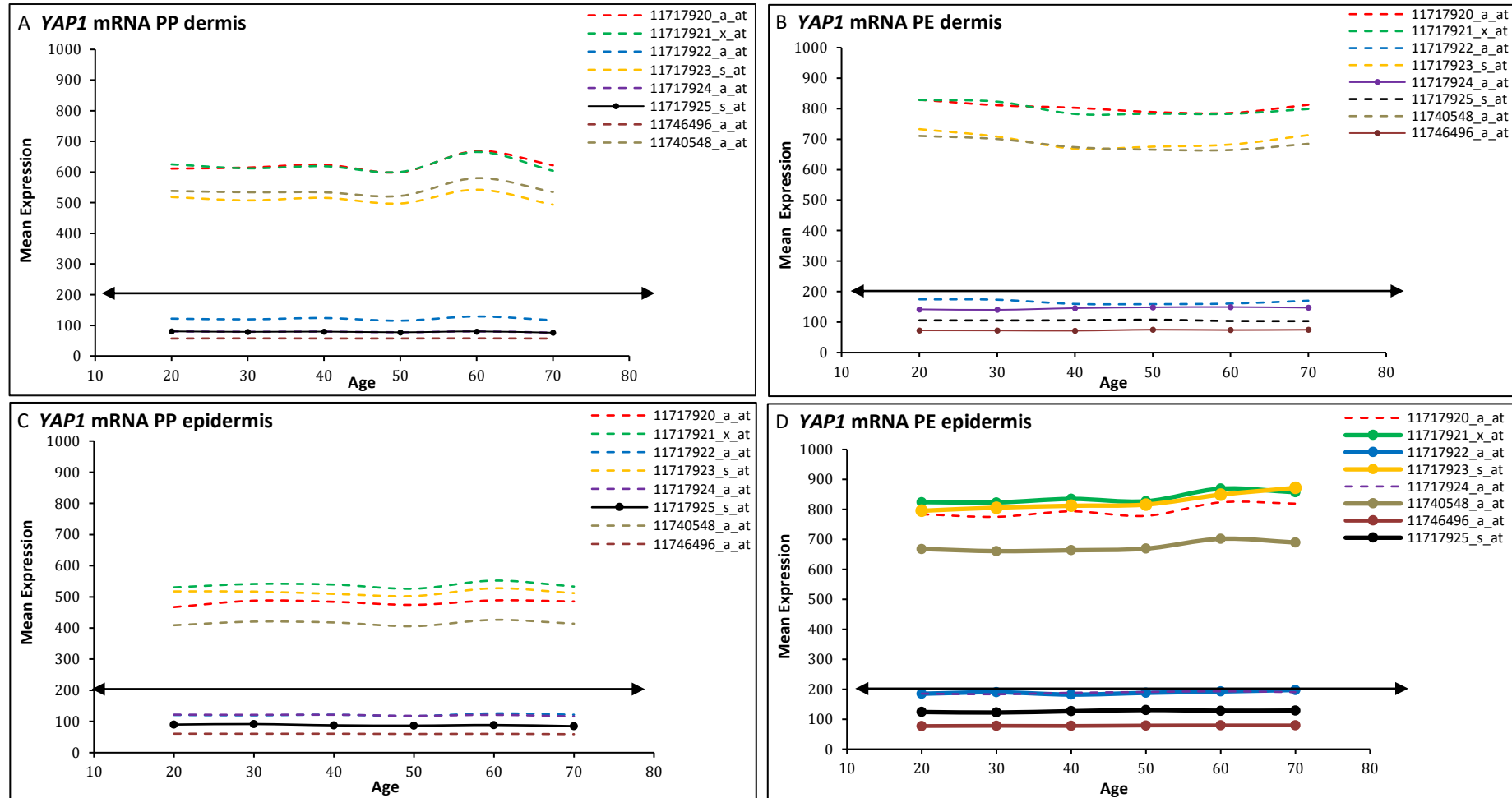
Figure 4.5.1: Microarray analysis of YAP1 in PP (A,C) and PE (B,D) isolated dermis and epidermis of individuals aged 20, 30, 40, 50, 60 and 70. Plots A-D show the change in mean signal expression of mRNA levels from the 2nd to 7th decade. The legend in the right hand corner of each plot depicts the colour and format applied to each probe set. Thin dotted lines show probe sets that did not significantly change in expression level with age. Thin uniform lines show probes that significantly change with age ($p \leq 0.05$). Thick uniform lines show probe sets that had a highly significant change with age ($p \leq 0.05 + q \leq 0.05$). Black double ended arrows indicate the threshold of mean expression considered to be above background levels (≥ 200).
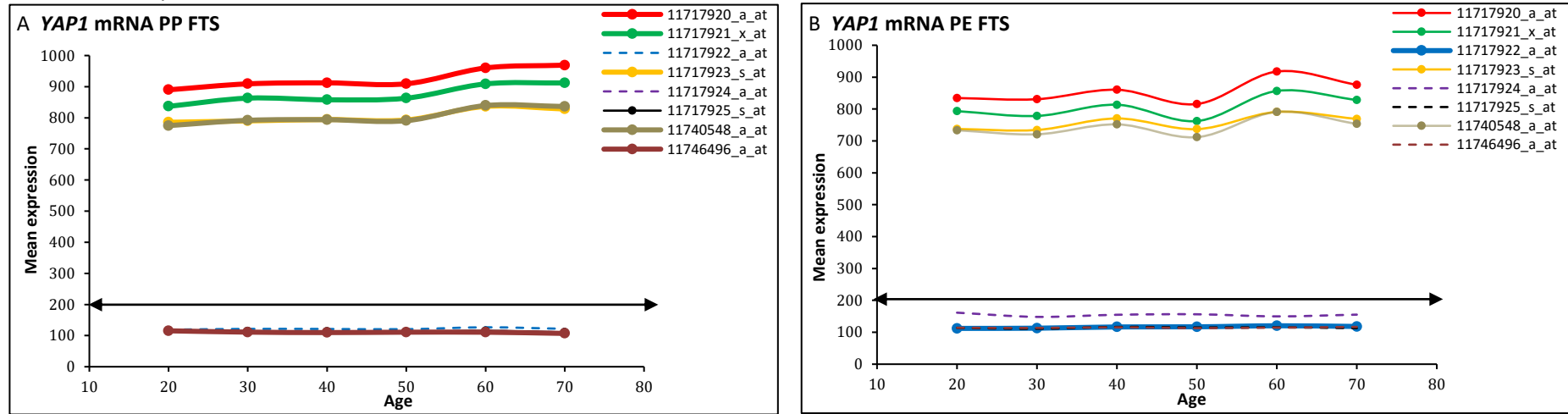
Figure 4.5.2: Microarray analysis of _YAP1_ in PP (A) and PE (B) Full thickness skin of individuals aged 20, 30, 40, 50, 60 and 70. Plots A and B show the change in mean signal expression of mRNA levels from the 2nd to 7th decade. The legend in the right hand corner of each plot depicts the colour and format applied to each probe set. Thin dotted lines show probe sets that did not significantly change in expression level with age. Thin uniform lines show probes that significantly change with age (p ≤ 0.05). Thick uniform lines show probe sets that had a highly significant change with age (p ≤ 0.05 + q ≤ 0.05). In (A) background level probes 11717925_s_at (black),11746496_a_at (brown) ,11717922_a_at (blue) and 11717924_a_at (purple) show overlap in their mean expression levels thus 11717925_s_at (black) and 11717924_a_at (purple) are obscured from view. In (B), 11717925_s_at (black) and 11746496_a_at (brown) also overlap. Black double ended arrows indicate the threshold of mean expression considered to be above background levels (≥ 200).

4.5.3   Changes to YAP1 mRNA with age as shown by 4 probe-sets with high mRNA binding

The probe sets in figure 4.5.1 A and 4.5.1 B, which document the change in mRNA levels in the isolated PP and PE dermis, are similarly organised and show little statistically significant change to *YAP1* levels with age. In both PP and PE skin, the *AT*-probe sets clustered together and showed levels of mRNA expression at ~500-700 units (PP skin) and ~650-850 units (PE skin). Figure 4.5.1 C and 4.5.1 D show the *YAP1* mRNA levels of the probe sets in the epidermal compartment during intrinsic (C) and photo-ageing 1D). In the *AT*-probe sets, mean expression was generally higher in the PE epidermis (~650-850 units), compared to the PP epidermis (~400-600).

Figure 4.5.2 A and 4.5.2 B show changes to *YAP1* mRNA in intrinsically aged (A) and photo-aged (B) FTS. The mean expression levels were slightly greater (~700-1000 units) for *AT*-probe sets in the PP FTS (A) compared to the separate epidermis (C: ~400-600 units) and dermis (A: ~500-700 units). In the PE skin a similar trend in the organisation of the probes was observed, with *AT*-probe-sets also having a higher level of expression (~700-900 units) in the FTS compared to the epidermis (D: ~650-850 units) and dermis (B: ~650-850 units).

4.5.4   YAP1 mRNA levels increase with intrinsic and photo-ageing.

Taking information from the *AT*-probe sets only, significant changes to mRNA levels with age were assessed using the P and Q values generated from Pearson's Rank Correlation tests completed on the data. The most robust changes were identified as those that had both significant P and Q values. The number of *AT*-probes sets that significantly changed expression levels with age provides a parameter of the extent of significant *YAP1* transcriptional changes, with greater numbers of significantly changing probe sets indicating a more robust change with age. These values are summarised in table 4.5.1 below.

Table 4.5.1: Details of statistically significant changes to *YAP1* mRNA probe sets with age within the different compartments of PP and PE skin. NP= no probe sets. The PE and PP compartments that showed the most significant changes are highlighted in orange (PE skin) and blue (PP skin)

Skin sample/condition	Signal expression range of statistically significant probes (to nearest 100)	Number of upregulated (+) or downregulated (-) probes statistically correlating with age with p ≤ 0.05. (numbers in parentheses indicate the number of these probes that also had q ≤ 0.05)
Photo-protected (PP) dermis	NP	NP
Photo-exposed (PE) dermis	NP	NP
Photo-protected (PP) epidermis	NP	NP
Photo-exposed (PE) epidermis	650-900	**+3** (1)
Photo-protected FTS (PP)	750-1000	**+4** (4)
Photo-exposed FTS (PE)	700-900	**+4** (0)

The FTS showed the most robust changes with all 4 *AT*-probes in both the PP and PE tissue increasing significantly in expression with age. This was particularly marked in the PP skin, where all 4 probes had both significant P and Q values. The only isolated compartment showing probes that statistically significantly changed their expression with age was the PE epidermis. In this compartment 3 probe-sets significantly increased their mRNA expression levels with age with one of these probe sets also having a significant Q-value. Taking all the data together, we concluded that YAP1 mRNA levels increased in the skin during both intrinsic and photo-ageing.

4.5.5   YAP1 protein expression in human skin as analysed by fluorescent immunohistochemistry.

Aside from fulfilling objective 2 (see 4.5.1-intro), changes in YAP1 mRNA were subsequently validated at the protein level for several reasons. Although the majority of the known mRNA transcripts transcribed from the *YAP1* gene yield functional proteins, there are still a number that do not. Microarray analysis quantifies all of the different mRNA variants together, and thus the proportion of protein-coding and non-protein coding transcripts that bound our microarray chips was not known. This introduces the possibility that the transcriptional changes we observed may not manifest to the same extent at the protein level.

Furthermore, the mRNA data for the PP skin showed a discrepancy given that the separate epidermal and dermal compartments showed no significant mRNA changes with age whereas there were highly significant changes present in the FTS. This suggests that the mRNA pools for the separate epidermal and dermal compartments were markedly different to the FTS although the epidermis and dermis constitutes part of the FTS. Finally, as objective 3 describes,

YAP1 sub-cellular localisation also contributes to its activity, and this information cannot be provided from mRNA data alone. The levels of YAP1 in human epidermis were therefore analysed using fluorescent immunohistochemistry (F-IHC) on human skin biopsies taken from young and old female subjects

The epidermis was chosen as the compartment to be analysed due to the fact that it is the most cell-rich compartment in the skin and the PE epidermal compartment had shown significant changes to YAP1 at the mRNA level with age. Furthermore, alluded to in the introduction to this thesis, previous publications have implicated the importance of YAP1 in epidermal biology. Confocal laser scanning microscopy (CLSM) presents a powerful tool to capture image data in both the X, Y and Z- dimensions. This tool was exploited to capture Z-stack images of immunofluorescence staining on human skin sections which formed the basis for analyses of both absolute levels of epidermal YAP1 and its localisation in both the nucleus and cytoplasm expressed as the nuclear to cytoplasmic ratio: N:C.

As shown in figure 4.5.3, which is a representative image of epidermal YAP1 staining taken from a 21 year old arm biopsy, both the levels of expression of YAP and its sub-cellular localisation were different in the various epidermal layers of skin. In the basal layer (bl-C and I), which consists primarily of un-differentiated, highly-proliferative stem-cells and progenitor cells, high levels of YAP were present as shown by the intense staining in this region (outlined with fine, dotted line, I). The localisation of YAP1 in the basal layer varied, with some cells showing YAP1 retained in the cytoplasm (green arrowheads, I) and others showing nuclear YAP1 (white arrowheads, I). In the supra-basal layers, YAP1 was predominantly retained in the cytoplasm. In addition, YAP1 expression levels were lower than in the basal layer, with the overall staining being less intense. Within the granular layer, where cells become flattened and lose their columnar/cuboidal morphology, YAP1 expression was high in the nuclei of the flattened cells, shown by the intense YAP1 staining overlying with the DAPI staining (white arrowheads, F). This was the most intense nuclear staining seen in all the layers of the skin, indicating that YAP1 becomes concentrated in the nuclei of these cells along with the cells of the basal layer.

The organisation of staining that was observed in human skin was consistent with those found online at the Human Protein Atlas. Like the staining here, these records show high YAP1 expression and nuclear localisation in the basal layer of the skin, cytoplasmic staining in the supra-basal layers and intense nuclear YAP staining in some cells of the granular layer. Given that the staining is in agreement to previous records, and the antibody specificity had already been confirmed using immunofluorescence and western blot (section 3.5.2 of this thesis) it was assumed that the staining observed was specific for YAP1 in human epidermis.
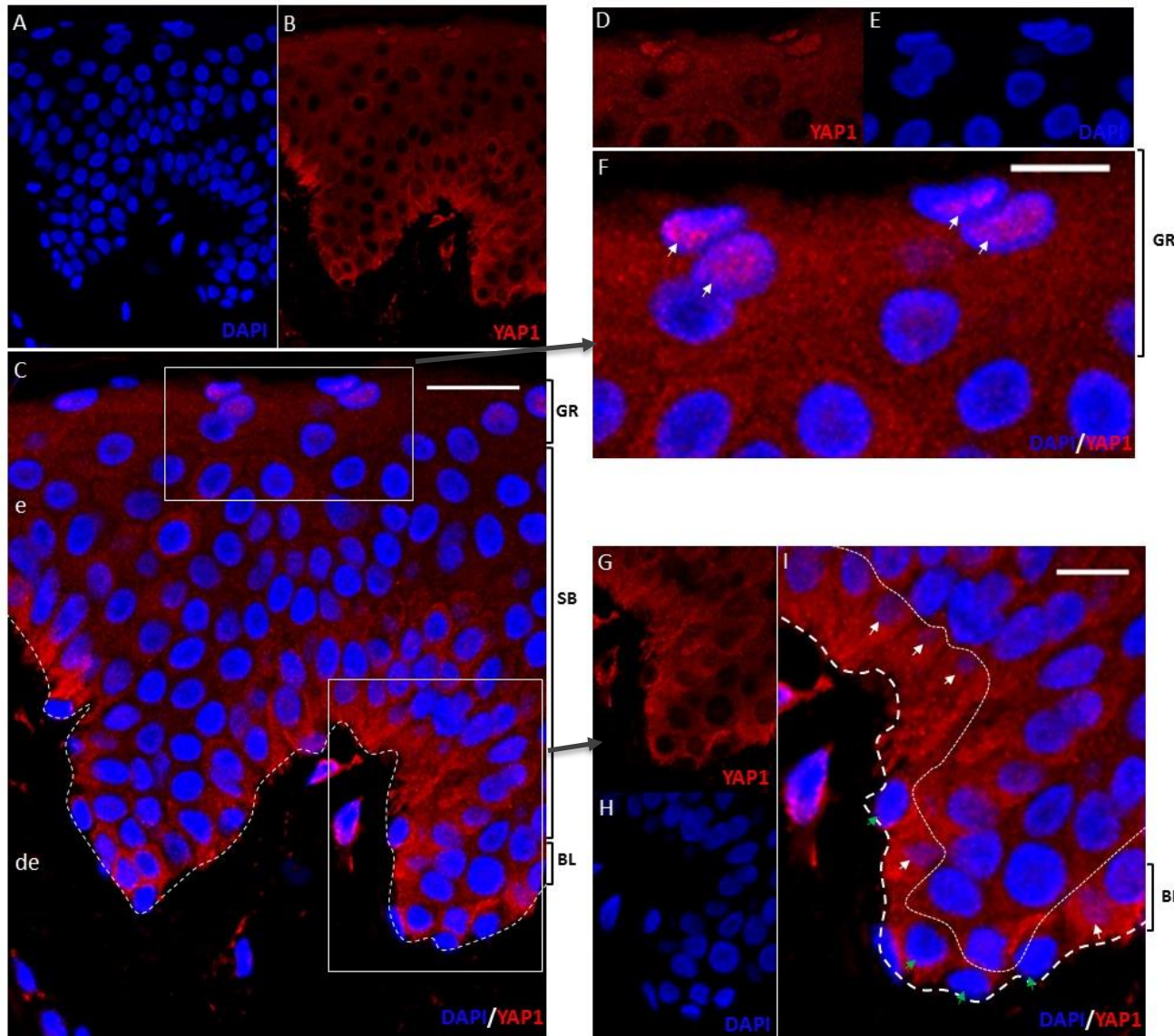
Figure 4.5.3: Overview of YAP1 immunofluorescence staining with Alexa 568 secondary antibody (red) with DAPI nuclear counterstain (blue) in young arm epidermis (21y) showing single channel images (A= DAPI, B=YAP1) and a merged image (C). BL= basal layer, SB= supra-basal layers, GR= granular layer. Coarse dotted line= dermal-epidermal junction. e= epidermis, de= dermis, scale bar= 20 μm.

D,E,F: Magnified inset showing the granular layer (GR). Single channel images (D=YAP1, E=DAPI). Merged image (F). YAP1 positive nuclei are marked with white arrowheads in F. Scale bar= 10 μm.

G,H,I: Magnified inset showing the basal epidermal layer (BL). Single channel (G= YAP1, H= DAPI). Merged image (I). The coarse dotted line indicates the DEJ and the fine dotted line outlines the region in the basal layer where strong YAP1 staining was present. Basal epidermal cells with nuclear YAP1 are marked with arrowheads, cytoplasmic YAP1, green arrowheads. Scale bar= 10 μm.

Figure 4.5.4 shows representative images of YAP1 staining in the epidermis and dermis of PP and PE young (21y) and old (64y) subjects. The epidermis of young arm and young buttock samples showed the same YAP1 organisation as seen in figure 4.5.3, with high levels of YAP1 in the basal layer with some of the YAP1 signal being localised to basal cell nuclei (white arrowheads, A, B). Lower YAP1 levels were retained in the cytoplasm in the supra-basal layers (green arrowheads, A,B) and intense nuclear YAP1 staining was detected in some of the flattened cells in the granular layer (white-arrowheads in upper epidermis, A,B).

In the old arm and old buttock samples the expression pattern of YAP1 was similar to younger tissues in the basal layer but in the supra-basal and granular layers there were considerably fewer cells, which manifested as epidermal thinning. Although fewer cells were present, the organisation of YAP1 in the supra-basal layers was generally uniform across the two different tissue biopsy sites and age groups with most cells retaining the transcription factor within the cytoplasm at relatively low levels compared to the basal layer. Interestingly, in the young buttock samples there were some instances of intense cytoplasmic staining in a cluster of cells in the supra-basal layers (white arrows, A). This area could represent part of a hair follicle or perhaps an area of wound healing, which is known to be associated with high levels of cellular YAP (Lee et al, 2014). The organisation of YAP1 in the granular layer was similar in all tissue samples with intense punctuate YAP1 nuclear staining present in some of the flattened nuclei in the outermost 2 layers of the epidermis (white arrowheads, upper epidermis C, D).
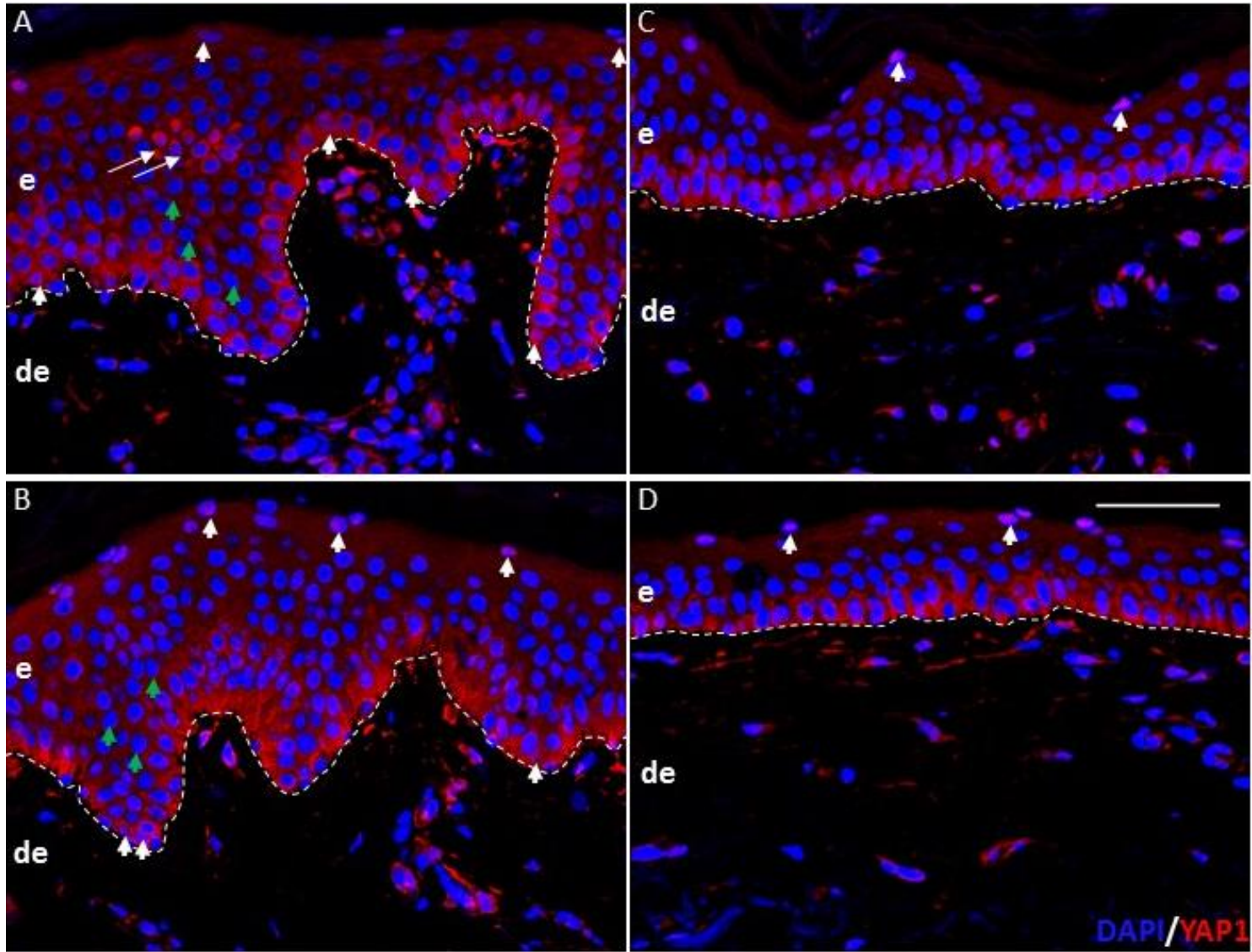
Figure 4.5.4: Representative low power images of PP and PE young (21y) and old (64y) epidermis and dermis stained with an Alexa 568-conjugated YAP1 antibody with DAPI nuclear counterstain. Skin was imaged on using CSLM using a 40x objective lens. A= young PP, B= young PE, C= old PP, D= old PE e= epidermis, de=dermis, scale bar= 50 μm. White arrowheads indicate examples of cells with high nuclear YAP1 and green arrowheads indicate examples of with low nuclear YAP1. Long arrows in A identify intense staining in suprabasal layers

4.5.6 YAP1 protein changes with age mirror mRNA changes.

The mean expression levels in the PP and PE epidermis of young (n=3) and old (n=3) subjects was quantified in Image J using 3 representative fields taken from the arm (PE) and buttock (PP) of each subject. Details of the analyses to generate mean levels of fluorescence intensity (FI) can be found in section 2.8.8-materials and methods. The data was collated to create figure 4.5.5, which shows the values of the mean epidermal protein levels of YAP1 for both PP and PE young and old skin.
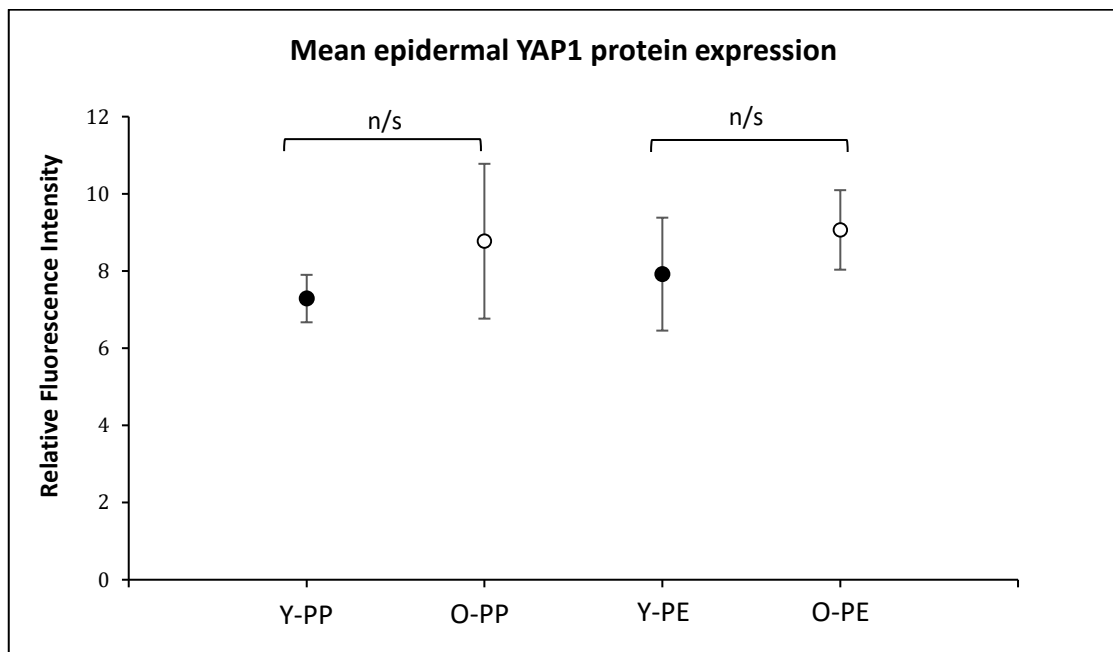
Figure 4.5.5: Mean expression levels of YAP1 protein in the epidermis of PP and PE biopsies of young (Y) and old (O) subjects. Each individual data point represents the mean pixel intensity of all of the fields taken from forearm and buttock of young (21-22y) and old (60-65y) subjects. Y-PP= young photo-protected, O-PP= old photo-protected, Y-PE = young photo-exposed, O-PE= old photo-exposed. Error bars represent standard deviations calculated from the mean pixel intensity values for all of the fields imaged within each condition. n/s=non-significant change.

As figure 4.5.5 shows, the mean expression levels of YAP1 increased with age in the PP and PE epidermis. Un-paired t-testing was used to assess the statistical significance of the difference between the mean expression of YAP1 between young and aged PP epidermis and as a separate analysis, young and aged PE epidermis. These tests showed that neither the increase observed in YAP1 levels in the epidermis of PP aged skin or PP aged skin was statistically significant, but the YAP1 increase with age was slightly more dramatic in the PE epidermis- p=0.15 compared to the PP epidermis–p=0.26.

4.5.7 YAP1 shifts to the nucleus in aged epidermis

As mentioned previously, the localisation of YAP1 determines its activity, with a nuclear localisation indicating active YAP1 that is able to bind its target genes and cytoplasmic YAP1 indicating it is transcriptionally inactive. Assessing the levels of nuclear YAP1 in PP and PE aged skin would therefore give a simple indication of potential changes to YAP1 activity with age during intrinsic and photo-ageing. The images which were previously used to generate the mean expression data shown in figure 4.5.5, were also used to calculate the Nuclear:Cytoplasmic ratio- N:C of YAP1 in the epidermis of the PP and PE young and old skin biopsies. The details of how binary masking was used to generate independent quantifications of nuclear and cytoplasmic levels of YAP1 for each image in order to calculate the N:C is detailed in materials and methods section 2.3.8 (same method used in both mouse and human skin). Figure 4.5.6 shows the results of these analyses.

In the epidermal regions of both PP and PE young and old skin the N:C ratio of YAP1 was below 1, indicating that regardless of age or biopsy site, there was more YAP1 present in the cytoplasm when all the cells of the epidermis are considered together. There was almost no difference between the N:C value in the PP young compared to the PP old skin. The difference between the PE young and old skin N:C values was greater (details- table 4.5.2).

Un-paired t-testing was used to assess the statistical significance of the difference between the mean N:C ratio of YAP1 between young and aged PP epidermis and as a separate analysis, young and aged PE epidermis. In the young vs old PP epidermis, this difference was not statistically significant (p=0.82). The difference between the N:C ratio of young and old PE epidermal tissue was much greater, and this was reflected in the fact that the p value generated in this test was much smaller: p=0.09 and was almost statistically significant.
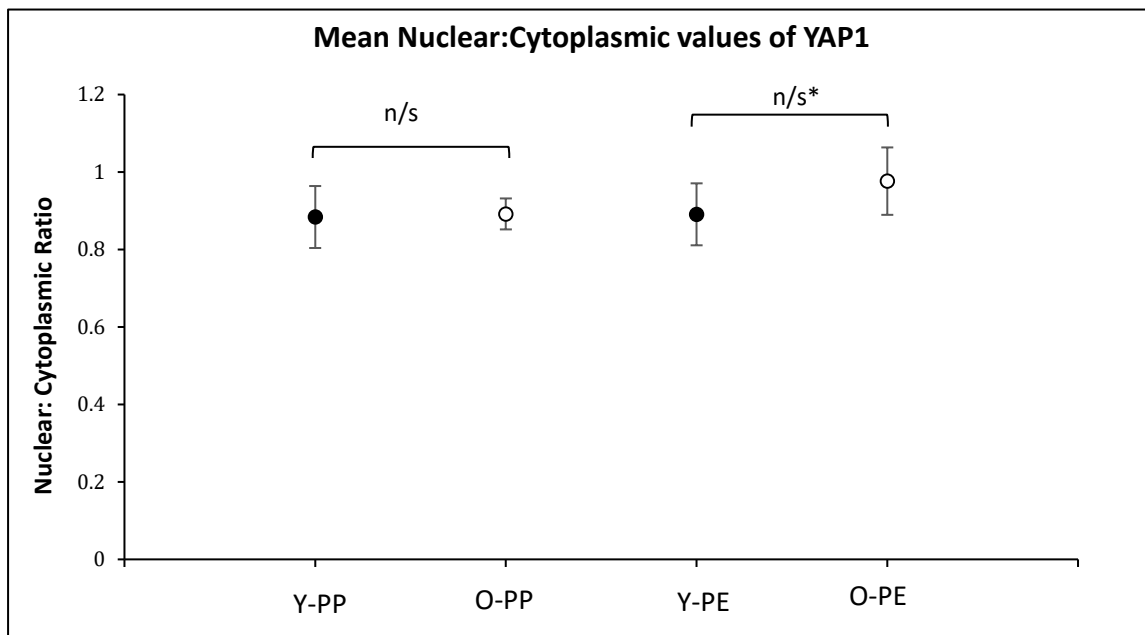
Figure 4.5.6: Mean N:C values of YAP1 protein in the epidermis of PP and PE biopsies of young (Y) and old (O) subjects. Each individual data point represents the mean N:C of all of the fields taken from forearm and buttock of young and old subjects. Y-PP= young photo-protected, O-PP= old photo-protected, Y-PE = young photo-exposed, O-PE= old photo-exposed. Error bars represent standard deviations calculated from the mean N:C values for all of the fields imaged within each condition. n/s=non-significant difference. n/s*= difference was close to conventional significance.

The analysis of mean epidermal YAP1 and the mean N:C in the epidermal compartments of both young and old PP and PE skin is summarised in 4.5.2 and 4.5.3 below which show that YAP1 protein level increased in both intrinsically aged and photo-aged epidermis but only photo-ageing appeared to cause movement on YAP1 into the nucleus (although not statistically significant).

Table 4.5.2: Mean epidermal expression levels of YAP1 and the mean nuclear to cytoplasmic ratio as calculated by the average fluorescence intensity in the different skin biopsy samples. Green fill indicates a decrease with age whereas orange fill indicates an increase with age. The numbers in brackets show the relative increase or decrease with age.

Epidermal sample/ condition	Mean YAP1 level- (fluorescence intensity)	Mean N:C of YAP1
PP- young (buttock)	7.29	0.88
PP- old (buttock)	8.77 (+1.48)	0.89 (+0.01)
PE- young (forearm)	7.92	0.89
PE- old (forearm)	9.06 (+1.14)	0.98 (+0.09)

Table 4.5.3: Summary of the p-values generated from statistical testing. Green fill represents the most significant results from all of the analyses.* Difference in mean expression level between PE young and old was smaller than PP young and old but there was less variation in mean expression in the PE old epidermis leading to a more significant result through statistical testing.

Epidermal sample/ condition	T-test p value: change in mean YAP1 level.	T-test p value: change in N:C value
PP- young (buttock)	PP young vs old	PP young vs old
PP- old (buttock)	0.26	0.82
PE- young (forearm)	PE young vs old*	PE young vs old
PE- old (forearm)	0.15	0.09

4.5.8   Discussion part 1: *YAP1* mRNA and protein increases during photo-ageing

The microarray data for YAP1 shows that there was a general trend for YAP1 mRNA levels to increase in the skin regardless of whether photo-exposure had occurred or not. By considering the number of probe sets that significantly changed in expression with age, how significant these changes were according to their P and Q values and the mean signal of these probe sets, the degree of change to mRNA levels in the different skin compartments (epidermis and dermis) as well as full thickness skin was assessed. The most significant increases in YAP1 mRNA were observed in the photo-exposed epidermal and full thickness compartments.

Each of the 8 different probe sets targeting *YAP1* mRNA in the Affymetrix Human U219 Array is formed of 11 short, 25-nucleotide long (25mer) sequences, with each probe set having sequences designed to target different areas of the *YAP1* mRNA transcripts. Online transcriptome resources such as ENSEMBL, NCBI's GenBank and NCBI's UniGene are used in probe design as these platforms provide large and regularly-updated bodies of information on different nucleotide sequences making up transcripts for a given gene. Thorough probe-set design is an important pre-requisite for good quality microarray results and thus using information from both a reputable and up-to-date resource is crucial (Liu et al, 2010). The quality of the Affymetrix probe design can be verified at their online analysis centre (https://www.affymetrix.com/analysis/netaffx/fullrecord), where probes are assigned an "Annotation Grade" of A-E indicating the quality of the probe design. "A" probes are those that match online transcript data (In this case taken from ENSEMBL and NCBI online databases) perfectly and are therefore considered to be of very high quality. All of the 8 probe sets that were designed to target the YAP1 gene had the highest quality "A" annotation grade assigned to them.

Despite this, it seemed that transcripts bound more efficiently to 4 probe sets out of the 8 used on the microarray chip. This suggests that use of online transcript data, which is a

common information source for probe-set design, should be coupled with empirical records of microarray experiments that detail the quality of mRNA binding to the probes. This would better inform the user of probe-sets showing robust changes in previous experiments. These records are widely available online at resources such as ArrayExpress: (www.ebi.ac.uk/arrayexpress)

Alternatively, the low levels of expression observed in some probe sets and not others may occur for biological reasons. YAP1 is also known to be subject to alternative splicing and has 8 different known protein isoforms (Sudol, M. 2013). It might therefore be the case that some of these isoforms are expressed at very low levels in the skin and are not modulated by the ageing process, meaning fewer of their encoding mRNA transcripts are present or showing modulation with age. This could explain the clear differential in the high expression levels in 4 of the probe sets and low expression levels in the other 4 remaining probe sets. In order to explore this further sequence alignment analyses could be carried out where sequences from each of the different 8 probe sets could be aligned with the most up-to-date versions of the different mRNA transcript variants to determine if the highly expressed probes aligned with transcripts coding for certain isoforms.

4.5.9 Discussion part 2: YAP1 protein changes with age are less marked that mRNA changes

The analyses indicated that the changes observed at the mRNA level were similar, but less marked at the protein level, and implicated photo-ageing as the only condition where both YAP1 level increases and nuclear localisation increases were borderline statistically significant. So why might photo-ageing in particular modulate the level and sub-cellular localisation of YAP1?

Changes to the protein composition of photo-aged dermis have been well publicised in the literature. Dermal ECM modifications are numerous, and reports indicate a reduction in type I and type III collagens as being a prominent change (Domyati et al, 2002). Additionally, this is something that we have observed in our photo-aged skin samples using Herovici staining. There is also an increased activity of ECM-degrading proteases (Naylor et al, 2011) and reduced collagen synthesis and accelerated collagen degradation results in dermal atrophy. Also characteristic of ageing skin is a loss of elastin and an increase in fibrosis (Cerimele et al, 1990). Together these processes cause tissue stiffening, which has been found to occur in human skin with age (Pawlaczyk et al, 2013). This stiffening impacts the mechanical properties of skin, causing it to be less resilient to deformation (Makrantonaki and Zouboulis, 2007).

As the stiffness of culture substrate has shown to modulate YAP1 sub-cellular localisation (see section 1.21 of thesis introduction), it is feasible that the epidermal

keratinocytes in PE aged skin are responsive to the mechanical changes that could be taking place in the underlying dermis during photo-ageing. This could explain the increases in the levels of nuclear YAP1 in the epidermis of photo-exposed skin, as stiffening of the dermal compartment below could modulate the localisation of YAP1 in the basal keratinocytes above. Photo-exposure has been shown to accelerate the ageing skin process (Naylor et al, 2011) This may explain why the change in YAP1 nuclear localisation was much more prominent in the photo-aged arm skin compared to the intrinsically aged buttock skin, as the mechanical changes associated with ageing skin could be more marked in the aged PE tissue compared to the intrinsically aged tissue.

At the molecular level, changes in the proliferative index of keratinocytes with age is well documented, with several reports indicating decreases in keratinocyte proliferation during intrinsic ageing (Gilhar et al, 2004; Waaijer et al, 2012). On the other-hand, there are also reports of instances of epidermal hyperplasia during photo-ageing (Armento et al, 2015), which creates epidermal thickening (Domyati et al, 2002). As nuclear YAP1 is associated with active cellular proliferation, and was found to be more abundant in the photo-exposed skin, it is possible that the increased YAP1 mRNA and protein levels in photo-exposed skin could be a result of photo-damaged induced hyperplasia. In order to conclude if this was the case, Ki67 staining could be carried out on human skin sections to indicate any change in the proliferative index of the keratinocytes in old PE epidermis compared to old PP epidermis.

Photo-exposure to the skin is highly associated with increased levels of DNA damage that can result in cellular apoptosis if the UV-induced insult is large enough (Lee et al, 2013). Photo-exposure is also commonly associated with carcinomas of the skin, indicating a causal link between UV exposure and skin cancers (de Gruijl et al, 2001). YAP1 has demonstrated specific roles in modulating DNA damage-induced apoptosis in epithelial cells in order to prevent oncogenic transformation (Cottini et al, 2014). The significant changes we observe in YAP1 mRNA levels in PE skin, and the movement of YAP1 into the nucleus could thus be a result of a protective cellular response to the presence of DNA damage due to UVA and UVB damaging irradiation during photo-ageing (Naylor et al, 2011). Future analysis of DNA damage levels in intrinsically aged and photo-aged skin would allow a more robust correlation to be drawn between nuclear YAP1 levels and the presence of DNA damage during photo-ageing.

Analysis of pixel data from high-quality confocal images presents a good early benchmark of indications of changes to protein expression levels with age. But several experiments could be done in future to improve this data. Microarray data results can vary greatly depending on sample preparation and platform use (Morey et al, 2006). To overcome discrepancies, several methods have been developed to validate microarray data, including the

use of RNA-Seq (RNA sequencing) and RT-PCR (Reverse transcription polymerase chain reaction) (Rajkumar et al, 2015). Use of these tools would provide further confirmation of transcriptional changes we have observed to YAP1 with age. Additionally, there are also more efficient methods to quantify protein levels within the skin, such as western blotting, and 2-Dimensional gel electrophoresis. Some of the changes we observed to YAP1 at the protein level during photo-ageing were close to being statistically significant. It may therefore be the case that more accurate methods of protein quantification might reveal true statistically significant changes in YAP1 epidermal levels and YAP1 nuclear localisation during photo-ageing.

Chapter 5: Thesis summary and final discussion

5.1   C57BL/6 mice demonstrate a skin ageing phenotype similar to human skin but future work is needed to understand the role of Hippo during epidermal ageing

Using C57BL/6 male mice taken from periodic stages in their lifespan, we have assessed the morphometric changes that occur to skin over time. Our findings showed that cellular loss was a hallmark of both epidermal and dermal ageing, and for the epidermal compartment this manifested as epidermal thinning and a reduction in the density of cells in the basal epidermal layer. Accompanying this change, we showed that the epidermal nuclei become less circular over time and that the nucleus adopts a flattened morphology in the aged basal epidermal cells.

Our subsequent studies within the murine epidermis showed that epidermal proliferation declined over time, and alongside this, we saw a reduction in lamin B1 expression. To our knowledge, this is the first report of decreased lamin B1 in aged mouse tissue, and it shows that like for human skin (Dreesen et al, 2013 and our data), lamin B1 loss is a marker of epidermal ageing. Curiously, our analysis of DNA damage alongside cell proliferation revealed an unexpected result. DNA damage levels increased between 3 mo and 24 mo animals, but in the 30 mo animals, where we may have expected DNA damage levels to be highest, DNA damage was actually reduced and cell proliferation was increased compared to the 24 mo animals. We suggest that mice living to this age may show survivorship effects, whereby selection bias over time allows this genotype to be revealed.

One caveat to this theory is given by the fact that there are known changes to the proliferative properties of aged basal epidermal cells. Charruyer et al (2009), have shown that aged murine epidermal stem cells produce greater quantities of transit amplifying cells (TA cells). As TA cells have the potential to show markers of proliferation like Ki67, it is possible that our observations of increased cell proliferation in the 30 mo animals compared to the 24 mo animals may reflect a greater TA cell population. Future work should explore why the oldest mice showed these unexpected changes, and an important subsequent experiment would be to assess whether the expression of DNA surveillance and repair genes, like RAD51 (Wood et al, 2001), are increased in these animals, as this could explain why they have reduced levels of DNA damage. Additionally, it is possible to distinguish between Epi SC's and TA cells in the basal epidermal layer by analysis of β1 integrin levels, as it has been shown that Epi SC's have greater expression of this marker compared to TA cells (Watt, F.M. 1998). This experiment would allow

us to uncover whether our increased observation of proliferation in the 30 mo animals is a result of a greater TA cell population.

Through Western blotting and immunofluorescence, we showed that the keratinocyte terminal differentiation protein loricrin was lost with age. Loricrin loss in aged human skin has been shown in previous reports (Rinnerthaler et al, 2013), so despite the fact that structurally, C57BL/6 mouse skin is different to human skin, it appears that the two show this common marker of epidermal ageing. An additional important finding that warrants future study was the observation that K14 levels were maintained in the aged epidermis whereas K10 and loricrin levels decreased. This finding is of notable importance when considering our observation of increased nuclear YAP1 in the aged epidermis.

YAP1 nuclear localisation can occur as a result of low-cell density conditions, stiffer ECM substrates, modulation of the actin cytoskeleton and mitogenic signalling (see thesis introduction parts 1.20-1.22). In our aged C57BL/6 epidermis, all four of these factors have the potential to modulate YAP1 localisation. We have seen that fewer nuclei are present in the epidermis, so cell density is reduced in this region and we have observed changes in the morphology of the basal epidermal cells that could impact their cytoskeletal properties. Additionally, our characterisation of the dermal and basement membrane collagens showed that collagen VII protein expression decreased in aged animals, and also that collagen III and collagen I protein levels decreased in the dermis. Changes in the levels of dermal and basement membrane collagens could impact the biomechanical properties of these skin regions, and as basal epidermal cells are connected to the basement membrane, changes in the biomechanical properties in the underlying skin layers could modulate the localisation of YAP1 in these cells.

Because all of these changes have the potential to drive nuclear localisation of YAP1, future work should aim to delineate the cause of this observation. Potential changes in the cytoskeletal properties of basal epidermal cells could be assessed by looking at F-actin and keratin expression and organisation, and analysis of changes to the stiffness of these cells using atomic force microscopy (AFM- see Achterberg et al, 2014) could be completed to assess if there is a difference in their biomechanical properties of epidermal keratinocytes that is driving nuclear localisation of YAP1.

It is important to mention one key, common limitation in some of our assessments; that we computed the change in the nuclear location of YAP1 and percentage of Ki67 positive cells using the *whole* epidermis over time. It is now clear that the cells of the different layers of the epidermis are not lost equally during C57BL/6 epidermal ageing, as cellular loss appears to occur mostly as a result of fewer terminally differentiated (K10 and loricrin positive) keratinocytes in aged skin. This raises the question as to what extent our observation of

increased nuclear YAP1 in the oldest 30 mo animals is simply representative of the maintenance of the K14-positive cells, which contribute to the actively proliferating basal epidermal layer during epidermal ageing and the loss of non-proliferating, differentiated keratinocytes of the spinous and granular epidermal layers.

Future work should aim to delineate this, and efforts should be focused on firstly un-covering the proportions of cells from the basal, spinous and granular layers that are lost during epidermal ageing. This can be completed by using markers of keratinocyte differentiation like K10 and loricrin with the basal epidermal makers K14. Following this, assessment of changes to YAP1 nuclear localisation and Ki67 expression in the basal epidermal cells *only* should be completed, as this will determine if our observed changes are specific to this compartment.

Finally, as this work was completed in an in-bred strain of mice with identical genomes, it is important to consider that our findings may be unique to this strain of mice only. Despite this limitation it is clear that the C57BL/6 strain shows characteristics of epidermal ageing that are also shown in humans and therefore analysis of ageing skin in this model is worthwhile in the consideration of intrinsic mammalian skin ageing. Our work focused heavily on the epidermal compartment, so future analyses must account for the role of the dermis and hair follicles in the ageing process of mice. Initial experiments could look at the change in the number of pilo-sebaceous units in this animal with age to determine the extent of hair follicle attrition during C57BL/6 skin ageing.

5.2   Identification of increased dermal and basement membrane collagen transcription in later life

Through our transcriptional analysis of collagen I, collagen III, collagen IV and collagen VII mRNA levels during intrinsic and photo ageing, we identified novel findings. Firstly, although collagen I and collagen III mRNA levels declined until the 5th decade as one might expect, we found that in the two last decades assessed (6th and 7th- so subjects in their 60's and 70's), increased collagen I and collagen III transcription was observed. We propose either that this observation occurs as a compensatory mechanism- to restore youthful dermal ECM composition or alternatively it may represent an age-associated fibrosis effect.

Like for collagens I and III, the mRNA expression of two particular alpha chains in the collagen IV protein family, collagen IV α5 and collagen IV α6, also showed increased mRNA expression during intrinsic and photo-ageing. However, un-like for the dermal collagens, mRNA levels increased steadily from the 2nd to 7th decades. Additionally, collagen VII mRNA levels increased steadily from the 2nd to 7th decades during intrinsic and photo-ageing. As the basement membrane houses the epidermal stem cell niche, it is possible that these

transcriptional increases over time occur in an attempt to maintain the integrity of the stem cell niche to be maintained during the ageing process.

What is clear from our analysis of skin using Herovici staining and antibody staining against collagen VII, is that these transcriptional increases did not cause collagen levels to be restored in the dermis or the basement membrane, as we observed degradation of type I and type III collagens during intrinsic ageing, and to a greater extent, during photo-ageing and loss of collagen VII in both conditions. This suggests a dramatic change in the collagen synthesis and degradation balance in the dermis and basement membrane, and shows that our work presents only a partial picture of collagen ageing dynamics in this cohort of females. Future work should look to understand why these transcriptional increases do not manifest at the protein level, as it could be caused by increased expression of enzymes like MMP-1 and MMP-9, that are able to degrade collagens. Alternatively, there could be an age-related perturbation in the protein synthesis and higher-order assembly of dermal and basement membrane collagens, perhaps due to reduced lysyl oxidase enzyme activity.

One key limitation in this work was the fact that the collagen IV antibody available to us targeted the α1 chain only. As our results clearly show that α5 chain and α6 chain transcription increases, future research should look to validate this at the protein level using a collagen IV antibody specific to α5 and α6 chains (see Hasegawa et al, 2007 who used chain-specific antibodies to show differential expression in young skin). Additionally, on a general note, our study cohort was all female, and it is important to note that the steroid hormonal profile of women and men is different, due to the different levels of testosterone and oestrogen. As these hormones can impact the dermal compartment through collagen synthesis (Thornton, M.J. 2013), it is possible that our observations are unique to women and therefore similar studies would be needed in males to confirm whether our observations are specific to the female gender or are universal.

5.3   YAP1 and lamin B1 transcriptional and protein changes occur during epidermal ageing in human skin. A more robust sample size should be used to confirm this at the protein level

From our transcriptional analysis of the nuclear lamins and YAP1, we identified robust changes. Expression of lamin A and YAP1 mRNA was increased during ageing, whereas lamin B1 mRNA levels decreased. Our validation of these changes at the protein level, however, gave less robust evidence for a statistically significant change in these observations. In addition, YAP1 nuclear localisation increased in the epidermis during ageing, but this was not significant. These observations suggest that decreased lamin B1 and increased nuclear YAP are common to

the ageing epidermis of C57BL/6 mice and humans, but unlike the mice used in our studies, our human tissue samples came from genetically heterogeneous females, and thus our sample size number for our human protein-based validations was small (n= 3). To confirm that decreased lamin B1 protein expression and increased nuclear YAP1 are common markers of epidermal ageing in both mice and humans, additional subjects should be used for protein-based validations in the human tissue cohort. A greater sample size will help to account for the genetic heterogeneity that is part of human tissue use, as a greater sample size increases the reliability of the data (Halsey et al, 2015).

Future work may also wish to consider the transcriptional fate of other components of the LINC complex during ageing. It is known that the nuclear lamins are crucial for assembly and stability of other parts of the LINC complex, like emerin (Vaughan et al, 2001) and also that nuclear lamins are required for the formation of cellular signalling complexes at the nuclear lamina, such as the formation of the complex of LAP2α and pRb (Markiewicz et al, 2002). It is therefore possible that several other components of the LINC complex show altered expression during ageing, which could be explored at the transcriptional and protein level in future studies. Finally, it is becoming increasingly well known that the homolog of YAP, TAZ, has its own unique roles in cell biology, which has been shown in the context of wound healing (Lee et al, 2014) and miRNA biogenesis (Moroishi et al, 2015). Future studies could therefore consider whether TAZ shows a differential modulation to YAP1 during epidermal ageing.

Chapter 6: References

Achterberg, V. F., L. Buscemi, H. Diekmann, J. Smith-Clerc, H. Schwengler, J. J. Meister, H. Wenck, S. Gallinat and B. Hinz (2014). "The nano-scale mechanical properties of the extracellular matrix regulate dermal fibroblast function." J Invest Dermatol 134(7): 1862-1872.

Ackerman, A.B. Boer, A. and Bennin, B. (2005) Histologic Diagnosis of Inflammatory Skin Diseases: An Algorithmic Method Based on Pattern Analysis. 3rd Edition .Available online at https://www.derm101.com/core-resources/histologic-diagnosis-of-inflammatory-skin-diseases/

Adam, L., P. Rosenbaum, A. Cosma, R. Le Grand and F. Martinon (2015). "Identification of skin immune cells in non-human primates." J Immunol Methods 426: 42-49.

Alvarado, J., C. Murphy and R. Juster (1983). "Age-related changes in the basement membrane of the human corneal epithelium." Invest Ophthalmol Vis Sci 24(8): 1015-1028.

Amano, S. (2009). "Possible involvement of basement membrane damage in skin photoaging." J Investig Dermatol Symp Proc 14(1): 2-7.

Aragona, M., T. Panciera, A. Manfrin, S. Giulitti, F. Michielin, N. Elvassore, S. Dupont and S. Piccolo (2013). "A mechanical checkpoint controls multicellular growth through YAP/TAZ regulation by actin-processing factors." Cell 154(5): 1047-1059.

Armento,A.J., Oldach, J., Stolper, G., Macwell, L., Bachelor, M.A. and Hayden, P.J. (2015) Evaluation of Cutaneous Damage and Repair Following Acute Solar Ultraviolet Radiation Exposure: Experiments with an In Vitro Reconstructed Human Skin Model and Excised Human Skin. Applied In Vitro Toxicology 1(2): 109-117

Aumailley, M. and T. Krieg (1996). "Laminins: a family of diverse multifunctional molecules of basement membranes." J Invest Dermatol 106(2): 209-214.

Bahar, R., C. H. Hartmann, K. A. Rodriguez, A. D. Denny, R. A. Busuttil, M. E. Dolle, R. B. Calder, G. B. Chisholm, B. H. Pollock, C. A. Klein and J. Vijg (2006). "Increased cell-to-cell variation in gene expression in ageing mouse heart." Nature 441(7096): 1011-1014.

Baker, D. J., T. Wijshake, T. Tchkonia, N. K. LeBrasseur, B. G. Childs, B. van de Sluis, J. L. Kirkland and J. M. van Deursen (2011). "Clearance of p16Ink4a-positive senescent cells delays ageing-associated disorders." Nature 479(7372): 232-236.

Bansal, A., L. J. Zhu, K. Yen and H. A. Tissenbaum (2015). "Uncoupling lifespan and healthspan in Caenorhabditis elegans longevity mutants." Proc Natl Acad Sci U S A 112(3): E277-286.

Barascu, A., C. Le Chalony, G. Pennarun, D. Genet, N. Imam, B. Lopez and P. Bertrand (2012). "Oxidative stress induces an ATM-independent senescence pathway through p38 MAPK-mediated lamin B1 accumulation." EMBO J 31(5): 1080-1094.

Barker, J. N., R. S. Mitra, C. E. Griffiths, V. M. Dixit and B. J. Nickoloff (1991). "Keratinocytes as initiators of inflammation." Lancet 337(8735): 211-214.

Barzilai, N., D. M. Huffman, R. H. Muzumdar and A. Bartke (2012). "The critical role of metabolic pathways in aging." Diabetes 61(6): 1315-1322.

Bazzoni, G. and E. Dejana (2002). "Keratinocyte junctions and the epidermal barrier: how to make a skin-tight dress." J Cell Biol 156(6): 947-949.

Behrens, D. T., D. Villone, M. Koch, G. Brunner, L. Sorokin, H. Robenek, L. Bruckner-Tuderman, P. Bruckner and U. Hansen (2012). "The epidermal basement membrane is a composite of separate laminin- or collagen IV-containing networks connected by aggregated perlecan, but not by nidogens." J Biol Chem 287(22): 18700-18709.

Benech, P. D. and A. Patatian (2014). "From experimental design to functional gene networks: DNA microarray contribution to skin ageing research." Int J Cosmet Sci 36(6): 516-526.

Benjamini, Y., D. Drai, G. Elmer, N. Kafkafi and I. Golani (2001). "Controlling the false discovery rate in behavior genetics research." Behav Brain Res 125(1-2): 279-284.

Bhattacharyya, T. K. and J. R. Thomas (2004). "Histomorphologic changes in aging skin: observations in the CBA mouse model." Arch Facial Plast Surg 6(1): 21-25.

Binic, I., V. Lazarevic, M. Ljubenovic, J. Mojsa and D. Sokolovic (2013). "Skin Ageing: Natural Weapons and Strategies." Evidence-Based Complementary and Alternative Medicine.

Boyer, B., P. Kern, A. Fourtanier and J. Labat-Robert (1991). "Age-dependent variations of the biosyntheses of fibronectin and fibrous collagens in mouse skin." Exp Gerontol 26(4): 375-383.

Brack, A. S., M. J. Conboy, S. Roy, M. Lee, C. J. Kuo, C. Keller and T. A. Rando (2007). "Increased Wnt signaling during aging alters muscle stem cell fate and increases fibrosis." Science 317(5839): 807-810.

Brandt, A., G. Krohne and J. Grosshans (2008). "The farnesylated nuclear proteins KUGELKERN and LAMIN B promote aging-like phenotypes in Drosophila flies." Aging Cell 7(4): 541-551.

Brehmer-Andersson, E.(2006) Chapter 2: The dermal blood vasculature. Dermatopathology:1st edition, Springer.

Brem, H., et al. (2007). "Molecular markers in patients with chronic wounds to guide surgical debridement." Mol Med **13**(1-2): 30-39.

Brincat, M. P., Y. M. Baron and R. Galea (2005). "Estrogens and the skin." Climacteric 8(2): 110-123.

Brizzi, M. F., G. Tarone and P. Defilippi (2012). "Extracellular matrix, integrins, and growth factors as tailors of the stem cell niche." Curr Opin Cell Biol 24(5): 645-651.

Broers, J. L., B. M. Machiels, G. J. van Eys, H. J. Kuijpers, E. M. Manders, R. van Driel and F. C. Ramaekers (1999). "Dynamics of the nuclear lamina as monitored by GFP-tagged A-type lamins." J Cell Sci 112 (Pt 20): 3463-3475.

Broers, J. L., F. C. Ramaekers, G. Bonne, R. B. Yaou and C. J. Hutchison (2006). "Nuclear lamins: laminopathies and their role in premature ageing." Physiol Rev 86(3): 967-1008.

Buchwalow, I., V. Samoilova, W. Boecker and M. Tiemann (2011). "Non-specific binding of antibodies in immunohistochemistry: fallacies and facts." Sci Rep 1: 28.

Burke, B. and C. L. Stewart (2013). "The nuclear lamins: flexibility in function." Nat Rev Mol Cell Biol 14(1): 13-24.

Burtner, C. R. and B. K. Kennedy (2010). "Progeria syndromes and ageing: what is the connection?" Nat Rev Mol Cell Biol 11(8): 567-578.

Callaghan, T. M. and K. P. Wilhelm (2008). "A review of ageing and an examination of clinical methods in the assessment of ageing skin. Part I: Cellular and molecular perspectives of skin ageing." Int J Cosmet Sci 30(5): 313-322.

Calleja-Agius, J., M. Brincat and M. Borg (2013). "Skin connective tissue and ageing." Best Pract Res Clin Obstet Gynaecol 27(5): 727-740.

Camargo, F. D., S. Gokhale, J. B. Johnnidis, D. Fu, G. W. Bell, R. Jaenisch and T. R. Brummelkamp (2007). "YAP1 increases organ size and expands undifferentiated progenitor cells." Curr Biol 17(23): 2054-2060.

Cameron, I. L. (1972). "Cell proliferation and renewal in aging mice." J Gerontol 27(2): 162-172.

Campisi, J. (1998). "The role of cellular senescence in skin aging." J Investig Dermatol Symp Proc 3(1): 1-5.

Campisi, J. and F. d'Adda di Fagagna (2007). "Cellular senescence: when bad things happen to good cells." Nat Rev Mol Cell Biol 8(9): 729-740.

Candi, E., R. Schmidt and G. Melino (2005). "The cornified envelope: a model of cell death in the skin." Nat Rev Mol Cell Biol 6(4): 328-340.

Cao, K., P. Ryvkin, Y. C. Hwang, F. B. Johnson and L. S. Wang (2013). "Analysis of nonlinear gene expression progression reveals extensive pathway and age-specific transitions in aging human brains." PLoS One 8(10): e74578.

Cerimele, D., L. Celleno and F. Serri (1990). "Physiological changes in ageing skin." Br J Dermatol 122 Suppl 35: 13-20.

Charruyer, A., C. O. Barland, L. Yue, H. B. Wessendorf, Y. Lu, H. J. Lawrence, M. L. Mancianti and R. Ghadially (2009). "Transit-amplifying cell frequency and cell cycle kinetics are altered in aged epidermis." J Invest Dermatol 129(11): 2574-2583.

Chase, H. B. and G. J. Eaton (1959). "The growth of hair follicles in waves." Ann N Y Acad Sci 83: 365-368.

Chen, C. C., P. J. Murray, T. X. Jiang, M. V. Plikus, Y. T. Chang, O. K. Lee, R. B. Widelitz and C. M. Chuong (2014). "Regenerative hair waves in aging mice and extra-follicular modulators follistatin, dkk1, and sfrp4." J Invest Dermatol 134(8): 2086-2096.

Chen, C. Y., Y. H. Chi, R. A. Mutalif, M. F. Starost, T. G. Myers, S. A. Anderson, C. L. Stewart and K. T. Jeang (2012). "Accumulation of the inner nuclear envelope protein Sun1 is pathogenic in progeric and dystrophic laminopathies." Cell 149(3): 565-577.

Chen, H., X. Zheng and Y. Zheng (2014). "Age-associated loss of lamin-B leads to systemic inflammation and gut hyperplasia." Cell 159(4): 829-843.

Cheng, W., R. Yan-Hua, N. Fang-Gang and Z. Guo-An (2011). "The content and ratio of type I and III collagen in skin differ with age and injury." African Journal of Biotechnology 10(13): 2524-2529.

Childs, B. G., M. Durik, D. J. Baker and J. M. van Deursen (2015). "Cellular senescence in aging and age-related disease: from mechanisms to therapy." Nat Med 21(12): 1424-1435.

Choi, H. R., S. Y. Byun, S. H. Kwon and K. C. Park (2015). "Niche interactions in epidermal stem cells." World J Stem Cells 7(2): 495-501.

Chomiczewska, D., E. Trznadel-Budzko, A. Kaczorowska and H. Rotsztejn (2009). "[The role of Langerhans cells in the skin immune system]." Pol Merkur Lekarski 26(153): 173-177.

Chrambach, A., R. A. Reisfeld, M. Wyckoff and J. Zaccari (1967). "A procedure for rapid and sensitive staining of protein fractionated by polyacrylamide gel electrophoresis." Anal Biochem 20(1): 150-154.

Cichorek, M., M. Wachulska, A. Stasiewicz and A. Tyminska (2013). "Skin melanocytes: biology and development." Postepy Dermatol Alergol 30(1): 30-41.

Clayton, E., D. P. Doupe, A. M. Klein, D. J. Winton, B. D. Simons and P. H. Jones (2007). "A single type of progenitor cell maintains normal epidermis." Nature 446(7132): 185-189.

Connelly, J. T., J. E. Gautrot, B. Trappmann, D. W. Tan, G. Donati, W. T. Huck and F. M. Watt (2010). "Actin and serum response factor transduce physical cues from the microenvironment to regulate epidermal stem cell fate decisions." Nat Cell Biol 12(7): 711-718.

Constantinescu, D., H. L. Gray, P. J. Sammak, G. P. Schatten and A. B. Csoka (2006). "Lamin A/C expression is a marker of mouse and human embryonic stem cell differentiation." Stem Cells 24(1): 177-185.

Contet-Audonneau, J. L., C. Jeanmaire and G. Pauly (1999). "A histological study of human wrinkle structures: comparison between sun-exposed areas of the face, with or without wrinkles, and sun-protected areas." Br J Dermatol 140(6): 1038-1047.

Coppe, J. P., C. K. Patil, F. Rodier, Y. Sun, D. P. Munoz, J. Goldstein, P. S. Nelson, P. Y. Desprez and J. Campisi (2008). "Senescence-associated secretory phenotypes reveal cell-nonautonomous functions of oncogenic RAS and the p53 tumor suppressor." PLoS Biol 6(12): 2853-2868.

Cottini, F., T. Hideshima, C. Xu, M. Sattler, M. Dori, L. Agnelli, E. ten Hacken, M. T. Bertilaccio, E. Antonini, A. Neri, M. Ponzoni, M. Marcatti, P. G. Richardson, R. Carrasco, A. C. Kimmelman, K. K. Wong, F. Caligaris-Cappio, G. Blandino, W. M. Kuehl, K. C. Anderson and G. Tonon (2014). "Rescue of Hippo coactivator YAP1 triggers DNA damage-induced apoptosis in hematological cancers." Nat Med 20(6): 599-606.

Coulombe, P. A., R. Kopan and E. Fuchs (1989). "Expression of keratin K14 in the epidermis and hair follicle: insights into complex programs of differentiation." J Cell Biol 109(5): 2295-2312.

Craven, N. M., R. E. Watson, C. J. Jones, C. A. Shuttleworth, C. M. Kielty and C. E. Griffiths (1997). "Clinical features of photodamaged human skin are associated with a reduction in collagen VII." Br J Dermatol 137(3): 344-350.

d'Adda di Fagagna, F., P. M. Reaper, L. Clay-Farrace, H. Fiegler, P. Carr, T. Von Zglinicki, G. Saretzki, N. P. Carter and S. P. Jackson (2003). "A DNA damage checkpoint response in telomere-initiated senescence." Nature 426(6963): 194-198.

Daigle, N., J. Beaudouin, L. Hartnell, G. Imreh, E. Hallberg, J. Lippincott-Schwartz and J. Ellenberg (2001). "Nuclear pore complexes form immobile networks and have a very low turnover in live mammalian cells." J Cell Biol 154(1): 71-84.

Dapson, R. W. (2007). "Macromolecular changes caused by formalin fixation and antigen retrieval." Biotech Histochem 82(3): 133-140.

Davalli, P., T. Mitic, A. Caporali, A. Lauriola and D. D'Arca (2016). "ROS, Cell Senescence, and Novel Molecular Mechanisms in Aging and Age-Related Diseases." Oxid Med Cell Longev 2016: 3565127.

de Gruijl, F. R., H. J. van Kranen and L. H. Mullenders (2001). "UV-induced DNA damage, repair, mutations and oncogenic pathways in skin cancer." J Photochem Photobiol B 63(1-3): 19-27.

De Sandre-Giovannoli, A., R. Bernard, P. Cau, C. Navarro, J. Amiel, I. Boccaccio, S. Lyonnet, C. L. Stewart, A. Munnich, M. Le Merrer and N. Levy (2003). "Lamin a truncation in Hutchinson-Gilford progeria." Science 300(5628): 2055.

Deplewski, D., K. Qin, N. Ciletti and R. L. Rosenfield (2011). "Unique mode of lipogenic activation in rat preputial sebocytes." J Nutr Metab 2011: 163631.

Di Lullo, G. A., S. M. Sweeney, J. Korkko, L. Ala-Kokko and J. D. San Antonio (2002). "Mapping the ligand-binding sites and disease-associated mutations on the most abundant protein in the human, type I collagen." J Biol Chem 277(6): 4223-4231.

Diekmann, J., L. Alili, O. Scholz, M. Giesen, O. Holtkotter and P. Brenneisen (2016). "A three-dimensional skin equivalent reflecting some aspects of in vivo aged skin." Exp Dermatol 25(1): 56-61.

Diezel, W., G. Kopperschlager and E. Hofmann (1972). "An improved procedure for protein staining in polyacrylamide gels with a new type of Coomassie Brilliant Blue." Anal Biochem 48(2): 617-620.

Dimri, G. P., X. Lee, G. Basile, M. Acosta, G. Scott, C. Roskelley, E. E. Medrano, M. Linskens, I. Rubelj, O. Pereira-Smith and et al. (1995). "A biomarker that identifies senescent human cells in culture and in aging skin in vivo." Proc Natl Acad Sci U S A 92(20): 9363-9367.

Dittmer, T. A. and T. Misteli (2011). "The lamin protein family." Genome Biol 12(5): 222.

Dos Santos, M., E. Metral, A. Boher, P. Rousselle, A. Thepot and O. Damour (2015). "In vitro 3-D model based on extending time of culture for studying chronological epidermis aging." Matrix Biol 47: 85-97.

Dreesen, O., A. Chojnowski, P. F. Ong, T. Y. Zhao, J. E. Common, D. Lunny, E. B. Lane, S. J. Lee, L. A. Vardy, C. L. Stewart and A. Colman (2013). "Lamin B1 fluctuations have differential effects on cellular proliferation and senescence." Journal of Cell Biology 200(5): 605-617.

Driskell, R. R., et al. (2011). "Hair follicle dermal papilla cells at a glance." J Cell Sci 124(Pt 8): 1179-1182.

Driskell, R. R., B. M. Lichtenberger, E. Hoste, K. Kretzschmar, B. D. Simons, M. Charalambous, S. R. Ferron, Y. Herault, G. Pavlovic, A. C. Ferguson-Smith and F. M. Watt (2013). "Distinct fibroblast lineages determine dermal architecture in skin development and repair." Nature 504(7479): 277-281.

Dupont, S., L. Morsut, M. Aragona, E. Enzo, S. Giulitti, M. Cordenonsi, F. Zanconato, J. Le Digabel, M. Forcato, S. Bicciato, N. Elvassore and S. Piccolo (2011). "Role of YAP/TAZ in mechanotransduction." Nature 474(7350): 179-183.

Eaton, S. L., S. L. Roche, M. Llavero Hurtado, K. J. Oldknow, C. Farquharson, T. H. Gillingwater and T. M. Wishart (2013). "Total protein analysis as a reliable loading control for quantitative fluorescent Western blotting." PLoS One 8(8): e72457.

Eckhart, L., S. Lippens, E. Tschachler and W. Declercq (2013). "Cell death by cornification." Biochim Biophys Acta 1833(12): 3471-3480.

Elbediwy, A., Z. I. Vincent-Mistiaen, B. Spencer-Dene, R. K. Stone, S. Boeing, S. K. Wculek, J. Cordero, E. H. Tan, R. Ridgway, V. G. Brunton, E. Sahai, H. Gerhardt, A. Behrens, I. Malanchi, O. J. Sansom and B. J. Thompson (2016). "Integrin signalling regulates YAP and TAZ to control skin homeostasis." Development 143(10): 1674-1687.

El-Domyati, M., S. Attia, F. Saleh, D. Brown, D. E. Birk, F. Gasparro, H. Ahmad and J. Uitto (2002). "Intrinsic aging vs. photoaging: a comparative histopathological, immunohistochemical, and ultrastructural study of skin." Exp Dermatol 11(5): 398-405.

Emes, R. D., L. Goodstadt, E. E. Winter and C. P. Ponting (2003). "Comparison of the genomes of human and mouse lays the foundation of genome zoology." Hum Mol Genet 12(7): 701-709.

Evans-Johnson, J. A., J. A. Garlick, E. J. Johnson, X. D. Wang and C. Y. Oliver Chen (2013). "A pilot study of the photoprotective effect of almond phytochemicals in a 3D human skin equivalent." J Photochem Photobiol B 126: 17-25.

Ewald, J. A., J. A. Desotelle, G. Wilding and D. F. Jarrard (2010). "Therapy-induced senescence in cancer." J Natl Cancer Inst 102(20): 1536-1546.

Farage, M. A., K. W. Miller, P. Elsner and H. I. Maibach (2008). "Intrinsic and extrinsic factors in skin ageing: a review." Int J Cosmet Sci 30(2): 87-95.

Farage, M. A., K. W. Miller, P. Elsner and H. I. Maibach (2013). "Characteristics of the Aging Skin." Adv Wound Care (New Rochelle) 2(1): 5-10.

Fisher, G. J., J. Varani and J. J. Voorhees (2008). "Looking older: fibroblast collapse and therapeutic implications." Arch Dermatol 144(5): 666-672.

Fisher, G. J., S. Kang, J. Varani, Z. Bata-Csorgo, Y. Wan, S. Datta and J. J. Voorhees (2002). "Mechanisms of photoaging and chronological skin aging." Arch Dermatol 138(11): 1462-1470.

Fitzgerald, A. M., J. J. Kirkpatrick, I. T. Foo and I. L. Naylor (1996). "Human skin histology as demonstrated by Herovici's stain: a guide for the improvement of dermal substitutes for use with cultured keratinocytes?" Burns 22(3): 200-202.

Flament, F., R. Bazin, H. Qiu, C. Ye, S. Laquieze, V. Rubert, A. Decroux, E. Simonpietri and B. Piot (2015). "Solar exposure(s) and facial clinical signs of aging in Chinese women: impacts upon age perception." Clin Cosmet Investig Dermatol 8: 75-84.

Foitzik, K., et al. (2003). "Prolactin and its receptor are expressed in murine hair follicle epithelium, show hair cycle-dependent expression, and induce catagen." Am J Pathol 162(5): 1611-1621.

Fornieri, C., D. Quaglino, Jr. and G. Mori (1989). "Correlations between age and rat dermis modifications. Ultrastructural-morphometric evaluations and lysyl oxidase activity." Aging (Milano) 1(2): 127-138.

Foster, C. R., S. A. Przyborski, R. G. Wilson and C. J. Hutchison (2010). "Lamins as cancer biomarkers." Biochem Soc Trans 38(Pt 1): 297-300.

Franceschi, C. and J. Campisi (2014). "Chronic inflammation (inflammaging) and its potential contribution to age-associated diseases." J Gerontol A Biol Sci Med Sci 69 Suppl 1: S4-9.

Franceschi, C., M. Bonafe and S. Valensin (2000). "Human immunosenescence: the prevailing of innate immunity, the failing of clonotypic immunity, and the filling of immunological space." Vaccine 18(16): 1717-1720.

Fratzl, P., K. Misof, I. Zizak, G. Rapp, H. Amenitsch and S. Bernstorff (1998). "Fibrillar structure and mechanical properties of collagen." J Struct Biol 122(1-2): 119-122.

Freund, A., R. M. Laberge, M. Demaria and J. Campisi (2012). "Lamin B1 loss is a senescence-associated biomarker." Mol Biol Cell 23(11): 2066-2075.

Fuchs, E. (1990). "Epidermal differentiation: the bare essentials." J Cell Biol 111(6 Pt 2): 2807-2814.

Fuchs, E. (2009). "The tortoise and the hair: slow-cycling cells in the stem cell race." Cell 137(5): 811-819.

Fuchs, E. and S. Raghavan (2002). "Getting under the skin of epidermal morphogenesis." Nat Rev Genet 3(3): 199-209.

Fujihara, S., C. Ward, I. Dransfield, R. T. Hay, I. J. Uings, B. Hayes, S. N. Farrow, C. Haslett and A. G. Rossi (2002). "Inhibition of nuclear factor-kappaB activation un-masks the ability of TNF-alpha to induce human eosinophil apoptosis." Eur J Immunol 32(2): 457-466.

Genevet, A., M. C. Wehr, R. Brain, B. J. Thompson and N. Tapon (2010). "Kibra is a regulator of the Salvador/Warts/Hippo signaling network." Dev Cell 18(2): 300-308.

Gerashchenko, B. I. and J. R. Dynlacht (2009). "A tool for enhancement and scoring of DNA repair foci." Cytometry A 75(3): 245-252.

Giangreco, A., M. Qin, J. E. Pintar and F. M. Watt (2008). "Epidermal stem cells are retained in vivo throughout skin aging." Aging Cell 7(2): 250-259.

Gilchrest, B. A. (2013). "Photoaging." J Invest Dermatol 133(E1): E2-6.

Gilchrest, B. A., M. S. Eller and M. Yaar (2009). "Telomere-mediated effects on melanogenesis and skin aging." J Investig Dermatol Symp Proc 14(1): 25-31.

Gilhar, A., Y. Ullmann, R. Karry, R. Shalaginov, B. Assy, S. Serafimovich and R. S. Kalish (2004). "Aging of human epidermis: reversal of aging changes correlates with reversal of keratinocyte fas expression and apoptosis." J Gerontol A Biol Sci Med Sci 59(5): 411-415.

Gineyts, E., P. A. Cloos, O. Borel, L. Grimaud, P. D. Delmas and P. Garnero (2000). "Racemization and isomerization of type I collagen C-telopeptides in human bone and soft tissues: assessment of tissue turnover." Biochem J 345 Pt 3: 481-485.

Glass, D., A. Vinuela, M. N. Davies, A. Ramasamy, L. Parts, D. Knowles, A. A. Brown, A. K. Hedman, K. S. Small, A. Buil, E. Grundberg, A. C. Nica, P. Di Meglio, F. O. Nestle, M. Ryten, U. K. B. E. consortium, T. c. Mu, R. Durbin, M. I. McCarthy, P. Deloukas, E. T. Dermitzakis, M. E. Weale, V. Bataille and T. D. Spector (2013). "Gene expression changes with age in skin, adipose tissue, blood and brain." Genome Biol 14(7): R75.

Goodpaster, T. and J. Randolph-Habecker (2014). "A flexible mouse-on-mouse immunohistochemical staining technique adaptable to biotin-free reagents, immunofluorescence, and multiple antibody staining." J Histochem Cytochem 62(3): 197-204.

Goodpaster, T., A. Legesse-Miller, M. R. Hameed, S. C. Aisner, J. Randolph-Habecker and H. A. Coller (2008). "An immunohistochemical method for identifying fibroblasts in formalin-fixed, paraffin-embedded tissue." J Histochem Cytochem 56(4): 347-358.

Graveley, B. R. (2001). "Alternative splicing: increasing diversity in the proteomic world." Trends Genet 17(2): 100-107.

Grove, G. L. and A. M. Kligman (1983). "Age-associated changes in human epidermal cell renewal." J Gerontol 38(2): 137-142.

Guilluy, C., L. D. Osborne, L. Van Landeghem, L. Sharek, R. Superfine, R. Garcia-Mata and K. Burridge (2014). "Isolated nuclei adapt to force and reveal a mechanotransduction pathway in the nucleus." Nat Cell Biol 16(4): 376-381.

Gunin, A.G., Petrov, V.V., Vasilieva, O.V and Golubtsova, N.N. (2015) Age-related changes of blood vessels in the human dermis. Advances in gerontology. 5 (2). pp 65-71

Gupta, M. A. and B. A. Gilchrest (2005). "Psychosocial aspects of aging skin." Dermatol Clin 23(4): 643-648.

Haigis, M. C. and B. A. Yankner (2010). "The aging stress response." Mol Cell 40(2): 333-344.

Hals, E. (1977). "Selective fluorescence of rat elastic fibers stained with acid fuchsin or fast green FCF." Scand J Dent Res 85(7): 542-548.

Halsey, L. G., D. Curran-Everett, S. L. Vowler and G. B. Drummond (2015). "The fickle P value generates irreproducible results." Nat Methods 12(3): 179-185.

Han, W., W. Wang, K. A. Mohammed and Y. Su (2009). "Alpha-defensins increase lung fibroblast proliferation and collagen synthesis via the beta-catenin signaling pathway." FEBS J 276(22): 6603-6614.

Hanif, M., Y. Rosengardten, H. Sagelius, B. Rozell and M. Eriksson (2009). "Differential expression of A-type and B-type lamins during hair cycling." PLoS One 4(1): e4114.

Hansen, L. S., J. E. Coggle, J. Wells and M. W. Charles (1984). "The influence of the hair cycle on the thickness of mouse skin." Anat Rec 210(4): 569-573.

Haratake, A., Y. Uchida, K. Mimura, P. M. Elias and W. M. Holleran (1997). "Intrinsically aged epidermis displays diminished UVB-induced alterations in barrier function associated with decreased proliferation." J Invest Dermatol 108(3): 319-323.

Harries, L. W., D. Hernandez, W. Henley, A. R. Wood, A. C. Holly, R. M. Bradley-Smith, H. Yaghootkar, A. Dutta, A. Murray, T. M. Frayling, J. M. Guralnik, S. Bandinelli, A. Singleton, L. Ferrucci and D. Melzer (2011). "Human aging is characterized by focused changes in gene expression and deregulation of alternative splicing." Aging Cell 10(5): 868-878.

Hasegawa, H., I. Naito, K. Nakano, R. Momota, K. Nishida, T. Taguchi, Y. Sado, Y. Ninomiya and A. Ohtsuka (2007). "The distributions of type IV collagen alpha chains in basement membranes of human epidermis and skin appendages." Arch Histol Cytol 70(4): 255-265.

Hayashi, H., T. Higashi, N. Yokoyama, T. Kaida, K. Sakamoto, Y. Fukushima, T. Ishimoto, H. Kuroki, H. Nitta, D. Hashimoto, A. Chikamoto, E. Oki, T. Beppu and H. Baba (2015). "An Imbalance in TAZ and YAP Expression in Hepatocellular Carcinoma Confers Cancer Stem Cell-like Behaviors Contributing to Disease Progression." Cancer Res 75(22): 4985-4997.

Henderson, K. D., L. Bernstein, B. Henderson, L. Kolonel and M. C. Pike (2008). "Predictors of the timing of natural menopause in the Multiethnic Cohort Study." Am J Epidemiol 167(11): 1287-1294.

Hewitt, G., D. Jurk, F. D. Marques, C. Correia-Melo, T. Hardy, A. Gackowska, R. Anderson, M. Taschuk, J. Mann and J. F. Passos (2012). "Telomeres are favoured targets of a persistent DNA damage response in ageing and stress-induced senescence." Nat Commun 3: 708.

Higgins, J. P. (2002). "Nonlinear systems in medicine." Yale J Biol Med 75(5-6): 247-260.

Hill, M. W. (1988). "Influence of age on the morphology and transit time of murine stratified squamous epithelia." Arch Oral Biol 33(4): 221-229.

Ho, C. Y. and J. Lammerding (2012). "Lamins at a glance." J Cell Sci 125(Pt 9): 2087-2093.

Hombach, S. and M. Kretz (2013). "The non-coding skin: exploring the roles of long non-coding RNAs in epidermal homeostasis and disease." Bioessays 35(12): 1093-1100.

Hsu, Y. C., L. Li and E. Fuchs (2014). "Emerging interactions between skin stem cells and their niches." Nat Med 20(8): 847-856.

Hutchison, C. J. (2002). "Lamins: building blocks or regulators of gene expression?" Nat Rev Mol Cell Biol 3(11): 848-858.

Hutchison, C. J. (2012). "B-type lamins and their elusive roles in metazoan cell proliferation and senescence." EMBO J 31(5): 1058-1059.

Hwang, K. A., B. R. Yi and K. C. Choi (2011). "Molecular mechanisms and in vivo mouse models of skin aging associated with dermal matrix alterations." Lab Anim Res 27(1): 1-8.

Indra, A. K. and M. Leid (2011). "Epidermal permeability barrier measurement in mammalian skin." Methods Mol Biol 763: 73-81.

Ishikawa, F. (2006). "Cellular senescence as a stress response." Cornea 25(10 Suppl 1): S3-6.

Ivell, R., K. Teerds and G. E. Hoffman (2014). "Proper application of antibodies for immunohistochemical detection: antibody crimes and how to prevent them." Endocrinology 155(3): 676-687.

Janson, D. G., G. Saintigny, A. van Adrichem, C. Mahe and A. El Ghalbzouri (2012). "Different gene expression patterns in human papillary and reticular fibroblasts." J Invest Dermatol 132(11): 2565-2572.

Janson, D., M. Rietveld, R. Willemze and A. El Ghalbzouri (2013). "Effects of serially passaged fibroblasts on dermal and epidermal morphogenesis in human skin equivalents." Biogerontology 14(2): 131-140.

Janus, C. and H. Welzl (2010). "Mouse models of neurodegenerative diseases: criteria and general methodology." Methods Mol Biol 602: 323-345.

Jeffery, I. B., D. G. Higgins and A. C. Culhane (2006). "Comparison and evaluation of methods for generating differentially expressed gene lists from microarray data." BMC Bioinformatics 7: 359.

Jeyapalan, J. C. and J. M. Sedivy (2008). "Cellular senescence and organismal aging." Mech Ageing Dev 129(7-8): 467-474.

Jeyapalan, J. C., M. Ferreira, J. M. Sedivy and U. Herbig (2007). "Accumulation of senescent cells in mitotic tissue of aging primates." Mech Ageing Dev 128(1): 36-44.

Jiao, Y., Z. Sun, T. Lee, F. R. Fusco, T. D. Kimble, C. A. Meade, S. Cuthbertson and A. Reiner (1999). "A simple and sensitive antigen retrieval method for free-floating and slide-mounted tissue sections." J Neurosci Methods 93(2): 149-162.

Johnson, R. and G. Halder (2014). "The two faces of Hippo: targeting the Hippo pathway for regenerative medicine and cancer treatment." Nat Rev Drug Discov 13(1): 63-79.

Jung, H. J., A. Tatar, Y. Tu, C. Nobumori, S. H. Yang, C. N. Goulbourne, H. Herrmann, L. G. Fong and S. G. Young (2014). "An absence of nuclear lamins in keratinocytes leads to ichthyosis, defective epidermal barrier function, and intrusion of nuclear membranes and endoplasmic reticulum into the nuclear chromatin." Mol Cell Biol 34(24): 4534-4544.

Kaeberlein, M. (2006). "Genome-wide approaches to understanding human ageing." Hum Genomics 2(6): 422-428.

Kalluri, R. (2003). "Basement membranes: structure, assembly and role in tumour angiogenesis." Nat Rev Cancer 3(6): 422-433.

Kanitakis, J. (2002). "Anatomy, histology and immunohistochemistry of normal human skin." Eur J Dermatol 12(4): 390-399; quiz 400-391.

Kazlouskaya, V., S. Malhotra, J. Lambe, M. H. Idriss, D. Elston and C. Andres (2013). "The utility of elastic Verhoeff-Van Gieson staining in dermatopathology." J Cutan Pathol 40(2): 211-225.

Keene, D. R., L. Y. Sakai, G. P. Lunstrum, N. P. Morris and R. E. Burgeson (1987). "Type VII collagen forms an extended network of anchoring fibrils." J Cell Biol 104(3): 611-621.

Kilkenny, C., W. Browne, I. C. Cuthill, M. Emerson, D. G. Altman and N. C. R. R. G. W. Group (2010). "Animal research: reporting in vivo experiments: the ARRIVE guidelines." Br J Pharmacol 160(7): 1577-1579.

Kim, N. G. and B. M. Gumbiner (2015). "Adhesion to fibronectin regulates Hippo signaling via the FAK-Src-PI3K pathway." J Cell Biol 210(3): 503-515.

Kim, Y., A. A. Sharov, K. McDole, M. Cheng, H. Hao, C. M. Fan, N. Gaiano, M. S. H. Ko and Y. Zheng (2011). "Mouse B-Type Lamins Are Required for Proper Organogenesis But Not by Embryonic Stem Cells." Science 334(6063): 1706-1710.

Kligman, A. M. and C. Koblenzer (1997). "Demographics and psychological implications for the aging population." Dermatol Clin 15(4): 549-553.

Kodaka, M. and Y. Hata (2015). "The mammalian Hippo pathway: regulation and function of YAP1 and TAZ." Cell Mol Life Sci 72(2): 285-306.

Koivunen, P., K. E. Salo, J. Myllyharju and L. W. Ruddock (2005). "Three binding sites in protein-disulfide isomerase cooperate in collagen prolyl 4-hydroxylase tetramer assembly." J Biol Chem 280(7): 5227-5235.

Koster, M. I. and D. R. Roop (2007). "Mechanisms regulating epithelial stratification." Annu Rev Cell Dev Biol 23: 93-113.

Lai-Cheong, J. E., K. Arita and J. A. McGrath (2007). "Genetic diseases of junctions." J Invest Dermatol 127(12): 2713-2725.

Langton, A. K., P. Halai, C. E. Griffiths, M. J. Sherratt and R. E. Watson (2016). "The impact of intrinsic ageing on the protein composition of the dermal-epidermal junction." Mech Ageing Dev 156: 14-16.

Lee, B. Y., J. A. Han, J. S. Im, A. Morrone, K. Johung, E. C. Goodwin, W. J. Kleijer, D. DiMaio and E. S. Hwang (2006). "Senescence-associated beta-galactosidase is lysosomal beta-galactosidase." Aging Cell 5(2): 187-195.

Lee, M. J., M. Ran Byun, M. Furutani-Seiki, J. H. Hong and H. S. Jung (2014). "YAP and TAZ regulate skin wound healing." J Invest Dermatol 134(2): 518-525.

Leenaars, M. and C. F. Hendriksen (2005). "Critical steps in the production of polyclonal and monoclonal antibodies: evaluation and recommendations." ILAR J 46(3): 269-279.

Lemons, J. M., X. J. Feng, B. D. Bennett, A. Legesse-Miller, E. L. Johnson, I. Raitman, E. A. Pollina, H. A. Rabitz, J. D. Rabinowitz and H. A. Coller (2010). "Quiescent fibroblasts exhibit high metabolic activity." PLoS Biol 8(10): e1000514.

Lener, T., P. R. Moll, M. Rinnerthaler, J. Bauer, F. Aberger and K. Richter (2006). "Expression profiling of aging in the human skin." Exp Gerontol 41(4): 387-397.

Levene, H. (1960). Robust tests for equality of variances. In Contributions to Probability and Statistics (I. Olkin, ed.)278–292. Stanford Univ. Press, Palo Alto, CA.

Li, R. and Y. Shen (2013). "An old method facing a new challenge: re-visiting housekeeping proteins as internal reference control for neuroscience research." Life Sci 92(13): 747-751.

Li, X., H. Xu, C. Xu, M. Lin, X. Song, F. Yi, Y. Feng, K. A. Coughlan, W. C. Cho, S. S. Kim and L. Cao (2013). "The yin-yang of DNA damage response: roles in tumorigenesis and cellular senescence." Int J Mol Sci 14(2): 2431-2448.

Liang, X. and S. A. Boppart (2010). "Biomechanical properties of in vivo human skin from dynamic optical coherence elastography." IEEE Trans Biomed Eng 57(4): 953-959.

Liao, C. Y. and B. K. Kennedy (2014). "Mouse models and aging: longevity and progeria." Curr Top Dev Biol 109: 249-285.

Libotte, T., H. Zaim, S. Abraham, V. C. Padmakumar, M. Schneider, W. Lu, M. Munck, C. Hutchison, M. Wehnert, B. Fahrenkrog, U. Sauder, U. Aebi, A. A. Noegel and I. Karakesisoglou (2005). "Lamin A/C-dependent localization of Nesprin-2, a giant scaffolder at the nuclear envelope." Mol Biol Cell 16(7): 3411-3424.

Lillie, R. D., R. E. Tracy, P. Pizzolato, P. T. Donaldson and C. Reynolds (1980). "Differential staining of collagen types in paraffin sections: a color change in degraded forms." Virchows Arch A Pathol Anat Histol 386(2): 153-159.

Lim, X. and R. Nusse (2013). "Wnt signaling in skin development, homeostasis, and disease." Cold Spring Harb Perspect Biol 5(2).

Lim, X., S. H. Tan, W. L. Koh, R. M. Chau, K. S. Yan, C. J. Kuo, R. van Amerongen, A. M. Klein and R. Nusse (2013). "Interfollicular epidermal stem cells self-renew via autocrine Wnt signaling." Science 342(6163): 1226-1230.

Lin, T. K., D. Crumrine, L. D. Ackerman, J. L. Santiago, T. Roelandt, Y. Uchida, M. Hupe, G. Fabrias, J. L. Abad, R. H. Rice and P. M. Elias (2012). "Cellular changes that accompany shedding of human corneocytes." J Invest Dermatol 132(10): 2430-2439.

Liu, X., H. Wu, M. Byrne, S. Krane and R. Jaenisch (1997). "Type III collagen is crucial for collagen I fibrillogenesis and for normal cardiovascular development." Proc Natl Acad Sci U S A 94(5): 1852-1856.

Llewylln, B. (2008) Differential staining with acid dyes.Caloundra, Queensland, Australia. Published online at https://stainsfile.info/StainsFile/downloads/tristain.pdf

Lo Sardo, F., Strano, S. and Blandino, G. (2014) The Hippo Kinase Pathway: a master regulator of proliferation, development and differentiation. Online at:http://atlasgeneticsoncology.org/Deep/HippoKinasePathwayID20125.html

Lovell, C. R., K. A. Smolenski, V. C. Duance, N. D. Light, S. Young and M. Dyson (1987). "Type I and III collagen content and fibre distribution in normal human skin during ageing." Br J Dermatol 117(4): 419-428.

Lu, C. S., S. C. Wu, J. W. Hou, C. P. Chu, L. L. Tseng and H. C. Lue (2013). "Restrictive dermopathy: report of two siblings." Pediatr Neonatol 54(3): 198-201.

MacRae, S. L., Q. Zhang, C. Lemetre, I. Seim, R. B. Calder, J. Hoeijmakers, Y. Suh, V. N. Gladyshev, A. Seluanov, V. Gorbunova, J. Vijg and Z. D. Zhang (2015). "Comparative analysis of genome maintenance genes in naked mole rat, mouse, and human." Aging Cell 14(2): 288-291.

Maharlooei, M. K., A. A. Mohammadi, A. Farsi, I. Ahrari, A. Attar and A. Monabati (2011). "A comparison between different existing methods used to separate epidermal cells from skin biopsies for autologous transplantation." Indian J Dermatol 56(6): 666-669.

Mahen, R., H. Hattori, M. Lee, P. Sharma, A. D. Jeyasekharan and A. R. Venkitaraman (2013). "A-type lamins maintain the positional stability of DNA damage repair foci in mammalian nuclei." PLoS One 8(5): e61893.

Mahfouz, S., S. Gabal, and M. Fawzy, "Immunohistochemical expression of E-cadherin in psoriasis", The Medical Journal of Cairo University, vol. 80, no. 2, 2012.

Makrantonaki, E. and C. C. Zouboulis (2007). "Molecular mechanisms of skin aging: state of the art." Ann N Y Acad Sci 1119: 40-50.

Makrantonaki, E., T. C. Brink, V. Zampeli, R. M. Elewa, B. Mlody, A. M. Hossini, B. Hermes, U. Krause, J. Knolle, M. Abdallah, J. Adjaye and C. C. Zouboulis (2012). "Identification of biomarkers of human skin ageing in both genders. Wnt signalling - a label of skin ageing?" PLoS One 7(11): e50393.

Mangelsdorf, S., et al. (2014). "Comparative study of hair follicle morphology in eight mammalian species and humans." Skin Res Technol 20(2): 147-154.

Manju, K., B. Muralikrishna and V. K. Parnaik (2006). "Expression of disease-causing lamin A mutants impairs the formation of DNA repair foci." J Cell Sci 119(Pt 13): 2704-2714.

Marji, J., S. I. O'Donoghue, D. McClintock, V. P. Satagopam, R. Schneider, D. Ratner, H. J. Worman, L. B. Gordon and K. Djabali (2010). "Defective lamin A-Rb signaling in Hutchinson-Gilford Progeria Syndrome and reversal by farnesyltransferase inhibition." PLoS One 5(6): e11132.

Marti, P., C. Stein, T. Blumer, Y. Abraham, M. T. Dill, M. Pikiolek, V. Orsini, G. Jurisic, P. Megel, Z. Makowska, C. Agarinis, L. Tornillo, T. Bouwmeester, H. Ruffner, A. Bauer, C. N. Parker, T. Schmelzle, L. M. Terracciano, M. H. Heim and J. S. Tchorz (2015). "YAP promotes proliferation, chemoresistance, and angiogenesis in human cholangiocarcinoma through TEAD transcription factors." Hepatology 62(5): 1497-1510.

Mascre, G., S. Dekoninck, B. Drogat, K. K. Youssef, S. Brohee, P. A. Sotiropoulou, B. D. Simons and C. Blanpain (2012). "Distinct contribution of stem and progenitor cells to epidermal maintenance." Nature 489(7415): 257-262.

Masoro, E. J. (2000). "Caloric restriction and aging: an update." Experimental Gerontology 35(3): 299-305.

Matera, A. G., R. M. Terns and M. P. Terns (2007). "Non-coding RNAs: lessons from the small nuclear and small nucleolar RNAs." Nat Rev Mol Cell Biol 8(3): 209-220.

Mays, P. K., R. J. McAnulty, J. S. Campa and G. J. Laurent (1991). "Age-related changes in collagen synthesis and degradation in rat tissues. Importance of degradation of newly synthesized collagen in regulating collagen production." Biochem J 276 (Pt 2): 307-313.

McBride, D. J., Jr., V. Choe, J. R. Shapiro and B. Brodsky (1997). "Altered collagen structure in mouse tail tendon lacking the alpha 2(I) chain." J Mol Biol 270(2): 275-284.

McClintock, D., D. Ratner, M. Lokuge, D. M. Owens, L. B. Gordon, F. S. Collins and K. Djabali (2007). "The mutant form of lamin A that causes Hutchinson-Gilford progeria is a biomarker of cellular aging in human skin." PLoS One 2(12): e1269.

McGrath, J. A., Eady, R. A. J. and Pope, F. M. (2004) Anatomy and Organization of Human Skin, in Rook's Textbook of Dermatology, 7th Edn Blackwell Publishing, Inc., Malden, Massachusetts, USA. doi: 10.1002/9780470750520.ch3

Meinke, P., T. D. Nguyen and M. S. Wehnert (2011). "The LINC complex and human disease." Biochem Soc Trans 39(6): 1693-1697.

Mienaltowski, M. J. and D. E. Birk (2014). "Structure, physiology, and biochemistry of collagens." Adv Exp Med Biol 802: 5-29.

Miller, R. A. and N. L. Nadon (2000). "Principles of animal use for gerontological research." Journals of Gerontology Series a-Biological Sciences and Medical Sciences 55(3): B117-B123.

Mine, S., N. O. Fortunel, H. Pageon and D. Asselineau (2008). "Aging alters functionally human dermal papillary fibroblasts but not reticular fibroblasts: a new view of skin morphogenesis and aging." PLoS One 3(12): e4066.

Mitnitski, A., S. E. Howlett and K. Rockwood (2016). "Heterogeneity of Human Aging and Its Assessment." J Gerontol A Biol Sci Med Sci.

Mody, L., D. K. Miller, J. M. McGloin, M. Freeman, E. R. Marcantonio, J. Magaziner and S. Studenski (2008). "Recruitment and retention of older adults in aging research." J Am Geriatr Soc 56(12): 2340-2348.

Moir, R. D., T. P. Spann, H. Herrmann and R. D. Goldman (2000). "Disruption of nuclear lamin organization blocks the elongation phase of DNA replication." J Cell Biol 149(6): 1179-1192.

Moiseeva, O., V. Bourdeau, A. Roux, X. Deschenes-Simard and G. Ferbeyre (2009). "Mitochondrial dysfunction contributes to oncogene-induced senescence." Mol Cell Biol 29(16): 4495-4507.

Moll, R., M. Divo and L. Langbein (2008). "The human keratins: biology and pathology." Histochem Cell Biol 129(6): 705-733.

Monteiro-Riviere, N. A., Y. B. Banks and L. S. Birnbaum (1991). "Laser Doppler measurements of cutaneous blood flow in ageing mice and rats." Toxicol Lett 57(3): 329-338.

Montes, G. S. and L. C. Junqueira (1991). "The use of the Picrosirius-polarization method for the study of the biopathology of collagen." Mem Inst Oswaldo Cruz 86 Suppl 3: 1-11.

Morey, J. S., J. C. Ryan and F. M. Van Dolah (2006). "Microarray validation: factors influencing correlation between oligonucleotide microarrays and real-time PCR." Biol Proced Online 8: 175-193.

Motta, P.M. and Ruggeri, A. (1984) Ultrastructure of the connective tissue matrix. Martinus Nijhoff publishing, Boston, USA.

Mouw, J. K., G. Ou and V. M. Weaver (2014). "Extracellular matrix assembly: a multiscale deconstruction." Nat Rev Mol Cell Biol 15(12): 771-785.

Muller-Rover, S., B. Handjiski, C. van der Veen, S. Eichmuller, K. Foitzik, I. A. McKay, K. S. Stenn and R. Paus (2001). "A comprehensive guide for the accurate classification of murine hair follicles in distinct hair cycle stages." J Invest Dermatol 117(1): 3-15.

Munakata, H., K. Takagaki, M. Majima and M. Endo (1999). "Interaction between collagens and glycosaminoglycans investigated using a surface plasmon resonance biosensor." Glycobiology 9(10): 1023-1027.

Nadon, N. L. (2006). "Of mice and monkeys: National Institute on Aging resources supporting the use of animal models in biogerontology research." Journals of Gerontology Series a-Biological Sciences and Medical Sciences 61(8): 813-815.

Nadon, R. and J. Shoemaker (2002). "Statistical issues with microarrays: processing and analysis." Trends Genet 18(5): 265-271.

Naidoo, S., K. J. Denby and D. K. Berger (2005). "Microarray experiments: considerations for experimental design." South African Journal of Science 101(7-8): 347-354.

Natsuga, K (2013). Chapter 2-Epidermolysis Bullosa Simplex, Current Genetics in Dermatology, Dr. Naoki Oiso (Ed.), InTech, DOI: 10.5772/54609. Available from: http://www.intechopen.com/books/current-genetics-in-dermatology/epidermolysis-bullosa-simplex

Naylor, E. C., R. E. Watson and M. J. Sherratt (2011). "Molecular aspects of skin ageing." Maturitas 69(3): 249-256.

Nelson, G., J. Wordsworth, C. Wang, D. Jurk, C. Lawless, C. Martin-Ruiz and T. von Zglinicki (2012). "A senescent cell bystander effect: senescence-induced senescence." Aging Cell 11(2): 345-349.

Nemes, Z. and P. M. Steinert (1999). "Bricks and mortar of the epidermal barrier." Exp Mol Med 31(1): 5-19.

Newman, A. B., S. Walter, K. L. Lunetta, M. E. Garcia, P. E. Slagboom, K. Christensen, A. M. *et al* (2010). "A meta-analysis of four genome-wide association studies of survival to age 90 years or older: the Cohorts for Heart and Aging Research in Genomic Epidemiology Consortium." J Gerontol A Biol Sci Med Sci 65(5): 478-487.

Nithya, S., T. Radhika and N. Jeddy (2015). "Loricrin - an overview." J Oral Maxillofac Pathol 19(1): 64-68.

Noursadeghi, M., J. Tsang, T. Haustein, R. F. Miller, B. M. Chain and D. R. Katz (2008). "Quantitative imaging assay for NF-kappaB nuclear translocation in primary human macrophages." J Immunol Methods 329(1-2): 194-200.

Oberg, P. and L. Tornstam (1999). "Body images among men and women of different ages." Ageing and Society 19: 629-644.

Oguchi, M., J. Sagara, K. Matsumoto, T. Saida and S. Taniguchi (2002). "Expression of lamins depends on epidermal differentiation and transformation." Br J Dermatol 147(5): 853-858.

Ohtani, N., A. Takahashi, D. J. Mann and E. Hara (2012). "Cellular senescence: a double-edged sword in the fight against cancer." Exp Dermatol 21 Suppl 1: 1-4.

Oikarinen, A. (1990). "The aging of skin: chronoaging versus photoaging." Photodermatol Photoimmunol Photomed 7(1): 3-4.

Olsen, D. R., J. Peltonen, S. Jaakkola, M. L. Chu and J. Uitto (1989). "Collagen gene expression by cultured human skin fibroblasts. Abundant steady-state levels of type VI procollagen messenger RNAs." J Clin Invest 83(3): 791-795.

Otberg, N., et al. (2008). "The role of hair follicles in the percutaneous absorption of caffeine." Br J Clin Pharmacol 65(4): 488-492.

Panich, U., G. Sittithumcharee, N. Rathviboon and S. Jirawatnotai (2016). "Ultraviolet Radiation-Induced Skin Aging: The Role of DNA Damage and Oxidative Stress in Epidermal Stem Cell Damage Mediated Skin Aging." Stem Cells Int 2016: 7370642.

Pasparakis, M., I. Haase and F. O. Nestle (2014). "Mechanisms regulating skin immunity and inflammation." Nat Rev Immunol 14(5): 289-301.

Pattison, D. I. and M. J. Davies (2006). "Actions of ultraviolet light on cellular structures." EXS(96): 131-157.

Paus, R. and G. Cotsarelis (1999). "The biology of hair follicles." N Engl J Med 341(7): 491-497.

Pawlaczyk, M., M. Lelonkiewicz and M. Wieczorowski (2013). "Age-dependent biomechanical properties of the skin." Postepy Dermatol Alergol 30(5): 302-306.

Pekovic, V., I. Gibbs-Seymour, E. Markiewicz, F. Alzoghaibi, A. M. Benham, R. Edwards, M. Wenhert, T. von Zglinicki and C. J. Hutchison (2011). "Conserved cysteine residues in the mammalian lamin A tail are essential for cellular responses to ROS generation." Aging Cell 10(6): 1067-1079.

Piccolo, S., S. Dupont and M. Cordenonsi (2014). "The biology of YAP/TAZ: hippo signaling and beyond." Physiol Rev 94(4): 1287-1312.

Plikus, M. V. and C. M. Chuong (2008). "Complex hair cycle domain patterns and regenerative hair waves in living rodents." J Invest Dermatol 128(5): 1071-1080.

Plotkin, J. B. (2010). "Transcriptional regulation is only half the story." Mol Syst Biol 6: 406.

Poljsak, B. and R. Dahmane (2012). "Free radicals and extrinsic skin aging." Dermatol Res Pract 2012: 135206.

Poschl, E., U. Schlotzer-Schrehardt, B. Brachvogel, K. Saito, Y. Ninomiya and U. Mayer (2004). "Collagen IV is essential for basement membrane stability but dispensable for initiation of its assembly during early development." Development 131(7): 1619-1628.

Prento, P. (1993). "Van Gieson's picrofuchsin. The staining mechanisms for collagen and cytoplasm, and an examination of the dye diffusion rate model of differential staining." Histochemistry 99(2): 163-174.

Qin, Z., J. J. Voorhees, G. J. Fisher and T. Quan (2014). "Age-associated reduction of cellular spreading/mechanical force up-regulates matrix metalloproteinase-1 expression and collagen fibril fragmentation via c-Jun/AP-1 in human dermal fibroblasts." Aging Cell 13(6): 1028-1037.-a

Qin, Z., P. Robichaud, T. He, G. J. Fisher, J. J. Voorhees and T. Quan (2014). "Oxidant exposure induces cysteine-rich protein 61 (CCN1) via c-Jun/AP-1 to reduce collagen expression in human dermal fibroblasts." PLoS One 9(12): e115402.- b

Quan, T., E. Little, H. Quan, Z. Qin, J. J. Voorhees and G. J. Fisher (2013). "Elevated matrix metalloproteinases and collagen fragmentation in photodamaged human skin: impact of altered extracellular matrix microenvironment on dermal fibroblast function." J Invest Dermatol 133(5): 1362-1366.

Rajkumar, A. P., P. Qvist, R. Lazarus, F. Lescai, J. Ju, M. Nyegaard, O. Mors, A. D. Borglum, Q. Li and J. H. Christensen (2015). "Experimental validation of methods for differential gene expression analysis and sample pooling in RNA-seq." BMC Genomics 16: 548.

Rawlings, A. V. (2010). "Recent advances in skin 'barrier' research." J Pharm Pharmacol 62(6): 671-677.

Redwood, A. B., S. M. Perkins, R. P. Vanderwaal, Z. Feng, K. J. Biehl, I. Gonzalez-Suarez, L. Morgado-Palacin, W. Shi, J. Sage, J. L. Roti-Roti, C. L. Stewart, J. Zhang and S. Gonzalo (2011). "A dual role for A-type lamins in DNA double-strand break repair." Cell Cycle 10(15): 2549-2560.

Reinhardt, H. C. and B. Schumacher (2012). "The p53 network: cellular and systemic DNA damage responses in aging and cancer." Trends Genet 28(3): 128-136.

Ressler, S., J. Bartkova, H. Niederegger, J. Bartek, K. Scharffetter-Kochanek, P. Jansen-Durr and M. Wlaschek (2006). "p16INK4A is a robust in vivo biomarker of cellular aging in human skin." Aging Cell 5(5): 379-389.

Richards, S. A., J. Muter, P. Ritchie, G. Lattanzi and C. J. Hutchison (2011). "The accumulation of un-repairable DNA damage in laminopathy progeria fibroblasts is caused by ROS generation and is prevented by treatment with N-acetyl cysteine." Hum Mol Genet 20(20): 3997-4004.

Righolt, C. H., M. L. van 't Hoff, B. J. Vermolen, I. T. Young and V. Raz (2011). "Robust nuclear lamina-based cell classification of aging and senescent cells." Aging (Albany NY) 3(12): 1192-1201.

Robinson, M. K., R. L. Binder and C. E. Griffiths (2009). "Genomic-driven insights into changes in aging skin." J Drugs Dermatol 8(7 Suppl): s8-11.

Romero-Calvo, I., B. Ocon, P. Martinez-Moya, M. D. Suarez, A. Zarzuelo, O. Martinez-Augustin and F. S. de Medina (2010). "Reversible Ponceau staining as a loading control alternative to actin in Western blots." Anal Biochem 401(2): 318-320.

Rong, Y. H., G. A. Zhang, C. Wang and F. G. Ning (2008). "[Quantification of type I and III collagen content in normal human skin in different age groups]." Zhonghua Shao Shang Za Zhi 24(1): 51-53.

Roy, E., Z. Neufeld, L. Cerone, H. Y. Wong, S. Hodgson, J. Livet and K. Khosrotehrani (2016). "Bimodal behaviour of interfollicular epidermal progenitors regulated by hair follicle position and cycling." EMBO J 35(24): 2658-2670.

Ryynanen, J., S. Sollberg, M. G. Parente, L. C. Chung, A. M. Christiano and J. Uitto (1992). "Type VII collagen gene expression by cultured human cells and in fetal skin. Abundant mRNA and protein levels in epidermal keratinocytes." J Clin Invest 89(1): 163-168.

Saito, K., I. Naito, T. Seki, T. Oohashi, E. Kimura, R. Momota, Y. Kishiro, Y. Sado, H. Yoshioka and Y. Ninomiya (2000). "Differential expression of mouse alpha5(IV) and alpha6(IV) collagen genes in epithelial basement membranes." J Biochem 128(3): 427-434.

Sandilands, A., C. Sutherland, A. D. Irvine and W. H. McLean (2009). "Filaggrin in the frontline: role in skin barrier function and disease." J Cell Sci 122(Pt 9): 1285-1294.

Sayama, A., T. Soushin, T. Okada, K. Doi and H. Nakayama (2010). "Morphological and Biochemical Changes During Aging and Photoaging of the Skin of C57BL/6J Mice." J Toxicol Pathol 23(3): 133-139.

Scaffidi, P. and T. Misteli (2006). "Lamin A-dependent nuclear defects in human aging." Science 312(5776): 1059-1063.

Schafer, I. A., M. Kovach, R. L. Price and R. B. Fratianne (1991). "Human keratinocytes cultured on collagen gels form an epidermis which synthesizes bullous pemphigoid antigens and alpha 2 beta 1 integrins and secretes laminin, type IV collagen, and heparan sulfate proteoglycan at the basal cell surface." Exp Cell Res 195(2): 443-457.

Shier, D., Butler, J., & Lewis, R. (2007). *Hole's human anatomy & physiology*. Dubuque, IA: McGraw-Hill.

Schlegelmilch, K., M. Mohseni, O. Kirak, J. Pruszak, J. R. Rodriguez, D. Zhou, B. T. Kreger, V. Vasioukhin, J. Avruch, T. R. Brummelkamp and F. D. Camargo (2011). "Yap1 acts downstream of alpha-catenin to control epidermal proliferation." Cell 144(5): 782-795.

Schneider, M. R., et al. (2009). "The hair follicle as a dynamic miniorgan." Curr Biol 19(3): R132-142.

Schuler, N. and C. E. Rube (2013). "Accumulation of DNA damage-induced chromatin alterations in tissue-specific stem cells: the driving force of aging?" PLoS One 8(5): e63932.

Schuster, E. F., E. Blanc, L. Partridge and J. M. Thornton (2007). "Estimation and correction of non-specific binding in a large-scale spike-in experiment." Genome Biol 8(6): R126.

Seppet, E., M. Paasuke, M. Conte, M. Capri and C. Franceschi (2011). "Ethical aspects of aging research." Biogerontology 12(6): 491-502.

Shackleton, S., D. T. Smallwood, P. Clayton, L. C. Wilson, A. K. Agarwal, A. Garg and R. C. Trembath (2005). "Compound heterozygous ZMPSTE24 mutations reduce prelamin A processing and result in a severe progeroid phenotype." J Med Genet 42(6): e36.

Shi, S. R., Y. Shi and C. R. Taylor (2011). "Antigen retrieval immunohistochemistry: review and future prospects in research and diagnosis over two decades." J Histochem Cytochem 59(1): 13-32.

Shimi, T. and R. D. Goldman (2014). "Nuclear Lamins and Oxidative Stress in Cell Proliferation and Longevity." Cancer Biology and the Nuclear Envelope: Recent Advances May Elucidate Past Paradoxes 773: 415-430.

Shimi, T., V. Butin-Israeli, S. A. Adam, R. B. Hamanaka, A. E. Goldman, C. A. Lucas, D. K. Shumaker, S. T. Kosak, N. S. Chandel and R. D. Goldman (2011). "The role of nuclear lamin B1 in cell proliferation and senescence." Genes Dev 25(24): 2579-2593.

Shoulders, M. D. and R. T. Raines (2009). "Collagen structure and stability." Annu Rev Biochem 78: 929-958.

Sieprath, T., R. Darwiche and W. H. De Vos (2012). "Lamins as mediators of oxidative stress." Biochem Biophys Res Commun 421(4): 635-639.

Sieprath, T., T. D. Corne, M. Nooteboom, C. Grootaert, A. Rajkovic, B. Buysschaert, J. Robijns, J. L. Broers, F. C. Ramaekers, W. J. Koopman, P. H. Willems and W. H. De Vos (2015). "Sustained accumulation of prelamin A and depletion of lamin A/C both cause oxidative stress and mitochondrial dysfunction but induce different cell fates." Nucleus 6(3): 236-246.

Signore, M. and K. A. Reeder (2012). "Antibody validation by Western blotting." Methods Mol Biol 823: 139-155.

Silvis, M. R., B. T. Kreger, W. H. Lien, O. Klezovitch, G. M. Rudakova, F. D. Camargo, D. M. Lantz, J. T. Seykora and V. Vasioukhin (2011). "alpha-catenin is a tumor suppressor that controls cell accumulation by regulating the localization and activity of the transcriptional coactivator Yap1." Sci Signal 4(174): ra33.

Simpson, C. L., D. M. Patel and K. J. Green (2011). "Deconstructing the skin: cytoarchitectural determinants of epidermal morphogenesis." Nat Rev Mol Cell Biol 12(9): 565-580.

Singh, M., C. R. Hunt, R. K. Pandita, R. Kumar, C. R. Yang, N. Horikoshi, R. Bachoo, S. Serag, M. D. Story, J. W. Shay, S. N. Powell, A. Gupta, J. Jeffery, S. Pandita, B. P. Chen, D. Deckbar, M. Lobrich, Q. Yang, K. K. Khanna, H. J. Worman and T. K. Pandita (2013). "Lamin A/C depletion enhances DNA damage-induced stalled replication fork arrest." Mol Cell Biol 33(6): 1210-1222.

Smalls, L. K., R. Randall Wickett and M. O. Visscher (2006). "Effect of dermal thickness, tissue composition, and body site on skin biomechanical properties." Skin Res Technol 12(1): 43-49.

Solanas, G. and S. A. Benitah (2013). "Regenerating the skin: a task for the heterogeneous stem cell pool and surrounding niche." Nat Rev Mol Cell Biol 14(11): 737-748.

Song, J. Y., R. Park, J. Y. Kim, L. Hughes, L. Lu, S. Kim, R. L. Johnson and S. H. Cho (2014). "Dual function of Yap in the regulation of lens progenitor cells and cellular polarity." Dev Biol 386(2): 281-290.

Spann, T. P., A. E. Goldman, C. Wang, S. Huang and R. D. Goldman (2002). "Alteration of nuclear lamin organization inhibits RNA polymerase II-dependent transcription." J Cell Biol 156(4): 603-608.

St Sauver, J. L., D. O. Warner, B. P. Yawn, D. J. Jacobson, M. E. McGree, J. J. Pankratz, L. J. Melton, 3rd, V. L. Roger, J. O. Ebbert and W. A. Rocca (2013). "Why patients visit their doctors: assessing the most prevalent conditions in a defined American population." Mayo Clin Proc 88(1): 56-67.

Steven, A. C. and P. M. Steinert (1994). "Protein composition of cornified cell envelopes of epidermal keratinocytes." J Cell Sci 107 (Pt 2): 693-700.

Stevenson, S. and J. Thornton (2007). "Effect of estrogens on skin aging and the potential role of SERMs." Clin Interv Aging 2(3): 283-297.

Steves, C. J., T. D. Spector and S. H. Jackson (2012). "Ageing, genes, environment and epigenetics: what twin studies tell us now, and in the future." Age Ageing 41(5): 581-586.

Sudol, M. (2013). "YAP1 oncogene and its eight isoforms." Oncogene 32(33): 3922.

Sund, M., Y. Maeshima and R. Kalluri (2005). "Bifunctional promoter of type IV collagen COL4A5 and COL4A6 genes regulates the expression of alpha5 and alpha6 chains in a distinct cell-specific fashion." Biochem J 387(Pt 3): 755-761.

Swift, J., I. L. Ivanovska, A. Buxboim, T. Harada, P. C. Dingal, J. Pinter, J. D. Pajerowski, K. R. Spinler, J. W. Shin, M. Tewari, F. Rehfeldt, D. W. Speicher and D. E. Discher (2013). "Nuclear lamin-A scales with tissue stiffness and enhances matrix-directed differentiation." Science 341(6149): 1240104.

Tasseff, R., A. Bheda-Malge, T. DiColandrea, C. C. Bascom, R. J. Isfort and R. Gelinas (2014). "Mouse hair cycle expression dynamics modeled as coupled mesenchymal and epithelial oscillators." PLoS Comput Biol 10(11): e1003914.

Thingnes, J., T. J. Lavelle, E. Hovig and S. W. Omholt (2012). "Understanding the melanocyte distribution in human epidermis: an agent-based computational model approach." PLoS One 7(7): e40377.

Tilli, C. M., F. C. Ramaekers, J. L. Broers, C. J. Hutchison and H. A. Neumann (2003). "Lamin expression in normal human skin, actinic keratosis, squamous cell carcinoma and basal cell carcinoma." Br J Dermatol 148(1): 102-109.

Tunggal, J. A., I. Helfrich, A. Schmitz, H. Schwarz, D. Gunzel, M. Fromm, R. Kemler, T. Krieg and C. M. Niessen (2005). "E-cadherin is essential for in vivo epidermal barrier function by regulating tight junctions." EMBO J 24(6): 1146-1156.

Vanhooren, V. and C. Libert (2013). "The mouse as a model organism in aging research: usefulness, pitfalls and possibilities." Ageing Res Rev 12(1): 8-21.

Varani, J., P. Perone, S. E. Fligiel, G. J. Fisher and J. J. Voorhees (2002). "Inhibition of type I procollagen production in photodamage: correlation between presence of high molecular

weight collagen fragments and reduced procollagen synthesis." J Invest Dermatol 119(1): 122-129.

Vaughan, A., M. Alvarez-Reyes, J. M. Bridger, J. L. Broers, F. C. Ramaekers, M. Wehnert, G. E. Morris, W. G. F. Whitfield and C. J. Hutchison (2001). "Both emerin and lamin C depend on lamin A for localization at the nuclear envelope." J Cell Sci 114(Pt 14): 2577-2590.

Vazquez, F., S. Palacios, N. Aleman and F. Guerrero (1996). "Changes of the basement membrane and type IV collagen in human skin during aging." Maturitas 25(3): 209-215.

Verbon, E. H., J. A. Post and J. Boonstra (2012). "The influence of reactive oxygen species on cell cycle progression in mammalian cells." Gene 511(1): 1-6.

Vergnes, L., M. Peterfy, M. O. Bergo, S. G. Young and K. Reue (2004). "Lamin B1 is required for mouse development and nuclear integrity." Proc Natl Acad Sci U S A 101(28): 10428-10433.

Vermeij, W. P., M. E. Dolle, E. Reiling, et al (2016). "Restricted diet delays accelerated ageing and genomic stress in DNA-repair-deficient mice." Nature 537(7620): 427-431.

Vigelso, A., R. Dybboe, C. N. Hansen, F. Dela, J. W. Helge and A. Guadalupe Grau (2015). "GAPDH and beta-actin protein decreases with aging, making Stain-Free technology a superior loading control in Western blotting of human skeletal muscle." J Appl Physiol (1985) 118(3): 386-394.

Waaijer, M. E., W. E. Parish, B. H. Strongitharm, D. van Heemst, P. E. Slagboom, A. J. de Craen, J. M. Sedivy, R. G. Westendorp, D. A. Gunn and A. B. Maier (2012). "The number of p16INK4a positive cells in human skin reflects biological age." Aging Cell 11(4): 722-725.

Wada, K., K. Itoga, T. Okano, S. Yonemura and H. Sasaki (2011). "Hippo pathway regulation by cell morphology and stress fibers." Development 138(18): 3907-3914.

Wakayama, T., Y. Kato, R. Utsumi, A. Tsuji and S. Iseki (2006). "A time- and cost-saving method of producing rat polyclonal antibodies." Acta Histochem Cytochem 39(3): 79-87.

Wang, C., D. Jurk, M. Maddick, G. Nelson, C. Martin-Ruiz and T. von Zglinicki (2009). "DNA damage response and cellular senescence in tissues of aging mice." Aging Cell 8(3): 311-323.

Wang, C., M. Maddick, S. Miwa, D. Jurk, R. Czapiewski, G. Saretzki, S. A. Langie, R. W. Godschalk, K. Cameron and T. von Zglinicki (2010). "Adult-onset, short-term dietary restriction reduces cell senescence in mice." Aging (Albany NY) 2(9): 555-566.

Wang, L., S. Shi, Z. Guo, X. Zhang, S. Han, A. Yang, W. Wen and Q. Zhu (2013). "Overexpression of YAP and TAZ is an independent predictor of prognosis in colorectal cancer and related to the proliferation and metastasis of colon cancer cells." PLoS One 8(6): e65539.

Wang, M. and P. J. Casey (2016). "Protein prenylation: unique fats make their mark on biology." Nat Rev Mol Cell Biol 17(2): 110-122.

Wang, Y., A. A. Panteleyev, D. M. Owens, K. Djabali, C. L. Stewart and H. J. Worman (2008). "Epidermal expression of the truncated prelamin A causing Hutchinson-Gilford progeria syndrome: effects on keratinocytes, hair and skin." Hum Mol Genet 17(15): 2357-2369.

Watson, R. E., N. K. Gibbs, C. E. Griffiths and M. J. Sherratt (2014). "Damage to skin extracellular matrix induced by UV exposure." Antioxid Redox Signal 21(7): 1063-1077.

Watt, F. M. (2002). "Role of integrins in regulating epidermal adhesion, growth and differentiation." EMBO J 21(15): 3919-3926.

Watt, F. M. and H. Fujiwara (2011). "Cell-extracellular matrix interactions in normal and diseased skin." Cold Spring Harb Perspect Biol 3(4).

Yang, S. H., H. J. Jung, C. Coffinier, L. G. Fong and S. G. Young (2011). "Are B-type lamins essential in all mammalian cells?" Nucleus 2(6): 562-569.

Yang, S. H., S. Y. Chang, L. Y. Yin, Y. P. Tu, Y. Hu, Y. Yoshinaga, P. J. de Jong, L. G. Fong and S. G. Young (2011). "An absence of both lamin B1 and lamin B2 in keratinocytes has no effect on cell proliferation or the development of skin and hair." Human Molecular Genetics 20(18): 3537-3544.

Young, P., O. Boussadia, H. Halfter, R. Grose, P. Berger, D. P. Leone, H. Robenek, P. Charnay, R. Kemler and U. Suter (2003). "E-cadherin controls adherens junctions in the epidermis and the renewal of hair follicles." EMBO J 22(21): 5723-5733.

Younis, S., M. Komine, M. Tomic-Canic and M. Blumenberg (2014). Skinomics: A New Toolbox to Understand Skin Aging. Textbook of Aging Skin. M. A. Farage, K. W. Miller and H. I. Maibach. Berlin, Heidelberg, Springer Berlin Heidelberg: 1-19.

Yu, F. X. and K. L. Guan (2013). "The Hippo pathway: regulators and regulations." Genes Dev 27(4): 355-371.

Yuan, R., S. W. Tsaih, S. B. Petkova, C. M. de Evsikova, S. Q. Xing, M. A. Marion, M. A. Bogue, K. D. Mills, L. L. Peters, C. J. Bult, C. J. Rosen, J. P. Sundberg, D. E. Harrison, G. A. Churchill and B. Paigen (2009). "Aging in inbred strains of mice: study design and interim report on median lifespans and circulating IGF1 levels." Aging Cell 8(3): 277-287.

Yue, F., Y. Cheng, A. Breschi, J. Vierstra, W. Wu, T. Ryba, R. Sandstrom, *et al* (2014). "A comparative encyclopedia of DNA elements in the mouse genome." Nature 515(7527): 355-364.

Zhang, H., H. A. Pasolli and E. Fuchs (2011). "Yes-associated protein (YAP) transcriptional coactivator functions in balancing growth and differentiation in skin." Proc Natl Acad Sci U S A 108(6): 2270-2275.

Zhao, B., L. Li, L. Wang, C. Y. Wang, J. Yu and K. L. Guan (2012). "Cell detachment activates the Hippo pathway via cytoskeleton reorganization to induce anoikis." Genes Dev 26(1): 54-68.

Zouboulis, C. C. and E. Makrantonaki (2011). "Clinical aspects and molecular diagnostics of skin aging." Clin Dermatol 29(1): 3-14.